Springer Series in Materials Science

Volume 267

The Springer Series in Materials Science covers the complete spectrum of materials physics, including fundamental principles, physical properties, materials theory and design. Recognizing the increasing importance of materials science in future device technologies, the book titles in this series reflect the state-of-the-art in understanding and controlling the structure and properties of all important classes of materials.

More information about this series at http://www.springer.com/series/856

Sergey F. Ermakov · Nikolai K. Myshkin

Liquid-Crystal Nanomaterials

Tribology and Applications

Springer

Sergey F. Ermakov
V.A. Belyi Metal-Polymer Research Institute
National Academy of Sciences of Belarus
Gomel
Belarus

Nikolai K. Myshkin
V.A. Belyi Metal-Polymer Research Institute
National Academy of Sciences of Belarus
Gomel
Belarus

ISSN 0933-033X ISSN 2196-2812 (electronic)
Springer Series in Materials Science
ISBN 978-3-319-74768-2 ISBN 978-3-319-74769-9 (eBook)
https://doi.org/10.1007/978-3-319-74769-9

Library of Congress Control Number: 2017964449

© Springer International Publishing AG, part of Springer Nature 2018
This work is subject to copyright. All rights are reserved by the Publisher, whether the whole or part of the material is concerned, specifically the rights of translation, reprinting, reuse of illustrations, recitation, broadcasting, reproduction on microfilms or in any other physical way, and transmission or information storage and retrieval, electronic adaptation, computer software, or by similar or dissimilar methodology now known or hereafter developed.
The use of general descriptive names, registered names, trademarks, service marks, etc. in this publication does not imply, even in the absence of a specific statement, that such names are exempt from the relevant protective laws and regulations and therefore free for general use.
The publisher, the authors and the editors are safe to assume that the advice and information in this book are believed to be true and accurate at the date of publication. Neither the publisher nor the authors or the editors give a warranty, express or implied, with respect to the material contained herein or for any errors or omissions that may have been made. The publisher remains neutral with regard to jurisdictional claims in published maps and institutional affiliations.

Printed on acid-free paper

This Springer imprint is published by the registered company Springer International Publishing AG part of Springer Nature
The registered company address is: Gewerbestrasse 11, 6330 Cham, Switzerland

Preface

The monograph is devoted to a topical issue of the study of lubricity of liquid-crystal (LC) nanomaterials and systems and their application in engineering and medical fields. The theoretical and experimental results of the study of friction, wear, and lubrication of both technical friction units and natural joints containing liquid-crystal cholesterol compounds are adequately presented. Current conceptions of friction and wear of solids, including biopolymers, are given. Moreover, the author's explanation of boundary lubrication in the presence of cholesteric liquid-crystal nanomaterials in a friction area is set out in the monograph. It is noted that liquid-crystal state of synovia is of essence for reduction of intra-articular friction due to the presence of cholesteric liquid-crystal nanomaterials.

A brand-new conception of lubricity of cholesteric liquid-crystal nanomaterials at friction of articular cartilages with friction surfaces anisotropy peculiar to them on submicroscopic layer has come out of the experimental work. An advantage of this conception is that it is based only on physical or rather energetic interpretations not considering the nature of dynamically contacting solids and so can be applied to not only cartilage but any surfaces and friction pairs. Experimental data confirming this concept are also presented.

Many issues on structural organization and biochemical characteristics of synovial mediums taking part in joint moving and friction are discussed. The results of studies on creation of artificial joint fluids containing liquid-crystal nanomaterials inherent to natural synovia and exhibiting its lubricating and biochemical properties are given.

The results of research on change in concentration of mineral and synthetic lubricating mediums containing LC-nanocompounds and taking place in the process of static and dynamic contacting with various materials are well covered in the monographs. It is shown that adsorption of cholesteric liquid-crystal nanomaterials from their oil solutions occurs only at dynamic contact of the friction surfaces, and there is no adsorption at static contact. The direct link is established for pair steel–steel between adsorption of CLCC nanomaterial molecules, inductive when dynamic interaction (triboinduced), and change of friction coefficient.

Authors have paid special attention to description of patent-protected original methods and techniques for tribophysical studies of natural and technical dissipative systems, as well as for control of phase states and phase transmission temperatures of LC-nanomaterials and systems. Precision devices and systems based on the digital circuitry methods are in use. It helps to considerable decrease in measurement errors and gets the high precision of the experiments. With all the above mentioned, we can make a conclusion that the presented experimental material is important for engineering and medicine, which makes the work useful for professionals in friction and wear of solids as well as for medical specialists dealing with problems of prevention and treatment of arthropathy.

Gomel, Belarus

Sergey F. Ermakov
Nikolai K. Myshkin

About the Book

The monograph gives the research results of tribological, rheological, and optical properties of liquid-crystal nanomaterials, as well as lubricant media and preparations on their basis. Information of high lubricating and screening action of cholesteric liquid-crystal compounds both in technical friction units and in natural human and animal joints are presented. Some connections between tribological and physical properties of liquid-crystal cholesterol compounds are shown. A conceptual model of lubricity of cholesteric-nematic liquid-crystalline nanostructures is proposed on the basis of physical interpretations. It is noted that this model is general and valid for all surfaces and friction pairs, including biopolymer ones. It also presents applications of cholesteric liquid-crystalline nanomaterials in different friction units and tribosystems, as well as in the medical treatment of joint diseases.

Contents

Acronyms and Nomenclature

AFM	Atomic-force microscope
AM	Arithmetic mean
CE	Cholesterol ester
CLC	Cholesteric liquid crystal
CPG	Cylinder-piston groups
ERF	Electrorheological fluids
FRM	Fuel run-in additive
HUA	Hyaluronic acid
ICE	Internal combustion engines
LC	Liquid crystal
LCCC	Liquid-crystal cholesterol compounds
LM	Lubricating materials
Na-CMC	Sodium carboxymethyl cellulose
OA	Oleic acid
PES-5	Polyethyl siloxane fluid
PG	Plastic greases
PS	Pseudo-synovia
PTFE	Polytetrafluoroethylene
RSR	Relative specific radioactivity
SR	Specific radioactivity
SAA	Surface active agent
SCMC	Sodium carboxymethyl cellulose modulus of tension
SF	Synovial fluid
UDD	Ultradispersed diamonds
UDDG	Ultradispersed diamond–graphite charge
UHMWPE	Ultrahigh molecular weight polyethylene
UPTFE	Ultradispersed polytetrafluoroethylene
VO	Vaseline oil
D	Liquid crystal order parameter
E	Modulus of tension

F_{a}	Adhesion component of friction
F_{c}	Cohesion component of friction ия
F_{f}	Friction force
G	Coefficient of rigidity
I_{fl}	Fluorescence strength
K	Forces of action of body weight part
K_{22}	Elastic constant
M	Forces of action of lateral abductor muscles
R	Resulting compressive forces
S	Lead of the cholesteric spiral
$\mathrm{S}/2$	Minimal thickness of liquid-crystal layer or film
T	Temperature
W	Free energy of liquid crystal
W_{s}	Surface energy of liquid crystal
W_e	Elastic energy liquid crystal
b	Extrapolative path
d	Thickness of liquid crystal
h	Thickness of lubricant layer
h_i	Range of sinusoidal relief
h_l	Thickness ratio of lubricant layer
Δh	The thickness of the specimen
Δl	Deformation
$\vec{n}$	Unit vector (director)
P	Pressure
$\tilde{p}$	Dimensionless pressure
Δp	Differential pressure
t	Time
v	Speed
Φ	Pressure in the fluid
Θ	Calorific endothermal effect
Ψ	Pressure in the articular cartilage
α	Angle
γ	Angle polarization plane rotation
η	Viscosity
φ	The angle of molecular orientation in cholesteric
λ	Wavelength of sinusoidal relief
θ	The angle of director orientation $\vec{n}$ relatively to the instantaneous direction of the cholesteric major molecule axis
τ	Dimensionless time parameter

Introduction

Analysis of tribology and condensed-matter physics shows that realization of LC-state of boundary layers lattice-ordered on nanolevel in dynamic contact area of bodies of different nature and investigation of their properties are becoming increasingly more important, as the use of rheological and constitutive models developed in liquid crystal physics can be effective for lubricity problem solving and for development of effective methods and means of control of frictional interaction and topography on nanolevel of surfaces of different nature [1–3]. It should be noted that cholesteric liquid-crystal substances occupy a special place and they are considered to be classified as nanomaterials and nanocomponents, as they meet all criteria (molecule size, twisted structure, mesomorphous-ordered state, dependence of spiral lead on definite parameters, etc.). Moreover, they are sometimes quoted as on example of these materials, in which properties are widely used in nature to form unique nanoconstruction, e.g., nucleic acid and the like.

What is more, such liquid-crystal substances are quite often used in nanotechnologies as standard for creation of ordered nanotextures, e.g., mesoporous systems, nanostructured electrodes, and more. Also, introduction of carbon nanotubes into cholesteric LC-basis as advanced sensitizer can contribute to increasing electrical and thermal conductivity and heat resistance, improving mechanical characteristics, changing structure of LC-matrix, and making it with new functional properties [4–6]. Moreover, the molecules' capacity for self-assembly in supramolecular assemblies makes the liquid-crystal compounds the most important material for nanotechnologies [7–9].

At the same time, a great attention to using structured-ordered organic compounds as additive, including biogenic, is representative of present-day tribology. Cholesteric LC-nanomaterials are of the great interest among such materials, in other words the materials which can structure not only at bearing surfaces but at a distance of it under certain thermodynamic conditions due to their chemical structure and also possess properties of liquid.

However, to give a more detailed picture of principles of such liquid-crystal nanomaterials is necessary to examine in more detail what liquid-crystal compounds represent in general and what is their ranking among well-known solids, liquids, and gases according to their aggregative state, structure, and properties.

The features of the structural behavior, tribology, and lubricity laws of the cholesteric liquid-crystal nanomaterials being developed on the basis of modern concepts of adsorption decreases of solid strength and structural mechanics of boundary layers are presented in the work. A special place is occupied by investigation of friction in biological joints as unique natural rubbing organs. Moreover, the book discusses development of brand-new principles of high-precision tribometry and creation of original devices and hardware for estimation of microstructural properties and phase state of liquid-crystal nanomaterials as well as natural and artificial lubricating media and preparations with them.

References

1. A.S. Akhmatov, *Molecular Physics of Boundary Friction* (Fizmatgiz, Moscow, 1963), p. 472 (in Russian)
2. N.K. Myshkin, C.K. Kim, M.I. Petrokovets, *Introduction to Tribology* (CMG, Seoul, 1997), p. 292
3. S. Ermakov, A. Beletskii, O. Eismont, V. Nikolaev, *Liquid Crystals in Biotribology* (Springer, 2016), p. 212
4. E.G. Rakov, Nanotubes and fullerenes, in *Proceedings of Allowance* (Universitetskaya kniga, Logos, Moscow, 2006), p. 376 (in Russian)
5. M.G. Tomilin, S.M. Pestov, *Properties of Liquid Crystalline Materials* (SPb.: University of Technology, Moscow, 2005), p. 296 (in Russian)
6. M.V. Yacemseva, I.V. Novikov, N.V. Usol'tseva, The Influence of dispersed carbon nanotubes on physical properties of cholesteric mesogens. Liq. Cryst. Pract. Use **4**, 98–106, (2010) (in Russian)
7. Y. Evdokimov, Nucleic acids, liquid crystals and secrets of nanoconstruction. Sci. Life. (4), 18–24, (2005) (in Russian)
8. N.V. Usol'tseva, O.B. Okopova, V.V. Bikova, A.I. Smirnova, S.A. Pikin, *Liquid Crystals: Discotic Mesogens* (University Publishers, Ivanovo, 2004), p. 546 (in Russian)
9. Y.M. Evdokimov, M.A. Zakharov, S.G. Skuridin, Nanotechnology based on nucleic acids. Bull. Russ. Acad. Sci. **76**(2), 112–120, (2006)

Chapter 1
Structure and Properties of Liquid-Crystal Nanomaterials

Aggregative states of matters are governed by ratio of average kinetic energy of molecular heat motion and their potential energy. Intermolecular forces are short-term; they reveal itself at low distances comparable with molecular size, unlike the long-tern forces (gravitational, electromagnetic etc.). There are three aggregative states of the substance: liquid, solid and gaseous, different by various order degrees [1–3].

Solid bodies are characterized by long-range ordering. Molecular heat motion is less than interaction range, and then motion in formed material (e.g., crystal latitude) is impossible. Gases are substances in which kinetic energy is far in exceed of molecular potential energy. Thus, molecular interaction is disordered and they can be free to move for large distance and fill available space full. Aggregative state of liquids takes an intermediate position between solid and gaseous. That's why they possess properties of both solid (volume conserving, surface formation, breaking strength) and gaseous states (conforming to the shape of the vessel, shape variability). Short-range order and little difference between potential interaction energy and kinetic energy of molecular heat motion are inherent for liquids. The major properties of liquid-***fluidity***—goes with it [1, 3].

At present, a large class of organic substances formed from elongated molecules is distinguished. These substances in smelting transit to the ***mesomorphous*** state (that has properties of fluids and solid crystals) rather than to the liquid state [4–6]. Both fluidity and long-range order are typical for such liquid-crystal substances.

S. F. Ermakov and N. K. Myshkin, *Liquid-Crystal Nanomaterials*, Springer Series in Materials Science 267, https://doi.org/10.1007/978-3-319-74769-9_1

1.1 Classification and Structure of Liquid-Crystal Nanomaterials

According to rheological property liquid-crystal (LC) substances take an intermediate position between real solid crystals and isotropic liquids. They are fluid, but anisotropic. These organic compounds show a structure similar to solid and isotropic liquid states, meaning they behave in the same way as liquids, but possess properties of ordered structure [7–12]. Such structure of LC-substances is defined by order parameter D. It describes an averaged molecular orientation to the normal unit vector $\vec{n}$ called "director", that aligns with the primary direction of major LC-compounds molecule axes. As a result, director assumes the most probable direction of molecular orientation in LC-nanomaterial.

For quantification of the averaged LC-substances molecular orientation the order parameter D is used [13, 14], defined by the relation (1.1):

$$D = 1/2(3\cos 2\theta - 1), \tag{1.1}$$

where θ is the angle between the position of the director $\vec{n}$ and the immediate direction of the long axis of the molecules.

Reference to (1.1) shows that the parameter D can take the value from 0 to 1. Herewith, D depends of temperature. The higher the value of the temperature of the transition LC-compounds to isotropic liquid, the higher ordering degree at room temperature. $D = 1$ is according to full orientation order in LC, in other words the direction of major LC-compounds molecule axes align with a director orientation $\vec{n}$. Conversely, $D = 0$ indicates full orientation disorder, i.e. LC has already transited to isotropic liquid.

There are two chief classes of LC-substances.

Liotropic liquid crystals are the first class. They take an intermediate position between solids and dilute homogeneous solution. They form liquid crystal phases in a certain concentration range. They can be found in binary and multicomponent systems of solvent compounds [6, 7, 15]. Liotropic liquid crystals occurs widely in nature. Among these are lipids—the large class of organic compounds including neutral lipids, phospholipids, glycolipids, terpenoids etc. Simple lipids are esters of fatty acids and various alcohols. Cholesterol (Fig. 1.1) and fatty acids form esters taking place in living systems and having LC properties within a strictly certain range of concentrations and temperatures.

As a rule, liotropic LC-substances are generated by the interaction between amphiphilic molecules (having both hydrophilous and hydrophobic groups) and solvent (e.g. water). Among them are phosphatidylcholine (lecithin) and phosphatidylethanolamine (cephalin).

Shown on Fig. 1.2 is structural formula of one of them. When dissolving these compounds in polar solvent (water etc.), they form micellar solutions [6, 7, 15], having outward polar heads interacting with water molecules and inward hydrocarbon tails contacting with each other (Fig. 1.3b). Conversely, in case of nonpolar

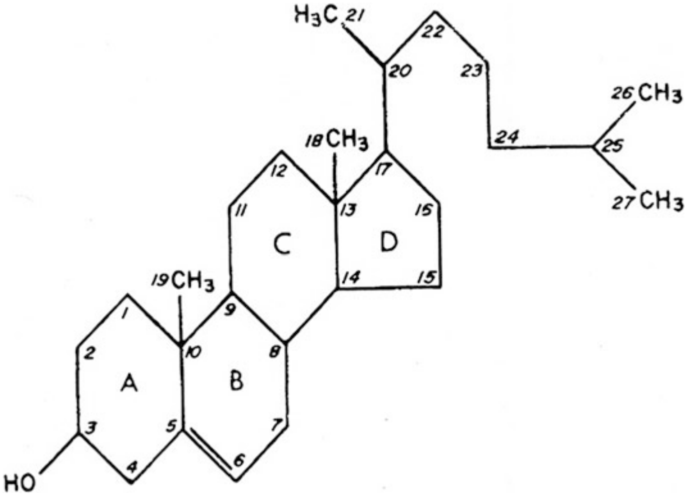

Fig. 1.1 Chemical structure of cholesterol

Fig. 1.2 Model of a molecule of phospholipid—lecithin

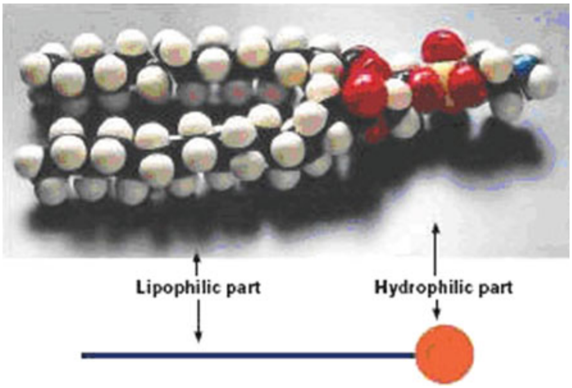

liquids (benzol etc.) hydrocarbon tails turn outward and contact with nonpolar solvent just as polar heads face each other inside micelles (Fig. 1.3c).

Eventually, the more complex system matching properties of two ordered structure of such amphiphilic molecules could be formed (Fig. 1.3d). That is peculiar to complex biosystems. It should be noted that phospholipids are able to form real solvents at very low concentrations. Thus, micelles is a structural unit with right spatial arrangement of amphiphilic molecules, which possess anisotropic properties and provide liquid-crystal state according to their concentration in liotropic LC-substances.

The second class called ***thermotropic liquid crystal*** goes into liquid-crystal state in a certain range of temperature between solid (crystal) state and isotropic liquid. In other words, thermotropic liquid crystals are connections, which transit to the

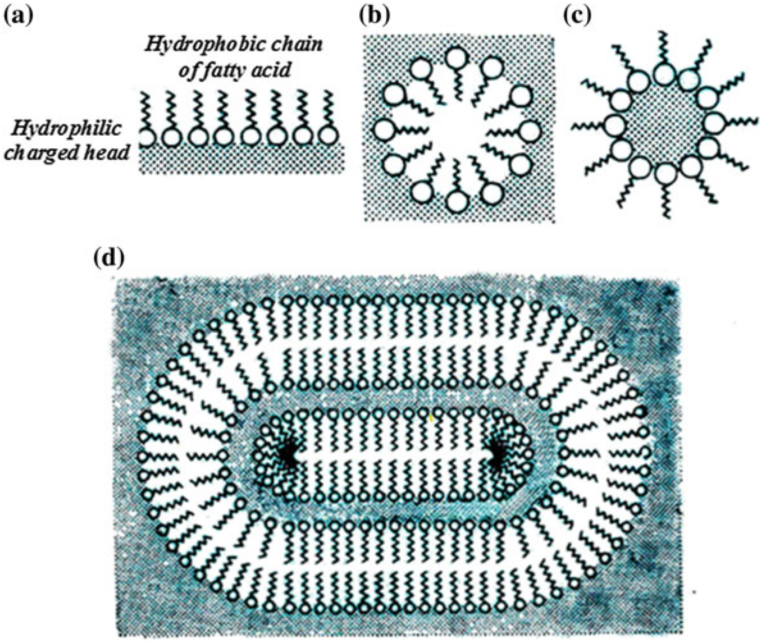

Fig. 1.3 Various phospholipid molecular arrangement [15] (circle—hydrophilic head; zigzag—hydrophobic chain of fatty acid): **a** monolayer on polar liquid, e.g. water; **b** phospholipid micelle in polar liquid (with outward charged phosphates); **c** phospholipid micelle in non-polar liquid, e.g. benzole (with outward charged phosphates); **d** (**b**–**c**) combination

mesomorphic state with increasing temperature. The temperature of the transition the solid in the liquid-crystal state is called the temperature of ***temperature of melting*** $\boldsymbol{T_m}$. The temperature of transition from liquid-crystal state to isotropic liquid state is called is the ***temperature of the enlightenment*** $\boldsymbol{T_e}$. The term is due to the fact that many of the substances in the liquid-crystal state being turbid liquids, scatter light. In other words, the substances becomes transparent in the transition in the isotropic liquid.

The dominant role in discovery of liquid-crystal state of substances belongs to Austrian botanist Reinitzer and German physicist Leman [16–19]. They observed and interrogated unusual behavior of cholesterol (cholesterolbenzoate) ester on heating. The compound had two melting points turning from solid crystal into turbid ($\boldsymbol{T_m}$) and then into transparent liquid ($\boldsymbol{T_e}$) (Fig. 1.4).

Numerous investigations arrived Leman to a conclusion that some organic compounds have intermediate phase. He proposed the term “liquid crystal” to distinguish above-described phase state from the others (crystalline, liquid and gaseous states). However, it took two decades to recognize his invention.

French physicist Fridel first classified such group of substances affirming the existence of the fourth phase state. The term “***mesomorphous*** (i.e. intermeadiate) ***state***”, suggested by Fridel, is still in use as synonym of “liquid crystal”. At present

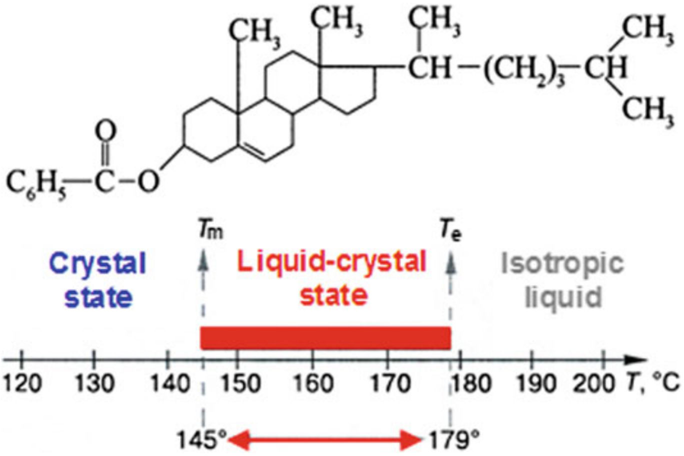

Fig. 1.4 Phase-transition points of cholesteryl benzoate liquid-crystal compound [17]

the term "liquid crystal" in common usage for designation of chemical agent which can form mesophase within certain temperature range. Such substance is said to be ***mesogenic***.

Thermotropic liquid-crystal nanomaterials by the pattern of molecular arrangement are divided into four kinds of LC-compounds: ***nematics, smectics, discotics and cholesterics*** (Fig. 1.5). Variously shaped molecules form all of these LC-substances. The most typical examples of chemical compounds which structure depends on the molecular shape are listed in the Table 1.1 [17].

Molecules in ***nematics*** align parallel and can move in three ways and roll around an axis (Fig. 1.5c). As a rule these compound consist of asymmetric scapiform molecules. That's why this molecules are called "***calamitics***" (*calamic* from the Greek word is meaning cane) [6, 17, 20] (Table 1.1). As cholesterics also fall into calamitics, significant period of study of liquid-crystal structures associates with calamitic types of molecules. Long-range order are not typical for nematics (Fig. 1.5c). The director $\vec{n}$ major axis orientation is random.

Smectics are more ordered LC-nanomaterials (Fig. 1.5d). Molecules are oriented to layer by different ways. By seven subgroups of smectic structures are known (smectics A, B, C etc.). The ***structured*** and ***non-structured*** smectic liquid crystals there are. In the structured smectic liquid crystals is provided long-range order of the molecules in the layers and is formed a two-dimensional lattice.

The layered molecular arrangement of ***discotics*** there are. The molecules of discotics represent the cyclical forms which are located on the flat discs (Fig. 1.5d). In discotics there are many molecular layers with a hexagonal packing (Table 1.1).

Strap-shaped mesogen **sanidics** (from the Greek word *sanidis* meaning strap [17]) are frequently found in nature along with discotic LC-compounds (Table 1.1). The mutual slip of layers incline to all types of LC-compounds as distinct from solid crystals.

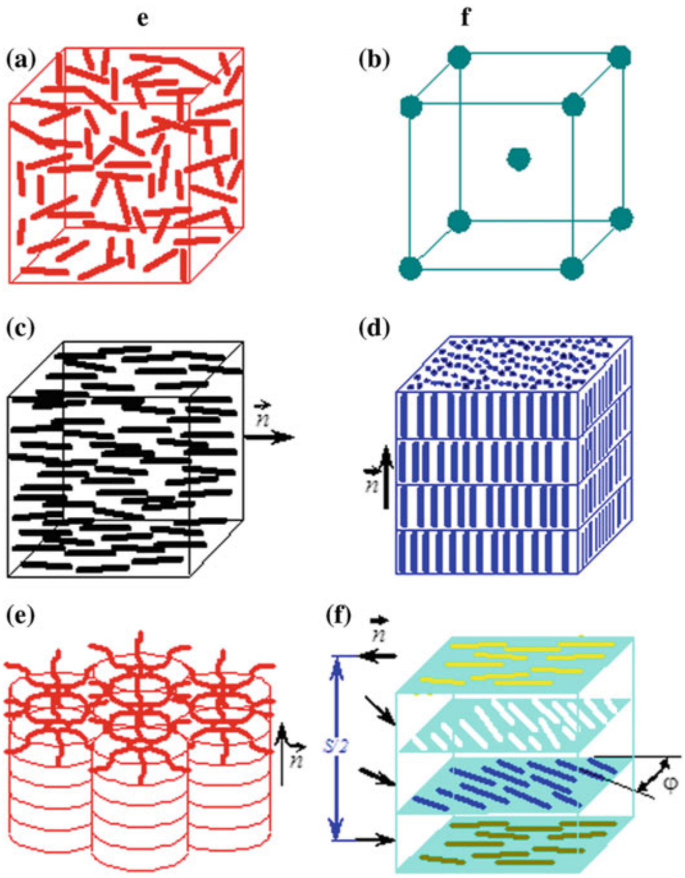

Fig. 1.5 Molecular arrangement: **a** liquid; **b** crystal; **c** nematic liquid crystal; **d** smectic liquid crystal (type A); **e** discotic liquid crystal; **f** cholesteric liquid crystal (S/2 minimal thickness of liquid-crystal layer or film)

As noted earlier, cholesterics and nematic-cholesterics belong to calamitics (Fig. 1.5, Table 1.1). Their structure is more complex than structure of pure nematic liquid-crystal compounds. Cholesterics were first discovered among cholesterol esters. Later it is found that a number of optically active organics and its compounds can be structured similary. Such substances are named ***chiral nematic liquid crystals***.

Thus, an asymmetrical shape of molecules providing anisotropic properties in the mesomorphous state and ordered parallel arrangement along major (calamitics and sanidics) or minor (discotics) axes is a distinctive feature of liquid-crystal compounds [17].

Table 1.1 Typical examples of chemical compounds forming liquid-crystal phase from molecules with various forms

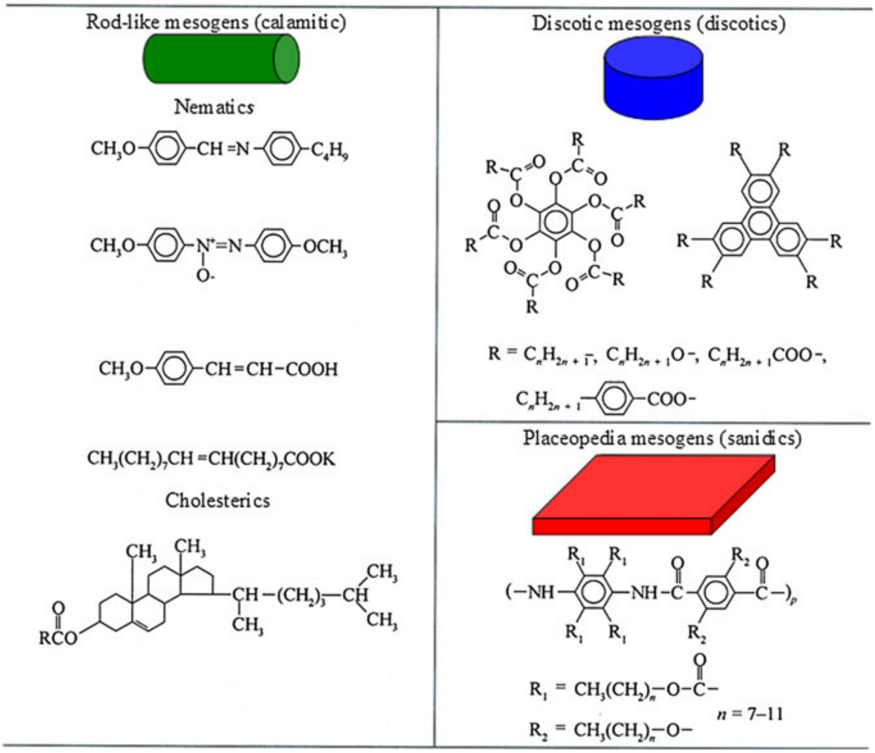

Rod-like mesogens (calamitic)

Nematics

$CH_3(CH_2)_7CH=CH(CH_2)_7COOK$

Cholesterics

Discotic mesogens (discotics)

$R = C_nH_{2n+1}$–, $C_nH_{2n+1}O$–, $C_nH_{2n+1}COO$–,

Placeopedia mesogens (sanidics)

$R_1 = CH_3(CH_2)_n{-}O{-}\overset{O}{\overset{\|}{C}}{-}$

$R_2 = CH_3(CH_2)_n{-}O{-}$

$n = 7{-}11$

1.2 Mesomorphous and Optical Properties of Cholesteric Liquid-Crystal Nanomaterials

Cholesteric LC-nanomaterials demonstrate layer-by-layer organization in addition to orientation order of molecules (Fig. 1.5, *f*). LC-substances contains the twisted structure of molecular layers for nematics. The director lies in the layer plane. In result motion from one molecular layer to another, the director rotates by an angle (about 0.4°–0.6°). Thus as director moves along a spiral (Fig. 1.5, *f*). The step of the spiral S is

$$S = \frac{2 \cdot \pi}{\alpha} d, \tag{1.2}$$

where α is angle of the director when you move from layer to layer; d is the thickness of the one layer of the cholesteric liquid-crystal nanomaterial. Taking twist angle of spiral cholesteric LC-nanomaterial α is 0.4°–0.6° and diameter of molecules $d = 0.6$ nm we identify that the step S of the cholesteric spiral equals 300–600 nm. When rotated at angles 0°, 180° and 360° to the major axes of liquid crystal molecules have the same orientation.

The molecular orientation in cholesteric liquid-crystal nanomaterials is repeated through a period $S/2$. The molecules can move freely from one to another layer but their spiral structure remains unchanged.

Such cholesteric structure can be easy found by optical properties [5]. When observed under the polarizing microscope, the image of thin layer of cholesteric LC-nanomaterial changes depending on orientation of the cholesteric axis (Fig. 1.6). If it is parallel to microglass (a), the light and dark lines alternate between crossed polaroids (a′); if it is perpendicular (b), thick darkness is seen through the eyepiece (b′).

Formation of such alternate layers can be also observed at planar arrangement of molecules between microglasses in a wedge-shaped specimen [18, 19]. In that case the undistorted spiral structure can exist where the thickness of LC-nanomaterial specimen is multiple of the half of the spiral half-lead (Fig. 1.7a). The spiral deforms on the adjacent sectors by around a quarter lead. Then the lead of the spiral step up to half-period. As a result special lines—linear disclinations—appear as optical discontinuity at a distance equal to $S/2$ (Fig. 1.7b). These linear disclinations are evident in wedge-shaped specimen of cholesteric LC-nanomaterials and named Cano-Grandjean lines.

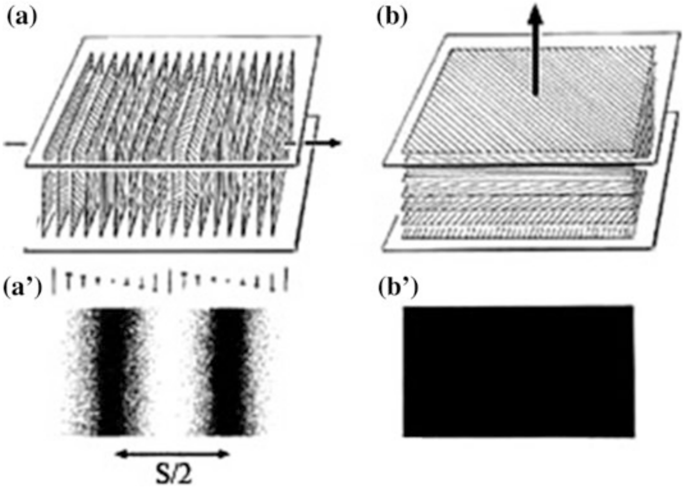

Fig. 1.6 Optical properties of cholesteric structure: **a** cholesteric axis is parallel to microglasses; **b** cholesteric axis is perpendicular to microglasses [5]

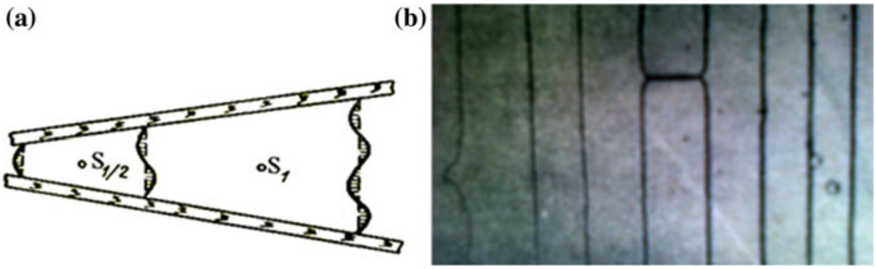

Fig. 1.7 Wedge-shaped specimen of cholesteric LC-nanomaterial between microglasses: **a** cholesteric spiral arrangtment in the wedge-shaped specimen; **b** micrograph of linear disclinations in the wedge-shaped specimen (Cano-Grandjean lines) [19]

Right and left Cano-Grandjean lines [18] can be formed when cholesterics with planar molecular arrangement are between spherical lens and flat glass surface. Wherein the right and left spirals are opposite in sign of rotation, that enables to determine the sign of rotation of the cholesteric planar texture. This method can be used for measurement of a lead and sign of spiral packing of cholesteric liquid-crystal nanomaterials. It is evident that the distance between spirals changes when Cano-Grandjean lines opposite in sign are mixed.

The leap of the spiral may vary over a wide range—from a few tens of angstroms to few micrometres. If the lead S of the cholesteric spiral has the same order of visible light wavelength λ_0, Bragg light diffraction scattering occurs due to periodicity of the structure. In that case, the cholesterics get a certain color. So the lead of the spiral is often measured by selective scattered light wavelength: $\lambda_0 = Sn$ (n—refraction coefficient) or by the inverse the lead of the spiral $\lambda_0^{-1} = (Sn)^{-1}$. The studies show that the inverse the spiral lead λ_0^{-1} is practically a linear function of concentration of given components (Fig. 1.8) [18, 21].

Nonlinearity is observed just when the concentration is similar to the original one. At mixing of the right and left cholesterics, λ_0^{-1} crosses the zero-axis. It is mean that cholesterics compensate each other and become nematics at certain concentrations. Similar trends are also valid for pure nematic and cholesteric mixtures. It is established that mixtures of nematics and cholesterics with a left spiral remain left at any concentration.

At the same time, mixtures of nematics and cholesterics with the right spiral do not follow this pattern. They remain right at high concentrations. The lead of the spiral gradually increases at cholesteric concentration drop and pure nematic phase is formed at certain concentration (about 40–50 mol.%). Then nematic phase turn into cholesteric with a left spiral at further increasing the nematic concentration. Therefore, nematics in mixtures with cholesterics act as if they had a left spiral.

According [18] it is explained as follows:

A steroid nucleus of cholesteric molecule is right. At the same time, the lateral carbon chain of the same fatty acid radical reduces a right twist value. The linear

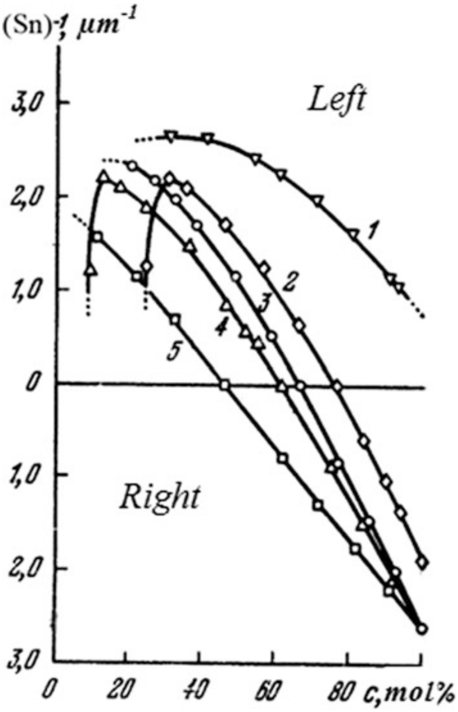

Fig. 1.8 Dependence of the inverse the spiral lead on cholesterylformiate, cholesterylbromide и cholesterylchloride molarity for binary mixtures: *1*—cholesteryllaurate-cholesterylformiate (40 °C); *2*—cholesteryllaurate-cholesterylbromide (50 °C); *3*—cholesteryllaurate-cholesterylchloride (60 °C); *4*—cholesterylpelargonate-cholesterylchloride (60 °C); *5*—cholesterylpropionate-cholesterylchloride (60 °C) [18, 21]

crossing the zero-axis dependence of the inverse the spiral lead on the length d of lateral carbon chain are observed in the wide range of chemical compounds peculiar to the right and left cholesterics (Fig. 1.9) [18].

If length of the lateral carbon chain is less than 2.08 Å, the molecule as a whole is right; otherwise it is left. It should be noted that cholesterol has $d = 0$, i.e. it forms the right spiral. Nematics in mixtures with cholesterics seek to be parallel to a steroid nucleus in each layer.

As a result, the arrangement of nematic molecules between the cholesterics leads to increase in right spiral step; and the more nematic concentration in the binary mixture, the more the step is.

Complex of molecular and quasi-nematic layers within a half-step of the spiral $S/2$ are considered as ***monocrystal films*** of cholesteric liquid-crystal materials. Such films can arise, for example, at frictional interaction of various solids at high pressure between friction surfaces [4, 22]. However, much more monocrystal layers of cholesterics are formed between bearing surfaces (Fig. 1.10).

This condition causes unique optical properties of the cholesteric LC-nanomaterials. They are able to reflect selectively incident light like a diffraction lattice due to regular twist structure.

When reflected light wavelength λ is comparable to the spiral lead S of cholesteric LC-nanomaterial, its film changes to the same color.

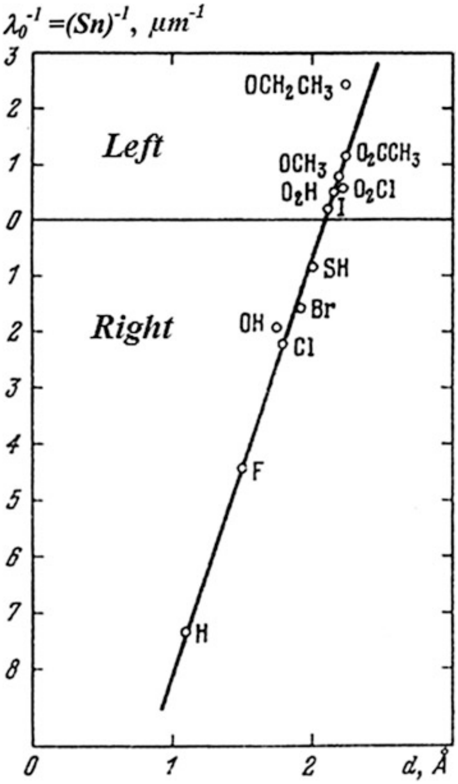

Fig. 1.9 Behavior of inverse selective reflection wavelengths for right and left cholesterics depending on the length of lateral carbon chain [18]

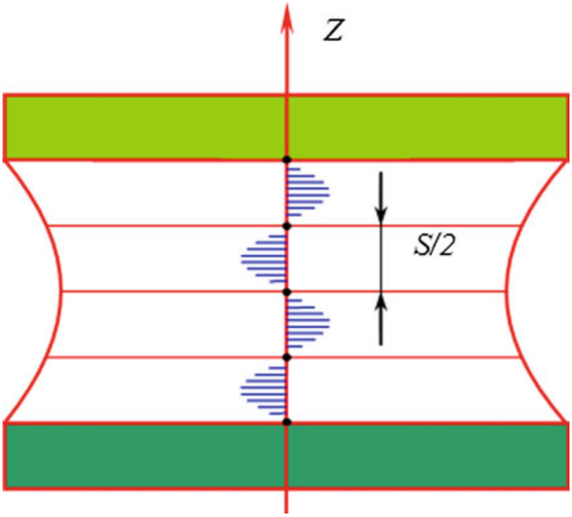

Fig. 1.10 Formation of cholesteric LC-nanomaterial monocrystal layers between bearing surfaces

The lead of the spiral of a number of cholesteric LC-nanomaterials decreases in the mesomorphous state with a rise in temperature. As the lead S of spiral molecular packings of a cholesteric in a mesophase is sensitive to changes in temperature, the selective reflection wavelength λ and color of film can vary over a wide range. It is illustrated with cholesteryl pelargonate and cholesteryl caprinate in Fig. 1.11 [17, 18]. It is shown that the selective reflection wavelength λ exponentially decays at increase in temperature, i.e. there is a transition from red spectrum area to the blue.

LC-nanomaterials with such properties are in widespread use of national economy. In particular, color-temperature ratio makes it possible to determine the temperature distribution on the studied surface of certain chemical cholesteric compound by its color [23].

Shown on Fig. 1.12 are standard dependences of various cholesterics. Depending on the type of color-temperature ratio cholesterics can be divided into monochrome (selective reflection wavelength varies insignificantly with elevating temperature; and cholesterics are the same color) and enantiochrome (selective reflection wavelength varies over a broad range).

Such character of color-temperature ratio is valid for both individual cholesteric LC-nanomaterials and its mixtures. Unexpected changes of color and temperature depending on component concentration can be observed in response to mixing of cholesterics.

It is illustrated by the example of temperature dependence of selective reflection wavelength in binary cholesteryl chloride and cholesteryl pelargonate mixtures

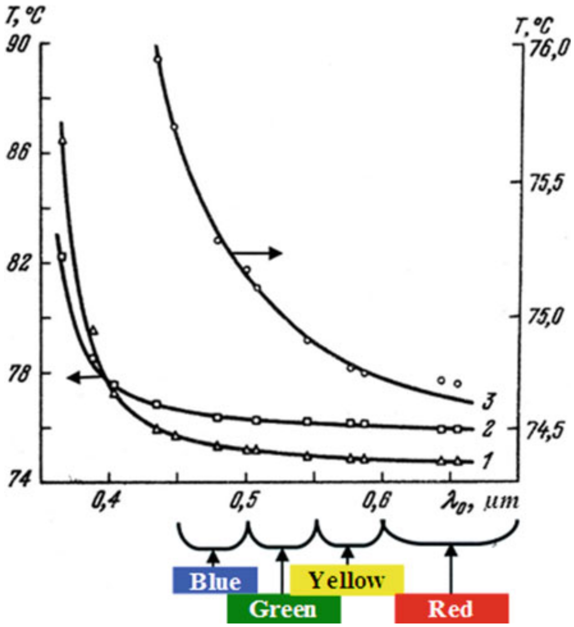

Fig. 1.11 Dependence of the selective reflection wavelength λ_0 on temperature T for cholesterylpelargonate (*1*, *3*) and cholesterylcaprinate (*2*) [17, 18]

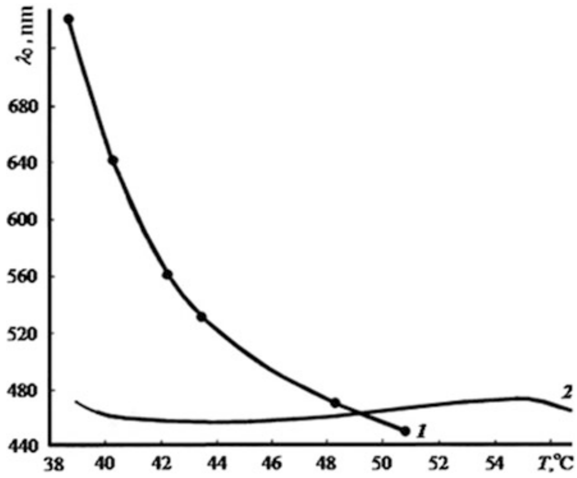

Fig. 1.12 Color and temperature characteristics of cholesteric LC-nanomaterials: *1*—enantiochrome; *2*—monochrome

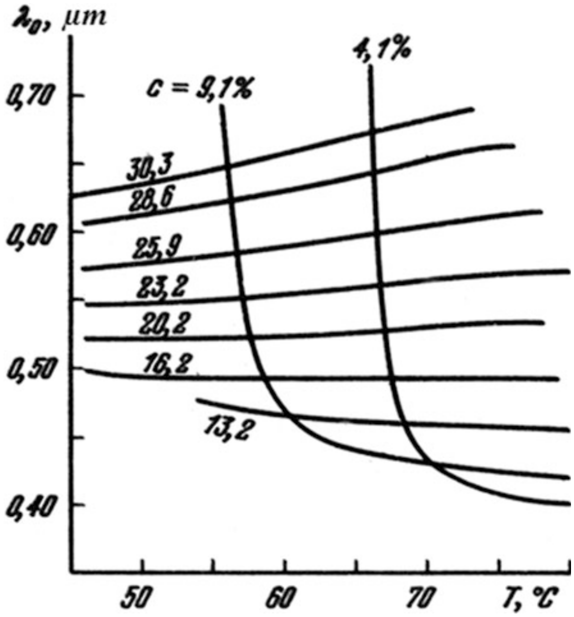

Fig. 1.13 Temperature dependences of selective reflection wavelength in cholesterylchloride-cholesterylpelargonate mixtures (*C*—weight concentration of cholesterylchloride) [18]

(Fig. 1.13). Individually they behave like enantiochrome cholesterics [18]. Nevertheless, they possess properties of both enantiochrome and monochrome cholesterics according to component concentration.

Chromatic and temperature characteristics of mixture with minor cholesteryl chloride are similar to cholesteryl pelargonate. However, with elevating cholesteryl chloride concentration C, compensations of spiral structures start affecting. So at $C = 16.2$ и 23.2%wt. cholesteryl chloride in the mixture a selective reflection wavelength hardly depends on temperature *T*, i.e. mixtures of these cholesterics turn pure monochrome in fact. Then, selective reflection wavelength rises with elevating temperature at increased cholesteryl chloride concentration in mixture.

Enantiochrome cholesteric LC-nanomaterials possess reversible properties, i.e. they recolour at temperature increase and decrease without any hysteresis phenomena. Selective light reflection temperatures (t_1 и t_2) and temperature range of cholesteric mesophase (Δt) are their operational characteristics. Values of t_1 и t_2 show what kind of problem can be solved with given cholesteric LC-compounds, Δt characterizes the cholesteric sensitivity.

Color-temperature ration is not typical for monochrome liquid-crystal cholesterol compounds. However, color disappears at elucidation temperature and does not appear during temperature decrease. i.e. they have the thermal storage effect. Selective reflective light wavelength λ_0 qualificative a cholesteric color under the certain conditions and elucidation temperature T_e are the mail variables of monochrome liquid-crystal cholesterol compounds.

In turn, thermotropic LC-compounds are divided into ***enantiothropic***, forming a mesomorphous state both at heating and on cooling the substance, and ***monothropic*** forming a mesomorphous state only on cooling the isotropic liquid. It should be noted that as homologon number C_n increases (Table 1.2), mesomorphous properties of cholesteric LC-nanomaterials vary in cholesterol n-alkane family as follows: monothropic cholesterics (C_1–C_2)—enantiothropic cholesterics (C_3–C_6)—enantiothropic cholesterics available for monothropic smecic forming (C_7 and further).

These experimental data have shown that most of LC-compounds passes a number of mesophase change during temperature variations although several of them have just one mesophase. Such behavior is called polymesomorphism of LC-nanomaterials.

During transition from solid crystal through various mesophases to isotropic liquid the succession of mesophases with decreasing the order strength is observed, namely smectic, cholesteric and nematic. It is also valid for smectic mesophase. In smelting of solid crystal at first smectics with structural layers are formed, then at higher temperature smectics with structureless layers are.

Evaluation of experimental data from the Table 1.2, Figs. 1.11, 1.12 and 1.13 has shown that if color of plane texture varies during change of temperature, a selective reflection wavelength increases with drop of temperature.

It should be noted that the above colors of diffuse plane texture are observed only on cooling of the test liquid-crystal specimens. Nevertheless, chromatic and temperature characteristics of cholesteric binary mixtures are typically found in temperature range between the phase transitions temperatures of primary components [18, 23].

So, ester homologs of cholesterol and aliphatic monocarboxylic acids can be used as a matter of actual practice, e.g. as a component of cholesteric LC-nanomaterials for creation of temperature indicator. At the same time, field-proven low-temperature liquid-crystal complexes are satisfactory for using as other component. For example *t*1 = 20 °C for temperature indicator (ТУ-6-09-06-1065-82).

Table 1.2 Phase change temperatures and colors of selective reflection of cholesterol n-alkanes plane textures

Number of carbon atoms (C_n) in the lateral chain of radical	n-alkanes of cholesterol[a]	Chemical formula	Phase change temperature, °C			Colors of plate texture observed by reflected light on cooling to crystalline phase or smectic mesophase
			Smectic mesophase	Cholesteric mesophase	Isotropic liquid	
C_1	Formiate	$C_{28}H_{46}O_2$		(60.5)	97.5	Colorless or subtle red (crystallization)
C_2	Acetate	$C_{29}H_{48}O_2$		(94.5)	116.5	Green–yellow–red (crystallization)
C_3	Propionate	$C_{30}H_{50}O_2$		102	116	Violet–blue–green–yellow–orange (crystallization)
C_4	Butyrate	$C_{31}H_{52}O_2$		102	112	Violet–light–violet (crystallization)
C_5	Valerate	$C_{32}H_{54}O_2$		93	101.5	
C_6	Capronate	$C_{33}H_{56}O_2$		99.5	101.5	Violet–blue–and–green (crystallization)
C_7	Enanthate	$C_{34}H_{58}O_2$	(92.5)	(95.5)	114	Violet (crystallization)
C_8	Caprylate	$C_{35}H_{60}O_2$	(69.5)	(96.5)	110	Violet–(blue–green–yellow–orange–red). Colors within the brackets refer to narrow versicolor spectrum and antecede the smectic mesophase
C_9	Pelargonate	$C_{36}H_{62}O_2$	(77.5)	80.5	92	
C_{10}	Caprynate	$C_{37}H_{64}O_2$	(81.5)	85.5	92.5	
C_{11}	Undecylate	$C_{38}H_{66}O_2$	(81.9)	(90)	92.5	
C_{12}	Laurate	$C_{39}H_{68}O_2$	(83.5)	(90)	93	Subtle violet (smectic mesophase)
C_{13}	Tridecylate	$C_{40}H_{70}O_2$	63.5	78.8	84.8	
C_{14}	Myristate	$C_{41}H_{72}O_2$	71	81	86.5	
C_{15}	Petadecylate	$C_{42}H_{74}O_2$	70	78.3	83	
C_{16}	Palmitate	$C_{43}H_{76}O_2$	(78.5)	79	83	

[a] Chemical formula of cholesterol—$C_{27}H_{46}O$

Use of cholesteric LC-nanomaterials with such properties makes it possible to get cholesteric LC-nanomaterials with the lead of the spiral measurable in the visible region and scaleable over a wide range of phase transition temperature including isotropic transition temperature [24].

Decrease the isotropic transition temperature or elucidation temperature during lateral carbon chain elongation (Table 1.2) is typical for cholesteric LC-nanomaterials. According to [25] it is explained as follows.

Thermodynamic mean endpoint distance of cholesteric molecular lateral chains is always less than their geometrical length owing to thermal fluctuation of side-chain conformation. It reduces molecular anisotropy in general and the anisotropic interaction causes orientation order. As a result, a thermal motion effect becomes more and more essential at increase in molecular length. Therefore, the isotropic transition temperature decreases during elongation of the lateral carbon chain of fatty acid radical. Exemption is possible if only elongation of the lateral carbon chain affects molecular elongation in whole, i.e. lead to anisotropy raise. It is valid at the beginning of homologous series and for cholesterylformiate e.g. Table (1.2).

Thus, owing to the given optical properties, the cholesteric LC-nanomaterials can be applied in science and engineering, especially, for nondestructive testing methods.

1.3 Physical Anisotropy and Application of Cholesteric Liquid-Crystal Nanomaterials

It is known that liquid-crystal materials, as well as solids, possess ***anisotropy of properties***, which are intimately associated with molecular shape, and structure anisotropy. LC-substances are generally formed from organic compounds with elongate cigar-shaped molecules, i.e. possess evident molecular shape anisotropy. Prolate molecular form due to free energy minimum principle causes mutual arrangement of molecules in the mesophase. Orientation order in the mesophase state is the main LC-nanomaterials structural member. It takes place in consequence of molecular irregular shape and structural organization of LC-compounds. It is obvious that such orientation order causes physical anisotropy of LC-nanomaterials.

For example, the anisotropic molecular forms of nematics and cholesterics give place to ***double refraction***. This confirms the anisotropy of dielectric permittivity (ε) and anisotropy of the refractive index (n) of LC-nanomaterials. The dielectric anisotropy of the liquid-crystal substance is called of difference ($\Delta\varepsilon$). Double refraction (Δn) and dielectric anisotropy ($\Delta\varepsilon$) are result from anisotropy of liquid crystal molecules, their structure and properties. It should be noted that the dielectric anisotropy can be both positive and negative.

LC-nanomaterial temperature increase reduces the orientation order and leads to Δn и $\Delta\varepsilon$ monotonic decrease. Herewith anisotropy of properties vanishes in the anisotropic transition point.

Liquid-crystal nanomaterials also possess the anisotropy of magnetic properties. In result are provides the possibility of the orientation of liquid crystal molecules of under external effects of magnetic and electric fields. The sign of the dielectric and diamagnetic anisotropies respectively govern the direction of major axes of liquid crystal molecules in these fields. The major axes of molecules are parallel to the field direction if the anisotropy is positive, and, on the contrary, the orientation is perpendicular, if the anisotropy is negative.

A most of works on electrooptics deals with research of nematic LC-compounds with various molecular orientation in an electrooptics cell (Fig. 1.14) [17–19, 26].

At planar molecular orientation and $\Delta\varepsilon > 0$ liquid-crystal film specifies by double refraction Δn (Fig. 1.14b). As vector of enclose electric field is directed against the elastic force of interaction between nematic and electrode surface, nematic molecule bending deformation occurs under strength between electrodes. Under certain strength director reorients normally to electrodes, then double refraction vanishes (Fig. 1.15). The effect of changes in the nematic orientation in electric field is called the transition of Frideriks.

In case the nematic molecules characterized by homeotropic orientation (the molecules are perpendicular to the surfaces of electrodes, Fig. 1.14c) and at $\Delta\varepsilon < 0$, an original LC-film does not possess double refraction. At imposition of electric field a liquid crystal undergo buckling deformation due to $\Delta\varepsilon < 0$, molecules reorient parallel to electrode surface and nematic LC-film turns doubly refractive.

In helically-coiled molecules of LC-compounds (Fig. 1.14d) molecules in adjacent zone possess planar orientation, the major axes of top electrode are in the picture plane, they of bottom electrode are oriented perpendicular to the plane. Such orientation is reached by special surface treatment, for example, diversely

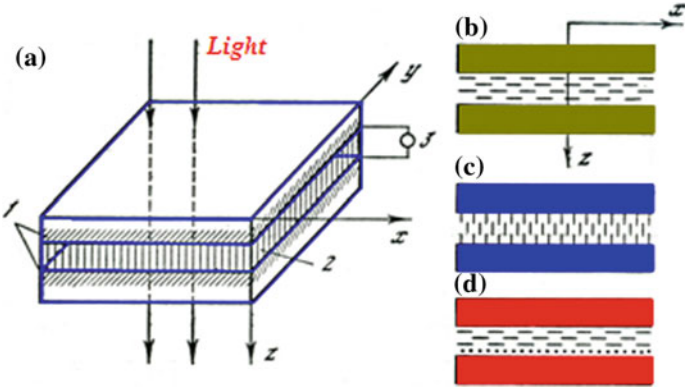

Fig. 1.14 Electrooptics cell (**a**) and various molecular orientation between electrodes; **b** planar; **c** homeotropic; **d** twisted [26]

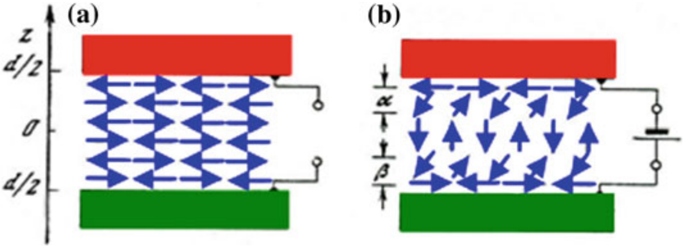

Fig. 1.15 Frideriks effect in nematic LC-nanomaterials: **a** original molecular orientation; **b** orientation under strength over threshold [26]

cover-glass rubbing (of top and bottom electrodes respectively) or with special substances providing the given molecular orientation.

Liquid-crystal nanomaterials can effect on orientation molecules of dissolved substances parallel to director in electric field. This effect is called the effect of "guest-host".

It should be noted that electrooptical effects in LC-nanomaterials determined not only by dipole spatial arrangement relatively to major molecular axis and conductivity. If molecules have the non-rodlike shape a polar order (electromechanical effect) can take place at imposition of electric field. Such deformation leads to electrode charge, and, on the contrary, the electric field focusing dipoles promotes emergence of nematic crystal deformation.

The anisometric structure of liquid crystal molecules influences their rheological behavior. In most cases the viscosity rises. Jump-like viscosity rise is sometimes observed in mesomorphous state at temperature elevation. Such behavior of LC-substance can be explained as follows.

Liquid crystal viscosity depends on director orientation relatively to flow direction. Nematic magnetic field orientation perpendicularly to the capillar axis leads to flow time increment (due to molecular buckling deformation) and viscosity growth. If magnetic field aligns with the capillar axis, flow time decreases. It proves ***the anisotropy of liquid-crystal viscosity***. As molecules align with flow direction, the coefficient of viscosity is less. Anisotropy of LC-nanomaterial viscosity occurs only at low flow rate. Otherwise orientation effect of magnetic and electric fields is significant, so as orientation in LC-nanostructure flow has an impact.

Such jump-like viscosity rise of cholesterics at transition to mesophase is characterized by a few orders. For example the viscosity of cholesteryl acetate is growing by approximately six orders of magnitude at the point of enlightenment. At the same time, the measurement of the viscosity of other cholesteric LC-nanomaterials has not shown so large rise of viscosity within that temperature range.

It should be noted that isotropic fluid for all types of liquid crystals behaves as the Newtonian fluid.

It is of importance that the spiral step and selective refraction wavelength of cholesteric plate textures and their mixtures are sensitive not only to thermal, but to other external factors. As it is known, temperature, electric and magnetic fields as well as chemical composition of environment, various radiations, shear deformation and others are refer to such factors. The dependence of spiral structure and selective refraction wavelength of cholesteric plate textures and their mixtures on various factors become common use in science and technology, especially in diagnostic and nondestructive testing methods.

Effective microwave holography imagining method has been developed by now: the thin coat of selected cholesteric LC-nanomaterials, smeared on studied surface, discolor with microwave radiation intensity variation [27].

Use of cholesteric LC-nanomaterial with ultrasonic is also actual application field. Viscoelastic layer absorbs ultrasonic radiation passing the specimen and turns it into thermal emission, affecting liquid-crystal layers. Ability of ultrasonic waves to pass though solid opaque layers enables to get an image of structural changes and defects.

Such methods are also used within other frequency ranges. Special films with a base absorbing infrared radiation and coated by liquid-crystal layer acting on infrared radiation are used to turn infrared radiation into visible.

Cholesteric LC-nanomaterial become widely used not only in engineering, but also in medicine, say for inflammatory process diagnostics. In that case, LC-nanomaterial cover open skin areas; then occurrence and pattern of inflamed areas are determined from the temperature pattern. They are commonly used along with nematic LC-nanomaterials in electrooptic displays and light modulators.

Consequently, study of temperature and other structurally sensitive parameters, as well as behavior of LC-nanostructures in different conditions and on various surfaces allows making an evidence-based choice the LC-nanomaterials and mixtures for comprehensive use in science and engineering. Ordering LC-nanostructures can be in use of tribophysics and arthrology, especially for reduction of friction, increase wear resistance and load capacity of various friction surfaces including human and animal joints.

Such experimental data on unique behavior of cholesteric LC-nanomaterials at frictional interaction of technical and biological objects are discussed in the following chapters of the monograph.

References

1. A.M. Prokhorov (ed.), *Physical Encyclopedic Dictionary* (Great Russian Encyclopedia, Moscow, 1995), p. 944 (in Russian)
2. A.G. Gurevich, *Solid State Physics. Textbook for Universities.* (SPb.: Nevsky Dialect, BHV–Petersburg, 2004), p. 320
3. V.A. Goldade, L.S. Pinchuk, *Condensed Matter Physics* (Nauka, Minsk, Belarus, 2009), p. 657
4. S.F. Ermakov, V.G. Rodnenkov, E.D. Beloenko, B.I. Kupchinov, *Liquid Crystals in Engineering and Medicine* (Asar, Moscow, CheRo, Minsk, 2002), p. 412 (in Russian)
5. S. Ermakov, A. Beletskii, O. Eismont, V. Nikolaev, *Liquid Crystals in Biotribology* (Springer, 2016), p. 212

6. N.V. Usol'tseva, O.B. Okopova, V.V. Bikova, A.I. Smirnova, S.A. Pikin, *Liquid Crystals: Discotic Mesogens* (University Publishers, Ivanovo, 2004), p. 546 (in Russian)
7. A.S. Sonin, N.A. Churochkina, A.V. Golovanov, Composite with lyotropic liquid crystals. Liq. Cryst. Pract. Use. **2**(28), 89–91 (2009) (in Russian)
8. G.E. Nevskaya, M.G. Tomilin, V.G. Chigrinov, Achievements in liquid crystals orientation. Liq. Cryst. Pract. Use. **1**(27), 5–23, (2009) (in Russian)
9. A.A. Sonin, *The Surface Physics of Liquid Crystals* (Gordon and Breach Publishers, Amsterdam, 1995), p. 192
10. N.A. Plate, V.P. Shibaev, *Comb-like Polymers and Liquid Crystals* (Chemistry, Moscow, 1980), p. 304 (in Russian)
11. L.M. Blinov, V.G. Chigrinov, *Electrooptic Effects in Liquid Crystal Materials. Series: Partially Ordered Systems* (Springer, Berlin, 1996), p. 296
12. S. Pestov, V. Vill, *Physical Properties of Liquid Crystals. Series: Landolt-Börnstein: Numerical Data and Functional Relationships in Science and Technology*–New Series (Springer, Berlin, 2003), p. 2805
13. V. de Gennes, *Physical Properties of Liquid Crystalline Substances* (Mir, Moscow, 1982), p. 160 (in Russian)
14. Yu.B. Americ, B.A. Krentsel, *Chemistry of Liquid Crystals and Mesomorphic Polymer Systems* (Nauka, Moscow, 1981), p. 288 (in Russian)
15. G.H. Brown, J.J. Wolken, *Liquid Crystals and Biological Structures* (Academic Press, New York, 1979), p. 316
16. A.S. Sonin, *A Way Century Long. History of Discovery and Study of Liquid Crystals* (Nauka, Moscow, 1988), p. 224 (in Russian)
17. V.P. Shibaev, Unusual crystals or mysterious liquid. Soros Educ. J. **11**, 37–46 (1996) (in Russian)
18. V.A. Belyakov, A.S. Sonin, *Optics of Cholesteric Liquid Crystals* (Nauka, Moscow, 1982), p. 360 (in Russian)
19. A.S. Sonin, *Introduction to Physics of Liquid Crystals* (Nauka, Moscow, 1983), p. 320 (in Russian)
20. S.V. Blokhina, N.V. Usol'tseva, M.V. Olkhovich, A.V. Sharapova, Influence calamitoso and discotic liquid crystals on phase state of the dendrimer polypropylenimine, in *Progress in the Study of Liquid Crystalline Materials* (Ivanovo: Ivan. State University, 2007), pp. 73–79 (in Russian)
21. G.M. Zharkova, The effect of external influences on the pitch of cholesteric spiral, in *Cholesteric Liquid Crystals (Collection of Papers)* (Novosibirsk University, Novosibirsk, 1976), pp. 56–66 (in Russian)
22. S.F. Ermakov, V.V. Mulyarchik, A.L. Bogdanov, A.P. Svirsky, The role of liquid-crystal nanomaterials in tribology. Friction Lubr. Mach. Mech. **1**, 23–30 (2011) (in Russian)
23. S.V. Shevchuk, A.P. Mahotella, V.G. Tishchenko, Thermoindicators film containing cholesteric liquid crystals, in *Cholesteric Liquid Crystals (Collection of Papers)* (Novosibirsk: Novosibirsk University, 1976), pp. 67–69 (in Russian)
24. S.F. Ermakov, R.A. Shyldikov, A.V. Mikalaynis, Tribological aspects of reversible control of the frictional interaction between solids in the presence of liquid crystals, in *Proceedings of the 6th International Symposium on Friction Products and Materials "YAROFRI-2006"*, (Yaroslavl, 2006), pp. 59–65 (in Russian)
25. L.N. Lisetskii, V.G. Tishchenko, Some problems of the theory of cholesteric liquid crystals, in *Cholesteric Liquid Crystals (Collection of Papers)*, (Novosibirsk University, Novosibirsk, 1976) pp. 14–26 (in Russian)
26. S.A. Pikin, L.M. Blinov, Liquid crystals (Nauka, Moscow, 1982), p. 208 (in Russian)
27. A.I. Dudarchyk, V.A. Semin, B.I. Gorbunov, *Control of Semiconductor Devices with Liquid Crystals* (Minsk, Science and Technology, 1983), p. 119

Chapter 2
Tribology and Lubrication of Solids

We meet friction processes quite often in everyday life. As for instance, when we move bodies relative to each other (***kinetic friction***) or try to put in motion various bodies at rest (***static friction***) [1–8]. Friction occurs when two bodies rub along external surfaces (***external friction***) or when atom or molecules inside the material move relative to each other (***internal friction***). The latter can take place in liquids, gases and solid materials. Measure of friction is resistance to friction balanced by contact force when relative motion between the two. Thermal, electric and magnetic together with mechanical phenomena are under way at friction [1, 2, 5–8].

Moreover, current practice shows that friction interaction between solid bodies can be changed over a wide range using various means and methods aimed to both decrease and decrease friction in dynamic contact area. Sometimes these processes can be reversible. It emerges especially clearly in the presence of lubricating material (LM) in contact zone. There are two ways to control friction, that are different in mechanism and activity rates of control when friction interaction of solids.

"***Passive control***" of friction coefficient is the most common and widely known method of friction control by means of change in components and chemically different addition in dynamically contacting bodies, lubricants and systems [9].

Systems of "***active control***" of coefficient of friction are also known in current practice. In that case, friction interaction can be regulated by variation of load on sliding surfaces or friction force in dynamic contact zone changing shear resistance to LM or contact surfaces of solids [9, 10]. Nature and structural properties of LM in use are proved to be of great importance in that case. Therefore, we try to enlarge upon various materials and surfaces in the presence of wide range of LM with or without additives.

S. F. Ermakov and N. K. Myshkin, *Liquid-Crystal Nanomaterials*, Springer Series in Materials Science 267, https://doi.org/10.1007/978-3-319-74769-9_2

2.1 Modern Antifriction and Antiwear Additives in Tribology (Passive Friction Control)

The more detailed classification of types of friction is presented in the Table 2.1 [6].

It is known that the presence of protective films, which prevent the seizure of solids in contact, takes on crucial importance during friction, when no hydrodynamic wedging of the surfaces by the lubricant can occur [1–7, 10–13]. In boundary friction, in addition to the physical bond of the lubricant with a metal, boundary films such as metallic soaps appear as a result of chemical reactions between the active metals (Sn, Cu, Zn, and others) with fatty acids contained in the lubricant. Secondary structures in the form of thin adhesive films—particles of graphite, sulfides, and so on—are also formed [11, 12]. The films can be repeatedly generated during friction owing to the active environment in which lubricity is realized. Temperature elevation in the contact zone reduces the lubricant viscosity and the lubricating film thickness and can result in the rupture of the boundary film [12]. However, the modern practice of using lubricants shows that the wear of the surfaces in contact does not necessarily relate to the lubricity indicator since it is often caused by other factors [14]. For this reason, when determining the lubricity, it is necessary first of all to take account of the peculiarities of the physical–chemical processes that evolve in the area of fricnion between the solids and result in integral effects, i.e., lubricity; it is also important to find the dependence of the pattern of these processes on the properties of the friction surfaces and lubricant [14–17].

In recent years, the use of lubricants of various type and origin is one of the most profitable ways to achieve a high lubricity of oils, which are necessary for friction units to operate. Oils with additives of lamellar solid lubricants play a significant role in providing the durability and operational stability of friction units within wide load and velocity ranges [11, 18–21]. Such substances include dichalcogenides of *d*-transition metals from the fourth to sixth groups of the periodic table (disulfides and diselenides of molybdenum, tungsten, etc.), in addition to the well-known graphite. They have a hexagonal lattice structure like 2H–MoS_2 [18, 20, 22]. The lubricity of such additives is caused by the characteristics of the boundary films that situated in the friction contact zone and undergo permanent changes during friction [11, 18, 20]. The fields of application of these materials is being widened and

Table 2.1 Types of friction [6]

Criterion	Types of friction		
Moving	Kinetic	Sliding, rolling and sliding-rolling friction	Boundary conditions at friction
	External	Of solid bodies	Dry, liquid, boundary
Location	Internal	In liquid or gases	Liquid and boundary friction
		In solid bodies	Plastic strain

research aimed at improving their tribological performance by modification is progressing rapidly [20, 22–25]. It is noted in some papers [22, 26, 27] that the modification of solid lubricants with structure like 2H–MoS_2 by metals and other substances which affect actively the mechanochemical processes evolving on the friction surfaces enhances greatly their tribological characteristics. For example, the authors of [26, 27] have demonstrated that the alloying of solid lubricants based on molybdenum and tungsten diselenides with gallium–indium alloy, which reduces the harmful effect of oxides, increases considerably the wear resistance of the friction surfaces lubricated by them.

With the use of lamellar solid lubricants with the structure like 2H–MoS_2, all processes accompanying friction are localized in a solid lubricant film, even though the latter is thick and the contact pressure is heavy [20]. The film thickness affects greatly the friction coefficient, whose dependence under various conditions is governed by the mode of contact deformation and can be descending, ascending, etc. There is a critical thickness of the solid lubricant film, above which the tribological characteristics become independent of the film thickness and reach the values typical for the friction of bulk materials. The thickness of solid lubricant films plays an important role in providing a high wear resistance and carrying capacity of friction units; the antifriction performance of a friction unit can be passively controlled to a marked extent by modifying the thickness of the lubricant film.

It is well known that dichalcogenides of the *d*-transition metals possess the best antifriction performance in vacuum and inert gases [11, 18, 28]. Molybdenum and tungsten disulfides, as well as niobium diselenide, are the best studied and most extensively used at present under these conditions [18]. Molybdenum disulfide retains its lubricating performance in vacuum and inert gases up to the dissociation temperature (>1000 °C). The tribological characteristics of natural molybdenum disulfide are improved by purifying it of abrasive impurities and adding various alloying elements, e.g., stibium [29, 30] and selenium [31], to it. The study of the tribological behavior of the original molybdenum disulfide when it is intercalated by different elements is of special importance. The durability of molybdenum disulfide films increases greatly if they are deposited on a solid sublayer in combination with films of other substances. For example, it is shown in [32] that the wear resistance of TiN and MoS_2 sandwich films on tool steel is much higher than that of MoS_2 films themselves. It is noted that the adhesion to the materials of the friction unit, i.e., the structural materials of the friction members, is the deciding factor which affects the durability of these tribosystems.

In the modern view of high-temperature solid lubricants applied in vacuum and air, the majority of these substances contains the most active chemical elements or metalloids such as fluorine, sulfur, oxygen, and selenium [18, 28]. The shear resistance of these substances themselves is quite low. However, wide experience of their application suggests that their basic role in friction is their liberation in active form (as atoms and ions) on real contact areas under the effect of elevated temperatures and tribological transformations. They react with the metallic surfaces to form protective films of chemically active compounds such as fluorides, sulfides, and oxides having a low shear resistance. This favors the protection of the friction surfaces against seizure and reduction of the friction coefficient [18].

Another method of passive friction control and improvement of the lubricity of oils that is in progress in recent years is to introduce additives of lamellar solid substances, which form colloidal solutions in oils and oil-soluble compounds, into the oils [19, 21, 33, 34]. Such additives are especially promising since they facilitate the formation of stable solutions [21, 33]. A peculiar feature of the effect of the oils containing such compounds is that they possess an induction period, after which they become most effective [19]. The duration of this period depends on the composition and structure of the friction modifier and on the testing conditions.

New methods of the synthesis of molybdenum trisulfide nanoparticles have been proposed. Unlike molybdenum disulfide nanoparticles, they have good solubility in oils and exhibit quite high activity as antifriction and antiwear additives [33]. The reactions of ammonium thiomolybdate with tetraalkyl ammonium halogenides containing alkyl groups of various origin have yielded substances which are precursors of the formation of molybdenum trisulfide nanoparticles. Different types of tribometers have been employed to demonstrate the antifriction and antiwear activity of both tetraalkyl ammonium derivatives of thiomolybdates and molybdenum trisulfide nanoparticles [33]. The latter have been found to be prone to tribochemical transformations resulting in the appearance of molybdenum disulfide in the friction zone. Thus, it has been shown that the behavior of oil-soluble molybdenum compounds is governed by the peculiarities of the mechanism of their effect. They undergo a series of subsequent transformations during friction, when they decompose due to elevated temperatures to form reaction products more simple than the original compounds [33]. The transformations evolve, first of all, in boundary films resulting in the formation of surface compounds with the friction pair metal that provide the effectiveness of the application of these compounds. Laminar solid substances have other interesting specificity. Particularly, graphite is prone to organized adsorption on solid surfaces [14, 35]. This can reduce the surface tension of the fluids contacting metallic surfaces; owing to this, oil films spread well over the surfaces and friction conditions improve considerably [35]. The presence of solid lubricants in oils has also been found to be effective, through the widening of the oils' working temperature range, has during fluid friction due to stronger adhesion of graphite to the oil. The temperatures at which oil is retained on graphite are higher compared to the case of common metallic surfaces. An adsorption layer of graphite flakes having a lamellar-hexagonal structure and oriented normally to the metal surface makes the profile of the latter closer to flat [14]. Secondary adsorption of active molecules of the lubricant, e.g., fatty acid, occurs on surfaces smoothed by graphite, leading to the localization of shear stresses in the ordered structured lubricant films. This is favorable for the boundary friction process.

Subsequently it was explicitly proven that high antifriction properties of graphite can manifest themselves upon the adsorption and intercalation of other substances [11, 18]. To improve the antifriction and strength characteristics of graphite and carbon–graphite materials, they are impregnated by polymers such as phenol formaldehyde resin, PTFE, and others and metals such as babbit and lead bronze [18, 36]. However, the working temperatures of such materials are restricted by the temperatures of polymer destruction and metal melting. A rich variety of graphite-based materials has been developed containing boron nitride, silicon carbide, silicon, ultraphosphates, etc., in addition to the above-mentioned fillers and alloying elements. Siliconized graphite produced by impregnating porous graphite material with silicon has found wide application. Materials on its basis are extensively used in seals operating in fluids. Also of interest are other modifications of carbon materials such as pyrolitic graphite, carbon pyrocerams, glassy carbon, nanotubes, fullerenes, etc.

It is known [11, 18] that, unlike materials based on molybdenum disulfide, graphite materials have a quite high friction coefficient in vacuum. However, if tribochemical reactions between them and the components of the composite material or the counterbody material yield substances which facilitate the mutual sliding of graphite crystallites, the friction coefficient may decrease considerably. This mechanism of friction reduction is most effective, e.g., in case of the contact of a graphite material in vacuum with corundum ceramics at temperatures of >500 °C. This can be explained by the fact that tribochemical reactions between corundum ceramics and the graphite material produce aluminum carbide, as well as atomic oxygen and carbon oxides that facilitate the mutual sliding of graphite planes. Owing to this, the friction pair graphite material–corundum ceramics has an abnormally low friction coefficient in vacuum at temperatures of >500 °C [18].

A variety of hypotheses have been proposed to interpret the low shear of lubricants containing lamellar solid substances. Hypothesis, which explains the mechanism of the lubricity of both lamellar solid substances and high-molecular linear polymers, is put forward in [37]. Its essence is as follows.

The low resistance shear of solid lubricants requires the surface energy over their cleavage planes or surfaces of two-dimensional molecules (lamels) to be low and the interplanar interaction to be quite weak. The absence of sufficiently high potential barriers and the relative constancy of the values of the potential energy of the estimated slip planes are also necessary conditions. These conditions entail that atoms or molecules of chemically adsorbed compounds can easily migrate over the surface under certain conditions, behaving as a so-called two-dimensional gas or fluid. Such behavior is possible for physically adsorbed molecules but it is hardly probable in the case of chemisorption. Therefore, if the surface energy decreases upon physical adsorption and the interplanar spacing increases when molecules are situated in interlaminar spaces, the friction coefficient must decline. If the adsorbed molecules or atoms react with the surfaces in contact, they hinder the easy mutual sliding of the surfaces, thus increasing the friction coefficient and wear.

Such behavior explains as the high so low resistance shear of lamellar solid substances under various operating conditions. Practice shows that these conditions much influence the energy of the bonds between the slip planes, as well as the pattern of the adsorption interaction of the molecules and their capacity for easy migration over the friction surfaces; i.e., they significantly affect the tribotechnical performance of lamellar lubricants overall [19, 21, 37–39].

It is obvious that the effective protection of friction surfaces requires the presence in the contact zone of a lubricating system meeting the above demands. Modern nanotechnologies hold an important place in this field; they allow considerable improvement, e.g., of the unique antifriction properties of graphite materials in combination with other chemically active elements and compounds in boundary lubrication with oils [40]. The idea of this research trend is as follows. It is believed that the graphite–graphite pair has one of the lowest friction coefficients [11, 14, 18]. Moreover, in the presence of a small amount of oil, the friction coefficient is still lower. On the other hand, if the friction surfaces in the contact zone have additional elasticity, the friction force can be reduced still further, by two or even three orders of magnitude [40].

In other words, it is necessary to develop a lubricating composition which does not change the properties of the oil; is not entrapped by an oil filter; is deposited on the friction surfaces, specifically on the most heavily loaded sites; and which fills the excessively widened gaps. According to the data from [40], this problem has been solved. A composition was developed containing nanopowders of silicon dioxide, aluminum trioxide, and plasma-expanded graphite in addition to the base oil (Fig. 2.1a). All components were dispersed in neutral oil compatible with any mineral or synthetic oils.

As a result, oil molecules are incorporated into the protective film of the complex lubricant on contact sites with a heavy pressure and high temperature, thus yielding an elastic base for the graphite particle layer that covers the "puff pastry" composed of aluminum trioxide and silicon dioxide nanoparticles (Fig. 2.1). Oil molecules bound in a spatial structure by silicon oxide particles form the basis of the protective nanocrystalline film with a gel-like consistency; they make up a sort of colloidal solution. Aluminum trioxide particles serve as a substrate, while a thin film of plasma-expanded graphite protects the outer surface. According to the data from [40], the protective nanocrystalline film grows most rapidly in the zones with a heavy pressure and elevated temperature, i.e., on the most heavily loaded sites, which require the most careful treatment and reliable protection. As the protective

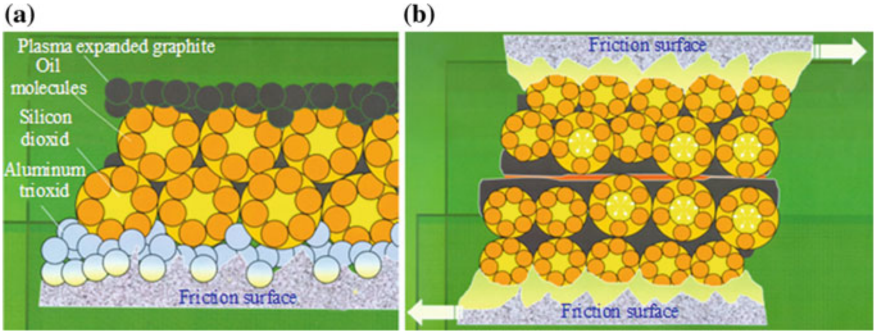

Fig. 2.1 Structure and main components (**a**) and schematic of operation (**b**) of nanocrystalline jellous protective lubricating film

film continues growing, friction on these sites diminishes and the film growth rate also decreases. At the same time, such protective nanocrystalline films appear and grow on other more heavily loaded sites of the friction surfaces, whereon the pressure is redistributed. The positive effect of the new protective films becomes more pronounced with increasing pressure and temperature. Thus, the most heavily loaded friction members turn out to be most protected. Under real conditions, similar structures of the protective nanocrystalline films are formed on the surfaces in contact; hence, friction is mainly reduced to the friction of the graphite–graphite pair with a low shear resistance (Fig. 2.1b).

In the present view, there are “nanophase” and “nanocomposite” materials [41]. The first are objects for which the size of particles, crystals, or phases does not exceed 100 nm. By contrast, nanocomposite materials, or nanocomposites, are systems consisting of a matrix over which nanosized particles or their clusters are distributed chaotically or in a particular arrangement [41]. The above mechanism of the formation of protective nanocrystalline lubricating films from silicon dioxide, aluminum trioxide, and plasma-expanded graphite nanopowders allows us to assign them to the second type of nanomaterials, namely, nanocomposites.

A rich variety of nanosized particles with different origin and properties are currently used to produce nanophase and nanocomposite materials, including lubricants. For example, a rather large number of lubricants with powders of nanodispersed particles of metals, oxides, carbon, and polymers are known [41]. However, in the development of lubricants, unlike structural materials, the capacity of nanomaterials to form separating films in the friction zone, which prevent direct contact of the sliding surfaces and have a low shear resistance, is of great importance, in addition to the necessity of the homogeneous distribution of nanoparticles in the base oil up to the molecular level.

The effect of improving the tribological performance of nanolubricants manifests itself when modifiers of various types are used. The application of powder dispersions of thermoplastic nanocomposites based on polyolefines and polyamides, as well as fillers such as metallic powders produced by the thermolysis of precursors in a melt or detonation synthesis of carbon particles, enhances considerably the wear resistance and loading characteristics of lubricants [13, 41–50].

The idea of developing lubricants that generate tribopolymers is based on the formation on rubbing metallic surfaces of polymer films possessing antiwear, antiscoring, and antifriction effects. It is supposed that such films will appear, first of all, on the local sites of the friction surfaces on which the contact pressure and temperature are highest. According to the data from [13], the mechanism of the formation of these transfer polymer films is complicated and involves the following.

Tribochemical transformations of the lubricants that generate tribopolymers in the zone of dynamic contact yield a set of products including low-molecular components, linear oligomers with a relatively small molecular weight, more high-molecular weakly soluble products, and cross-linked insoluble residue. The low-molecular components can be additive products of the formation of the high-molecular products of the tribochemical transformations or of the mechanodesturction of the high-molecular products in friction. The oligomers are considered to be products of the initial stages of the tribochemical transformations in the friction zone. They contain the basic structural elements of the original additive that generates the tribololymer. At the same time, the more high-molecular compounds are weakly soluble and form slightly cross-linked polymer structures. These compounds contain a great amount of coordination bonded iron, which is probably an important source of the formation of polymer grid nodes. The insoluble polymer is the product of the deep transformation of the original additive under the prolonged effect of high temperatures and pressures, as well as the catalytic action of the metal. It has a closely cross-linked structure and contains unpaired electrons and coordination bonded iron. The latter is found in the tribopolymerization products and participates in the formation of polymer grid nodes. It can be supposed that to some degree it also participates in the cross-linking of the polymer grid which appears on the friction surface to this surface. As a result, the compounds of the additives that generate tribopolymers may transform on the surfaces to complexes with iron atoms located on them; i.e., they are more effectively retained on the surfaces.

Thus, the friction of the original surfaces gives way to the friction of the polymer materials formed in the contact zone; hence, the surfaces become better separated. It is well known that polytetrafluoroethylene (PTFE) and composites on its basis have the best tribological characteristics among polymers. Fluorine-containing oligomers with various composition and structure serve as effective antiwear and antifriction additives [41–43]. The basic mechanism of the effect of such polymer additives is the formation of chemisorbed films with a high strength and thermal stability on the metallic friction surfaces; through tribochemical transformations, they prevent the direct contact of microasperities, keep the fluid-phase component of the lubricant on the friction surface, and produce metal fluorides. The latter substances are good antiscoring additives [41]. In addition, oligomer molecules make up oriented films on the friction surfaces (Fig. 2.2).

Depending on the oligomer composition, adsorbed films have a different structure; thus, their tribological characteristics vary. Lubricant molecules are oriented under the effect of the force field of nanoparticles, which possess a noncompensated charge, and due to the appearance of juvenile surfaces owing to the polishing action of the nanoparticles. The nanodispersed particles are capable of

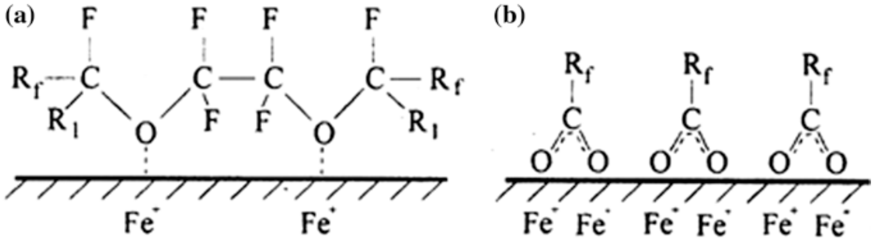

Fig. 2.2 Schematic diagrams of interaction of molecules of fluorine-containing oligomers of types (R_f–COOH) (**a**) and (R_f–R_f) (**b**) with metal surface [41]

forming oriented structures similar to "charge clusters" that have a pronounced structuring effect in polar and nonpolar media. This increases the thickness and carrying capacity of the boundary lubricating film and improves its loading capacity and reduces the friction coefficient.

According to the data from [51, 52], modern methods of producing fluorine-containing oligomers play an important role in achieving the unique antifriction and anticorrosion properties of materials. The method of the thermogas dynamic synthesis of ultradispersed PTFE (UPTFE) is finding ever-wider application. It involves the production of an aerosol mixture from monomers and oligomers that condenses, under certain thermodynamic conditions, to form powdery ultradispersed PTFE (the FORUM trade mark) [51]. The FORUM ultradispersed powder fabricated using this method contains mainly spherical particles 0.6 µm in diameter and has a stronger adhesion to metallic surfaces while keeping high antifriction characteristics; for this reason it is applied as an antiwear and antifriction additive to oils. As reported in [52], the mechanism of the lubricity of such compounds is that FORUM particles become trapped between two sliding surfaces and disintegrate into nanofilms under the effect of impacts. The films are subminiature and have a great charge; they adhere rapidly to the metal, fill micro- and nanocracks, and smooth out scores and asperities, thus producing a perfectly smooth and superslick coating, whose friction coefficient is close to that of the wet ice–wet ice pair (Fig. 2.3). Charged FORUM nanoparticles are attracted, first of all, by the sites with the most severe friction and highest hydraulic impact load.

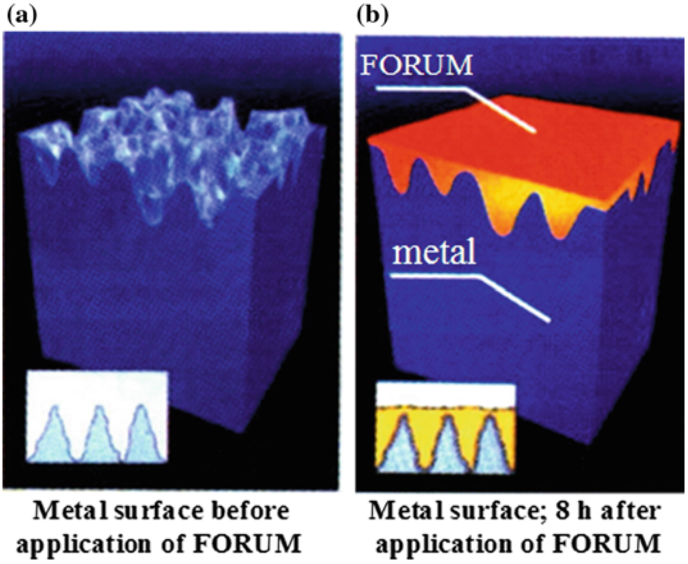

Fig. 2.3 Illustration of mechanism of lubricity of UPTFE (FORUM trade mark) involving formation of ideally smooth superslick film with friction coefficient typical for wet ice–wet ice pair [52]: **a** metal surfaces; **b** film formed

Thus, tribochemical transformations in lubricating compositions containing oligomers promote the formation of separating antiwear films that reduce the probability of scoring and microseizure. As a result, fluorine-containing oligomers may serve as a complex functional additive that enhances the wear resistance of the tribosystems.

The introduction of nanosized materials, e.g., ultradispersed diamonds (UDD), into the polymer matrix may yield even better effects. For example, it is noted in [53] that the introduction of 2 wt% of detonation synthesis UDD into PTFE reduces its wear rate 100–150 times. According to the data from [50, 53], UDD nanoparticles are linked together through coordination bonds in the PTFE amorphous phase, thus reinforcing it. This increases the compressive strength (to 42%) and hardness (to 14%) of the polymer.

Other authors have demonstrated that the introduction of nanodispersed particles of diamond–graphite charge into PTFE leads to not only a considerable rise of the wear resistance of the composite but also a decrease in its friction coefficient [51, 54, 55]. However, to disperse the dry UDD powder in oil is problematic. Mechanical (disintegration) and acoustic (ultrasonic) methods of dispersion of nanodiamonds are inadequate to produce stable oil suspensions. The chemical modification of UDD has yielded the best results in achieving stable (up to a year) suspensions of UDD in oils. It is aimed at the blocking of the surface hydrophilic functional groups and eliminating the intermediate precipitation of UDD as a solid phase (a dry powder) [51].

It has been found that the modification of the lubricating composition containing UPTFE by UDD varies significantly the characteristics of the friction pair. The joint introduction of UPTFE and UDD, which are specific structuring agents, improves the mechanical properties of the polymer film, thus yielding stable temperature and friction force during the whole testing period. According to the data from [51], the incorporation of UDD into the UPTFE matrix favors a decrease in the shear resistance between the layers of the polymer matrix perpendicular to the sliding velocity and also reduces the deformation component of the friction force and increases the wear resistance of the tribosystem.

A similar mechanism of friction, but with a much better effect of wear rate reduction (more than 300 times), occurs in the steel–steel pair upon the introduction of carbon nanotubes into PTFE [50, 56]. As the results of work [50] show, the high lubricity of such tribosystems is attributed to the improvement of the resistance of the polymer matrix to shear stresses which arise in friction; the growth of the hardness of the surface layers of the rubbing polymers; the accumulation of carbon nanotubes in the transfer film on the metallic counterface; and, as a result, the decrease in the penetration depth of microasperities on the surfaces in contact and the reduction of the deformation component of the friction force. Depending on the nature of the matrix polymer, the presence of carbon nanotubes in it may either reduce (PTFE and polyimide) or increase the friction coefficient. Such ambiguous behavior is explained, on the one hand, by the enhancement of the strength characteristics of the polymers and the lubricating effect yielded by carbon nanotubes, and, on the other hand, by increasing frictional losses due to the growth of the shear resistance of transfer films and, on the contrary, the abrasive effect of nanoparticles and their clusters leading to the rupture of the films during friction [50, 57].

However, the high lubricity of carbon nanotubes is beyond doubt and has been confirmed for other friction pairs. It has been found that the introduction of 0.1% of multiwalled carbon nanotubes into oil I-20A reduces considerably (3.5–5.5 times) the friction coefficient of the ceramics ($\alpha - Al_2O_3 + \gamma - Al_2O_3$)–steel pair within the 30–50 MPa pressure range [58]. It has been noted that the best effect is observed under heavy pressures. At the steady wear stage, the friction coefficient is 0.015–0.020 under 50 MPa and 0.010–0.012 at 30 MPa. At the same time, it has been shown that the introduction of carbon nanotubes into oil I-20A reduces the wear of the ceramics many times within the whole load range. The latter fact can be explained by the generation of a thin ($\approx$200 nm) film on the ceramic, which probably consists of radicals and nanosized ceramics and steel wear debris cross-linked by carbon nanoparticles. The film adheres strongly to the original surfaces and serves as a good separating layer between them.

The application of polymer compounds together with fullerene-containing additives also holds promise in tribology [50, 59]. It has been found that the introduction of fullerene soot into fluoroplastics reduces considerably the friction coefficient and increases the antiwear properties of friction units within a wide range of the contact pressure. The mechanism of their effect can be explained by the fact that the macroradicals resulting from the destruction of PTFE are chemically grafted to fullerene molecules and form a fullerene-like grid with a high wear resistance. At the same time, the growing microcracks that appear in the surface layer of the polymer film in friction are "healed" on fullerene-containing particles rather than rounding them as common inclusions. This is caused by the high electronegativity of the particles and the inhibition of free radicals.

The tribological performance can also be enhanced considerably by the use of fullerenes (mixtures of C_{60} and C_{70}) together with other polymer compounds, for example, polyimides. In this case, the sharp drop of the wear rate can be attributed to both the increased mechanical characteristics of the fullerene-containing polymer matrix and the inhibition of the thermal destruction of macromolecules by the fullerene additives, which may serve as "traps" for free radicals [50]. The application of nanoparticles with a high adsorption activity to form lubricating films having an improved resistance to rupture under the effect of shear stresses and high local temperatures and pressures is a promising trend in the development of lubricants [41, 51, 60, 61]. The accumulated experimental data show that the introduction of fine carbon-containing products of detonation synthesis (nanodiamonds and diamond–graphite charge), as well as fullerenes and fullerene-like structures, into lubricants promotes the formation of submicrocrystalline structures on friction surfaces [60, 61]. However, the study results indicate an ambiguous effect of the presence of diamond-containing nanoadditives in the friction zone, which depends greatly on the original structural state and properties of the materials in contact. It has been found, in particular, that in the case of annealed steel 45, the introduction of ultradispersed diamond–graphite charge (UDDG) into the lubricant accelerates the running-in of the friction unit and increases considerably its wear resistance and reduces its friction coefficient under heavy contact pressures [60]. At the same time, in the case of the hardened steel 45-hardened steel 45 pair the introduction of the UDDG into the lubricant accelerates both the running-in and wear of the pair.

The probable causes of the improvement of the tribological performance of annealed steel 45 in the lubricant modified by the UDDG are variations in the physical–mechanical properties of the lubricant (increase in the thermal stability and carrying capacity of the oil film) and the hardening of the steel surface layers by severe plastic deformation in friction [60]. As a result, if ultradispersed diamond–graphite additives are present in lubricants, an ultradispersed subgrain structure appears in the thin surface layers of the ductile materials at friction. The structure is characterized by a much smaller size of cells or blocks compared to that which appears in the testing of materials in the unmodified lubricant [60, 61]. Refining of the friction-induced subgrain structure is accompanied by a considerable (almost two-fold) rise of the microhardness of the surface layer, as well as a reduction of the resistance shear and in the wear of the friction unit.

It has been shown experimentally in works [60, 61] that the introduction of UDDG into the lubricant varies its properties in a complex manner. On the one hand, in the case of annealed materials, the addition of the ultradispersed modifier yields a positive effect since it causes the refinement of the subgrain structure appearing in the surface layers down to the nanocrystalline scale and the formation of a cellular substructure with a greater resistance to the nucleation and propagation of microcracks, which effectively absorbs the friction energy and improves the wear resistance of the tribosystem. On the other hand, in the case of high-strength hardened steel the additives of the UDDG to the lubricant intensify the wear of the friction surfaces.

The capacity of nanoparticles added to lubricants for influencing effectively the friction surfaces through variations in their microrelief, expansion of the real contact area, and reduction of the contact pressure is noted by other researchers under more intense conditions of dynamic contact [62]. In particular, under non-stationary friction conditions (repeated starts and stops) it has been found for the cast iron–steel pair that the introduction of a nanodispersed component—fullerene C_{60}—into motor oil reduces the wear rate of cast iron 1.62 times and that of steel 1.41 times. The capacity of oils for producing boundary adsorption films on the friction surfaces is a very important characteristic of their lubricating effectiveness under conditions of frequent starts and stops. According to the data from [62], the addition of a 20% suspension of fullerene C_{60} into motor oil causes the formation of stable boundary layers on the friction surfaces under these extreme conditions; the thickness of the chemisorbed films in these layers varies within 0.079–0.930 μm. It has been found that the polymerization of globular fullerene C_{60} molecules with hydrocarbon radicals on the metallic surface plays a leading role in the structuring of adsorption films if the boundary lubricating films are produced using the fullerene additive. This results in the appearance of a diamond-like layer that improves the wear resistance of the friction pair. It has been noted that the intensification of the mechanochemical processes on the metallic surface with increasing pressure enhances the polymerizing activity of the fullerene molecules still further (this agrees well with the results reported in [63, 64]) and induces the formation of a protective diamond-like layer on the surface. The appearance of this layer promotes a decrease in the intensity of the softening of the surface layers of high-strength hardened steel and the hardening of the surface layers of cast iron.

At the same time, the high production cost of fullerene C_{60} restricts its practical applicability for modifying lubricants. An alternative is the application of cheaper materials containing various soots, including those fabricated in fullerene production [65, 66]. It has been found that such substances as pure fullerenes C_{60} are most effective in friction pairs in which a high-strength hardened material contacts a more ductile one. In particular, the comparative tests of various carbon products carried out in work [65] have shown that for the steel roller–copper foil pair the addition of fullerene soots (before and after extracting bulk fullerenes from them) into industrial oil I-40A improves its antifriction and antiwear properties. This effect is comparable to the effect of the introduction of pure fullerene C_{60} into lubricants and in some cases can be ever better.

First, unlike the fullerene C_{60} powder, which is practically insoluble in a lubricant when introduced into it commonly in concentrations of <5 wt%, does not change the lubricant color, and precipitates quite rapidly, thus requiring special treatment before application, all soots (technical and fullerene) form sufficiently stable suspensions and impart a dark color to oils, which is retained during prolonged storage.

Second, structural examination of the friction surfaces have revealed that the mechanism of the effect of fullerene soots on the friction processes differs from the mechanism of the effect of C_{60}.

Third, since the content of C_{60} in soot is 15–20 wt%, the introduction of, e.g., 5 wt% of soot into the lubricant yields a much lower content of C_{60} in the latter of about 0.50–0.75 wt%. Nevertheless, according to the data from [65], such concentrations of C_{60} in fullerene soot are capable of producing at least four monolayers of densely packed C_{60} molecules on the friction surface; we note that this is quite sufficient to ensure a high lubricity of these tribosystems.

However, more comprehensive investigations have shown that the efficiency of the specimens of soot under study as additives to lubricants can be attributed not only to the presence of fullerene C_{60}. This is confirmed by the results of studying the additive of soot after the extraction of individual fullerenes C_{60} and C_{70} from it. This soot contains almost no pure fullerenes. It was applied in combination with another carbon-soot of P-514 grade, a byproduct of rubber production—in equal amounts (2.5 wt%) [65–67]. It was found that the use of such technical carbons in the lubricant for the steel–copper pair results in a much stronger effect than the use of the additive of pure fullerene C_{60}. With increasing contact pressure, the friction coefficient declines rather than grows; under loads of about 800 N it reaches very low and stable values (0.0135) and leads further to steady and long operation of the friction unit.

According to the data from [65], the pronounced effect of the joint application of soots containing almost no fullerene C_{60} is presumably caused by the activating action of the particles of soot P-514 on the process of fullerene formation during the friction of the other soot, which was exposed to the extraction of fullerenes C_{60} and C_{70}, as well as by the appropriate combination of the optimal content, dispersity, and activity of soot P-514. The combination of the properties of this soot eliminates the sintering of particles into a bulk agglomerate under conditions of heavy pressure and shear, which is typical for ultradispersed systems. The synergetic effect of the joint use of soots as an additive to lubricants has been confirmed experimentally and does not contradict the current views in this field [63–67], since shear deformation in the contact zone may promote the processes of the modification of carbon molecules at even lower temperatures and pressures.

Thus, the application of fullerene soot without fullerene C_{60} molecules and its composition with soot P-514 as an additive to oils is equally effective for transition to a very small resistance shear and wear as the addition of the powder of pure fullerene C_{60}. This opens ways of using a cheaper material-waste products of fullerene manufacture—as the source of the bulk of fullerenes. It also widens considerably the possibilities of the application of such substances as antifriction and antiwear additives to lubricants.

In addition to nanosized carbon products, nanoparticles of other chemical origin may have complex effects on a tribosystem, resulting in the formation of stable separating films on the friction surfaces, possessing low shear resistance and high wear resistance. They are also of a near-spherical shape. They include ultradispersed β-sialon, which is the solid solution of Al_2O_3 and AlN in β-Si_3N_4, having the general formula $Si_{6x}Al_xO_xN_{8x}$ and produced by plasmachemical synthesis at temperatures of 5600–6200 K [68–72]. It has been found that the application of nanosized β-sialon as an additive to lubricants improves considerably their performance, especially in heavy-duty friction units [68, 71, 72]. At the running-in stage under conditions of high shear forces typical for such friction units, β-sialon reduces the adhesion component of the friction force, thus protecting the contacting surfaces against local seizure and promoting the formation of smooth surfaces with high luster and a much larger real contact area. Surface examination by X-ray structure analysis has shown that the use of β-sialon as an additive results in the appearance of structures with a greater lattice parameter in the steel surface layer. They also have a reduction of microdeformations and dislocation density, that reduces greatly the friction coefficient and contact temperature. Thus, the high lubricating effect of the β-sialon in friction zone consists in the formation of a new structurally ordered surface layer with a minimal number of lattice defects and a high carrying capacity [71, 72].

Another type of silicate friction modifiers used as additives to lubricants are minerals like serpentinite containing siloxane or bridge bonds Si–O–Si, whose rupture yields noncompensated Si–O– dangling bonds owing to the destruction or refining of the mineral. These bonds are active acceptors of hydrogen in the form of H+ [73, 74]. Their interaction produces compensated silanol groups Si–OH. On the one hand, fine serpentine with a high specific surface and a great number of dangling siloxane bonds favors the bonding of active hydrogen present in the friction zone; i.e., it inhibits the reaction of hydrogen with the metal and hinders hydrogen wear. On the other hand, it has been found that the presence of such mineral modifiers in lubricating oils leads to the formation of a separating film with a two-level structure on the steel friction surface [73]. The film consists of a mineral "skeleton" with a rough surface and a layer of oil tribopolymerization products that is held by the skeleton. Such a structure of the lubricating system yields the stable performance of the friction unit under deficient lubrication, i.e., under so-called oil starvation. At the same time, comparison of the lubricity of serpentine minerals with cheaper and more abundant clay minerals from the kaolin group added into lubricants has shown that for these groups of minerals the mechanisms of the plating of the friction surface are similar both in the type of the chemical bond formed and in the ordering of the film that appears. Such ordering is observed in the plane film structures of the oxygen—containing compounds of silicon [74]. It has been found that kaolin ranks above serpentine in antifriction and antiscoring characteristics, and this is additionally confirmed by the lower bulk temperature of the lubricant and milder visible damage to the friction surface both during running-in and at the steady wear stage. However, kaolin has worse antiwear properties than serpentine. But we note that these groups of silicate minerals demonstrate a general pattern of behavior which is typical of most tribosystems and observed during rubbing of antifriction polymers and composites and in selective transfer. It involves, as a rule, the creation of a multilayer antifriction film in the process of friction.

Thus, numerous methods of producing antiwear and antiscoring films have been developed and are used widely. Under conditions of the effect of the environment (when grafted polymerization [75–77] occurs, the interface is irradiated [78, 79] and selective transfer develops [80–82]), friction induces the appearance of the thin lubricating film with small resistance shear that prevents the contact of the friction members. The lubricant composition has a marked effect on the kinetics of the formation of the lubricating films.

The lubricity of industrial, hydraulic, transmission, and motor oils with additives which contain coordination compounds of copper, zinc, nickel, and cobalt, as well as ligands and esters, has been studied quite well during recent years [83, 84]. It has been found that the joint application of these compounds in lubricants is most effective in the case of selective transfer in the steel–steel pair. The introduction of coordination compounds into lubricants in an amount of 0.1–0.3 wt% improves considerably their lubricity and increases the seizure load, as well as reducing the friction coefficient and wear rate of the wear tribosistem. Analysis of the kinetic dependences which characterize the adsorption of such compounds (Fig. 2.4) has revealed that during the initial period of friction a sharp drop of the concentration of the metal complex in the lubricant occurs, together with increase in the wear rate and decrease in the friction coefficient [84].

These changes, depending on the type of metal added to the lubricant, are accompanied by the formation of a thin metallic film which protects the steel surface against oxidation and mechanical wear. The next part of the lubricating film appears on it, i.e., a tribopolymer film. As a result, all characteristics of the pair stabilize and so-called wearless friction is attained (Fig. 2.4, curve *2*). The results of

Fig. 2.4 Variations in copper complex concentration (*1*), wear rate (*2*), and friction coefficient (*3*) in steel–steel pair in selective transfer [84]

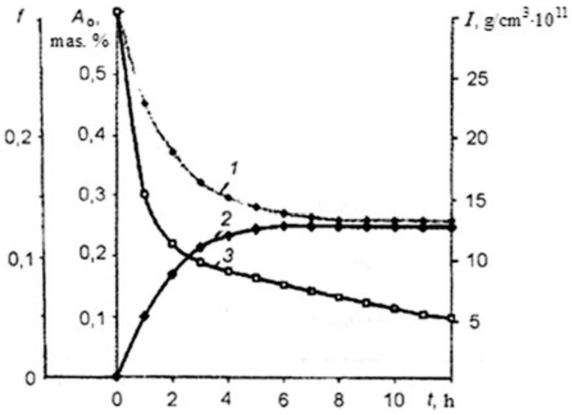

spectral examination have shown that the tribopolymer film contained in the lubricating layer includes carboxyl groups bonded to ions of the metals in contact.

Thus, it has been found that the presence of coordination compounds of copper, nickel, cobalt, and zinc in a lubricant is a necessary condition for selective transfer in steel–steel friction pairs. The lubricity of the oil improves in the following series of coordination compounds: copper, nickel, cobalt, and zinc [84]. The low friction coefficient of the steel–steel pair under these conditions is presumably explained by the jellous state and the liquid-crystal structure of the separating lubricating films.

This is also confirmed by our results of studying adsorption processes that evolve when individual liquid-crystal nanomaterials are added to lubricants [85, 86]. It has been found that in the case of the steel–steel friction pair the adsorption processes with participation of solutions of cholesteric liquid-crystal nanomaterials follow similar mechanisms. It has been demonstrated that the induced or triboinduced adsorption of molecules of liquid-crystal cholesterol compounds is correlated with kinetic changes—increase and subsequent stabilization—of the tribological characteristics of the steel–steel friction pairs, as in the case when coordination compounds of transition metals are added to lubricants [86].

The experimentally found relation between the stabilization of the concentration of the liquid-crystal nanomaterials in the lubricant under study and the onset of the sharp drop of the friction coefficient proves strongly that at this point in time an adsorbed liquid-crystal film with a high antifriction properties starts “operating” in this tribosystem. A mechanism of the lubricity of the liquid-crystal nanomaterials of the cholesteric type has been proposed, which involves the progressive wear of the friction surface that is gradual and governed by the influence of the liquid-crystal cholesterol compounds contained in the lubricant. It yields a smooth flat microrelief (Fig. 2.5e, g–i).

Such a situation is most favorable for reducing the local contact pressures in the friction zone and hence the heat generation and deformation loss [85, 86]. A continuous lubricating film that is typical for the given concentration of the

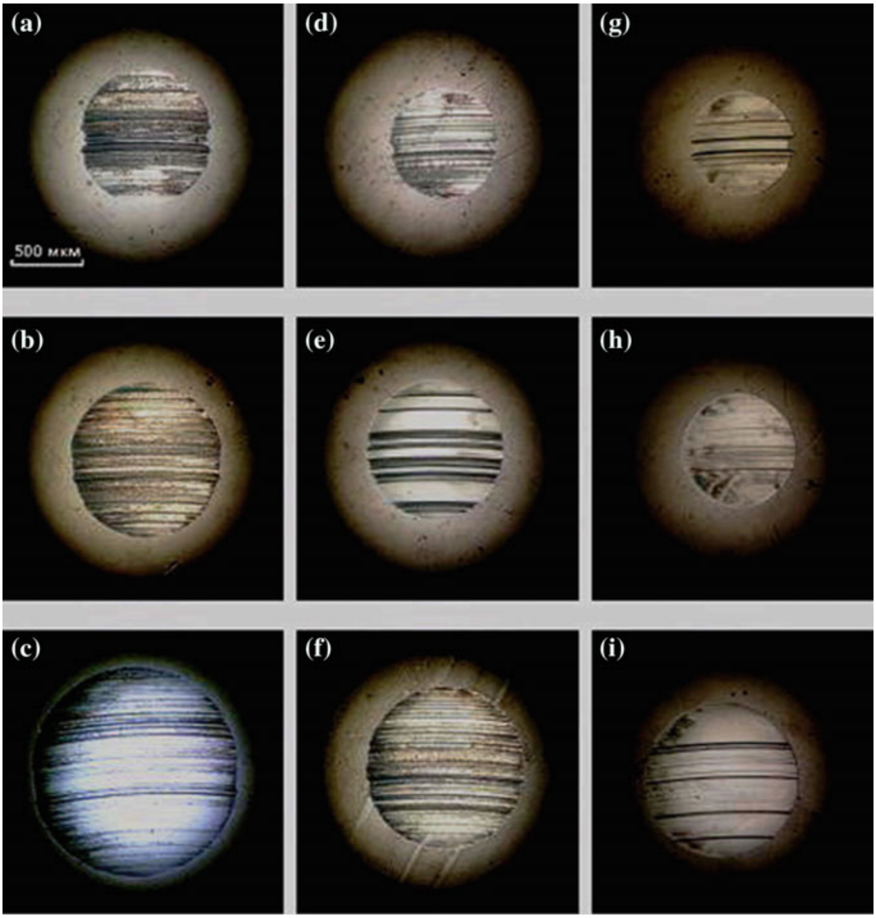

Fig. 2.5 Kinetics of variations in microrelief of surfaces of wear spots on steel balls lubricated with pure Vaseline oil (**a**–**c**) and Vaseline oil with additives of 1 wt% (**d**–**f**) and 3 wt% (**g**–**i**) of cholesteric liquid-crystal nanomaterials: **a**, **d**, **g** 2 h; **b**, **e**, **h** 4 h; **c**, **f**, **i** 8 h. Four-ball tests, load 333.2 N

liquid-crystal cholesterol compounds is formed on this microrelief. The film screens the surfaces and reduces the friction and wear of the solids (Fig. 2.6).

At the same time, wide experience of the application of lubricants has shown that inorganic compounds, which are also capable of dissolving in base oils, can serve as equally promising antiwear and antiscoring additives. They possess important advantages in the absence of organic cations and radicals that may induce the destruction of the lubricant during its use.

Heteropolyphosphates such as $M^{I}PMoO_6$ turn out to be well-soluble in natural oils in addition to molybdenum trioxide MoO_3 and some condensed metaphosphates of alkali metals. They have a cyclic structure, where M^{I} is the atom of a one-valent metal [87, 88].

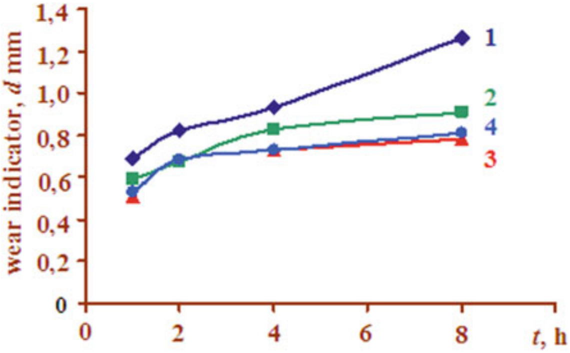

Fig. 2.6 Kinetic dependences of diameter of wear spots on steel balls lubricated with pure and modified Vaseline oil: *1*—pure oil; *2*, *3*, *4*—additive of cholesteric liquid-crystal nanomaterials in concentrations of 1, 3, and 10 wt%, respectively. Four-ball tests, load 333.2 N

It has been found that the introduction of the additives of heteropolyphosphates of alkali metals such as sodium, lithium, and nickel into lubricants reduces considerably the friction coefficient of the steel–steel pair, keeps the friction coefficient stable, increases the wear resistance, and smoothens the relief of the friction surfaces [87–89]. The effectiveness of such additives is caused by their molecular structure, possibilities of their reversible rearrangement under various operating conditions of friction units, and the capability of molybdophosphorous anions for integrating into the structure of oxide films on the metal surfaces. The application of quantum-chemical analysis has allowed us to suppose that the heteropolyphosphates of alkali metals possess properties of both surfactant additives (in the location of the linear chains relative to the metal surface and the resulting low friction coefficient) and chemically active additives (in the degree of the binding with the metal surface and the resulting high wear resistance of the metal) [89]. The use of modern testing methods has revealed that during friction, heteropolycompounds having a cyclic shape open and transform to linear chains [87–89]. Such structures integrate better in the crystalline texture of oxide films on steel friction surfaces. Therefore, the appearance of the linear form of the heteropolyphosphates of alkali metals and the formation of effective separating lubricating films on steel surfaces in friction is crucial for the wide application of these compounds as additives to lubricants.

The capability of a lubricant for forming strong boundary lubricating films of a sufficient thickness during relatively short time intervals governs strongly the durability and reliability of heavy-duty lubricated friction units operating under boundary lubrication conditions either permanently or periodically. To solve the problem of the adequate modeling of friction regimes and provision of the serviceability of friction units under various lubrication conditions it is worth while to use the Stribeck curve, which can easily be plotted from experimental data. It presents the dependence of the friction coefficient f on the dimensionless parameter $\eta\omega/p$, where η is the lubricant dynamic viscosity, N s/m^2; ω is the angular velocity, s^{-1}; and p is the pressure, MPa.

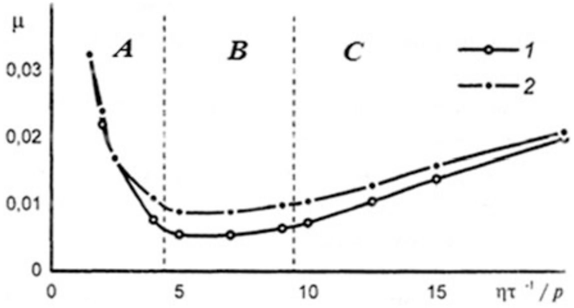

Fig. 2.7 Stribek curve for lubricated friction of composite aluminum material AlKS–1.5 Gr against steel: *1*—oil bath; *2*—deficient (drop) lubrication [12]

It is found in [12] that under various lubrication conditions (abundant or deficient oil supply in the friction zone) depending on the parameter $\eta\omega/p$ a common pattern of the friction curves is observed: gradual transition from the mixed mode (area *A*) to the boundary (area *B*) and hydrodynamic (area *C*) modes occurs (Fig. 2.7).

Nevertheless, the abundant lubrication of the specimens (in an oil bath) produces more favorable conditions than deficient oil supply in the friction zone, particularly in the case of drop lubrication. However, in almost all cases, i.e., regardless of the lubricating conditions, the lowest friction coefficient is registered in the case of boundary lubrication.

Lubricity in the boundary mode has an intricate mechanism. It is not dependent on the lubricant viscosity and chemical transformations in the area of contact of friction surfaces but is caused by both the formation of a specific boundary film and the effect of the active components of the lubricant on the mechanical properties of the surfaces [7, 10–12]. As a result of these processes, an adsorption film with a specific structure appears [5, 7, 14], on the one hand, and the adsorption plasticization of the friction surface occurs, on the other hand. This plasticization also contributes considerably to the lubricity [16, 90]. As a result, the processes of boundary friction evolve in the surface layers of the solids in contact and in the lubricating boundary film which separates this layers, the thickness of which is comparable to the layers' thickness. Analysis of numerous studies in this field has shown that the three-stage kinetic model of the wear process in boundary lubrication is the most suitable. It includes the following stages: 1—the stage of the adsorption of molecules on the friction surface; 2—the interaction of the molecules with the metal surface layer to form some secondary structures, the tribological characteristics of which differ from those of the original surface; 3—the stage of the disintegration of the structures followed by the exposure of the activated metal surface with the capacity for subsequent reaction with the lubricant [91, 92].

Since solid surfaces are rough, conditions for the appearance of adsorption films differ for different areas of the surface. There are three types of contact surface areas [14], namely, (a) the area formed by a polymolecular boundary film; (b) the area formed by a mono- or bimolecular film; (c) the area whereon the engagement of the asperities occurs and, in the case of shear, their deformation and fracture take place.

Correspondingly, at low slide velocities, when the thermal and tribochemical effects can be ignored, the total friction force consists of the following components: (a) the friction force in the polymolecular film; (b) the friction force of the surfaces separated by the monomolecular film; (c) the friction force in the surface layer of the solid. It has been found that the rate of the formation and the thickness of the polymolecular film depend greatly on the properties of the surfactant. Molecules with short or branched alkyl radicals form only thin boundary films or do not form them at all [14]. The length of the alkyl radical plays a decisive role in the formation of thicker boundary films [14, 93, 94]. Solutions of higher alcohols and amines are also capable of producing polymolecular boundary films, but these films are weaker than the films of fatty acids at equal lengths of the alkyl radical [14].

Experimental study of the lubricity of surfactant monomolecular films is difficult because of the inhomogeneity of the surface of real solids. In the case of a monomolecular adsorption film, the force of contact interaction depends, first of all, on the degree of filling of the film and is therefore related to the adsorption activity of surfactants. Then, unlike the polymolecular boundary film, the thickness of the adsorbed surfactant layer does not play an important role. If the adsorption film is unfilled, short-chain molecules may be more effective. It is for this reason the regularities relating the lubricity differ for poly- and monomolecular boundary films. For a polymolecular boundary film, the molecularkinetic factors which govern the resistance of the film to thinning are of crucial significance. In the case of a monomolecular adsorption film the strength of the adsorption bond and the kinetics of the renewal of the film on the juvenile surface are important. If adsorption plasticization occurs, the result depends on the diffusion of the molecules into defects in the surface layer of solid.

A more profound analysis leads us to the corollary that high lubricity at the boundary mode is reached when shear is localized totally or partially in the polymolecular boundary film, which has minimal shear resistance and incurs almost no wear [1–5, 14, 85]. This can be attained when boundary films in the friction area acquire a liquid-crystal structure [5, 94–96].

Temperature elevation in the contact zone reduces the oil viscosity and lubricating film thickness; it can also lead to rupture of the boundary film. The temperature at which the film is ruptured is the critical temperature for the given combination of the oil and the friction member materials [5, 91, 92]. The effect of the friction member materials consists in the fact that a decrease in its hardness causes a reduction of the critical temperature, all else being equal. The rupture of the lubricating film and the onset of seizure are more probable when the surfactants contained in the lubricant are desorbed [6, 97].

At the same time, it has been found that the lubricity of oils can also be enhanced by increasing the orienting capacity of the solid working surfaces themselves. This effect can be reached, e.g., by covering the surfaces with special orienting carbon

Fig. 2.8 Model of formation of structurally ordered epitropic liquid-crystalline (ELC) boundary lubricating layer [98]

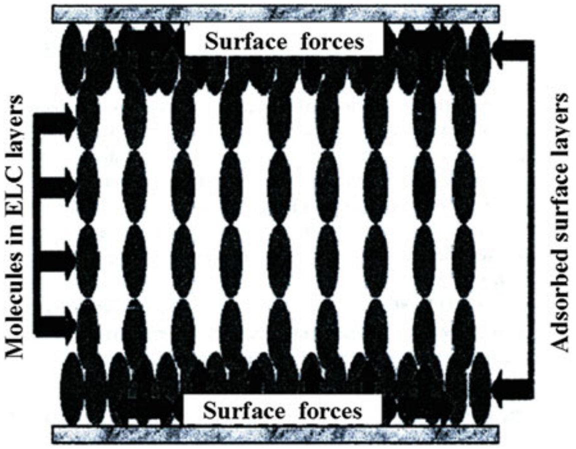

coatings that yield highly oriented boundary films; the latter copy the highly ordered structure governed by the coating surface (Fig. 2.8) [98, 99].

Analysis of the adsorption of oil molecules on the friction surfaces, which favor their orientation, has shown that the orienting coatings provide substantial structural ordering of the molecules in the boundary film, while amorphous coatings do not have an orienting effect on it. Highly oriented coatings yield the best lubricity and serviceability of boundary films within wider temperature and load ranges [99]. In addition, the application of these coatings makes it possible to simplify considerably the composition of oils by reducing the number of antifriction, antiwear, and other additives, and even altogether excluding their use.

Analysis of the adsorption of oil molecules on the friction surfaces, which favor their orientation, has shown that the orienting coatings provide substantial structural ordering of the molecules in the boundary film, while amorphous coatings do not have an orienting effect on it. Highly oriented coatings yield the best lubricity and serviceability of boundary films within wider temperature and load ranges [99]. In addition, the application of these coatings makes it possible to simplify considerably the composition of oils by reducing the number of antifriction, antiwear, and other additives, and even altogether excluding their use.

Thus, the lubricity of various tribosystems under conditions of boundary lubrication of solids results mainly from the formation in the contact zone of interphase films of molecules possessing a specific structure. The presence of orienting coatings on friction surfaces expands greatly the possibilities of such passive control over their lubricity through the preliminary directed modification of the surfaces. Such modification imparts specified structural peculiarities to the surfaces, thus enhancing the tribological performance of friction units.

2.2 Present-Day Advances in Control of Antifriction Behavior of Solids (Active Friction Control)

Active control over the friction of solids is one of the important problems of modern tribology. Active friction control is primarily characterized by a fast response of a tribosystem to the application and variation of the external energy, which is supplied to the tribosystem and improves its state by enhancing its tribological characteristics, in particular by reducing the friction force (and therefore the friction coefficient) directly during dynamic contact. In other words, during “active friction control” or “active friction regulation,” the response of the friction members to external energy is reversible and can be implemented automatically by using modern control systems and feedbacks; i.e., it can be directed exactly in the way that is required at the given moment of time. One striking example of the wide practical application of such active control in tribology is the use of antilock brake systems [9, 100, 101]. In such systems the braking torque is automatically varied for each wheel to achieve a suitable slip-to-rolling ratio at each moment of time; this is implemented by taking into account and selecting the individual response of each wheel sufficient for the attainment of the optimal contact between the tire and pavement, thus providing the most effective braking. Therefore, such tribosystems control friction by changing the load applied to the friction surfaces, rather than the friction force or friction coefficient.

From the viewpoint of tribology, active control over the friction coefficient is relevant. Studies in this field are constantly evolving and include several directions. In particular, according to the data from [9, 100, 101], the following two methods of active control over the friction coefficient can be distinguished. The first is control over the viscosity of a lubricating fluid, which changes the friction coefficient during hydrodynamic lubrication as the bulk viscosity of the lubricant varies. Another method is to change the state of surface films, which, in turn, varies the boundary friction coefficient. It should be noted that these methods of controlling the friction coefficient can be implemented by using both magnetic and electric fields applied to the friction zone. Below we shall consider in more detail each of the known ways of active control over the friction of tribosystems of various origin and performance.

Interest in the effect of magnetic field on friction and wear stems mainly from attempts to find simple and practically useful methods for controlling the processes which evolve during friction. Devices involving magnetic fluids as the working substance have been well tested [102]. There are two types of magnetic fluids whose response to applied magnetic field results from the magnetic properties of the solid particles dispersed in them. One of these types is made up of colloid solutions of magnetic particles so small that they undergo Brownian motion, hampering their sedimentation. Colloid particles of a magnetic material are one-domain zones whose magnetic moments interact with each other. To prevent the agglomeration of the particles, surfactants are added to the fluid base; the surfactants form protective adsorbed films or solvation shells on the particle surfaces. In stationary uniform magnetic field, the particles are drawn into the zone with stronger field. This motion is transmitted to the fluid base through Brownian motion, thus inducing force interaction between the magnetic fluid and field.

Another type of magnetic fluid is systems containing multidomain particles whose size exceeds by more than an order of magnitude the size of the individual particles in common magnetic fluids. Such systems are called magnetorheological suspensions and are suspensions of ferromagnetic particles, most often carbonyl iron powder, in mineral or organosilicon oils. These compositions have found application in magnetically operated clutches, brakes, and dampers. However, one of their disadvantages is the immiscibility of the fluid and solid phases after the deactivation of the magnetic field owing to the rather large size of the particles and their sedimentation under the effect of gravity; this causes the unstable performance of the devices.

Nevertheless, according to the data from [103], the introduction of colloid magnetic particles into the base oil under the effect of magnetic field can increase the oil viscosity two- to fourfold. The dynamic viscosity of the ferrofluid depends on the direction and induction of applied magnetic field; i.e., the fluid possesses the anisotropy of magnetic properties. At the same time, it has been shown that even without magnetic field the viscosity of the ferrofluid exceeds by 70–75% the base oil viscosity. As a result, the four-ball tests demonstrated a higher lubricity of the ferrofluid compared to that of common motor oils (Fig. 2.9).

It has been found that the carrying capacity of sliding bearings lubricated with the ferrofluid without magnetic field is approximately 70–80% higher than that of the bearings lubricated with the base oil. Thus, it has been shown that magnetic oils or ferrofluids themselves, i.e., without the application of magnetic field, can serve as effective lubricants for sliding bearings.

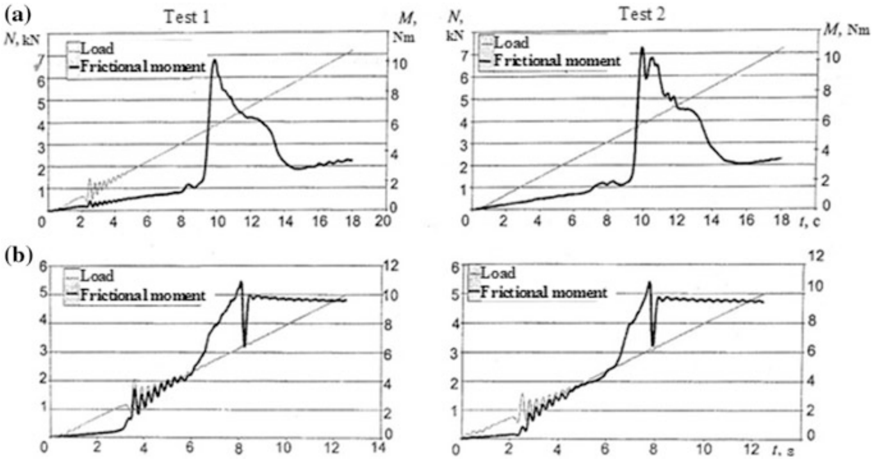

Fig. 2.9 Kinetic dependences of load and friction torque obtained during four-ball tests [103]: **a** ferrofluid; **b** base oil; *1*—load *N*; *2*—friction torque *M*

The possibility of entrapping a volume of the magnetic fluid affected by an external force using the magnetic field in a narrow clearance between the shaft and body of a friction unit is the principle of operation of most common devices with magnetic fluids or magnetic fluid seals [102, 104]. The magnetic lubricants containing magnetite colloid particles and surfactants are sometimes much more advantageous compared to common lubricants, even in traditional bearings [103]. The attraction of the magnetic particles to steel friction surfaces increases the lubricating film viscosity and the surfactants cover the solid surface with a hydrophobic film; this ultimately improves the antiwear and antiscoring properties of the friction surfaces.

The experience of the development and application of magnetic oils shows that their considerable potential can be fully realized only on the basis of the profound and comprehensive study of the lubricity mechanism [105, 106]. A great number of works deal with investigation of the effect of fine materials contained in oils on friction and wear. The possible mechanisms of the influence of the particles on friction are described and special attention is paid to the structure of the film separating the rubbing surfaces. To impart magnetic properties to oils, dispersed materials with a high saturation magnetization, usually Fe and Fe_3O_4, are added. The particle size does not exceed, as a rule, 1.5×10^{-8} m. According to the electron microscopy data, the particle shape is close to spherical. Owing to their small size, the magnetic particles have an almost defect-free structure and are in the one-domain state. It is assumed that during friction fine particles favor the healing of surface defects and reduction of contact deformation due to an increase in the real contact area and the localization of shear stresses in the boundary lubricating film [105].

The pattern and peculiarities of the effect of solid particles on friction depend on the ratio of their size to the surface asperity height and the thickness of the boundary lubricating layers. The size of the magnetic oil particles is one or two orders of magnitude less than the friction surface asperity roughness and comparable with the thickness of the boundary lubricating film. However, under all loads and for all materials an increase in the friction coefficient occurs, as a rule, with increasing particle concentration [105]. The particles between the moving surfaces apparently favor the adsorption of an additional share of the energy spent for the deformation of the adsorbed molecular layers and the surfaces.

According to the data of [105, 106], due the effect of nonuniform magnetic fields the Boltzmann redistribution of the concentration of the particles in magnetic oil occurs in the friction zone, resulting in a higher concentration of the particles near the contacting surfaces. This, in turn, increases the content of free surfactants since the equilibrium between the adsorption and desorption of the molecules which form solvating shells of the particles is accented. It is for this reason that the formation rate of new films, or the recovery rate of the ruptured boundary lubricating film in the nonuniform field, grows considerably. As a result, under the effect of nonuniform magnetic fields, friction declines by 10–15% owing to a decrease in the probability of the formation of contact between the juvenile surface portions.

However, practice has shown that this effect is profound only at low sliding velocities.

It has also been found experimentally that in nonuniform magnetic field the rate of the formation of the boundary lubricating film influences not only friction but also the degree of surface plasticization (the Rehbinder effect) [106]. It is noted that nonuniform magnetic field accelerates friction surface plasticization. For this reason, adsorption processes on the friction surfaces can be specifically controlled by changing locally the disperse particle concentration using magnetic field.

The introduction of special additives to magnetic oils makes it possible to vary their lubricity within a wide range. However, one of the specific features of magnetic oils compared to common ones is a much greater optimal additive content. The additive content in common oils is no more than 5%, while it may reach 15–20% in magnetic oils. The friction coefficient in magnetic oil can be reduced up to three times by varying the additive content and concentration and the wear rate can be reduced by an order of magnitude. Moreover, the application of special additives for treatment of the friction surfaces to make them lyophobic (Fig. 2.10) favors the so-called effect of the improvement of the sliding of structured magnetic fluid over a solid surface at the moments of start, i.e., when the transition from static friction to sliding friction occurs in magnetic fluid units [107].

Thus, it becomes possible to reduce not only the dynamic but also the static friction in magnetic fluid tribosystems and real methods for optimal control over the friction coefficient are proposed.

Many of the available studies deal with the development of systems with alternating electromagnetic fields, which can eliminate external friction almost completely. Friction and wear in traditional passive magnetic bearings decline owing to the prevention of mechanical contact between the mated surfaces. Self-unloading magnetic bearings have been developed, which combine a mechanical bearing and a magnetic unloading unit [108]. Self-unloading magnetic bearings are compact and have a simple design and a quite high unloading force since the clearance between the friction members with opposite magnetic interaction is very narrow.

It has been found that not only technical lubricants but also natural ones respond actively to electromagnetic field variation. Experiments have been carried out with the metal-ultrahigh molecular weight polyethylene (UHMWPE) pair under the effect of electromagnetic field of a solenoid installed in the support of a pendulum tribometer. It has been shown that the friction coefficient of the pair lubricated with physiological solution remains constant irrespective of the application of electromagnetic field to the polymer support [109]. However, the lubrication of the pair with natural lubricant taken from human and animal joints—synovial fluid (SF)—makes it sensitive to the presence of electric field in the support. It has been found that without field, the lubrication of the pendulum support with both healthy natural SF and blood serum (original and with hyaluronic acid additives) yields almost the same friction coefficients $\mu = 0.060 \pm 0.001$ (the pendulum mass is 2 kg). The application of field reduces μ with the use of any of the studied biological fluids for lubrication.

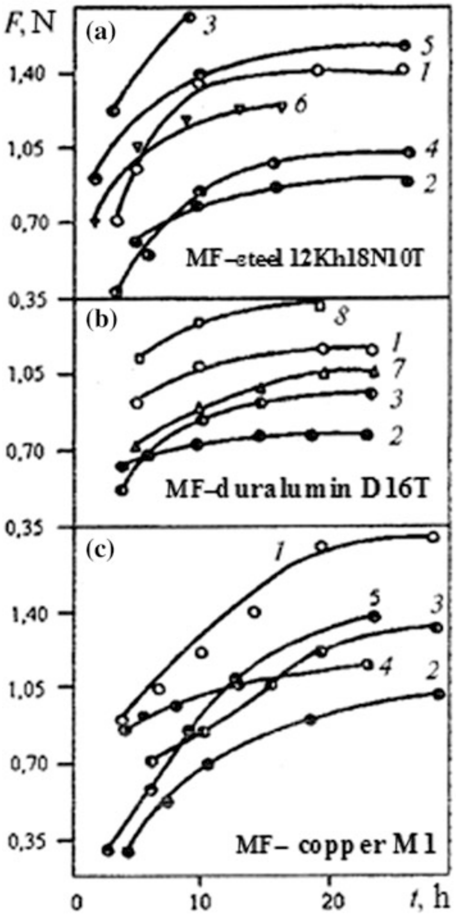

Fig. 2.10 Friction of magnetic fluid (MF) over surfaces of various nature [107]: *1*—pure fluid; *2*—alfanoks; *3*—sintanol; *4*—karbonoks; *5*—lauryl sulfate; *6*—solamin; *7*—fluoroplastic; *8*—notched surface; **a** MF—steel 12Kh18N10T; **b** MF—duralumin D16T; **c** MF—copper M1

These arguments lay the groundwork for a fundamentally new approach to the creation of a modern generation of substitutes of natural SF on the basis of blood serum [109–111]. Like the lubricity of healthy SF, their lubricity improves under the effect of electromagnetic field. When used to lubricate a pendulum tribometer support, their mixtures with hyaluronic substitutes of SF demonstrate the minimal friction coefficient at the concentration $C = 50\%$. According to the data of [109, 110, 112], such concentration minima at $C = 50\%$ correspond to the formation of complex structures—similar to those existing in healthy SF—including macromolecules of proteins, hyalurates, and cholesterol liquid-crystal compounds (LCCC).

In this connection, the authors have attempted to explain the results with account for the modern views on a specific spiral layer structural organization of LCCC in the friction zone. According to these ideas, the treatment of a liquid-crystal lubricating film in a solenoid field apparently favors the optimal—i.e., entailing the lowest friction loss-orientation of LC films relative to the friction direction. The structure of the lubricating film without magnetic field is not optimal and it cannot be optimized under lubrication with physiological solution. It can be assumed that in vivo the optimal orientation of the LC-components of SF occurs under the effect of joint biofield.

Convincing evidence of such unique behavior of biological lubricants in the presence of fields is provided by the experiments carried out on a pendulum tribometer to reveal the influence of the polarization of the polymer support on the friction coefficient of the studied lubricants [113]. These experiments showed that the friction coefficient of the metal-UHMWPE pair lubricated with physiological solution remains constant with a high reproducibility, all else being equal, both with and without the electric polarization of the polymer support. Conversely, lubrication with SF makes the pair sensitive to the presence of the polarization charge in the support. It has been found that the friction coefficient decreases twofold if the support is polarized. This effect is observed irrespective of the means of support polarization—either by the thermoelectret method or in corona discharge. It is noted that if the polymer surface is negatively charged, the friction coefficient of the pair lubricated with SF is much lower than that of the pair with the positively charged polymer surface.

Thus, it is proven in works [109–113] that the natural lubricant of joints-SF—is sensitive to electromagnetic field variations and its magnetic susceptibility may depend on many factors, for example, the presence of joint pathology, as well as the age and other characteristics of the individual organism.

However, the possibility of active control over tribological parameters of friction units can be realized in engineering by using other methods, in particular, by applying electric fields. The authors of [114] note that the application of a constant electric voltage of up to 8 V on the lubricated with mineral oil a friction pair "ball - steel disc" changes the tribological properties of the friction pair mainly during its running-in. Similar results were obtained when passing constant electric current with a strength of up to 10 A through pure mineral oil which lubricated the friction zone between a bearing steel journal and a carbon steel support. Ultimately, this also favored more effective operation of the unit and caused noticeable changes in its tribological characteristics [115]. These processes were generalized as effects induced by the intensive formation of oxide layers on the friction surface. It can be said that these studies evolved with studies on the influence of electric charging in situ on the friction coefficient using zinc organodithiophosphate additives to motor oils [116]. The pin-bowl tribosystem was tested with both members made of tool steel and a constant electric voltage of up to 20 V was applied between the insulated pin holder and the bowl. The experimenters revealed the accelerated formation of a film from the active additives to oil on the friction surfaces, which led to a reduction in the friction coefficient maximum by 35%.

According to the modern data, the possibility of active control over lubricity can be realized more broadly in engineering, namely, not only by using magnetically susceptible fluids or special additives to oils which respond to electric current, but also by lubricating friction joints with electrorheological fluids (ERF). Tribologists throughout the world pay great attention to the solution of these crucial problems. It is found that if a fluid, e.g., mineral oil, is filled by dielectric microparticles with specific properties, the viscosity of this suspension can be varied by applying electric fields. It is shown in [117–120] that silica (SiO_2) particles are such high-effective dielectric microparticles-fillers. Their introduction into mineral oil in an amount of up to 50% yields quite flowable ERF in the form of a homogeneous suspension. It is noted that the application of electric field to such ERF changes their viscosity within a wide range. In other words, the ERF viscosity can be varied by changing the electric field strength; the localization of such control in the friction contact zone during lubrication with these ERF is implemented in a quite simple way, namely, by connecting the friction members to the opposite poles of a power supply with varying output voltage. To avoid short circuit the friction surfaces are additionally insulated with, e.g., polymer coatings or coatings like an alumina film, i.e., oxide-ceramic coatings.

It is found experimentally [119] that with increasing strength of the electric field induced in the clearance between the friction surfaces separated by ERF, the friction coefficient diminishes to a certain value and then grows slightly and stabilizes within a definite range. This can be explained by the fact that the lubricating film thickness increases and boundary friction transits to fluid friction as the electric field strength and the related ERF viscosity grow. This changes the mode of friction and reduces the friction coefficient. Simultaneously, resistance to motion due to ERF viscosity variations increases. This causes a slight augmentation of the friction coefficient. As a result, the growth of the voltage between the contacting surfaces covered with oxide-ceramic coatings yields nonlinear variations in the friction coefficient and the thickness lubricating layers. Nevertheless, according to the data of [119], a quite good correlation between changes of the friction coefficient and the thickness lubricating layers is observed.

Thus, the use of ERF based on mineral oils to lubricate friction joints whose contacting surfaces are covered with insulating oxide-ceramic coatings results in reversible changes of the sliding friction coefficient depending on the applied voltage. This makes it possible to provide effective control over the tribological characteristics of the joints owing to variations in the rheological properties of the lubricant and the transition of the tribosystem to elastohydrodynamic contact. The results show that the purposeful application of ERF makes it possible to develop friction joints with controllable tribological parameters—viscosity and thickness of lubricating films, friction force, etc.—and therefore to affect actively the improvement of the durability of such tribosystems, especially those undergoing frequent starts and stops, by means of greatly increasing their wear resistance.

The use of structure-sensitive substances, e.g., liquid-crystal (LC) compounds, as lubricants is another convincing proof of the possibility of active reversible control over the tribological characteristics of friction pars by applying electric field and of the effect of the latter on lubricant behavior [9, 100, 101]. Liquid crystals attract more and more attention of tribologists as potential lubricants with unique properties [85, 86, 95]. On the one hand, the anisotropy of the viscosity of LC compounds is of great interest to tribologists. On the other hand, the application of such compounds in watch and computer displays demonstrates clearly the possibility of varying their properties in wide ranges through the use of electric fields. This has resulted in the idea that, if the state of LC layers can be controlled by applying electric fields, active control over the friction coefficient of the tribosystems with these layers can be implemented. It can be achieved not only owing to viscosity variations, i.e., during hydrodynamic friction, but also during boundary lubrication, e.g., due to the abovementioned structure reordering of lubricating layers under the effect of electric fields [9, 101].

Detailed studies of a number of nematic LCs carried out on a rotation viscometer in uniform electric field applied across a LC film placed between rotating cylinders show that the LC viscosity can indeed change within a quite wide range (up to three times) as the electric field strength grows from zero and reaches saturation in quite strong fields (Fig. 2.11a) [2].

Since at temperatures in range of LC states at which the experiment was performed the nematic phase is characterized by molecular-oriented ordering (the director is parallel to the long axes of the molecules), the LC director also tends to become parallel to the field direction. However, this increases additionally the resistance of the LC during its flow between the rotating cylinders since it flows across the field direction; this ultimately yields a quite great growth of the viscosity. This effect is called the electroviscous effect. The results also show that the viscosity of such nematic LC systems at mesomorphic state temperatures depends on the shear rate but within a much narrower range than in the case of electric field application. Since the lubricant viscosity is the dominating factor for the friction coefficient during hydrodynamic lubrication and the data of [9, 100, 101] demonstrate clearly that the viscosity of nematic LCs can be varied within a wide range by applying electric field, the real possibility exists of using such LSs as lubricants to provide active control over the tribological characteristics of tribosystems during hydrodynamic friction.

However, more detailed studies show that the effect of active reversible control over the friction coefficient of the tribosystems with nematic LCs can also be realized during boundary friction [9, 101]. In particular, the pendulum tribometer was used to test a pin 2 mm in diameter and 30 mm long—the expected contact spots on the pin surface were covered with a SiO_2 thin insulating film—in pair with four bearing balls 4.76 mm in diameter made of tool steel and immersed in a bath filled with the nematic LCs under testing. The active effect of the applied electric voltage (up to 30 V) on the friction coefficient of the pair has been found (Fig. 2.11b). It is shown that there is a threshold electric voltage (about 5 V in this case), below which the relative friction coefficient diminishes considerably until reaching ≈0.75 at 30 V. It is noted that this change in the friction coefficient with

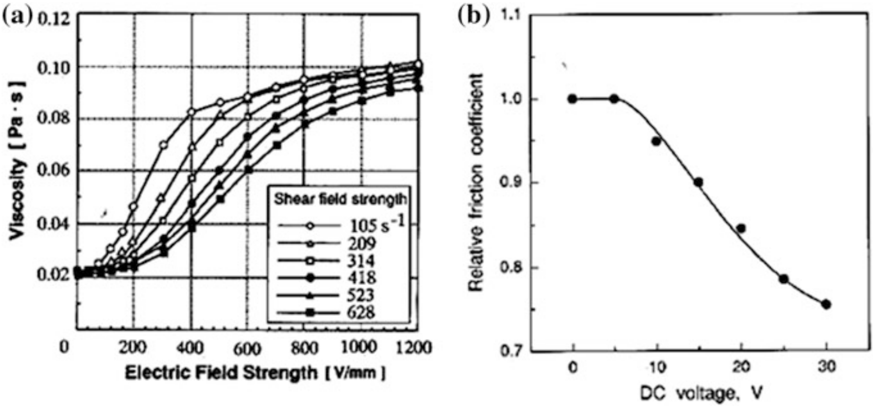

Fig. 2.11 Electroviscous effect (**a**) and decrease in relative friction coefficient of samples of nematic LCs depending on applied electric voltage (**b**) within temperature range 30–40 °C [100, 101]

varying electric voltage is reversible: upon application of an electric voltage of, e.g., 20 V, the friction coefficient decreases by ≈18%, while it reaches its initial values after voltage disconnection.

Thus, the authors of works [9, 100, 101] proved convincingly that nematic LCs have a unique peculiarity: their viscosity and friction force can be changed through the use of electric fields across the LC films; the fields provide active and reversible control over the friction force directly during the friction of solids. The practical application of such tribosystems will apparently expand with the evolution of the technology of LC compounds, first of all, with account for the achievement of the required antifriction characteristics and the reduction of LC cost.

2.3 Effect of Lattice-Ordered Lubricant Film on Friction of Solids

Now it is fully certain that the lubricating effect of substances most closely relates to their nature and the complex of phenomena evolving during lubrication of the solid body surface [85]. As a rule, the lubricating material is adsorbed on the solid body contact. As it was observed already in the epoch of formation of the classic theory of capillarity, the appearing properties of the adsorption layer differ from the volume properties of the substance. The idea of the boundary state of matter was intensively developed in the twentieth century by Adam, Devot, Marceline, Frumkin, Rebinder, Deryagin et al. The problem of boundary friction was furthered by Hardy, Deryagin, Rebinder, and Bowden.

2.3.1 Structure of Fine Fluid Layers on the Solid Body Contact

Direct studies of the structure of adsorption films by the method of X-ray diffraction revealed that a layer 10–100 nm directly on the solid contact has its molecules oriented. According to [121] this orientation appears in the boundary layer of a non-polar oil when polar molecules of a fatty acid are added. A. S. Akhmatov in his classic works formulated the idea about the smectic-like structure of fatty acid layers. The fatty acid dimers produce the smectic layers and they are bimolecular [121, 122]. B. V. Deryagin applied his own method of boundary-layer blowing to the method of vapor adsorption [123] and demonstrated that the boundary properties of polar substances change rather in leaps than continuously as they move away from the contact until certain thickness is reached. A relatively high resolution of the blowing method enabled to establish that non-polar substances, e.g., highly pure Vaseline oil, retain constant viscosity equal to the volume viscosity when approaching to the substrate to a distance ≈1 nm [124]. Taking into account that viscosity is a structurally sensitive property of a fluid, it was concluded that no structuring existed in the interface between the solid substrate and the Vaseline oil layer. In contrast, polar fluids or fluids containing polar additive do not reveal any change in the viscosity of the layer 10–100 nm thick.

A specific state of the fluid in the boundary structured layer was called by B. V. Deryagin the "boundary phase" Later it was called the epitropic liquid-crystal phase.

Development of methods of dichroism in intensive absorption bands [125] led to a new level of studies of boundary layers. It is due to the fact that it enables to determine the thickness of the structured layer, to find the pattern of its transition into the volumetric isotropic fluid, the type of the order of molecules in the layer adjacent to the wall, ad the parameter of the structural order.

The method is based on the dependence of the light absorption coefficient on the orientation substance molecules in respect of the light wave vector of the absorbing oscillator. In a majority of cases, the direction of the absorption oscillator coincides with the direction of the longer axis of the molecule. Then, according to [126], when the structure is homeotropic and the light is normal to the layer the coefficient of absorption $\mu_\perp$ is minimal because, when the direction of oscillations of the electric vector of the light wave is perpendicular to the structure orientation, the absorption of natural light is determined by the averaged absorption coefficient:

$$\mu_{\mathrm{area}} = 1/2(\mu_\parallel + \mu_\perp), \tag{2.1}$$

where $\mu_\parallel$—the maximum absorption coefficient observed when the plane of oscillations of the electric vector of the light wave is parallel to the absorption oscillator. The absorption coefficient of an isotropic fluid is determined according to [126] as:

$$\mu_0 = 1/3(\mu_{\|} + \mu_{\perp}) \tag{2.2}$$

In case of axial symmetry of absorption the ratio between the coefficients of absorption of the natural light, homeotropic, planar oriented structures and isotropic fluids is the following:

$$\mu_{\perp} < \mu_0 < \mu_{\text{area}}. \tag{2.3}$$

According to the laws of Lambert-Booter the dependence of the logarithm of intensity of the passed light (ln *I*) on the thickness of the drug layer *d* of a uniphase system has a linear pattern:

$$\ln I = \ln I_0 - \mu_0 d, \tag{2.4}$$

where I_0—intensity of incident light; μ_0—the absorption coefficient from the experimental data is determined by the tangent of the angle of inclination of dependence (2.4) to the abscissa angle. Incase of structural inhomogeneity of the preparation the absorption coefficient according to (2.3) does not remain constant and dependence (2.4) is violated. When there is a structured fluid layer adjacent to the contact with the substrate boundary, the light absorption coefficient, when $\mu' \neq \mu_0$, dependence (2.4) becomes:

$$\ln I = \ln I_0 - \mu' d \quad \text{at}\, d < d_{\text{bond}}$$

and

$$\ln I = \ln I_0 - \mu' d_{\text{rp}} - \mu_0 (d - d_{\text{rp}}) \quad \text{at}\, d > d_{\text{bond}},$$

where d_{bond}—the thickness of the boundary of the structured layer.

In the simplest case, when μ' is constant within the boundary layer there is an interface between the structured boundary layer and the volumetric fluid. The graph of dependencies ln $I = f(d)$ is broken, convex or concave depending on the ratio between the values μ_0 and μ' (Fig. 2.12). In case of inconstancy of μ' within the boundary layer, i.e. when $\mu' = f(d)$, the initial portion of the dependence ln $I = f(d)$ is nonlinear, and when it is approaching to d_{bond}, it becomes smoothly a straight line (Fig. 2.12c). If the boundary structured layer turns gradually into a volumetric fluid, the dependence ln $I = f(d)$ within the region d_{bond} has a transition portion Δd (Fig. 2.12d).

Thus, from the experimental dependencies of ln *I* on the thickness of the preparation layer the thickness of boundary structured layers, their structural homogeneity and the pattern of transition from the boundary layer to the volumetric fluid can be determined. The values of light absorption coefficients of the boundary layer μ' and the volume of fluid μ_0 calculated with the experimental dependencies ln $I = f(d)$, with the account of relation (2.3), enable to determine also the type of orientation of molecules in the boundary layer and calculate the structural order

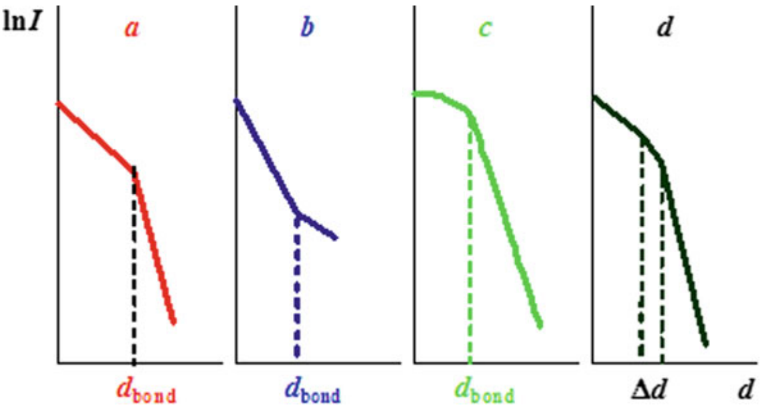

Fig. 2.12 Dependence of logarithm of intensity of light that passed through fluid layer on its thickness: **a** homeotropic orientation of boundary layer; **b** planar orientation of boundary layer; **c** complex structure of boundary layer; **d** smooth transition of homeotropically oriented layer into volumetric fluid

parameter S in it. The later relates to the dichroic coefficients $N = \mu_{||}/\mu_{\perp}$ through expression [126]:

$$S = (N - 1)/(N + 2). \tag{2.5}$$

From relations (2.1), (2.2) and (2.5) it follows that:

$$S_r = 1 - \mu_{\perp}/\mu_0; \quad S_{area} = 1 - \mu_{||}/\mu_0,$$

where S_r, and S_{area}—parameters of the structural order of homeotropic and planar structures, respectively.

The experimental dependencies ln $I = f(d)$ are obtained by scanning of the wedge-like beaker full of the substance in question with a light beam. The experimental bench and methods of investigating the structural properties of fine fluid layers are described in [125].

Application of this method has revealed [127, 128] that the polar nitrobenzol lyophilized chromic acid produces in contact with quartz wall boundary layers 55 nm thick that show homeotropic orientation of molecules. The parameter of the structural order in the layer at temperature $T = 295$ K is $S = 0.27 \pm 0.01$. Any higher temperature reduces the layer according to the linear law (Fig. 2.13). The structured wall boundary layer becomes thinner too.

If the quartz contact is lyophilized with hydrogen flame instead of the chromic acid, the parameter a of the structural order and equilibrium boundary phase increase [127].

Similarly like nitrobenzol produces the epitropic phase, so do other ion-substituted benzols, such as aniline, acetophenol. Their molecules become in

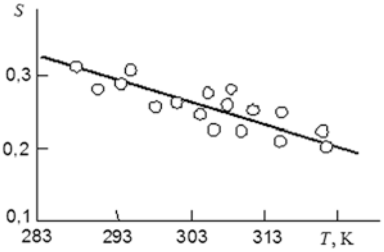

Fig. 2.13 Dependence parameter of S of boundary phase of nitrobenzol on temperature (surface is lyophilized with chromic acid) [127]

the epiphase structured homeotropically so that the plane of the benzol ring disposes normally to the contact quartz substrate. Further studies using thee method of dichroism of intensive absorption bands [129] have revealed that the homeotropic order and the thickness of the epiphases of homological series of benzoic acid esters ($C_6H_5CO_2(CH_2)_nCH_3$, $n = 0, 1, \ldots, 8$) increase as the concentration of carbon in the substitutor chain grows. Formation of the epiphases by weak polar benzoic acid esters has permitted the authors [129] to conclude that the polarization anisotropy plays an essential role in emergence of the epitropic phase rather than the rigid molecular dipole. Investigation of the epiphases of the chlorine-substituted benzol have revealed (Table 2.2) that there is no direction correlation between the magnitude of the dipole momentum of the molecules P_e, the parameter of the structural order S and the equilibrium thickness of the structured wall layer d.

Application of the method of dichroism in intensive absorption bands is attractive for studies if features of the structure liquid crystals in a superfine layer on the solid substrate [130, 131]. These studies were performed using nematic liquid crystals at temperatures near the point of transition of liquid crystals from the mesophase into the isotropic phase.

The authors [130] established strongly polar cyanobiphenyl (CB) in the mesomorphous phase having the general formula

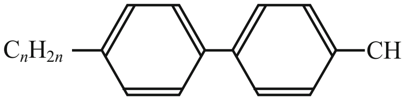

$n = (5, 7, 8)$

in a layer thinner than 80–90 nm have a high order strength, unlike the weakly polar MBBA (4-methoxybenzylidene-4′-n-butylamine). When the layer becomes thicker from 80 to 160 nm all the liquid crystals tend typically to lose the order

Table 2.2 Characteristics of epiphases of chlorine-substituted benzol [129]

Parameter	C_6H_5Cl	$C_6H_5CH_2Cl$	C_6H_5COCl	$CH_3C_6H_5Cl$
P_e	1.69	1.84	3.23	1.95
S	0.36	0.2	0.2	0.28
d (nm)	90	50	50	60

strength. The order strength of thicker layers remains unchanged after apparently reaching the values typical for the liquid crystal phase in the volume. Thus, the wall layer of liquid crystals has larger order strength versus the liquid crystal phase in the volume. The authors [130] attribute the different order strengths of fine layers of weakly and strongly polar nematics to the contribution of the permanent dipole moment into the orientation order and to dipole–dipole interactions between adjacent molecules. It is assumed also the limiting contacts play in narrow gaps the role of an external field that produces a stronger orienting effect than the molecules with a large constant dipole moment.

The fact in [130] is worth attention that one of the studied liquid crystals (8CB) is in the smectic phase at the temperature of the experiment and not in the nematic phase. However, the order strength of all the liquid crystals in the fine layer (<80 nm) has one and the same value. The fact that strongly polar nematics in the narrow clearances have the same order strength with the smectics proves it. Moreover, the order strength of the liquid crystals in question is independent of the temperature when the layer is <80 nm permitting to assume that the order strength in the contact with a solid body is sooner determined by the interaction of the liquid crystal with this surface than by the order strength in the liquid crystal volume. The structuring effect of the hard contact on the attached liquid crystal layers survives even at temperatures exceeding the temperature of transition from the mesophase to the isophase ($\mathbf{T_c}$) by several tens of degrees.

According to [131] the thickness and order strength of liquid crystals 5CB and 8CB in the wall layer are much higher than in the liquid crystal films >1.0 μm thick. When the overheating is increased $\Delta T = T - T,$ the structured layer becomes thinner and the degree of orientation of molecules within the layer decreases. However, intimately in contact (d = 20 + 30 nm) it remains still sufficiently high (Fig. 2.14) and exceeds the order strength of нemesogenes in the layer of the indicated thickness. Unlike the latter for which a distinct boundary is typical between the structured layer and the volumetric medium, it is not manifest in mesogenes starting from ΔT = 10 K.

Comparison of the dependencies in Fig. 2.14a, b, shows that the liquid crystals planar-oriented in the mesophase produce ordered layers in the isophase thinner than those that were previously oriented homeotropically.

From Fig. 2.15 it follows that the difference of thicknesses of the layers reduces as the overheating ΔT grows.

The thicknesses of the ordered wall layers of the planar orientation in the mesophase are almost two times less than the homeotropic ones. From study of the regularities of structural changes in wall layer, the authors [131] established that the pre-oriented planar specimens of liquid crystals in transition from the mesophase into the isophase pattern change orientation. The planar orientation in such transition transforms into the homeotropic orientation. The planar orientation in the liquid crystal phase, according to modern ideas, is due to reduction of elastic energy of mesogenous molecules that arrange along the grooves of the ordered microrelief of the substrate. The achievable energy gain is insignificant. It reduces strongly

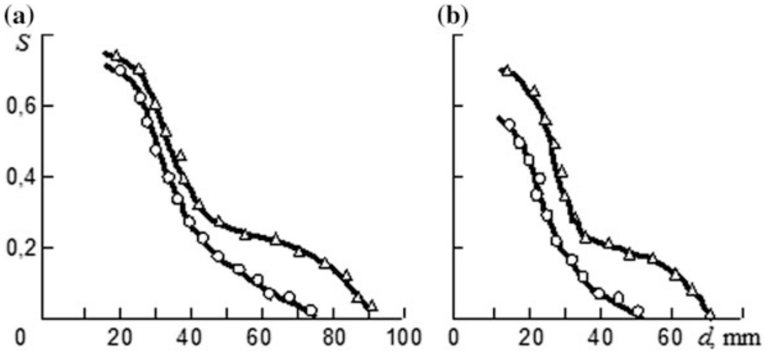

Fig. 2.14 Dependence of parameter of orientation order *S* on thickness of wall isophase liquid crystal layer *d* in original (in mesophase) homeotropic (**a**) and planar (**b**) orientation: **a** overheating of preparation ΔT = +3.1 K (*1*) and +8.3 K (*2*); **b** overheating of preparation ΔT = +0.8 K (*1*) and +6.5 K (*2*)

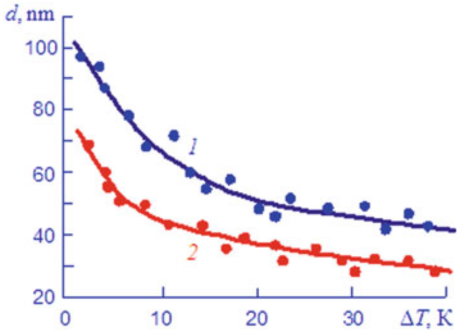

Fig. 2.15 Dependence thickness of boundary oriented ordered layer on overheating ΔT of drug pre-oriented homeotropically (*1*) and planarly (*2*)

during transition into the isotropic fluid phase due to the lessening of the moduli of elasticity as the temperature grows and a more energy gainful homeotropic orientation occurs.

Summarizing the above results of studies of structural characteristics of a fine layer of liquid substances in contact with a solid body the following conclusions can be drawn:

- the solid body surface produces a structure organizing effect on the interfaced fluid layers at least 100 nm thick;
- lyophilic surfaces of non-mesogenous substances with polar and asymmetric molecules acquire ordered boundaries with the surface of solid body layers. Polarization anisotropy plays a governing role in the appearance of these layers rather than the presence of a rigid molecular dipole;
- the ordered boundary layers of non-mesogenous substances have a finite thickness and they are confined by an unstructured fluid interphase boundary region;

- the order strength and thickness of the boundary layers of non-mesogenous substances reduce as the temperature rises;
- mesogenes in the liquid crystal phase in contact with a solid body are better ordered than in the volume, the structured layer being thicker than in the isophase;
- the order of the boundary layer of mesogenous substances withstands the temperatures exceeding the temperature of transition from the mesophase into the isophase. The thickness and order strength of these layers in the isophase changes in response to temperature similarly to the non-mesogenous substances;
- the layers of mesogenes oriented homeotropically in the mesophase become thicker during transition into the isophase as the temperature rises than the planar oriented layers;
- the planar orientation of molecules of mesogenes in the boundary layer to the homeotropic one during transition into the isophase as the temperature rises.

2.3.2 Surface Forces in Fine Fluid Interlayers

The above regularities of the behavior of mesogenous and non-mesogenous substances in a fine layer directly contacting a solid body are due to a complex of surface forces including electrostatic, molecular, and structural ones. Since the boundary structured fluid layers have finite dimensions, two situations of relatively structured surface forces are possible in the fluid interlayer between the surfaces of solid bodies as a function of spacing between them. Figure 2.16 shows them schematically. In the first case, the clearance L between the surfaces exceeds

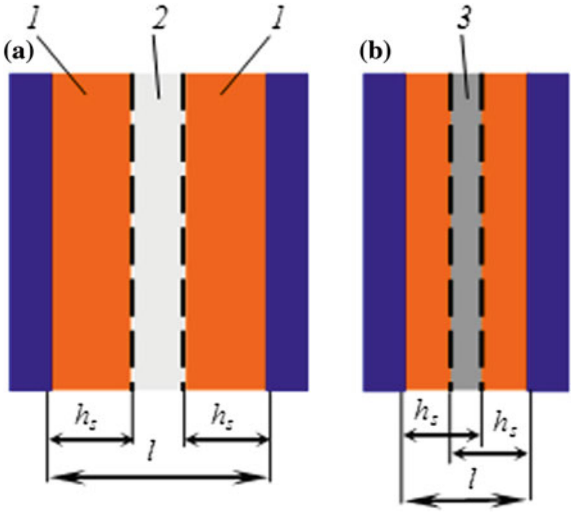

Fig. 2.16 Interaction of surfaces with structured and boundary layers when they do not overlap (**a**) and when they overlap (**b**): *1*—structured boundary layer; *2*—layer with volumetric fluid properties; *3*—region of overlapping of structured boundary layers

significantly the total thickness h_s of the structured boundary layers 1 ($L > 2h_s$). There is a fluid interlayer 2 in between with the properties that it has typically in the volume. In this situation, the surfaces interact due to electrostatic and molecular forces. The structured boundary layers can influence just the dispersive component of the molecular forces by changes in the frequency dependence of dielectric permeability when its structuring occurs and it becomes anisotropic.

In the second case of contact the solids approach mutually so much that the interlayer with the properties of a volumetric fluid is forced out and the boundary structured layers overlap.

It is apparent that the overlapping of boundary-structured layers is determined by the re-organization of their structure. The depth of restructuring is governed by the degree of overlapping of boundary-structured layers and is accompanied by destruction of a part of their volume. It changes the free energy of the system in question and to the appearance of structural forces [132–134]. Hence, in the situation in question, the surfaces interact both due to the electrostatic and molecular forces and to the structural forces too. It is noteworthy that, when the thickness of the interlayer L changes, the electrostatic and molecular forces can change too. However, the extent and range of action of the structural forces can exceed the surface forces of interaction between solids in the vacuum.

The above situations of intercontact interaction between the surfaces separated by a fluid interlayer relates utterly closely to the problem of boundary friction. A number of fundamental works [121–124, 132 etc.] has been accomplished to this end, however, those that appeared in the last decade contains the results of studies of surface forces attractive for tribologists. Therefore, we will discuss some of them relating to intercontact interactions in finest fluid interlayers. This matter is exhaustively discussed in [132].

The new results in the sphere of surface forces became feasible because of the experimental equipment developed by the authors of [135]. Two crossing glass cylinders are the main unit of their instrument, their working contact is covered with micaceous plates (the ruby-red muscovite) (Fig. 2.17). This choice is due to the

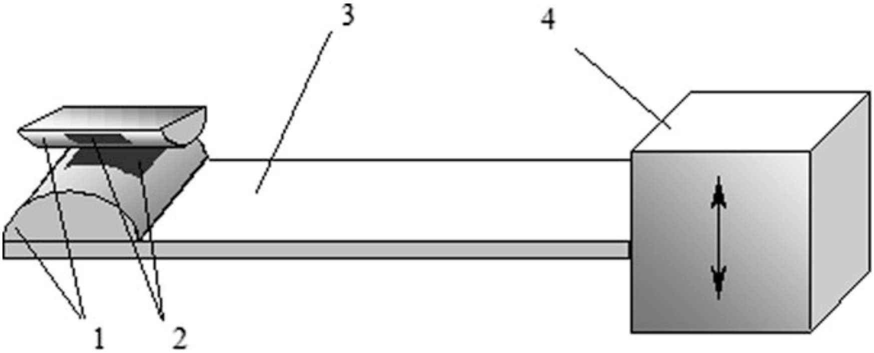

Fig. 2.17 Diagram of device for measuring forces of interaction between smooth: *1*—glass lenses with cylindrical working surfaces; *2*—mica plates; *3*—spring; *4*—its movable adjustable support

rigidity and chemical inertness of mica and by a chance to produce molecular-smooth surfaces when the mica crushes. The latter fact enables to achieve highly sensitive measurements and strongly reduce error.

The cylinders have the radius 1 cm. The distance between them is measured with an optical interferometer. The mica plates have the side facing the cylinder coated with silver to provide 95% reflection.

The optical system resolves the white light passing through the cylinders and the clearance with the fluid into components. Thus strips of equal thickness and of the same order of magnitude appear. The scheme enables to measure clearances up to 0.2 nm. A video camera at the spectrometer outlet serves for dynamic measurements; it records the motion of strips and reads time. A videorecorder registers the light wavelength. These features of the instrument enable the accuracy of measurement of the clearance ±0.1 nm.

To measure the forces of interaction one cylinder is mounted on a cantilever spring. Before measurements the cylinders are brought into contact in the nitrogen medium, then they are together with the spring are immersed into the fluid to be measured. The opposite end of the spring is driven (vertical oscillations) by a mechanical drive or a ceramic piezzotransducer.

It is a quite common idea based on the results of the fundamental work of B. V. Deryagin that surface forces between bodies recede as the spacing between them grows. However, application of the above method to measurements of surface forces between molecular-smooth mica surfaces revealed that this dependence is more complicated, specifically in case of small clearances (<10 nm) when structural forces come into play. Studies of polar and non-polar compounds, solutions and melts of polymers, smectic and nematic liquid crystals, revealed that in the majority of low-molecular substances the oscillation forces of interaction change together with the clearance within the indicated range [136, 137].

According to [138], for the series of *n*-alcanes from hexane to hexadecane the dependence of forces of interaction F between mica surfaces on the clearance L between them has an almost identical pattern. Variations of F are observed at $L < 3$ nm. At larger L the variations attenuate; the curve of dependencies $F = f(L)$ smoothly approaches to zero. The periodicity of the variations correlates with the mean diameters of molecules. This regularity permits to assume that the molecules of the n-alcanes in the boundary layer arrange in a parallel contact.

Non-polar low-molecular forces of the iconic fluid OMCTS (octamethyl cyclotetrasil oxane) have shown the same pattern of orientation of molecules and changes in the forces of interaction as the clearance reduces [139]. The dependence $F = f(L)$ both for them and n-alcanes shows not more than these minima (Fig. 2.18) that follow with the periodicity 0.8 nm corresponding to the mean diameter of OMCTS molecules. The study in [140] is worthwhile to discuss because one mica plate was replaced with a silver plate and the same non-polar OMCTS fluid was used.

Application of a metallic contact did not alter the results of measurements. They are practically the same like in the case of two mica surfaces. The differences were in reduction of the amplitude and range of oscillations in response to L. The latter

Fig. 2.18 Dependence of forces of interaction of surfaces lubricated in octamethylcyclotetrasiloxane on clearance: *1*—empirical ependence, *2*—dispersive attraction

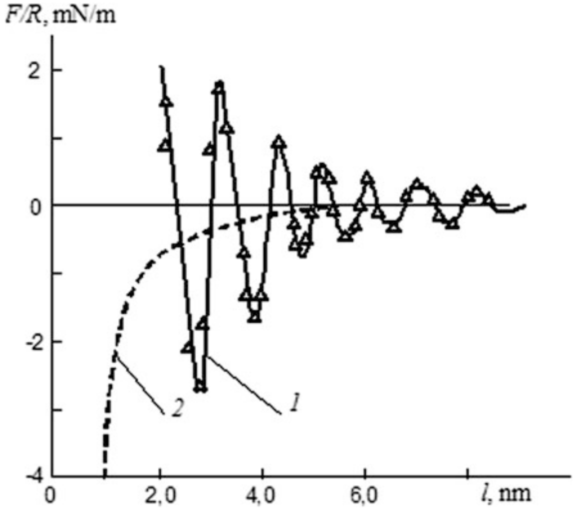

did not exceed 5 nm in this case. The rough microrelief of the metallic contact my cause it. The authors [140] believe that this factor and physical adsorption on the silver contact increasing the edge angle of its wetting with water may cause weak forces of interaction between the surfaces 40 mN/m versus 600 mN/m that two lubricated surfaces have.

The surface forces in polar fluids reduce to the electrostatic forces of repulsion in double electric layers and dispersion forces of attraction. The ideas about the additivity of these forces are supported by a number of experimental facts. One of them is the stability of weak aqueous colloid electrol solutions. Another proof was provided by the method of contact interactions between mica plates. However this method revealed also the inconsistency of ideas about the additivity of electrostatic and dispersion forces in fine, of the order of several nanometers, interlayers of polar fluids. It was shown that the forces vary with the above values of the clearances.

The interaction between mica surfaces in acetone (the dielectric permeability $\varepsilon = 21$ and dipole moment $p = 2D$) and in methanol ($\varepsilon = 33$, $p = 1.7D$) was studied in [141]. No electrostatic repulsion was discovered in the acetone, meanwhile weak and strong oscillating forces of attraction were discovered at large distances. No monotonous forces of attraction were observed. When mica surfaces converge at $L < 4.6$ nm, significant forces of attraction appear, then they converge in leaps to a distance of 2 nm, afterwards oscillations begin. Their period is 0.45 nm; it is quite close to the diameter of acetone molecules (0.46 nm). A similar pattern of changes of forces of interaction between mica surfaces was established in the methanol and propylene carbonate, a strong polar fluid too [142]. The latter has the dielectric permeability $\varepsilon = 65$, the dipole moment $p = 4.94D$ and is free of hydrogen bonds.

The method [135] was applied to a study of surface forces in liquid crystal interlayers [143]. The nematic 5CB and smectic 8CB liquid crystals were studied.

The homeotropically oriented 5CB showed loss of the monotonous growth of the forces of repulsion to $L = 15$ nm and appearance of five oscillations forces when L declines. The amplitude of oscillations grows exponentially. The period of oscillations is 2.5 nm coinciding with the length of molecules. In case of planar orientation of the molecules 5CB the three first oscillations have the period 0.5 nm (it corresponds to the diameter of molecules), later it increases to 0.6 nm. It is due to a larger motility of the molecules outward of the contact. The nematic 8CB at small distances also show intensive oscillations throughout five monolayers with a period equal to the diameter of molecules. When the clearance increases still more, the oscillations, though more dithered, have a high enough amplitude and remain up to an order of several micrometers until considerable clearances. It proves that, unlike the nematics, the laminar structure of the smectics is manifest both near the contact and at a considerable distance from it.

It is noted above that the structural forces include the forces that appear when the boundary structured layers overlap in the contact between solid bodies. The oscillating forces due to the discreteness of the substance structure also belong to the structural forces because they appear when boundary layers overlap. However, they differ from the structural forces by the range of action relating to changes in macroscopic properties of the fluid (heat capacity, dielectric permeability, etc.) in the boundary layers when they overlap. It is also possible that, in case of very fine fluid interlayers ($l < 2$ nm), the oscillating forces come to rule in the complex of structural forces due to the substance structure discreteness.

2.3.3 Effects Observed During Deformation of Structured Boundary Layers

The interaction oscillation forces relate to the thermodynamic efficiency of filling of the interlayer thickness with an integer number of molecular layers and to the instability of “fractional” states. Because of this, when the values L, of the multiple thickness of a monolayer d_0 (d_0 can equal the length or the diameter of molecules making up the boundary layer), the interlayer resists both thinning and thickening. In this case, it is thermodynamically stable. When L is not multiple of d_0 and has “fractional” values, the interlayer spontaneously tends to proceed into the state with the number of layers multiple to d_0 by thickening or thinning. This state of the interlayer is unstable. It was observed experimentally in [143]. When a fine interlayer is compressed, the smectic A between micaceous molecular-smooth surfaces is extruded in leaps in layers with a period 3.1 nm equal to the monolayer thickness. It was preceded by accumulation of 1–2% elastic compressive deformation. In tension the interlayer thickness grows in leaps with a period 3.1 nm due to drawing in of new моноlayers and after accumulating of come elastic deformation.

According to [122, 136] each monolayer possesses the properties typical for a fluid in its plane. As a whole, the system of such layers manifests the properties of the solid body in compression or tension in the direction normal to the layer. The modulus of compression or tension in this direction has an order of magnitude of 10 N/m for the smectic *A* and 10 N/m for the smectic *C*. During extrusion of layers from the interlayer, when interlayer shear occurs, the smectics *A* and *C* behave like a mean viscosity fluid. It is possible that this feature determines good lubricating properties of smectic like surfactant layers.

A sudden compression of the smectic in the direction normal to the layer results in a leap of stresses in the layer. However, they gradually relax almost exponentially. The time of relaxation is hundredth fragments of a second. It is apparent that smectic layer gets restructured within this period, e.g., by forcing out the monolayer, migration of molecules from one monolayer into other layers. It is believed that the median part of the compressible layer remains motionless. Changes, flow (possibly nematic too) in particular occur due to defective layers directly attached to the solid body [144].

The dislocation mechanism of flow of the smectic A during normal compression by the layer is validated in [145].

In a dynamic contact, the lubricating layer separating the friction contact is exposed to both compression and shear. Hence, the result in [146–148] are certainly appealing since they deal with the behavior of cholesteric liquid crystals in shear within a narrow clearance between limiting surfaces.

A mixture of cholesteryl chloride and cholesteryl oleyl carbonate was studied. Each of selected crystals had the melting temperature within ±1 °C of the known values. The specimens were prepared by mixing the melt of the original components. The obtained composition had a broad range of temperatures of the cholesteric mesophase, including the room temperature.

The studies were carried out with a Weissenberg modified rheometer. The standard cone and plate were replaced with two glass disks 15 cm in diameter. The disks were glued to the metallic cylinders that served to insert the new measuring system into the rheometer. The glass disks were adjusted to make then coplanar, then they were installed at a distance 100 μm one from the other. Structural changes in the liquid crystal were identified spectrometrically. For this purpose the transparent glass disks with the liquid crystal in the clearance between them were placed in the path of light through the spectrometer between the monochromator and the emission detector (Fig. 2.19).

They were arranged so that their plane would be normal to the light incidence. Measurements were performed within the wavelength range 450–750 nm. The intensity of light passing through the liquid crystal specimen depended on its wavelength and shear rate that varied within 10^{-3} to 10^{3} s^{-1}.

In addition to the spectroscopic studies the interlayer of cholesteric liquid crystals between the glass disk was examined visually and checked by polarization microscope in order to identify the appearing textures. Alongside the rheological properties were checked that appear during shear of the textures.

Rheometric measurements [146] have revealed that the cholesteric liquid crystals change their rheological nature in response the shear rate (Fig. 2.20). when the

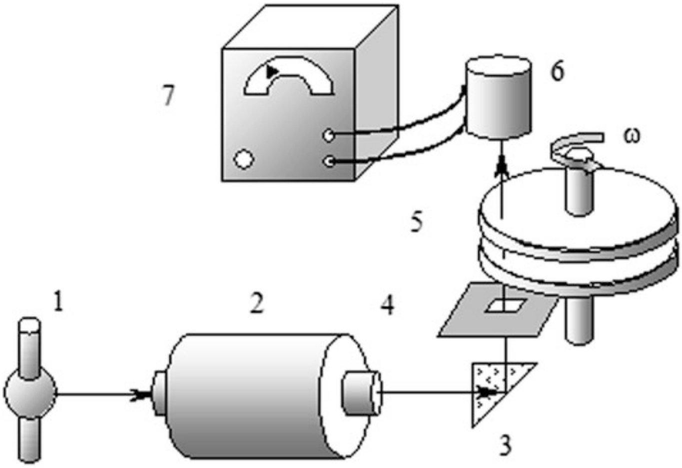

Fig. 2.19 Diagram of rheometer–spectrometer: *1*—light source; *2*—monochromator; *3*—full reflection prism; *4*—rotating glass disks; *5*—emission detector; *6*—indicator

Fig. 2.20 Dependence of relative viscosity logarithm ($\Delta\tau/\omega$) on speed of rotation of disks with clearance filled with liquid crystal: $\Delta\tau$—reaction of torsion moment meter of rheometer–spectrometer; ω—speed of rotation of disks, r.p.m

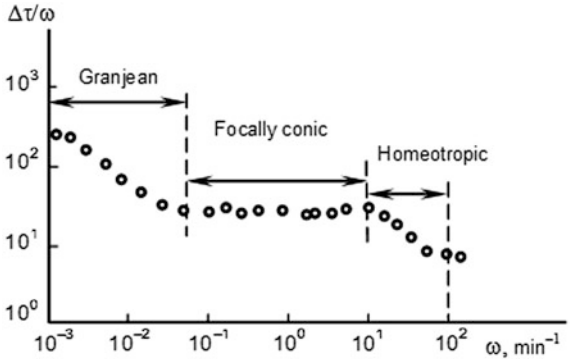

shear rate is high or low they behave as non-newton fluids, when the rte is intermediate they behave as newton fluids.

Low shear rates exist within the non-newton region and Granjean textures appear characterized by normal limiting surfaces of location of the cholesteric spiral axes. These textures possess high reflectivity. When the shear is zero the maximum reflection or minimum transmission of the Granjean texture is within the “red” spectral band [147] (Fig. 2.21).

Low shear rate move the minimum of transmission towards the blue spectrum. When shear ceases the minimum relaxes towards the original spectrum band. These changes in the spectra of transmission of the cholesteric mesophase when the shear is applied are explained in [148] by deformation of the axes of cholesteric spirals of the Granjean textures in the direction of shear. The fact of relaxation of the

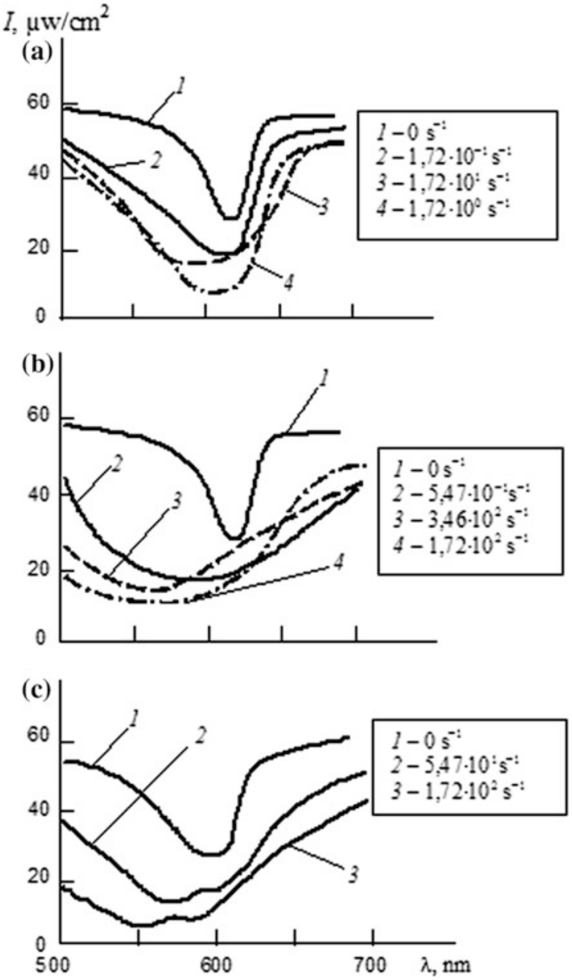

Fig. 2.21 Spectra of transmission of compositions of cholesteryl chloride and cholesteryl oleyl carbonate at different speeds of rotation of disks and ratio of components 20:80 (**a**, **b**), 27.2:72.8 (**c**)

minimum in the spectrum transmission when the shear is absent has compelled the authors to conclude that the cholesteric spirals responds to the shear rate less than 10 s^{-1} as a rigid rod.

In case of intermediate shear rates (>10^{-3} c^{-1}) the transmission spectrum has two minima that were clearly observe in [140] for the composition with 27.2% by mass of cholesteryl chloride and 72.8% of cholesteryl oleyl carbonate. One of them corresponds to the minimum in the spectrum when there is no shear, the second is displaced towards the short wave band волн. This spectral pattern is attributed to a combination of textures of cholesteric liquid crystals in the clearance between the glass disks. The major part of the clearance is occupied by dynamic focally conic textures, the region near the surfaces disks—Granjean or Granjean inclined structures. The dynamic focally conic textures produce dominating effect and govern the newton pattern of behavior of liquid crystals at shear rates. The minimum transmission spectrum within this region does not relax from the blue band into the red original spectral band when the field is removed implying that the dynamic focally conic textures produced by shear are stable in time. According to [146] these textures had existed for during 15 h after the shear ceased without any evident change. Rheometric measurements revealed that the viscosities produced by the shear rate acceleration and its reversal to the low shear range region differ. The viscosity of shear-produced dynamic focally conic textures at low shear rates is less than the viscosity of non-newton Granjean textures, existing in the liquid crystal that was not exposed to displacement or shear with a low rate. However, after opening of the glass disks with liquid crystal specimens and their repeated convergence the viscosity values within the region regain the values typical for the Granjean textures.

Dynamic focally conic and homeotropic textures are observed through the rotating glass disks visually within the range of high shear rates (>0.17 s^{-1}). They arrange in concentric rings. Homeotropic and the inner ring form the outer ring by dynamic focally conic textures. The interface between the textures is distinct and displaces toward the axis of rotation when one disk accelerates in respect to the other. When shear ceases the textures and the interface are observed during several days with the same distinction.

Displacement of the interface between the dynamic focally conic and homeotropic textures as the shear rate changes served to measure the viscosity of liquid crystals. The results of calculation and experimental results have shown that the former has the viscosity 1.6 and the latter 0.65 Pa s. The viscosity the homeotropic textures drops as the shear rate grows. At the same time, the viscosity of the dynamic focally conic textures does not depend on the rate. It is apparent that these changes in the nature of dependence of viscosity on shear rates in the region of transition of dynamic focally conic textures into homeotropic textures are due to a change in the rheological nature of the liquid crystal. It is remarked above that the homeotropic textures are non-newton fluids.

An assumption is made in [147] based on the results of spectroscopic studies and dynamic changes in the textures of the cholesteric liquid crystal composition during variations of the shear rate that the liquid crystal interlayer consists of 5 layers if the rate is >3 s^{-1} in the region of newton fluids. There are two non-inclined Granjean directly attached to the glass disks, two inclined Granjean interposed between the non-inclined layers, and one middle layer of dynamic focally conic textures. The axes of cholesteric spirals in the middle layer lie in the shear plane. Such arrangement has an irreversible pattern even at still lower shear rates.

It is noted above that the dynamic focally conic textures transform into homeotropic at shear rates exceeding 1.1×10^3 s^{-1}. They appear when the shear energy is sufficient to overcome the cohesive forces in the cholesteric spiral, i.e. friction its rupture and fragmentation with a spiral arrangement of molecules. The length of the fragments is a function of the applied shear rate. It is demonstrated in [148] that this growth of the shear rate shortens the spiral fragments from approximately 40–20 nm. The ultimate length that the authors of the referred paper observed was

10 nm. However, it is due to the maximum limit of the rate on the experimental bench. At very high shear rates it is assumed in [148] that the fragments can be substantially shorter, the homeotropic textures after destruction can result in fragments during intensive shear that are even possible with the composition of cholesteric liquid crystals in question in the isotropic phase.

Along with the described regularities of dynamics of transitions of the textures and changes in the rheological properties of the cholesterics under the effect of shear stresses it is undoubtedly peculiar for tribologists how the normal stresses appear that described in [146–148] that tend to increase the clearance between the glass disks. Their appearance is due to the effect of Weissenberg when a non-newton fluid tends to "creep" over the rotating shaft immersed into the fluid instead of being pushed away by centrifugal forces. The effect of Weissenberg is observed also, when the fluid rotates and the shaft or another subject stays motionless and the fluid tries to expel it.

According to [146] the magnitude of the normal stresses in the above-described compositions of cholesteric liquid crystals varies from 10^3 to 10^4 Pa within the range of shear rates 10^2–10^4 s^{-1} under the conditions in question. Table 2.3 lists specific values of normal stresses for the compositions of cholesteryl oleyl carbonate (COC) and cholesteryl chloride (CC) at various rates borrowed from [148]. According to Table 2.3, the magnitude of the normal stresses depends on both the liquid crystal composition and the shear rate. When it intensifies, the normal stresses grow. Appearance of normal stresses in cholesterics exposed to intensive shear is due to the homeotropic textures that form in the system in question. According to [148] the spiral fragments have for days later a behavior resembling that of a rod rotating in the fluid stream. A similar model of fluid that is treated as a solution of rod-like macromolecules is analyzed theoretically in [149]. The authors used the general theory of irreversible processes [150] to calculate normal stresses

Table 2.3 Values of normal stresses in the compositions of cholesteryl oleyl carbonate (COC) and cholesteryl chloride (CC)

Composition	Ratio between COC/CC (% by mass)	Shear rate (s^{-1})	Normal stresses (kPa)
1	100/0	1.69×10^3	8.30
2	83.7/16.3	2.68×10^2	1.32
		8.48×10^2	5.98
3	76.7/23.3	2.69×10^2	3.32
		8.48×10^2	9.30
4	77/23	2.69×10^2	4.23
		8.48×10^2	8.45
		2.69×10^3	21.1
5	73.1/26.9	2.69×10^2	1.66
		8.48×10^2	6.64

in macromolecular solution and to propose several hypotheses in order to uncover the nature of the effect of Weissenberg.

They demonstrated that, taking into account the hydrodynamic interactions in the system in question, the normal stresses appear that depend on the shear rate and constants of rotational diffusion. To explain the sense of the notion «rotational diffusion» note that the rotary motion of molecules even of comparatively simple (bi-atom) fluids at moderate temperatures has mostly the pattern of rotational oscillations near equilibrium orientations governed by the influence of the surrounding molecules and changes in time in leaps. In case of the fluids with small molecules, and during these leapwise changes in the orientation they can rotate through larger angles. The rotational oscillations near the equilibrium orientations of the fluids with large anisotropic molecules (e.g., liquid crystals) alternate with comparatively gradual changes of the latter. This slight change in the orientation from the analogy with slight (of the order of 0.1 nm) translational changes in the position of centers of gravity of molecules of simple fluids in Brownian or diffusive motion is considered rotational diffusion. It produces a significant effect in the orientation-ordered systems, such as, e.g., as boundary systems with surfaces of solid body layers of liquid crystals or substances with biphilic molecules. Rotational viscosity relates to rotational diffusion. The order of magnitude of rotational viscosity is equal to dynamic viscosity [150].

To describe the behavior of fluids the rotational motion of molecules is to be taken into account, so they were termed as "momentary" or "micropolar," according to [151].

Appearance of normal stresses in shear in the wedge-like clearance (the sliding bearing model) is shown in [152, 153] for smectic liquid crystals.

To this end, the fundamental postulates were used relating to the fluidity of liquid crystals of the smectic type. The dynamics of shear flow in the wedge are considered in [152] during exposure to external forces when the upper plate is mobile and the lower one is fixed in case the smectic layer is exposed to dislocations. It was shown theoretically that, when the dislocations are affected, if the upper plate moves towards a wider clearance, there appears a bearing forces tending to displace the plate apart. According to [152], the force can exceed the bearing forces at the oil wedge 10 times with the same clearance geometry. Direct experiments with a wedge-like cell filled with the smectic octicyan biphenyl (8CB) confirmed the calculations.

The problem of the smectic flow in the wedge-like clearance is treated in [154, 155] using a different approach and in a more general form but with the same rheological model of the continuous medium. The physical idea of the microstructure in this model proposed in [154, 155] is that the space in the clearance is filled with layers separated by porous plates that, in their turn, are interconnected by (Fig. 2.22).

The fluid flow parallel to the planes according to the law of Newton as if no plate existed whatsoever. The fluid meets in the direction normal to the layers the resistance of the porous medium proportional to the gradient of normal pressure.

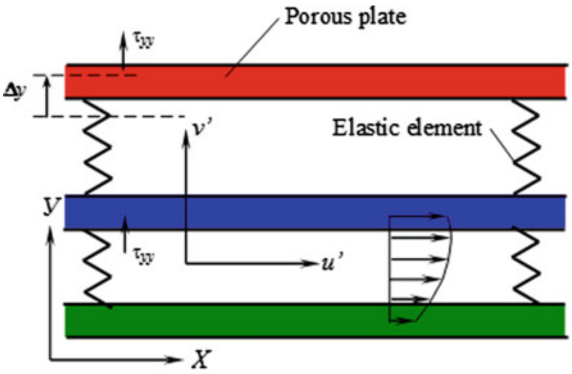

Fig. 2.22 Rheological model of smectic liquid crystal according to [155]

This resistance is similar as if the flow was resisted by smectic dislocations discussed in [142].

The permeability characteristics of the porous plate are entered into the dimensionless permeability modulus

$$N = \frac{H^4}{\eta\lambda_n B^2}, \tag{2.6}$$

where H—the width of the wedge-like clearance at the axis; B—its length, m; η—viscosity, Pa s; λ_n—the permeability coefficient, m/Pa s.

According to the dimensionality, the λ_n expresses the thickness of the layer of penetration of lubricating medium per area unit of the porous plate at the viscosity of the penetrating medium 1 Pa s. Hence, the permeability parameter apparently determines the nature of the flow process and the layer structure.

Using the model, the authors of [155] demonstrated that the stresses bearing load in the smectic liquid crystal lubricant have the order of magnitude $N^{1/2}$ in case of large values of the parameter N. In case N is small, the bearing loading is proportional to N. If $N = 10^4$, the loading in the bearing smectic lubricant model in question exceeds 200 times that in the traditional oil lubricant.

The authors [155] that this model yields the order of prediction in case of the most complicated problems and needs extra studies. Among numerous problems to be solved there are more detailed measurements of the properties of liquid crystals, integration of dislocations into models and numerical solution of equation for arbitrary N. The model used ignores the specific properties liquid crystal layers adhering to limiting surfaces.[1]

The problem of lubrication effectiveness with nematic liquid crystals is treated in [156]. Its author applied the theory of continuous mechanical flow proposed in [157] to description of lubrication with nematic liquid crystals. It is solved in the

---

[1] The circumstance is noteworthy that the terms "scale effects", "Adhesive lay", "micropolar fluid" are often used to designate special properties of subsurface layers.

manner that any other of the geometry of the lubricating clearance can be used; the angles of director orientation, effective viscosity, normal stresses, forces a and friction coefficient are calculated as the functions of the parameter of adhesive viscosity that is determined as a relation between the viscous forces affecting the director orientation forces of the magnetic field that similarly influence the director.

The elastic forces that appear in the interface between the nematic layer and the solid body are taken into account; however, they are ignored in the calculation because of their insignificance and limited effect.

Dependence of the angle θ of director orientation and the dimensionless functions of effective viscosity η* on the parameter of adhesive viscosity ε are shown in Fig. 2.23. It is apparent that θ and η* approach to fixed values and the nematic behaves like a quasi-newton fluid both in case the values of ε (dominant viscous forces) are large and ε (dominant magnetic field forces) are small. When the magnetic field forces the viscous forces ($\varepsilon \ll 1$), nematic molecules orient in the magnetic field direction normally to the smectic flow direction in the clearance e ($\theta \to 90°$), and effective viscosity:

$$\eta^* = 1/2\left(\alpha_4^* + \alpha_5^* - \alpha_2^*\right). \tag{2.7}$$

In case the dominant viscous forces are ($\varepsilon \gg 1$), the flow orients molecules and, according to [156], they arrange in располагаются relation to the flow direction at the angle $\theta \to \arccos(-\gamma_1^*)$. Then the effective viscosity

$$\eta^* \to 1/2\left[\alpha_4^* + \alpha_1^*\left(1 - \gamma_1^*\right)\gamma_5^* - \left(\alpha_5^* - \alpha_2^*\right)\left(1 - \gamma_1^*\right) + \left(\alpha_6^* + \alpha_3^*\right)\gamma_1^{*2}\right]. \tag{2.8}$$

The values α_1^*, α_6^*, γ_1^* are dimensionless viscosity coefficients. Lesley used [156] the following values of the coefficients: $\alpha_1^* = -0.0826$; $\alpha_2^* = -0.9848$; $\alpha_3^* = 0.0152$; $\alpha_4^* = -1.0572$. $\alpha_5^* = -0.5883$. $\alpha_6^* = 0.4371$ and $\gamma_1^* = -0.9895$. These values yield $\eta^* \to 1.3$ in the first case when $\theta \to 90°$, $\eta^* \to 0.3$ in the second case when $\theta \to 4'$. It is apparent that changes of the director orientation from being normal to the flow to an almost coinciding one with its direction reduce the viscosity of the nematic.

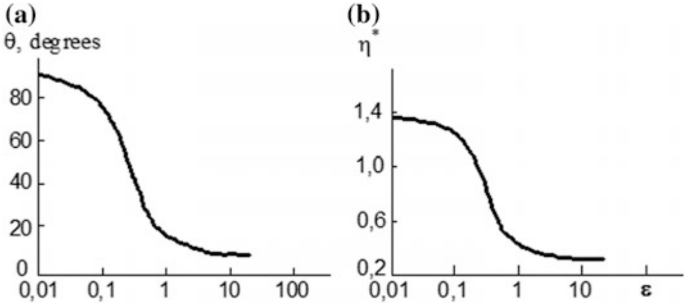

Fig. 2.23 Dependence of angle θ of director orientation (**a**) and dimensionless effective viscosity η* (**b**) on adhesive viscosity parameter

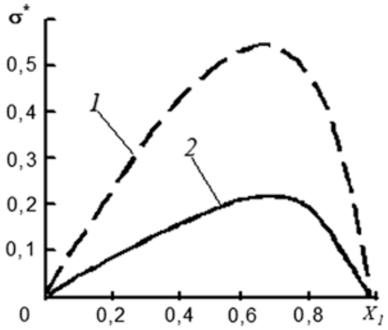

Fig. 2.24 Distribution of dimensionless loading (σ*) along wedge clearance at ε = 1 and tangent of wedge clearance resolution tgα = −0.5 of nematic liquid crystal (*1*) and newton fluid (*2*)

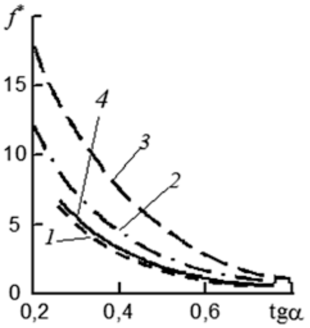

Fig. 2.25 Dependence of dimensionless friction coefficient *f** on tangent of wedge clearance resolution (tgα) at ε = 0.05 (*1*); 0.2 (*2*); 1.0 (*3*); 5 (*4*)

Figure 2.24 shows the curve of normal pressure distribution along the wedge-like clearance when the viscosity forces and magnetic field forces are equivalent (ε = 1) and the tangent of the wedge resolution angle is equal to −0.5.

The same Figure shows a similar curve for the newton fluid viscosity equal to the effectively nematic viscosity. It is apparent that the load bearing capacity of the newton fluid is much stronger in case of nematic lubrication. However, friction coefficients of nematics with large and small ε are equivalent to the newton fluid (Fig. 2.25). The largest deviations towards greater friction coefficients are observed at ε = 1.

The above results of calculation of the friction coefficients differ strongly from the above-described experimental data [158], according to the latter the friction coefficient of the nematic liquid crystal H-8 is 4–5 smaller than that of the mineral oil.

It may be due to the fact calculations in [156] are based just on a single combination of dimensionless parameters of materials borrowed from publications. It is apparent that the trend of the lubricating effect of nematics described in [156] can be strongly modified by changing the values of the parameters; this requires further measurements of the properties of nematic liquid crystal materials.

2.3.4 The Concept of the Micropolar Fluid and Related Hydrodynamic Effects

Extensive studies of boundary fluids with the surfaces of finest solid body layers permit to consider it proven that their molecules are oriented in an orderly manner. A number of media, such as liquid crystals, magnetic fluids, slurries, etc., have their pattern of internal microstructure. According to [159], it seems quite apparent that laminar arrangement of molecules in the boundary lubricating films should at once facilitate sliding of surfaces separated by these layers, i.e. reduce the friction coefficient, and to boost resistance if the clearance to thinning under the effect of loading. Deryagin [159] emphasized that the anisotropic fluid hydrodynamics are necessary to describe theoretically interrelation between the specific structures of boundary layers with effects observed in boundary lubrication.

It was developed in the subsequent years and it was demonstrated that theoretical description of microstructural media should consider both their translational motion of particles or molecules of the fluid and their proper rotation with angular speed different from the angular speed of rotation where a portion of the medium is contained as an integrity. The classic hydrodynamics of Navies–Stocks considers the latter, but ignores the first rotation. It necessitated developing a model of the fluid with internal microstructuresой and respective equations for mathematical description of such media.

Because the subject of the present work does not include discussion of theories of micropolar fluids, a review of the subject can be obtained from [151, 160, 161].

The micropolarity of the internal microstructure is manifest in the fine layer: the finer the layers the more pronounced are the micropolar properties of the medium. A typical and very frequent in engineering is fluid flow in a very narrow clearance when a fine layer of the lubricating material flows in a sliding bearing. The conditions cause the medium to demonstrate micropolarity: (a) the clearance is sufficiently narrow, particularly in boundary friction; (b) the lubricating material having additives (e.g., a liquid crystal) in the clearance in the bearing can be considered a micropolar medium. Hence, it is apparent that it is clever to apply a theory of micropolar fluids to describe the lubrication hydrodynamics theoretically. Studies in this direction began over 20 years ago. During this era of the hydrodynamic theory of lubrication, a large number of publications appeared dealing with a variety of aspects of application of model fluids that would take into account proper rotation of their molecules.

A detailed analysis of these works requires additional discussion. Therefore, leaving alone mathematical consideration, let us discuss some, most interesting, in our view, results of the studies that treat the effect of micropolarity on the load bearing capacity of lubrication layer, force friction and its coefficient.

Paper [161] deals with the problem of compression of a fine micropolar fluid layer between parallel disks (Fig. 2.26).

The upper disk moves in compression with the speed v_0 towards the fixed lower disk. It is believed that fluid on the surfaces of the disks adheres fully; the pressure

Fig. 2.26 Diagram of compression of fine lubrication layer between disks

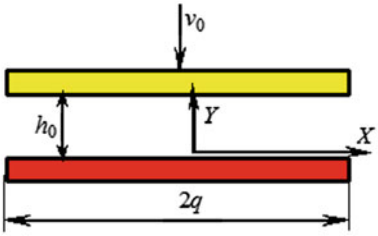

gradient from the centers of the disks outward is such that the pressure along the disk edge ($r = a$) reaches some constant value ($p = p_a$).

Full adhesion implies that the molecules of the fluid in the boundary layer lack both proper rotation and translational motion. Taking into account these conditions, an expression of dimensionless variables of the fluid layer load bearing capacity in the clearance between the disks was derived:

$$\overline{W} = h^{-3}\left[\frac{1}{12} + (L\cdot H)^{-2} - \frac{N}{2L\cdot H}cth\frac{N\cdot L\cdot H}{2}\right]^{-1}, \tag{2.9}$$

where $H = h/h_0$; $L = h_0/l$; h_0 = the layer initial thickness. The Parameter N is called the bonding parameter, l—the material length. These parameters are the characteristics of fluid micropolarity. When $N \to 0$, the fluid is described by common equations of Navies-Stocks.

Figure 2.27 shows how the parameters N and l affect the load bearing capacity of the lubrication layer.

It follow from the shown distributions that the more the fluid micropolarity is pronounced ($N \to 1$, $l \to \infty$), the higher is the load bearing capacity of the

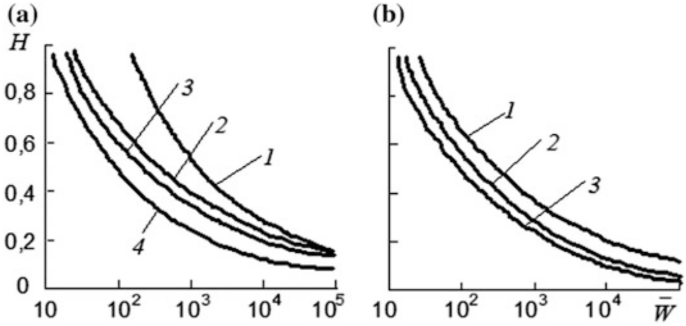

Fig. 2.27 Distribution of load bearing capacity of lubrication layer $\overline{W}$ through layer height H: **a** at $N^2 = 0.9$ for different parameters $L = 0$ (*1*); 9 (*2*); 15 (*3*); → ∞ (*4*); curve 4 corresponds to newton lubricant; **b** at $L = 9$ for different values of $N^2 = 0.9$ (*1*); 0.5 (*2*); 0 (*3*); curve 3 corresponds to newton lubricant

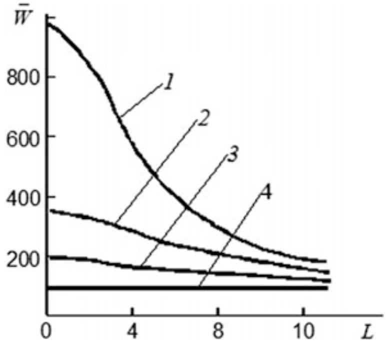

Fig. 2.28 Load bearing capacity W at different values of N^2 depending on parameter L: *1*—$N^2 = 0.9$; *2*—0.7; *3*—0.5; *4*—0; curve 4 corresponds to newton lubricant in [163]

lubrication film. When the thickness h of the micropolar fluid layer reduces, it goes up considerably.

Since larger particles or molecules correspond to a larger typical material length l when their dimensions are comparable with the clearance value h, the medium micropolarity grows and boosts larger load bearing capacity of the lubrication layer (Fig. 2.28).

From the dependencies in Figs. 2.27 and 2.28, it follows that the load bearing capacity of micropolar fluids is always than that of the newton fluids. It is also shown in [162] where the micropolar fluid flow is considered in the wedge-like clearance.

The authors demonstrated that the lubricant micropolarity in the sliding bearing both boosts the load bearing capacity and reduces the friction coefficient proving that the boundary lubrication layer adheres fully.

The work [164] deals with the effect of lubricant micropolarity on the lubricant's main hydrodynamic characteristics in a radial bearing shown schematically in Fig. 2.29.

The numerical analysis of the expressions for pressure in the clearance and friction coefficients are shown in Figs. 2.30 and 2.31.

From Fig. 2.30 it is apparent that the lesser is $L = h_0/l$ the larger is the parameter N, the higher is the pressure, hence, the heavier loading can the bearing withstand. The friction coefficient of the micropolar fluid (Fig. 2.31) has lower values for values micropolar lubrication versus the newton fluid in case of the wedge clearance in the flat sliding bearing. However, it has a minimum in the radial bearing at a definite $L_{\min}$ that depends on N.

Studies of the radial bearing filled with a micropolar lubricant with the account of dry friction are specifically worthwhile [165]. Two model cases of roughness are considered: longitudinal, when the lubricant flow coincides with the direction of the grooves of the microrelief; transverse, when the lubricant crosses the grooves. Both like in case of micropolar and newton lubrication, roughness the first case reduces the load bearing capacity and boosts the friction coefficient, and produces the opposite effect in the second case. However, the lubricant micropolarity boosts the rate of changes in the load bearing capacity, the larger the parameter N the stronger

Fig. 2.29 Diagram of radial bearing

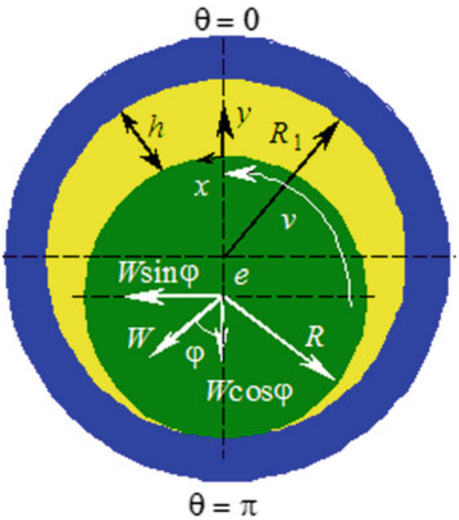

Fig. 2.30 Load bearing capacity $\overline{W}$ as function of L at $N^2 = 1$ (*1*); 0.9 (*2*); 0.5 (*3*); 0 (*4*); curve *4* corresponds to newton lubrication [163]

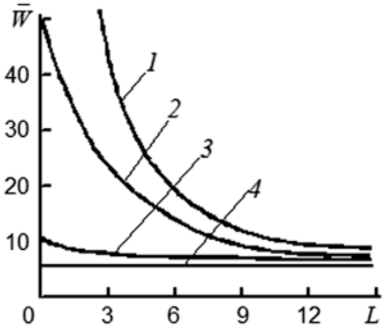

Fig. 2.31 Dependence of dimensionless friction coefficient f^* on parameter L at $N^2 = 0$ (newton lubrication) (*1*); 0.1 (*2*); 0.5 (*3*); 0.7 (*4*); 0.9 (*5*) [163]

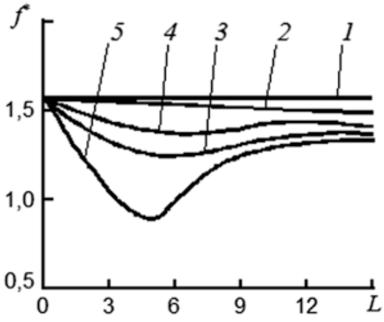

the changes. As regards the friction coefficient, the lubricant micropolarity intensifies it as longitudinal roughness increases. As regards the cross roughness growth, the rate of reduction of the friction coefficient goes down at smaller L values; it augments at larger L versus the newton lubricant.

Performance of the bearings with micropolar lubrication is treated exhaustively in [155] dealing with the effect of the degree of retardation of proper rotation of the micropolar fluid by thee friction forces and friction coefficient as well as with the effect of the load bearing capacity of the lubrication layer.

In addition, the performance of the bearing is analyzed under the effect of the elasticity of its material in micropolar lubrication. It is shown that during external contact between the cylinders, when the load is constant and other conditions of operation of the bearing are equal, growth of the parameter of material length l doubles and increases even more the clearance thickness увеличивается (the cylinders are moved apart). In this case, the forms of the clearance remain practically unchanged during divergence of the cylinders. It enables to draw a conclusion that the scratching of contacting surfaces becomes less probable. It is shown that the load bearing capacity has an extreme pattern depending on the contact stretch and dimensionless parameter D_1 characterizing the yield (elasticity) of the bearing walls (Fig. 2.32). If the contact stretch is the micropolar lubrication produces 4–5-fold rise of the load bearing capacity compared with the classic newton lubrication.

It follows from the above brief review and according to [155] that the hydrodynamics of fluids with degrees of freedom of rotation enables to construct a theory of lubricating effect that would result in a generalized Reynolds equation in which the shear viscosity assumes the type of a definite function of thickness of the clearance. When the clearance is very fine this function has sense of the boundary viscosity as a material characteristics of the fluid. Higher values of the boundary viscosity than those of the volumetric fluid due to retardation of rotation of molecules in the contact with the solid body and determine higher efficiency of the micropolar lubrication versus the newton lubrication. This conclusion results from the concepts of the micropolar fluid taken into account in hydrodynamic calculation.

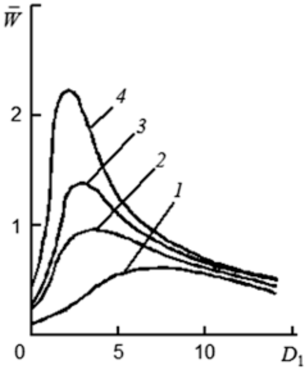

Fig. 2.32 Dependence of load bearing capacity $\overline{W}$ on yield parameter of cylinder D_1 (external contact between cylinders): *1*—l/h = 0; *2*—0.2; *3*—0.4; *4*—1.0 [155]

Nevertheless, abnormally low friction and wear of the cartilages are observed in the living joints for a long time, namely, throughout the life cycle of a person and animal [85, 136]. So, let us now consider in detail the issues of tribophysics and friction efficiency in the living joints.

2.4 Tribology of Synovial Joints—Unique Natural Rubbing Organs

The literature of recent years contains a large body of information both on living o in is biomechanics and results of research into synovia specific features, and the role of synovial fluid and cartilage in its realization [122, 166, 167]. Obviously, the variety and complexity of physicochemical processes occurring in the synovia, as well as a set of biomechanical properties inherent to separate components, play an important part in the lubrication mechanism of living joints.

Owing to these processes and properties, animal joints are unusually effective kinematic pairs to realize extremely low coefficients of friction and lubrication for long periods of action. However, analysis of mechanical systems shows the most complex ones to have tribological characteristics similar to living joints [93, 122]. The causes of such behavior have not been fully understood. Therefore, the problem of lubrication in living joints as unique tribosystem remains a central one in the medicine and tribology [85, 122, 136].

2.4.1 *Theories and Hypotheses About Lubrication in the Living Joints*

Attempts to study low friction in living joints have been made ever since G. Hunter in 1743 drew attention that synovial fluid is used as lubricant for the living joints [166, 167]. Activities in this field were only continued at the beginning of the twentieth century, when in 1925 Beninghoff suggested that cartilage elasticity may result from liberation and repeatable absorption of synovial fluid [167]. This statement had remained unnoticed for many years.

In 1959 McCutchen used a cartilage-glass system to show that after every period of liquid absorption the friction coefficient of the pair reduced considerably. The shear resistance is significantly increased if the exudation from the cartilage stopped. In view of this, McCutchen anticipated synovial joints to be lubricated with the interstitial fluid released from the cartilage tissue under compression. He used the term “weeping lubrication” to describe the case where inteistitial fluid gets released from the cartilage and creates hydrostatic pressure capable of maintaining surfaces at a microscopic distance. Such a system favours further development of a general lubrication mechanism for living joints [166]. The weeping lubrication theory assumes that synovial fluid moves both between the two rubbing cartilage surfaces and in the cartilage bodies. In other words, according to the work [166], the interstitial fluid secreted from the cartilages took the load during dynamic contact acting on the mutually rubbing articular surfaces.

Consequently, the "weeping lubrication" helped to explain the minimum shear resistance in joint elements, especially at the termination of the relative movement of the rubbing of the cartilage surfaces. However, despite advantages of this theory, the question—whether the liquid exuded from the cartilage tissue is sufficient to form the liquid film required for successful functioning of living joints—was and still remains the subject of much dispute. Nevertheless, the recognition of cartilage and synovia roles in living joint lubrication, along with new advanced methods developed for structure investigations, stimulated further interest in arthrology. In particular, significant success in the development of scanning electron microscopy allowed to investigate the ultrastructural features of the articular cartilage and to recognize the general morphological concepts [167, 168]. More detailed research showed the surface layer of cartilage matrix to differ markedly from other subsurface zones in the structure and properties; most investigators had associated this with an important role of the former in living joint lubrication [169]. Of no small importance was Weiss's theory that the surface layer of cartilage matrix functions as a membrane [170]. Subsequently, many researchers supported this theory after analyzing the chemical and morphological characteristics research data of the articular cartilage. According to this conception, cartilage matrix surface layer is highly permeable to water, nutrients, and some other low-molecular compounds [171–173].

New data on structural and mechanical properties of separate interacting components of synovia have promoted further development of new joint lubrication theories. An essential role was played by numerous scientists observations, which demonstrated that: (1) hyaluronic acid from synovia can be adsorbed by the cartilage surface to form a protective layer essential for the joint operation [174, 175]; (2) the synovia viscosity can change depending on the shear rate and surface pressure acting upon joint surfaces; (3) pliable cartilage surfaces can serve as a support for the compressed liquid film which thickness can consequently reach tens of micrometers, when joint surfaces approach each other, and separate the rubbing surfaces completely, or almost completely. In addition to those data, Walker and coworkeis, in late 60s, published their results of scanning electron microscopy stating that synovial fluid gets entrapped and retained between asperities on cartilage surfaces [176, 177]. They underlined the liquid film thickness to vary from 1/4 to 10 μm [177, 178].

Accordingly, a theoretical viscosity of fluid was calculated for given experimental conditions and it was established the synovia to be a concentrated fluid unlike the fluid found in the joint bulk. The same was supported by the friction studies [178]. A more detailed study of concentration effect revealed a longer duration of compression of the lubricating film [179]. As a result of those experiments, a conclusion was made that synovial fluid was captured in the course of joint operation, concentrated or enriched through the liberation of low-molecular weight components into cartilage pores. So, Walker and other investigators proposed a modified type of lubrication accompanied by compressing the film when the molecular structure of synovial fluid, as well as the elasticity, porosity and surface characteristics of joint cartilages facilitate an increased durability of lubricating films which separate the cartilage surfaces [176, 179].

This type of lubrication is known as «boosted lubrication». It means that articular cartilages come in contact at friction and synovia thickening happens between the cartilage surface irregularities due to extraction of more low-molecular components through the cartilage pores. As a result, real contact area of the cartilage grows but the local loads reduce. Summing up what has been said, even formal comparison of the boosted and weeping lubrication theories shows that they differ from each other. Indeed, the weeping lubrication implies release of interstitial fluid, whereas the boosted one implies absorption of fluid by the joint cartilage under load at motion, i.e. these two lubrication modes seem mutually exclusive. Linn, however, trying to eliminate the contradictions between the two lubrication modes, using the known mechanical and physical properties, as well as the latest findings on cartilage tissue ultrastructure obtained by the scanning electron microscopy, had proposed a new model of joint cartilage [174].

In this model the synovial-type joint is represented as two round porous elastic discs compressed and separated by a fluid film that can create certain resistance under tension and compression owing to liquid absorption or exudation. In conformity with Linn's parametrical solution for the given system, two time-dependent modes of lubrication exist in synovial joints (Fig. 2.33).

Initially (τ = 0) the fluid flows into cartilage in their central part ($\varphi - \Phi$), while in the external circular region the picture is reversed, i.e. in the initial period of cartilage compression the fluid seems to be absorbed by the middle region of the

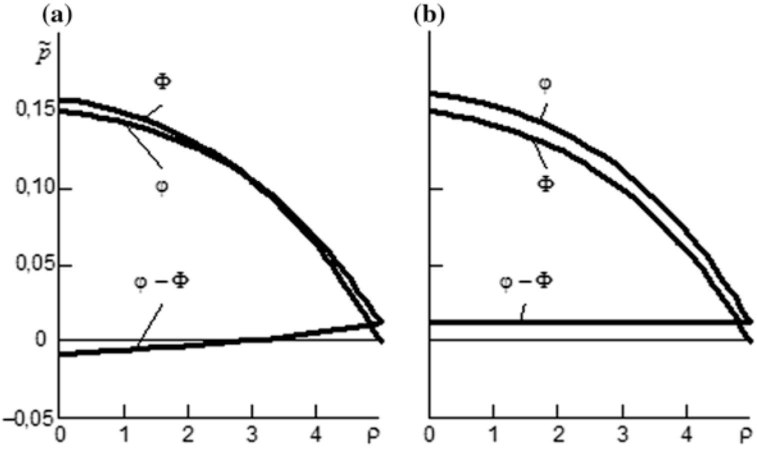

Fig. 2.33 The behavior of the dimensionless pressure in the liquid film (Φ) and in articular cartilage (φ) depending on the radius (ρ) and time (τ): **a** τ = 0 (τ = 3); **b** τ = 6

cartilage bodies and released through pores near their periphery (Fig. 2.33a). Such a situation, as Linn believed, remains during the following time period ($\tau = 3$). Some time later ($\tau = 6$), when the cartilage continue to be compressed, fluid flows from the cartilage bodies to the clearance (Fig. 2.33b). Thus, Linn argued that at initial loading both boosted and weeping lubrication mechanisms are in action, since fluid circulates from the clearance to the cartilage bodies, then returns to the clearance. After a while only weeping lubrication begins to act, i.e. fluid will flow in one direction only, namely, from the cartilage bodies to the clearance between them.

In this way, using the data obtained from models of synovial joints, Linn smoothened to some extent previous contradictions between the boosted and weeping lubrication theories of living joints.

Some investigators, however, considered that an exact way of forming the lubricating film on the surface of cartilage does not confirm McCutchen's guesswork on weeping lubrication or Walker's postulate on boosted lubrication in living joints [180, 181]. The following facts support this approach. On the one hand, several workers reported [174, 182] that enzymic decomposition of hyaluronic acid by selective action of hyaluronidase upon synovial fluid, when the latter was loosing rheological qualities, did not influence the friction characteristics of joint elements. This fact caused doubts about the basic principles of the boosted lubrication theory of living joints.

On the other hand, proceeding from the analytical study of transient oscillating characteristics sliding under pressure on a laminated porous permeable elastic surface, it was shown that the weeping lubrication proposed by McCutchen could exist, most probably only if no sliding occurred in the joint.

However, other studies of action of the load along the similar laminated porous elastic surface has shown, that if materials were used which properties were similar to those of healthy joints and sub-cartilage bone substance, then interstitial fluid would be exuded along the moving-load-front line and near it, and would be absorbed by the joints cartilage surface near and behind the moving-load line [180]. Such circular patterns of the fluid flow field were registered by different authors. As the result of those findings, it was assumed, that the natural lubrication mechanism for a normal joint depends on circular motion of fluid flow at rubbing joint surfaces. At first this assumption was based on the models in which a joint cartilage was treated in the form of single layer porous systems. In reality, the mechanical characteristics of the cartilage vary with depth. Research performed by Mansour and Maw [180, 183] were helpful for taking these facts into consideration, and hence, for developing the hypothesis.

These authors believed the three-dimensional model could represent the tribological properties of healthy and not healthy cartilage tissues, since biochemical and ultrastructural changes in the latter could be accounted for by varying the parameters of porosity, permeability, as well as rigidity of the three-layer composite material proposed to model the cartilage. As a result, in conformity with this hypothesis, a new pattern of liquid lubrication was postulated implying a two-directional fluid flow between a synovial cavity and joint cartilage (Fig. 2.34). It should be noted that—according to the authors of this hypothesis—such a pattern

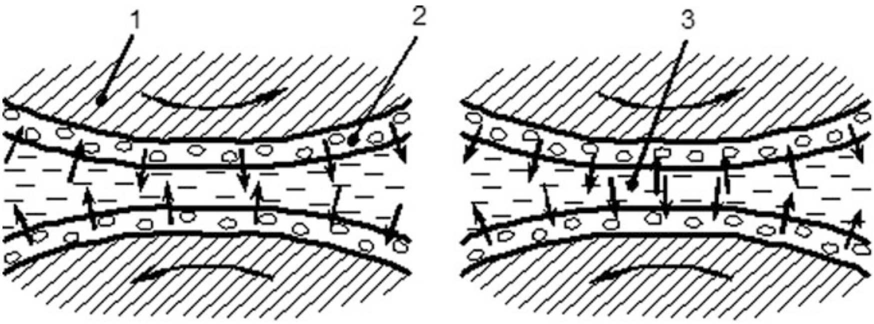

Fig. 2.34 Fluid flow in joint cartilage: left-hand picture representing a normal cartilage; right-hand one a pathologically changed cartilage [166]: *1*—subcartilage bone; *2*—joint cartilage; *3*—synovial fluid

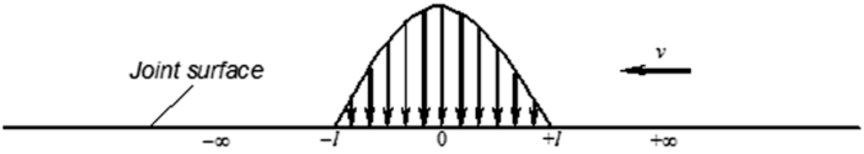

(Case) - Cartiage / v, m/s	Consumption of fluid through joint				Total consumption
	I	*II*	*III*	*IV*	
(1)-Normal /0,0254	0,0080 ↑	0,0492 ↑	0,0178 ↓	0,0197 ↓	0,0198 ↑
(2)-Normal /0,0508	0,0064 ↑	0,0265 ↑	0,0084 ↓	0,0243 ↓	0,0003 ↑
(3)-Normal /0,0762	0,0056 ↑	0,0231↑	0,0044 ↓	0,0215 ↓	0,0027 ↑
(4)-Normal /0,0254	0,0079 ↑	0,0205 ↑	0,0126 ↓	0,0145 ↓	0,0013 ↑
(5)-Pathologically/0,0254	0,0097 ↑	0,1046 ↓	0,0411 ↑	0,0545 ↑	0,0006 ↑
(6)-Pathologically/0,0254	0,0097 ↑	0,1046 ↓	0,0411 ↑	0,0545 ↑	0,0006 ↑

Fig. 2.35 Flow rates of interstitial fluid through cartilage (arrows stand for ↑—liberation, ↓—absorption of fluid by cartilage) [180]

is caused by fluid flow in conjugated cartilages caused during motion by compaction of the cartilage tissues [183, 184]. Indeed, the calculated flow fields of interstitial fluid showed, that materials which properties are similar to those of a normal healthy joint cartilage, form a surface lubricated in the natural manner.

The processes described are illustrated quite well by the calculated flow rate of interstitial fluid through the cartilage (Fig. 2.35) [180].

According to the obtained results for normal cartilage (case 1–4) the amount of liquid absorbed in region *III* will be less than liberated from cartilage. Therefore, under such conditions a normal joint appears able to generate the lubrication fluid. However, for case *5* when the increase of surface porosity up to 60% caused a greater permeability and reduced surface area, and for case *6* which the elastic modulus of the subcartilage substance increased with variations in properties of the cartilage surface layer, the quantity of liberated fluid within region *I* appeared insufficient to provide the lubricating layers in the area *II*. Thus, in diseased joints the natural lubrication mechanism of joint cartilage is obviously violated.

Thus, in conformity with the given concept, the natural lubrication of joints depends fully on movement of interstitial of interstitial fluid; normal healthy cartilage tissues can generated and maintained the fluid film on the rubbing surfaces, whereas this is impossible for diseases cartilage. Thus this concept gives the most acceptable picture of joint lubrication. However, it does not fully reflect real processes occurring in synovial joints, the same as many other theoretical works. Particularly, describing quite adequately the properties of a cartilage matrix to release and absorb fluid, this theory does not account for the effect of the physical nature of lubricant materials on cartilage friction. However, numerous investigators showed the latter to play significant role in tribology joint.

The experimental work pointed out to this [185]. It revealed that the resistance of shear of cartilage bodies in synovia was considerably lower, than in other lubricants, for example, in the physiological solution.

Meanwhile, more detailed investigations allowed us to obtain new data on the friction of the joints in the presence of liquid lubricants. This was facilitated by further improvement of tribometric techniques intended to study them. Thanks to a pendulum machine direct measurements of friction characteristics in a pair of friction “cartilage–cartilage” became possible. It was established that sudden loading of the hip joint lubricated with synovial fluid led to an extremal dependence of the resistance of shear on the time [186].

At the same time, under conditions of sudden loading of an unlubricated joint, and also in the case of preloaded joints, both lubricated with synovial fluid or unlubricated, a different behavior is observed, namely, with a larger number of pendulum oscillations the friction coefficient is decreasing in a monotonous manner. The causes of such a behaviour of the friction coefficient were tried to be explained by the authors by various loading conditions in joints. For example, summarizing their observations under conditions of sudden joint loading, the authors concluded that conditions are created typical of hydrostatic lubrication effect with a compressible film. In particular, according to them, at the beginning of a test when the hip head sinks into the liquid lubricant film—as the film thickness reduces—friction will grow; after some time the re comes a moment when the film thickness is governed by the sliding velocity and the load. It could be expected that with the completely damaged film resistance of shear would rise and lead to the experiment interruption.

At the same time, this does not happen in the tests with natural living joints. This unusual behavior can probably be explained, according to the authors, by the fact that at a certain trial moment the friction force equals the force developed simultaneously with the pendulum deviation at shear displacement of the cartilage tissue. In favour of the latter, as the authors believe, evidences the increase in the friction coefficient observed in metal-polymer joints possessing higher shear moduli than those of the cartilage tissue [184].

Later, such an interpretation of the phenomenon was doubted. Prokhorova [147] showed the earlier assumption on the relation between the maximum and decreased

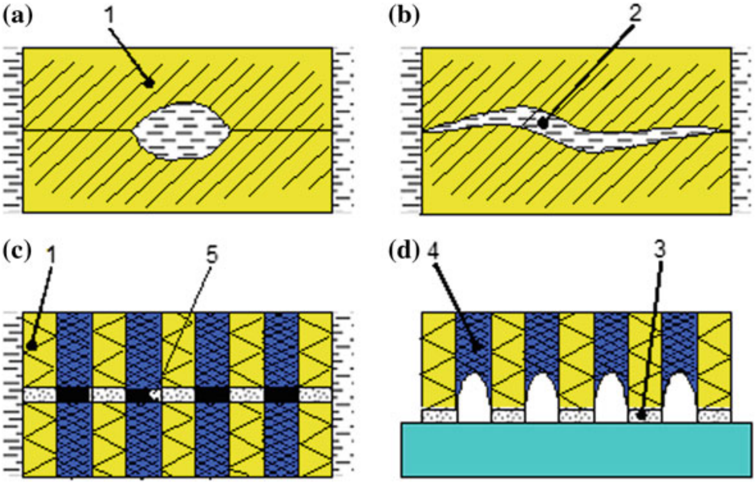

Fig. 2.36 Schematical diagram of “living friction” mechanism: **a** zones of pair “cartilage–cartilage” at the moment of macrorasperity loading; **b** same at moving; **c** contact in pair “cartilage–cartilage” at high pressure; **d** contact in pair “cartilage–cartilage” at low pressure; *1*—cartilage; *2*—synovial fluid; *3*—boundary film (contact Type I); *4*—interstitial fluid; *5*—liquid film (contact Type II)

force with the transition from the sliding friction to elastic shear in the cartilage matrix to be absolutely wrong. The investigator assumes the resistance force, recorded in the joint elements in the area of maximum friction and in the area where the dependences discussed fall down, is related to the sliding and results from activation of the so-called “living friction” mechanism. According to this mechanism, under normal loading when rubbing cartilage macroasperities get compressed (Fig. 2.36a, b), areas of real contact appear in their contour contact zones provided by two elements (Fig. 2.36c, d), namely, the area of actual contact through of elastic matrix cartilage elements via the boundary film (actual contact Type I) and through interstitial fluid microcolumns (actual contact Type II) [187].

In addition, these authors showed analytically that in the course of contour contact area life the contacting microcolumns of interstitial fluid can undergo elastic compression and support practically the whole load, while a negligible part of the load is supported by micro frictional contacts where boundary friction occurs. The authors of the “living friction” mechanism believe that friction fully through interstitial fluid film provides until the film thickness separating contacting cartilages of the hip head and cotyloid cavity, studied in the above experiments on hip joints, remains sufficiently large.

The mechanism of “living friction” cannot operate under such conditions, as interstitial fluid microcolumns press, in fact, against the compressed film of synovia, whereas their rigidity does not correspond to the bulk compressive modulus of interstitial fluid for this time period. It is anticipated that with increasing number of test cycles, when the synovia film thickness reduces and approaches the boundary one, the rigidity of interstitial fluid microcolumns becomes corresponding to the bulk compression modulus of this fluid, thus providing a liquid-lubricated contact. As a result, the resistance of shear stops rising and the friction coefficient drops.

At the same time, according to the same researchers, during the first time interval no contact between the compressed film and interstitial fluid microcolumns can be realized, because the fluid content is insufficient in cartilage matrix micropores (Fig. 2.36d), but the increased friction coefficient is associated with the compression of the synovia film which finally leads to a completely boundary contact of elastic cartilage matrix elements. Later this contact becomes the contact of interstitial fluid microcolumns with activation of living friction mechanisms, owing to cartilage tissue creep. However, this would contradict with the basic concept of "living friction" mechanism, in conformity with which the portion of boundary lubrication is negligible. This, probably, is the cause why the researchers of the "living friction" neglect the influence of the lubricant physical nature on cartilage friction, though they had obtained different results when cartilages were lubricated with synovial fluid and physiological solution.

At the same time, it is quite obvious that "living friction" mechanism also cannot explain these experimental findings.

2.4.2 Conceptual Approaches to the Explanation of Low Friction in the Joints

The ambiguity of living joint lubrication theories forced investigators to make more thorough analyses of rubbing cartilage surfaces and treat them not as inert structureless layers, but as dynamic structures capable of active interaction with synovia components [122, 167].

Of considerable importance was the fact that protein polysaccharide complexes being tremendous molecular accumulations of hyaluronic acid (HUA) and proteins were detected in synovia [188, 189]. In recent years there were two different approaches explaining the formation of such complexes in synovia [190]. On the one hand, proteins were assumed to be a link helping HUA to adsorb on the cartilage surface: on the other—proteins were considered as adsorbents hydrogen molecules in disaccharide chains of HUA.

Protein polysaccharide complexes tend to adopt spherical configurations owing to their high electronegativity in solutions [189]. Structures of such a shape measuring between 100 and 1000 nm were first detected both in synovia samples and on cartilage surfaces by using special preparation techniques in scanning electron microscopy [176]. Nevertheless, their origin and role in the living joint friction mechanism a long time remained uncertain.

Only in mid-80-s a more detailed research was made [191, 192]. Pavlova and Kumanin reported that rubbing surfaces of menisci and joint cartilages pretreated in

2%-glutar aldehyde, subsequently rinsed in a phosphate buffer, and in running water were covered with drop-like oval structures of size between 100 and 2800 nm.

The authors believe the drop-like oval structures occurring on cartilage surfaces to result from specific features of their hystological structure. Because of diffusive metabolism, in agreement with [191], metabolic products come out from the cartilage matrix and contacting the synovial fluid. On the border of two media differing in their chemical and physical properties, these products get aggregated to form globules. The latter consist, probably, of a more dense matter than synovia, and the spherical shape is preserved in synovia owing to the effect of surface tension forces. It was noted, that no proteoglycanes were detected in the globule composition.

The experimental data from [191] were used to suggest that the globules detected on the friction surfaces of cartilage have the protein origin. This hypothesis was further developed later [192]; Chikama verified it with electron-microscopic and tribological findings; the data were obtained on a pendulum tribometer and a reciprocating wear machine. They showed trypsin added not to have influenced the synovia viscosity, but deteriorated the lubricity several times; hyaluronidase inducing enzymic decomposition of HUA-molecule and reducing synovia viscosity [182], influenced markedly the lubricity, but alter a sufficiently long period of time. The electron microscopic investigations revealed that along with HUA, having a shapeless mass measuring between 200 and 500 nm spherical particles of 20–30 nm were detected in synovia samples tested. The deep coloring of the latter with ruthenium red, as well as their disappearance, if synovia was subjected to enzymic treatment with trypsin, made the author to believe the particles detected consist mostly of protein. As the particles were spherical in shape, and treatment of the test material with trypsin led to both complete disappearance and sharp deterioration in the synovia lubricity, the results from [192] appeared helpful in designing a rolling friction model for living joint lubrication (Fig. 2.37).

In this model, HUA molecules surround spherical particles of protein, which can rotate freely similar to ball-bearing rotating elements.

However, despite a wealthy material reported in [191, 192] in favour of the above hypothesis, it should be noted, that the guess of spherical structures formed in the test samples, is controversial, since aggregation of synovial components into spherical particles can depend considerably on the conditions at which the material was prepared for electron microscopic studies, which had been indicated earlier [176]. Nevertheless, the research data reported elsewhere [191, 192] are of great significance, as they point out to an important role of proteins in living joint lubrication.

There is another point of view on the protein lubricity [193]. It rests on the reports of numerous authors [182, 192] stating that the efficiency of cartilage lubrication does not depend on the synovia viscosity, which agrees with the provisions of boundary lubrication.

Experimental data on friction of different surfaces in synovial fluids and in 0.15 M solution of NaCl, and also in view of the fact that glycoprotein (LGP-1) identified earlier in synovia by Swann and his colleagues, possesses high lubricity

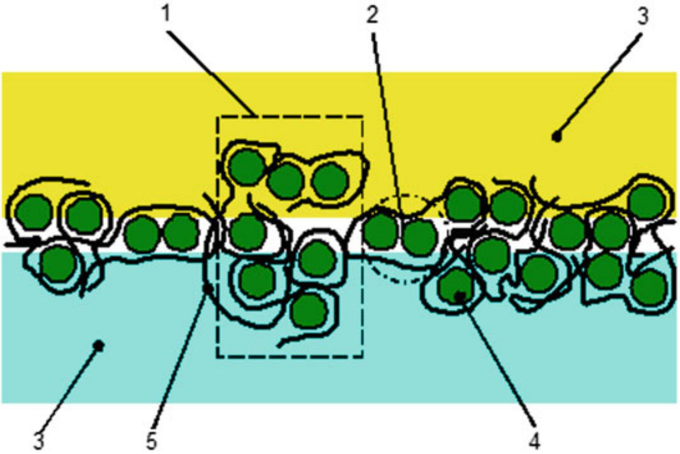

Fig. 2.37 Schematic representation of joint fabrication model based on roiling friction: *1*—zone of elastohydrodynamic lubrication; *2*—zone of rolling friction; *3*—joint cartilage; *4*—spherical particles of protein; *5*—hyaluronic acid (HUA)

[194–196], Davis et al. [193] proposed a boundary lubrication model, based on hydrophilic characteristics of the cartilage surface and structurization of adsorption layers of glycoproteins and water molecules (Fig. 2.38). In accordance with this model, as with any boundary lubrication system, a lubricant should adhere to the surfaces of friction through ionic, covalent, hydrophobic–hydrophylic or hydrophylic–hydrophilic chains.

Since glycoprotein identified by Swann [194] contains hydrophobic and hydrophylic areas, at same radioactive LGP-1 exhibits good adhesion to cartilage surfaces [166], the investigators of this model suggest that such bonds are theoretically admissible in joint cartilages. Therefore, in conformity with the results from [193], glycoprotein boundary layers and electrostatic repulsion participate in efficient separation of rubbing cartilage surfaces.

If this is true, then in view of electronegativity of cartilage surfaces owing to proteoglycane macromolecules being present in cartilages, with fixed negatively charged groups, cationic surfactant lubricating layers should behave preferably compared to anionic surfactants in cartilage friction. However, data [197] state the opposite. Consequently, low friction of cartilages it is impossible to explain through electrostatic forces only. In this regard, other mechanisms of molecular interaction should be taken into consideration when treating the processes in question.

One of such mechanisms can be that based on liquid-crystalline state of synovia in joints. Research that has been conducted in recent years points out in favour of this hypothesis. By way of example, liquid-crystalline compounds were detected in synovial fluid; their importance in friction and biomechanical properties of joint cartilages was underlined; ways of intrajoint transport of the said compounds in living organisms were understood [198–209].

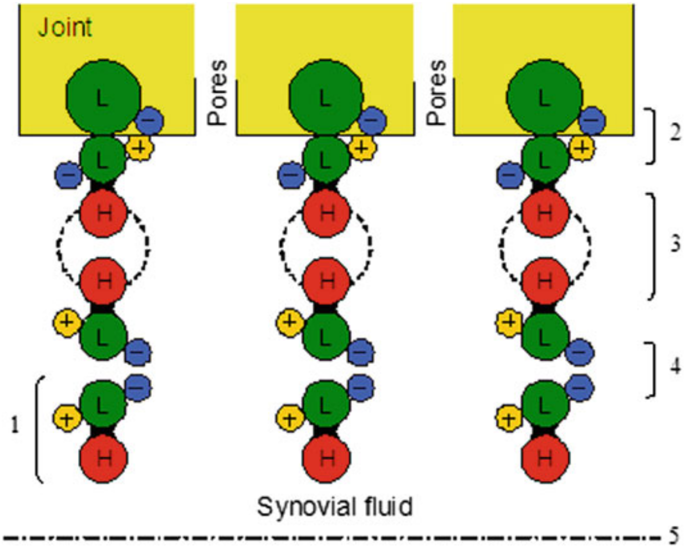

Fig. 2.38 Diagram of boundary frictional model of joint cartilage: *1*—subelement of lubricating glycoprotein LGP-1 (*L*—hydrophylic region of glycoprotein; *H*—hydrophobic region); *2*—region of ionic attraction of glycoprotein hydrophylic areas to hydrophylic areas on cartilage surface; *3*—attraction region of glycoproteins hydrophobic areas (large shear resistance); *4*—region of ionic attraction of glycoprotein hydrophilic areas (small shear resistance); *5*—symmetry line

The study of the joint cartilage structure has shown that the surface microrelief contains marked parallel ridges and groves [136, 185]. The thorough examination of the cartilage surface topography by the scanning electron microscopy shows that bundles of collagen fibers on the surfaces and microgrooves between them are oriented in the direction of displacements dominating in the joint (Fig. 2.39).

The study of the friction of the cartilages with the orientation of collagen fibers along and across the sliding direction against glass has shown the regular structure of the cartilage surface layer to affect considerably the friction coefficient of the cartilage–glass pair lubricated with synovia. In sliding along the fibers the friction coefficient is lower compared with transverse sliding showing higher friction coefficients. Similar results were obtained for cartilage friction in the model lubricants with the additive of liquid-crystal cholesterol compounds. It is typical that the similarity of the tribological behavior of the cartilage–glass pair in synovia and model lubricants includes not only close friction coefficients but also the same dependencies of them on the orientation of the cartilage specimens under testing.

Thus, a close interrelation between the cartilage surface microstructure and the antifriction behavior of the cartilage–synovia system has been found whose qualitative and quantitative characteristics apparently depend on the deformation properties of the cartilage matrix, first of all.

To determine these specific features we compared the friction of the cartilage against glass in synovia and in the model lubricant with liquid-crystal cholesterol

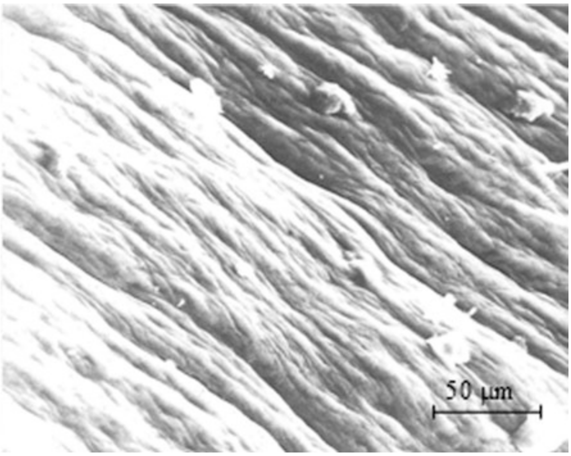

Fig. 2.39 Regular structure of the cartilage surface layer

compounds, as well as in the organosilicon fluid ПМС-300 which is used for joint lubrication [206]. The cartilage was loaded stepwise from 0.2 to 6.0 MPa and after 50 min of testing it was rapidly unloaded to the initial state.

It is seen that the cartilage deformation in loading does not depend on the lubricant composition and antifriction properties (Fig. 2.40c). Similarly to the results of other researchers [122, 136] we observed initially instantaneous elastic deformation followed by creep that is explained by the properties of collagen at the initial stage and by the removal of the liquid phase from it at the creep stage.

When unloading the cartilage time variations in its tribological characteristics depend on the lubricant composition (Fig. 2.40d). It is found that in case of natural synovia and model lubricant with liquid-crystal cholesterol compounds cartilage unloading initially causes the friction coefficient to rise and after 20–25 min of testing it decreases to its initial value.

Close values and the similar pattern of the time dependence of the friction coefficient during unloading prove that the cartilage show similar tribological behaviors in friction with synovia and the model lubricant containing cholesterol compounds. In contrast, when the cartilage rubs against glass in lubricants without liquid crystal additives, e.g. the organosilicon fluid, unloading increases the friction coefficient 1.5–2 times compared with the initial values. Synovia and the model lubricant containing liquid crystal additive provide a greater recovery of the cartilage matrix dimensions in unloading than other lubricants without liquid crystals.

The above effect of the regular structure of surfaces and the deformation properties of the cartilages on their friction can be explained basing on the properties of the liquid crystal compounds contained in synovia [122]. According to the data reported in [85, 96], there is a close interrelation between the regular pattern of the solid surface microrelief and the formation of planar liquid crystal films. The orientation of the major axes of liquid crystal molecules along microrelief grooves corresponds to their minimal elastic energy, hence to the thermodynamically stable

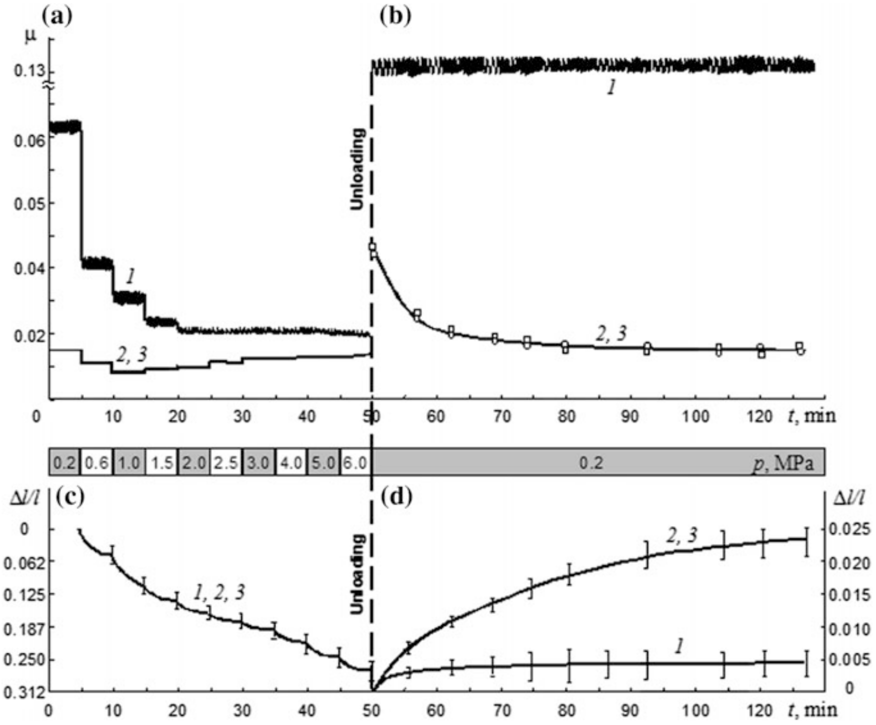

Fig. 2.40 Time dependence of friction coefficient μ (**a**, **b**) and relative change of cartilage sample thickness Δ*l*/*l* (**c**, **d**) at friction against glass in organo-silicon fluid PMS-300 (*1*), synovial fluid (*2*) and pseudosynovial fluid doped with LS (*3*). Loading regimes: **a**, **c** under stepwise loading from 0.2 to 6.0 MPa; **b**, **d** after unloading to 0.2 MPa

state being more profitable from the energy viewpoint. If the molecules are perpendicular to the grooves they are bent and have a higher elastic energy.

Moreover, the adhesion of the liquid crystal molecules to the surface depends on the surface relief characteristics and, as it is shown in [85, 96], has the maximum when the size of the molecules (1–10 nm) is comparable with the width of the grooves, i.e. when the surface has the submicroroughness.

To study the cartilage surface roughness more thoroughly we use the results of the analysis of collagen structure biosynthesis (Fig. 2.41) [122, 189]. It is seen that, in addition to macro- and microasperities [93, 210], the cartilage surface has submicroasperities resulted from the microfibrillar (3–5 nm) and fibrillar (20–100 nm) structure of collagen fibers (Fig. 2.42).

The strict order being the basis of the micro- and macromorphology of the cartilage provides the regular structure of its surface at submicrolevel. This surface topography promotes the strong adhesion of liquid crystal molecules and their orientation along surface microrelief grooves covered with planar liquid crystal films (Fig. 2.43) [122, 136]. The structure of the films resembles that of solid

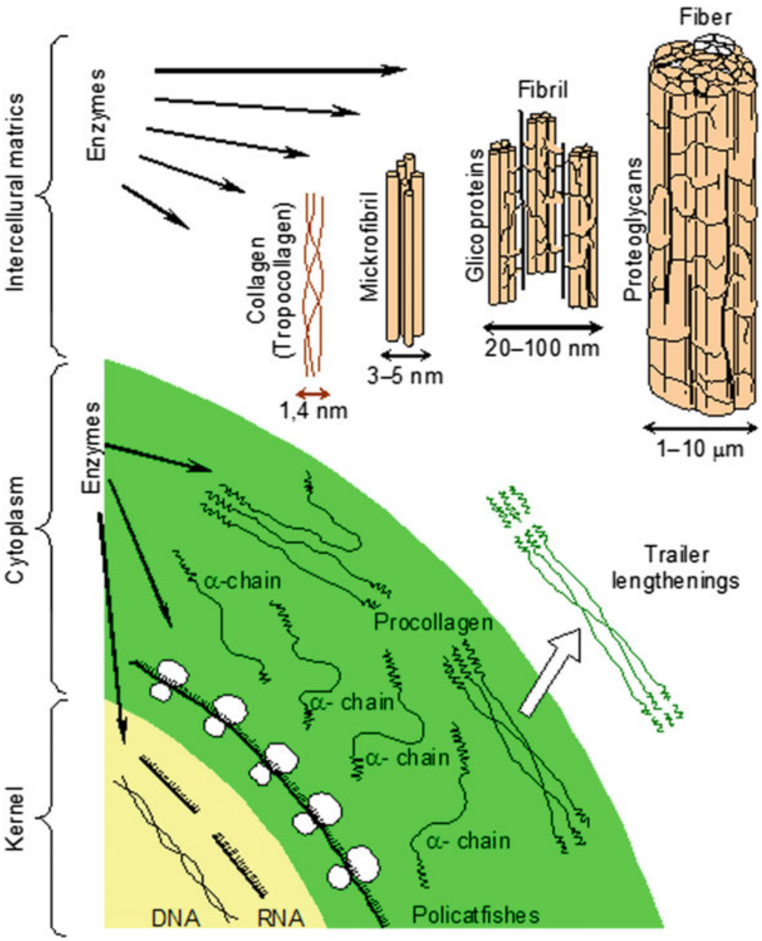

Fig. 2.41 The biosynthesis of collagen structures

lubricants such as graphite, MoS_2 etc., but is characterized by considerably weaker interaction between single layers due to their liquid-crystalline state. As a result, in sliding shear is localized in interlayer regions of the liquid-crystalline structure and weak interaction between layers provides low friction in the joint that is confirmed experimentally (Fig. 2.43b, c). The above explanation is supported by the fact that the lubricating behavior of the model lubricants with liquid crystal compounds is similar to that of natural synovia.

It was noted, that in addition to high antifrictional qualities, model systems containing liquid-crystalline compounds, exhibit a powerful biological effect, so that useful medicinal preparations can be developed to correct tribology in arthrosoarthritis affected living joints [200–209].

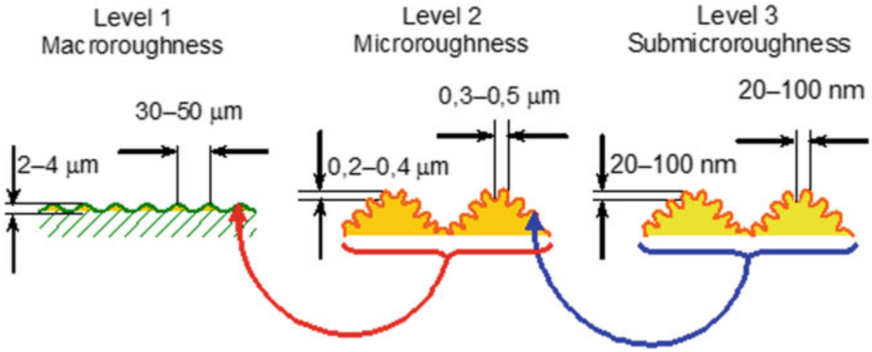

Fig. 2.42 The scheme of multilevel surface relief of the cartilages

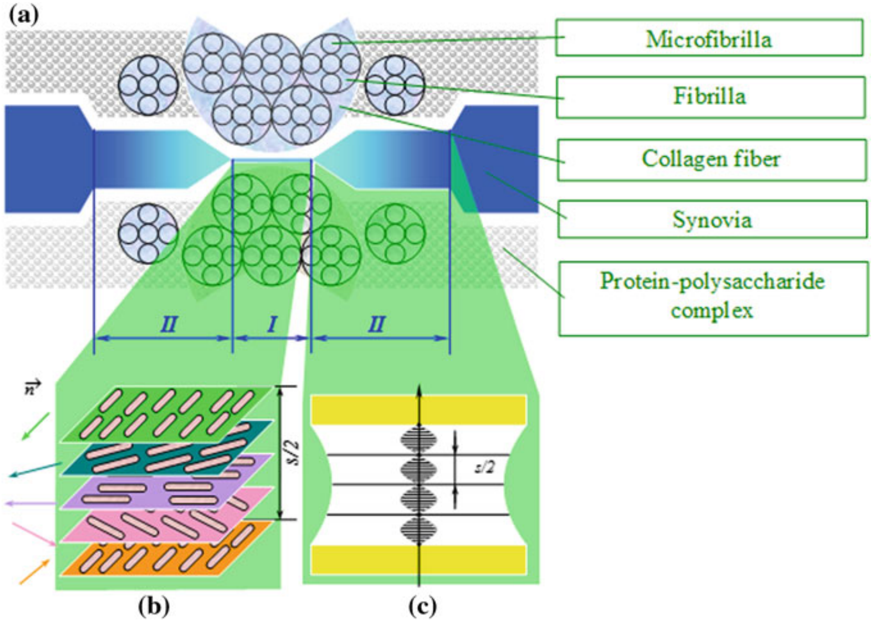

Fig. 2.43 Model of the liquid-crystalline state of lubrication in the living joints: **a** contact of the cartilage at intra-articular friction in the synovial fluid; **b** monocrystalline film of cholesteric type in the contact of the collagen fibers (I); **c** multi-molecular film of cholesteric type on the contact edges (II) of collagen fibers

It is obvious that detailed experimentations in this area is impossible on industry-standard friction machines. Consequently, the creation of original device and equipment is required. That's why in the following chapter we elaborate on some issues of practical implementation and application of developed method and means of triboengineering tests to investigate of friction processes of natural and artificial tribosystems.

References

1. B.N.J. Persson, *Sliding Friction: Physical Principles and Applications* (Springer, Berlin, 2000), p. 516
2. N.K. Myshkin, C.K. Kim, M.I. Petrokovets, *Introduction to Tribology* (CMG, Seoul, 1997), p. 292
3. N.K. Myshkin, A.I. Sviridenok, D.V. Tkachuk, New Tendencies in Tribology in Relation to the Scientific Heritage of I.V. Kragel'skii, J. Friction Wear **29**(4), 251–258 (2008)
4. K.C. Ludema, *Friction, Wear, Lubrication: A Textbook in Tribology* (CRC Press Inc., Boca Raton, 1996), p. 257
5. V.A. Belyi, K.C. Ludema, N.K. Myshkin (ed.), *Tribology in the USA and the Former Soviet Union* (Allerton Press, NY, 1994), p. 456
6. I.V. Kragelsky, V.V. Alisin, N.K. Myshkin, M.I. Petrokovets (ed.), *Tribology—Lubrication, Friction, and Wear, Handbook* (PEP Publishers, London, 2001) p. 948
7. P.N. Bogdanovich, V.Y. Prushak, *Friction and Wear in Machines* (Vysheishaya Shkola, Minsk, 1999), p. 374 (in Russian)
8. N.K. Myshkin, I.G. Goryacheva, Tribology: Trends in the Half-Century Development, J. Friction Wear **37**(6), 513–616 (2017)
9. Y. Kimura, K. Nakano, T. Kato, S. Morishita, Control of friction coefficient by applying electric fields across liquid crystal boundary films. Wear **175**, 143–149 (1994)
10. F.P. Bowden, D. Tabor, *The Friction and Lubrication of Solids* (Clarendon Press, Oxford, 1964), p. 544
11. A.P. Semenov, Antifriction materials: experience of application and perspectives. Trenie Smazka Mash. Mekhan. **12**, 21–36 (2007) (in Russian)
12. A.T. Volochko, Antifriction properties of composite aluminum materials under liquid and boundary friction. J. Friction Wear **26**(6), 67–72 (2005)
13. R.N. Zaslavskii, Perspectives of tribopolymer—producing compounds for lubrication material production. Trenie Smazka Mash. Mekhan. **3**, 21–33 (2006) (in Russian)
14. P.A. Rebinder, E.D. Shchukin, Surface phenomena in solids during the course of their deformation and failure. Sov. Phys. Usp. **15**, 533–554 (1973) (in Russian)
15. D.N. Garkunov, *Triboengineering* (Mashinostroenie, Moscow, 1989), p. 328 (in Russian)
16. A.S. Akhmatov, *Molecular Physics of Boundary Friction* (Fizmatgiz, Moscow, 1963), p. 472 (in Russian)
17. V.A. Belyi, A.I. Sviridenok, Actual directions of development of study in the region of friction and wear. Sov. J. Friction Wear **8**(1), 1–16 (1987)
18. A.P. Semenov, High-temperature solid lubricating substances. J. Friction Wear **28**(4), 401–407 (2007)
19. A.B. Vipper, V.L. Lashkhi, Y.A. Mikutenok, Effect of friction modificators on engine oil properties. Sov. J. Friction Wear **2**(5), 55–58 (1981)
20. T.A. Lobova, E.A. Marchenko, Interaction between friction surfaces and lubricating materials of the 2H–MoS_2 type. J. Friction Wear **29**(4), 295–301 (2008)
21. V.L. Lashkhi, A.B. Vipper, V.V. Kulagin, Oil-soluble organic compound of molibdenum—additives to lubricating oils. Khimiya i Tekhnologiya Toplivi Masel **1**, 56–58 (1984) (in Russian)
22. N.M. Reniver, J. Hampshiere, V.C. Fox, Advantages of using self-lubricating, hard, wear-resistant MoS_2–based coating. Surf. Coat. Techn. **142–144**, 67–77 (2001)
23. S. Watanabe, J. Noshiro, S. Miyake, Tribological characteristics of WS_2/MoS_2 solid lubricating multilayer films. Surf. Coat. Technol. **183**, 347–351 (2004)
24. C. Donnet, A. Erdemir, Historical developments and new trends in tribological and solid lubricant coatings. Surf. Coat. Technol. **180–181**, 76–84 (2004)
25. D.C. Teer, New solid lubricant coatings. Wear **251**, 1068–1074 (2001)
26. T.A. Lobova, E.A. Marchenko, Tribological properties of W(Mo)Se_2–Ga/In coatings. Trenie Smazka Mash. Mekhan. **11**, 27–31 (2006) (in Russian)

27. T.A. Lobova, E.A. Marchenko, Modified solid lubricating coatings on tungsten diselenide. J. Friction Wear **28**(2), 193–199 (2007)
28. V.N. Puchkov, A.P. Semenov, V.G. Pavlov, Solid lubricants: experience of application and perspectives. Trenie Smazka Mash. Mekhan. **11**, 36–46 (2007) (in Russian)
29. W.J. Bartz, X. Jinfen, Wear behaviour and failure of bonded solid lubricants. Wear **148**(1), 231–246 (1991)
30. T. Shimizu, A. Iwabuchi, H. Mifune, K. Kishi, M. Arita, The frictional properties of a spray bonded MoS_2/Sb_2O_3 film under the fretting in vacuum. Lubr. Eng. **52**(12), 943–948 (1996)
31. A.A. Zuev, Antifriction and antiwear characteristics of silid-lubricant components from chromium and selenium disulfide. J. Friction Wear **13**(4), 131–133 (1992)
32. N. Stephanolopulos, V. Bellido-Gonzalez, J. Hampshire, D.G. Teer, Tribological study of optimized MoS_2 coatings on tool steel specimen pre-coated with TiN. Tribologic et Inginierie des Surfacts (Journees d'etudes, 1995). STF, SIRPE, 57–66 (1996)
33. O.P. Parenago, G.N. Kuz'mina, D.V. Terekhin, Mechanism of MoS_3 triboactive particle formation, in *Proceedings of International Scientific and Technical Conference "Polycomtrib–2011"* (IMMS NANB, Gomel, 2011), pp. 170–171
34. V.G. Novitskii, V.P. Gavrilyuk, D.D. Panasenko, N.A. Kal'chuk, V.Ya. Khoruzhii, The effect of lubricating material and thermal treatment on the resulting subsurface layers and wear resistance of 40X steel in sliding friction. J. Friction Wear **23**(2), 82–86 (2002)
35. A.T. Volochko, G.L. Tsarev, Properties of powder composite materials with lead and graphite. Izv. Akad. Nauk BSSR, Ser. Fiz. Tekh. Nauk. (1), 12–16 (1989) (in Russian)
36. B.N. Arzamasov, T.V. Solov'eva, *A Handbook on Construction Materials* (Mos. Gos. Tekh. Univ., Moscow, 2005), pp. 147–172 (in Russian)
37. A.P. Semenov, M.V. Nozhenkov, About mechanism of lubricating action of solid antifriction materials. Sov. J. Friction Wear **5**(3), 16–22 (1984)
38. J. Congrad, *Alignment of Nematic Liquid Crystals and Their Mixtures* (Gordon and Breach, London, 1982), p. 104
39. A.A. Markov, Y.V. Lun'kov, T.N. Nazarova, V.K. Gusev, Experimental study of adsorption influence of lubricating oils on wear-resistance of metals. J. Friction Wear **5**(3), 123–126 (1984)
40. D. Bobrov, About friction, Graphite and nanotechnologies. Nauka i zhizn' **2**, 97–100 (2008) (in Russian)
41. M. Luty, G.A. Kostyukovich, A.A. Skaskevich, V.A. Struk, O.V. Kholodilov, Methods of creating of lubricating materials with nanomodifiers. J. Friction Wear **23**(4), 48–59 (2002)
42. S.P. Zharinov, Fluorine-containing surfactants for wear-resistant coatings and lubricants. J. Friction Wear **20**(1), 86–93 (1999)
43. Yu. Podgurskas, R. Rukuiza, V.A. Gubanov, P.E. Troichanskaya, Influence of fluoroligomeric materials on operation conditions of precision and sealing friction pairs. J. Friction Wear **21**(1), 51–57 (2000)
44. N.K. Myshkin, A.I. Sviridenok, K. Fridrikh, Development of tribology of polymer materials, in *Proceedings of International Scientific and Technical Conference "Polycomtrib–2011"* (IMMS NANB, Gomel, 2011), pp. 3–4
45. A.P. Krasnov, O.V. Afonicheva, V.B. Bazhenova, V.A. Mit, Tribochemical processes and nano-dimension in polymer systems, in *Proceedings of International Scientific and Technical Conference "Polycomtrib–2009"* (IMMS NANB, Gomel, 2009), pp. 4–5
46. A.P. Krasnov, N.V. Tokareva, V.K. Popov et al., Friction and properties of Ultrahigh-Molecular Weight Polyethylene (UHMWPE), finished by supercritical carbon dioxide. J Friction Wear **24**(4), 429–435 (2003)
47. Y.M. Pleskachevskii, V.E. Agabekov, Achievements of chemistry as fundamental base of material science, in *Proceedings of International Scientific and Technical Conference "Polycomtrib–2011"* (IMMS NANB, Gomel, 2011), pp. 5–7
48. V.P. Sel'kin, A.V. Makarenko, A.Z. Skorokhod et al., The effect of radiation-induced cross-linking on the wear rate of polyvinylidene fluoride during friction in a liquid. J. Friction Wear **29**(1), 45–49 (2008)

49. I.V. Pogotskaya, S.A. Chizhik, T.A. Kuznetsova, Statistical power spectroscopy of nanostructured Langmuir–Blodgett films, in *Proceedings of International Scientific and Technical Conference "Polycomtrib–2011"* (IMMS NANB, Gomel, 2011), pp. 181–182
50. S.S. Pesetskii, S.P. Bogdanovich, N.K. Myshkin, Tribological behavior of nanocomposites produced by the dispersion of nanofillers in polymer melts. J. Friction Wear **28**(5), 457–475 (2007)
51. M.G. Ivanov, V.V. Kharlamov, V.M. Buznik et al., Tribological properties of the grease containing polytetrafluorethylene and ultrafine diamonds. J. Friction Wear **25**(1), 89–92 (2004)
52. *Forum—The Newest Technologies of Struggle with Friction and Wear* (Vladforum, Vladivostok). http://www.forumshop.ru
53. A.A. Okhlopkova, Properties of polytetrafluorethylene modified by ultradispersed diamonds. Mat. Tekhnol. Instrumenty **4**(3), 60–63 (1999) (in Russian)
54. A.M. Malevich, E.V. Ovchinnikov, YuS Boiko, V.A. Struk, Tribological properties of PTFE modified by ultra-dispersed clusters of synthetic carbon. J. Friction Wear **19**(3), 71–74 (1998)
55. A.N. Popov, V.P. Kazachenko, A.V. Rogachev, Structure and triboengineering properties of polytetrafluorethylene coatings, dispersly-strenghtening by nanoparticles formed from active gaseous phase, in *School on Plasmochemistry for Young Scientists of Russia and Union of Independent Countries* (RAN–IGKhTU, Moscow, 2001), pp. 1–3
56. W.X. Chen, F. Li, G. Han, J.B. Xia, L.Y. Wang, J.P. Tu, Z.D. Xu, Tribological behavior of carbon-nanotube-filled PTFE composites. Tribol. Lett. **15**, 275–278 (2003)
57. I.I. Vasiliyev, A study of triboengineering characteristics of fine fullerene films. J. Friction Wear **25**(4), 61–64 (2004)
58. V.I. Komarova, A.I. Komarov, Effect carbon nanotubes introduced in lubricant on triboengineering properties and structure of MDO coatings, in *Proceedings of International Scientific and Technical Conference "Polycomtrib–2011"* (IMMS NANB, Gomel, 2011), pp. 117–118
59. B.V. Ginzburg, D.G. Tochil'nikov, Effect of fullerene-containing additives on the bearing capacity of fluoroplastics under friction. Tech. Phys. **46**(2), 249–253 (2001)
60. P.A. Vityaz', V.I. Zhornik, V.A. Kukareko, A.I. Kamko, Formation of wear-resistant surface structures and mechanism of their damage at friction with lubricant modified by ultradispersed diamond–graphite additives. Part I. Tribological behavior. J. Friction Wear **27**(1), 55–61 (2006)
61. P.A. Vityaz', V.I. Zhornik, V.A. Kukareko, A.I. Kamko, Formation of wear-resistant surface structures and mechanism of their damage at friction with lubricant modified by ultradispersed diamond–graphite additives. Part II. Model of destruction. J. Friction Wear **27**(2), 67–70 (2006)
62. N.F. Dmitrichenko, R.G. Mnatsakanov, O.A. Mikosyanchik, A.I. Kushch, Wear kinetics of contact surfaces with use of C–60 fullerene additive to motor oil. J. Friction Wear **30**(6), 399–403 (2009)
63. H. Hirai, K. Kondo, N. Yoshizawa, M. Shiraishi, C–60 fullerene. Appl. Phys. Lett. **64**, 1797–1799 (1994)
64. O.G. Epanchitsev, A.S. Zubchenko, Y.D. Tret'kav, Shock wave synthesis of diamonds of micron size from fullerenes. Doklady Ross. Akad. Nauk **340**(2), 201–203 (1995)
65. O.F. Kireenko, B.M. Ginzburg, V.P. Bulatov, The effect of fullerene on the tribological characteristics of plastic greases. J. Friction Wear **23**(3), 64–68 (2002)
66. B.M. Ginzburg, O.F. Kireenko, D.G. Tochil'nikov, V.P. Bulatov, Formation of antiwear structure upon sliding friction of steel along copper in the presence of fullerene or fullerene carbon-black. Pis'ma Zh. Tekh. Fiz. **21**(23), 38–42 (1995)
67. A.A. Shepelevekii, L.A. Shibaev, B.M. Ginzburg, V.P. Bulatov, Effect of C–60 fullerene on lubricating process in steel–copper trubopair clearance. Zh. Prikl. Khim. **72**(7), 1198–1203 (1999)

68. V.G. Savkin, T.G. Chmykhova, I.O. Delikatnaya, E.N. Volnyanko, The influence of external effects on the structurization of lubricating materials. J. Friction Wear **28**(6), 557–560 (2007)
69. V.G. Savkin, V.A. Smurugov, T.G. Chmykhova, I.O. Delikatnaya, Wetting and spreading of oils containing surfactants and superdispersed fillers. J. Friction Wear **25**(4), 35–41 (2004)
70. E.F. Kudina, D.N. Kushnerov, S.I. Tyurina, T.G. Chmykhova, Effect of dispersed organic silica on the tribological behavior of greases. J. Friction Wear **24**(5), 77–80 (2003)
71. E.N. Volnyanko, S.F. Ermakov, V.A. Smurugov, Influence of a lubricant modified with fine-dispersed β-sialon on a steel surface structure under friction loading. J. Surf. Invest. X-ray, Synchrotron Neutron Tech. **2**(5), 738–743 (2008)
72. V.I. Kolesnikov, N.A. Myasnikova, E.N. Volnyanko, S.F. Ermakov, A.P. Sychev, A.A. Sychev, Lubricants with ceramic nanoadditives and wear-resistant surface structures of heavy-duty junctional joints. Russ. Eng. Res. **31**(5), 454–457 (2011)
73. K.N. Dolgopolov, D.N. Lyubimov, A.G. Ponomarenko et al., The structure of lubricating layers appearing during friction in the presence of additives of mineral friction modifiers. J. Friction Wear **30**(5), 377–380 (2009)
74. D.N. Lyubimov, K.N. Dolgopolov, A.T. Kozakov, A.V. Nikol'skii, Improvement of exploitation properties of lubricating materials by use of clay mineral additives, in *Proceedings of International Scientific and Technical Conference "Polycomtrib–2011"* (IMMS NANB, Gomel, 2011), pp. 144–145
75. R.N. Zaslavskii, V.D. Asrieva, Y.S. Zaslavskii, About mechanism of antiwear action and results of tests of plastic lubricant with tribopolymerformating stiffener. Sov. J. Friction Wear **2**(1), 96–101 (1981)
76. V.G. Lapteva, E.N. Dokuchaeva, V.F. Kaplina, Wear resistance of technological equipment friction pairs at the use of tribopolymerformating lubricating materials. Sov. J. Friction Wear **6**(1), 77–83 (1985)
77. L.S. Pinchuk, V.A. Gol'dade, *Electret Materials in Engineering* (Infotribo, Gomel, 1998), p. 288
78. A.A. Silin, Friction in cosmic vacuum. Trenie Iznos **1**(1), 168–178 (1980)
79. A.A. Silin, About behavior and stability of artificially activated tribosystems. Trenie Iznos Smaz. Mater. **2**, 296–299 (1985)
80. D.N. Garkunov (ed.), *Selective Transfer in Hardly Loaded Friction Joints* (Mashinostroenie, Moscow, 1982), p. 207
81. V.N. Litvinov, N.M. Mikhin, N.K. Myshkin, *Physico-Chemical Mechanics of Selective Transfer at Friction* (Nauka, Moscow, 1979), p. 187
82. M.L. Rybakova, L.I. Kuksenova, *Structure and Wear-Resistance of Metal* (Mashinostroenie, Moscow, 1982), p. 212
83. G.G. Chigarenko, A.G. Ponomarenko, A.S. Burlov, A.G. Chigarenko, Efficient additives on the basis of azo-(azomethine) coordination compounds of transition metals. J. Friction Wear **28**(4), 377–382 (2007)
84. G.G. Chigarenko, A.G. Ponomarenko, A.S. Burlov et al., Effect of chemical structure of coordination compounds of transient metals on lubricating characteristics of oils. J. Friction Wear **27**(2), 92–97 (2006)
85. S.F. Ermakov, V.G. Rodnenkov, E.D. Beloenko, B.I. Kupchinov, *Liquid Crystals in Engineering and Medicine* (Minsk, Asar, 2002), p. 412
86. V.I. Kolesnikov, S.F. Ermakov, A.P. Sychev, Triboinduced adsorption of liquid-crystal nanomaterials under friction interaction of solids. Dokl. Phys. **54**(6), 269–272 (2009)
87. V.I. Kolesnikov, M.A. Savenkova, S.B. Bulgarevich et al., Investigation of the triboengineering characteristics of plastic railway greases with inorganic polymeric additives. J. Friction Wear **29**(3), 200–204 (2008)
88. V.I. Kolesnikov, S.F. Ermakov, F. Daniel et al., Synthesis and study of triboengineering characteristics of a new nanosize ceramic nickel phosphoromolybdate additive to greases. J. Friction Wear **31**(6), 426–432 (2010)

89. V.I. Kolesnikov, A.T. Kozakov, Y.F. Migal, Study of friction and wear in the wheel-rail system by X-ray electron and auger-electron spectroscopy and quantum chemistry. J. Friction Wear **31**(1), 11–22 (2010)
90. P.A. Rebinder, *Physico-chemical Mechanics: Selected Papers* (Nauka, Moscow, 1979), p. 381
91. I.A. Buyanovskii, Application of the kinetic approach to description of the process of boundary lubrication. J. Friction Wear **24**(3), 72–80 (2003)
92. A.V. Chichinadze, I.A. Buyanovskii, B.E. Gurskii, The diagram of transitions and the screening effect of lubricating layer. J. Friction Wear **23**(3), 90–97 (2002)
93. D. Moore, *Principles and Applications of Tribology* (Pergamon Press, Oxford, 1975), p. 488
94. S.F. Ermakov, V.P. Parkalov, V.A. Shardin, R.A. Shuldykov, Effect of liquid-crystal additives on tribological performance of dynamically contacting surfaces and mechanism of their friction. J. Friction Wear **25**(2), 87–91 (2004)
95. G. Biresaw (ed.), *Tribology and the Liquid-Crystalline State* (American Chemical Society, Symposium Series, 1990) (441), p. 130
96. A.S. Sonin, *Introduction in Liquid Crystal Physics* (Nauka, Moscow, 1983), p. 104
97. I.A. Buyanovskii, Y.N. Drozdov, Z.N. Ignat'eva et al., Effect of orienting coatings on the apparent activation energy of boundary film destruction. J. Friction Wear **28**(1), 12–18 (2007)
98. I.A. Buyanovskii, V.A. Levchenko, Z.N. Ignat'eva, V.N. Matveenko, Nanostructured carbon coating-orientant and its interaction with boundary lubricating layers. J. Friction Wear **30**(6), 415–419 (2009)
99. I.A. Buyanovskii, Z.N. Ignat'eva, V.A. Levchenko, V.N. Matveenko, Orientation ordering of boundary layers and lubricity of oils. J. Friction Wear **29**(4), 282–287 (2008)
100. S. Morishita, K. Nakano, Y. Kimura, Electroviscous effect of nematic liquid crystals. Tribol. Int. **26**, 399–403 (1993)
101. Y. Kimura, K. Nakano, S. Morishita, Liquid crystal as potential lubricant—possibility of active control of friction coefficient, in *Proceedings of the 6th Nordic Symposium on Tribology*, vol. 2 (1994), pp. 313–322
102. V.E. Fertman, *Magnetic Fluids: A Textbook* (Minsk, Vysheishaya Shkola, 1988), p. 184
103. A. Mishchak, tribological properties of ferrofluid. J. Friction Wear **27**(3), 81–86 (2006)
104. A.N. Bolotov, S.N. Grigor'ev, I.V. Gorlov, Magnetopowder method of abrasive medium confinement. Sov. J. Friction Wear **10**(6), 91–93 (1989)
105. A.N. Bolotov, K.K. Sozontov, D.V. Orlov, Role of structural components of machine oil in boundary lubrication conditions. Sov. J. Friction Wear **12**(5), 44–49 (1991)
106. A.N. Bolotov, N.V. Lochagin, YuO Mikhalev, Magnetic field role at friction of surfaces, Lubricated by machine oil. Sov. J. Friction Wear **9**(5), 80–86 (1988)
107. A.N. Bolotov, V.V. Novikov, O.O. Novikova, Friction of a structured magnetic fluid sliding over a solid surface. J. Friction Wear **27**(4), 46–51 (2006)
108. N.B. Demkin, A.N. Bolotov, Self-unloading magnetic bearings. Sov. J. Friction Wear **6**(1), 1–6 (1985)
109. E.D. Beloenko, YuM Chernyakova, L.S. Pinchuk, Tribological foundation of hondroprotection method with the help of blood auto-serosity and hyaluronates. Dokl. Nat. Akad. Nauk Belarusi **51**(2), 72–75 (2007)
110. L.S. Pinchuk, Y.M. Chernyakova, V.A. Gol'dade, The tribology of joints and problems of modern orthopedics. J. Friction Wear **29**(3), 224–233 (2008)
111. YuM Chernyakova, ZhV Kadolich, L.S. Pinchuk et al., Electromagnetic field effect on tribological characteristics of synovial fluid. Trenie Iznos **24**(6), 50–55 (2003)
112. L.S. Pinchuk, YuM Chernyakova, S.F. Ermakov, *Tribophysics of Synovial Fluid* (Minsk, Belaruskaya Navuka, 2010), p. 382
113. L.S. Pinchuk, E.A. Tsvetkova, Z.V. Kadolich, Electromagnetic field effect on friction in endoprostheses of joints. J. Friction Wear **22**(5), 69–73 (2001)
114. Y. Yamamoto, J. Yagi, H. Higaki, Effect of electric field externally applied on friction and wear characteristics. Trans. Jpn. Soc. Mech. Eng. **57C**, 2734–2739 (1991)

115. A. Takeuchi, M. Sato, H. Aoki, Effect of electric current on advance of running-in. Japanece J. Tribol. **35**, 1385–1395 (1990)
116. S.C. Tung, S.S. Wang, In-situ electro-charging for friction reduction and wear resistant film formation. Tribol. Trans. **34**, 479–488 (1991)
117. E.V. Korobko, R.G. Gorodkin, V.V. Mtlnichenko, Boundary effects at ERF spreading in electric field. Int. J. Modern Phys. B **10**(23), 3357–3365 (1996)
118. E.V. Korobko, *Electrostructured (Electroreological) Fluids: Hydrodynamic Peculiarities and Possibilities of Use* (Minsk, ITMO, 1996), p. 189
119. V.L. Basinyuk, E.V. Korobko, E.I. Mardosevich et al., Tribotechnical parameter control of friction interfaces. J. Friction Wear **24**(6), 96–102 (2003)
120. V.I. Komarova, V.L. Basinyuk, A.I. Komarov, N.E. Senokosov, New composite friction pairs of friction. Nauka Proizvodstvu **19**(6), 52–53 (1999)
121. V.A. Belyi, C. Ludema, N.K. Myshkin (ed.), *Tribology. Studies and Applications: The Experience in the USA and CIS States* (Moscow, 1993), p. 432 (in Russian)
122. S. Ermakov, A. Beletskii, O. Eismont, V. Nikolaev, *Liquid Crystals in Biotribology. Synovial Joint Treatment* (Springer, Heidelberg, 2016), p. 211
123. B.V. Deryagin, G.K. Strakhovskii, D.A. Malysheva, Measurement of viscosity the boundary (surface) layers of liquids by the method of deflation. J. Exp. Theor. Phys. **16**(2), 171–182 (1946) (in Russian)
124. V.V. Karasev, B.V. Deryagin, Measurement of viscosity the boundary (surface) layers of liquids by the method of deflation. Colloid J. **15**, 1235–1241 (1953) (in Russian)
125. B.A. Altoiz, Measurement of viscosity the boundary (Surface) layers of liquids by the method of deflation, in *Physics of Air-Borne Dispersed Systems*, 21 edn. (Vysheishaya Shkola, Kiev, 1981), pp. 35–40 (in Russian)
126. L.M. Blinov, V.G. Chigrinov, *Electrooptic Effects in Liquid Crystal Materials. Series: Partially Ordered Systems* (Springer, Berlin, 1996), p. 296
127. B.A. Altoiz, Study of the structural characteristics of the boundary (LCD) nitrobenzene layer on the surface of the quartz, in *Problems of Physics of Form Appearance and Phase Transformations* (Kalinin, 1981), pp. 80–86 (in Russian)
128. Y.M. Popovskii, B.A. Altoiz, Study of structural regularity boundary of multimolecular layers of nitrobenzene formed on liofilizirovanny solid support. Colloid J. **43**(6), 1177–1179 (1981) (in Russian)
129. B.V. Deryagin, B.A. Altoiz, I.I. Nikitenko, Study of the structural characteristics epitropic LCD phases of some organic liquids. Trans. USSR Acad. Sci. **300**(2), 377–380 (1988) (in Russian)
130. I.A. Klejman, I.E. Tomashevskii, Features structural regularity near the boundary between the liquid crystal substrate. Crystallography **29**(6), 1214–1215 (1984) (in Russian)
131. B.A. Altoiz, AYu. Popovskii, The study wall of ordering in liquid crystals freeze solid substrate. Colloid J. **19**, 419–423 (1987) (in Russian)
132. B.V. Deryagiin, N.V. Churaev, V.M. Mullur, *Surface Forces* (Nauka, Moscow,1987), p. 202 (in Russian)
133. B.V. Deryagin, N.V. Churaev, Trans. USSR Acad. Sci. **207**(3), 572–575 (1972) (in Russian)
134. B.V. Deryagin, N.V. Churaev, Croat Chem. Acta. **50**(4), 187–195 (1977) (in Russian)
135. J.N. Israelachvili, E.E. Adams, Measurement of forces between two mica surfaces in aqueous electrolyte solution in the range 0–100 nm. J. Chem. Soc. Faraday Trans. **74**(4), 975–1001 (1978)
136. S.F. Ermakov, *Tribology of Liquid-Crystalline Nanomaterials and systems* (Belarusian Nauka, Minsk, 2012), p. 380 (in Russian)
137. E.L. Aero, N.M. Bessonov, Micromechanics of structural liquid layers between solids in contact, in *Itogi Nauki I Tekhniki. Ser.: Mechanics of Fluids and Gases*, vol. 23. (VINITI, Moscow, 1989), pp. 237–315 (in Russian)
138. N.K. Christenson, D.W.R. Gruen, R.G. Horn, J.N. Israelachvili, Structuring in liquid alcanes between solid surfaces: force measurements and mean-field theory. J. Chem. Phys. **87**(3), 1834–1841 (1987)

139. D.I.C. Chan, R.G. Horn, The drainage of thin liquid films between solid surfaces. J. Chem. Phys. **83**(10), 5311–5324 (1985)
140. J.L. Parker, H.K. Christenson, Measurements of the forces between a metal surface and mica across liquids. J. Chem. Phys. **88**(12), 8013–8014 (1988)
141. H.K. Christenson, DLVO (Derjaguin–Landau–Verwey–Overbeek) theory and salvation forces between mica surfaces in polar and hydrogen-bonding liquids. J. Chem. Soc. Faraday Trans. **80**(7), 1933–1946 (1984)
142. H.K. Christenson, R.G. Horn, Direct measurement of the force between solid surfaces in a polar liquid. Chem. Phys. Lett. **98**(1), 45–48 (1983)
143. R.G. Horn, J.N. Israelachvili, E. Perez, Forces due to structure in a thin liquid crystal films. J. Phys. **42**(1), 39–52 (1981)
144. K. Bartolino, G. Durand, Mechanical behavior of the smectic phases near the phase transitions. Solid State Commun. **54**(4), 301–304 (1985)
145. P. Oswald, Fluage en Compression d'un Smectique. J. Acad. Sci. Ter. 2. **296**(18), 1385–1388 (1983)
146. J.M. Pochan, P.T. Erhardt, Shear-induced texture changes in cholesteric liquid-crystal mixtures. Phys. Rev. Lett. **27**(12), 790–791 (1971)
147. J.M. Pochan, D.G. Marsf, Mechanism of shear-induced structural changes. J. Chem. Phys. **57**(3), 1193–1200 (1972)
148. P.P. Erhardt, J.M. Pochan, W.C. Richards, Normal stress effects in cholesteric mesophases. J. Chem. Phys. **57**(9), 3596–3601 (1972)
149. T. Koraka, Note on the normal stress effect in the solution of rodlike macromolecules. J. Chem. Phys. **30**(6), 1566–1567 (1959)
150. J.G. Kirkwood, Rec. Trav. Chim. **68**, 649 (1949)
151. A.C. Eringen, Theory of micropolar fluid. J. Math. and Mech. **36**(1), 1–16 (1966)
152. P. Oswald, M. Kleman, Theorie de Lubrication Appliquee aux Smectiques. C. R. Acad. Sci. Ser. 2. **294**(17), 1057–1060 (1982)
153. Orsay Group in Liquid Crystals, On some flow properties of smectic A. J. Physigue Cl, 305–313 (1975)
154. P.M. Leslie, *Theory of Flow Phenomena in Liquid Crystals. Advances in Liquid Crystals*, ed. by G.H. Brown (Academic Press, NY, 1979), p. 23
155. E.L. Aero, N.M. Bessonov, Hydrodynamic mode of operation of the elastic bearing is slipping boundary conditions in the viscosity. J. Friction Wear **13**(1), 116–124 (1992)
156. J.A. Tichy, Lubrication theory for nematic liquid crystals. Tribol. Trans. **33**(3), 363–370 (1990)
157. J.L. Ericksen, Continuum theory of nematic liquid crystals. Res. Mechanica. **21**, 381–392 (1987)
158. A.S. Vasilevskaja, E.A. Dukhovoj, A.A. Silin, Effect of nematic ordering on sliding friction. Correspondence J. Tech. Phys. **12**(12), 750–752 (1986) (in Russian)
159. B.V. Deryagin, The theory of boundary friction, in *Progress of the Theory of Friction and Wear* (Moscow, 1957), pp. 15–26 (in Russian)
160. E. Cosserat, F. Cosserat, *Theorie des Corp Deformables* (Hermann, Paris, 1909), p. 226
161. S.J. Alien, K.A. Kline, The effect of concentration in fluid suspension. Trans. Soc. Rheol. **12** (3), 457–468 (1968)
162. S.J. Alien, K.A. Kline, Lubrication theory for micropolar fluid. Trans. ASME. E **38**(4), 646–656 (1971)
163. J. Prakash, P. Sinha, Squeeze film theory for micropolar fluids. Trans. ASME. F **98**(1), 139–144 (1976)
164. J. Prakash, P. Sinha, Lubrication theory for micropolar fluids and its applications to a journal bearing. Int. J. Eng. Sci. **13**, 217–232 (1975)
165. P. Sinha, Ch. Singh, Lubrication of rough surfaces. Int. J. Mech. Sci. **24**(10), 619–633 (1982)
166. R.A. Brand, Joint lubrication. Ch. 13. in *The Scientific Basis of Orthopaedics*, 2nd edn. (1987), pp. 373–386

167. S.F. Ermakov, Biomechanics of synovia in living joints. 1. Modern concepts of living joints friction, wear and lubrication. J. Friction Wear **14**(6), 97–109 (1993)
168. H. Muir, P. Bullough, A. Maroudas, The distribution of collagen in human articular cartilage with some of its physiological implications. J. Bone Joint Surg. **52B**, 554–563 (1970)
169. H. Lipshitz, R. Etheredge, M.J. Climcher, In vitro studies of the wear of articular cartilage. The wear characteristics of chemically modified articular cartilage when worn against a highly polished characterized stainless steel surface. J. Biomech. **13**, 423–436 (1980)
170. C. Weiss, L. Rosenberg, A.J. Helfet, An ultrastructural study of normal young adult human articular cartilage. J. Bone Joint Surg. **50A**, 663 (1968)
171. A. Maroudas, P. Bullough, S.A.V. Swanson, M.A.R. Freeman, The permeability of articular cartilage. J. Bone Joint Surg. **50B**, 166 (1968)
172. A. Maroudas, H. Muir, The distribution of collagen and glycosaminoglycans in human articular cartilage and the influence on hydraulic permeability. Chem. Mol. Biol. Intercell. Matrix **3** (1970)
173. F.F. Jaffe, H.J. Mankin, C. Weiss, A. Zarins, Water binding in the articular cartilage of rabbits. J. Bone Joint Surg. **56A**, 1031 (1974)
174. F.K. Linn, Lubrication of joints in animals. Problems of friction ad lubrication. ASME Trans. **2**, 141−153 (1969)
175. C.W. McCutchen, Boundary lubrication by synovial fluid: demonstration and possible osmotic explanation. Federat. Proceed. Lubric. Biomech. **25**, 1061–1068 (1966)
176. P.S. Walker, J. Sikorski, D. Dowson et al., Behavior of synovial fluid on surfaces of articular cartilage: a scanning electron microscope study. Ann. Rheum. Dis. **28**(1), 1–14 (1969)
177. P.S. Walker, A. Unsworth, D. Dowson et al., Mode of aggregation of hyaluronic acid protein complex on the surface of articular cartilage. Ann. Rheum. Dis. **29**, 591–602 (1970)
178. P.S. Walker, B.L. Gold, Comparison of the bearing performance of normal and artificial human joints. Trans ASME. F **95**(3), 333–341 (1973)
179. D. Dowson, A. Unsworth, V. Wright, Analysis of boosted lubrication in human joints. J. Mech. Eng. Sci. **12**, 364–369 (1970)
180. J.M. Mansour, V.C. Mow, On the natural lubrication of synovial joints: normal and degenerate. Trans. ASME F **99**(2), 163–173 (1977)
181. P.A. Torzilli, Mechanical response of articular cartilage to an oscillating load. Mech. Res. Commun. **11**(1), 75–82 (1984)
182. V. Wright, D. Dowson, J. Kerr, The structure of joints. IV. Articular cartilage. Int. Rev. Connect. Tissue Res. **6**, 105–124 (1973)
183. V.C. Mow, J.M. Mansour, The nonlinear interaction between cartilage deformation and interstitial fluid flow. J. Biomech. **10**(1), 31–39 (1977)
184. A. Unsworth, D. Dowson, V. Wright, D. Koshal, The frictional behavior of human synovial joints. 2. Artificial joints. Trans. ASME **F97**(3), 377–382 (1975)
185. I.C. Clarke, R. Contini, R.M. Kenedi, Friction and wear studies of articular cartilage: a scanning electron microscope study. Trans. ASME F **97**(3), 358–368 (1975)
186. A. Unsworth, D. Dowson, V. Wright, The frictional behavior of human synovial joints. Part 1. Natural joints. Trans. ASME **F97**(3), 369–376 (1975)
187. T.A. Prokhorova. O.V. Oganesjan, V.K. Mikhajlov. Problem of the mechanism of low friction of articular cartilages, friction, wear and lubricants, in *Proceedings of the International Science Conference* (Moscow, 1985), pp. 15−16 (in Russian)
188. V.K. Mow, Role of lubrication in biomechanical joints. J. Lubr. Technol. **91F**(2), 320–328 (1969)
189. V.N. Pavlova, *Synovial Medium in Joints* (Meditsina, Moscow, 1980), p. 296 (in Russian)
190. P.C. Seller, D. Dowson, V. Wright, The rheology of synovial fluid. Rheol. Acta. **10**, 2–7 (1971)
191. M.N. Pavlova, B.N. Kumanin, The ultrastructure of rubbing surfaces in a joint. Anat. Histol. Embryol. Arch. **8**, 38–42 (1983) (in Russian)
192. H. Chikama, The role of the protein and the hyaluronic acid in the synovial fluid in animal joint lubrication. J. Jpn. Orthop. Ass. **59**(5), 559–572 (1985)

193. W.H.J. Davis, S.L. Lee, L. Sokoloff, A proposed model of boundary lubrication by synovial fluid: structuring of boundary water. Trans. ASME J. Biomech. Eng. **101**(3), 185–192 (1979)
194. D.A. Swann, *Macromolecules of Synovial Fluid. The Joints and Synovial Fluid*, ed. by L. Sokoloff (New York, 1978), p. 374
195. D.A. Swann, E.L. Radin, M. Nazimiec et al., Role of hyaluronic acid in joint lubrication. Ann. Rheum. Dis. **33**, 318–328 (1974)
196. D.A. Swann, R.B. Hendren R.B., E.L. Radin, The lubricating activity of synovial fluid glycoproteins. Arthritis Rheum. **24**, 22 (1981)
197. D. Gvozdanovic, V. Wright, D. Dowson, Formation of lubricating monolayers at the cartilage surface. Ann. Rheum. Dis. **34**, 100–106 (1975)
198. B.I. Kupchinov, V.G. Rodnenkov, S.F. Ermakov et al. The problem of the mechanism of functioning of the joint as a rubbing body. Trans. Belarusian Acad. Sci. **29**(5), 463−465 (1985) (in Russian)
199. B.I. Kupchinov, S.F. Ermakov, V.G. Rodnenkov, S.N. Bobrysheva, E.D. Beloenko, I.R. Voronovich, Y.M. Pleskachevskii, V.A. Belyi, Property of synovial medium to ensure the high antifriction of cartilages in joints of humans and animals, in *Nauchnye otkrytiya* (Scientific Discoveries) (Moscow, 1999), pp. 14−16
200. Pat. 5,238,929 US, A 61 K 31/56. Correction of tribology of arthritis-affected joints and medicine for its implementation/B.I. Koupchinov, S.F. Ermakov, E.D. Belojenko, V.G. Rodnenkov, V.N. Kestelman, N 779,490. Filed 22.10.91. Published 24.08.93
201. S.F. Ermakov, E.D. Beloenko, O.L. Eismont, Role of liquid crystals in tribological behavior of joint cartilages. J. Friction Wear **25**(5), 31–35 (2004)
202. B.I. Kupchinov, S.F. Ermakov, V.G. Rodnenkov, Role of liquid crystals in the lubrication of living joints. Smart Mater. Struct. **2**, 7–12 (1993)
203. S.F. Ermakov, B.I. Kupchinov, E.D. Beloenko, Liquid crystalline components of synovia and their role in the joint tribology, in *Proceedings of Symposium "Inzynieria Ortopedyczna i Protetyczna"* (Belostok, 1997), pp. 125−131
204. B.I. Kupchinov, S.F. Ermakov, V.G. Rodnenkov, E.D. Beloenko, O.L. Eismont, Some results of studies in liquid-crystalline state of synovial lubricant in joints. J. Friction Wear **23** (3), 69–75 (2002)
205. B.I. Kupchinov, S.F. Ermakov, V.G. Rodnenkov, Study of cartilage tribological properties. Sov. J. Friction Wear **9**(4), 73–77 (1988)
206. S. Ermakov, B. Kupchinov, E. Beloyenko, A. Suslov, O. Eismont, The effect of liquid crystals on tribomechanical properties of cartilages, in *Inzynieria Ortopedyczna i Protetyczna – IOP 99: Proceedings of the Sympozjum* (Bialystok, 1999), pp. 93−99
207. B.I. Kupchinov, S.F. Ermakov, V.G. Rodnenkov, E.D. Beloenko, Relation of the structural-mechanical and antifriction properties of the synovial medium of the joints. Mech. Compos. Mater. **24**(2), 188–194 (1988)
208. E.D. Beloenko, S.F. Ermakov, B.I. Kupchinov, V.G. Rodnenkov, O.L. Eismont, Liquid crystal state of joint synovial lubricating medium. Experimental substantiation. Acta Bioeng. Biomech. **3**(1), 24–32 (2001)
209. E.D. Beloenko, O.L. Eismont, L.A. Pashkevich, I.A. Chved, S.F. Ermakov, Effectiveness of medication containing bioactive cholesteric-nematic liquid crystals substance in treatment of experimental osteoarthritis. Proc. Nat. Acad. Sci. Belarus Med. Ser. **1**, 5–8 (2005)
210. P. Walker, J. Sikorski, D. Dowson, Lubrication mechanism in human joints, bio-engineering group on human joints (University of Leeds, 1966–67), pp. 49−56

Chapter 3
Engineering and Technique of Experimental Tests of Liquid-Crystal Nanomaterials

At the present time there is no doubt that precision tribotechnic tests can be implemented using the methods and devices which are based on modern advances in digital circuitry. Thus, using them methods some fundamental results in the friction of solids have been obtained. It was shown that the pendulum method is fairly sensitive when studying both dry and lubricated friction. The latter is caused by the fact that depending on the thickness of lubricating films formed by polar molecules and the roughness of rubbing surfaces the oscillations of the pendulum differ not only by the amplitude but also by the mode of their attenuation. The application of recent advances in the area of precision tribometrical of tests is the best prerequisite for simulation and investigation of the mechanisms of friction and wear of solids.

3.1 Triboengineering Tests

3.1.1 Triboengineering Tests on Standard Equipment

Triboengineering laboratory tests of steel 45–steel 45 pair are carried out using «partial insert–disc» and «pin–disc» schemes (Fig. 3.1). A serial friction machine SMT-1 is used in the former case (test pattern is shown in Fig. 3.1a). In the latter case—various pin-on-disc friction setup (b contact area is shown schematically in Fig. 3.1; design of pin-on-disc friction setup and its units is given below) is which three rotating cylindrical samples ("pins") contact with the stationary low-slung flat disk are used. Shifting samples are set up in the equilateral triangle tops. Load is applied to a disc on the underside.

Counterfaces for SMT-1 are made in the form of rollers («shaft») $d = 40$ mm in diameter and $h = 20$ mm width and in the form of sectors («partial insert») with a curve radius of a work surface $r = 20$ mm and width $h = 10$ mm.

S. F. Ermakov and N. K. Myshkin, *Liquid-Crystal Nanomaterials*, Springer Series in Materials Science 267, https://doi.org/10.1007/978-3-319-74769-9_3

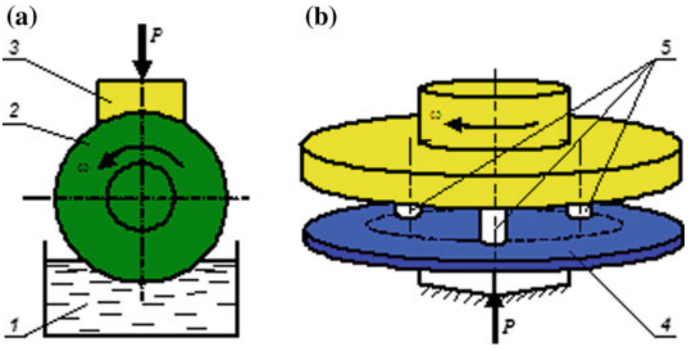

Fig. 3.1 Schemes of tribotests on SMT-1 friction machine (**a**) and pin-on-disc friction setup (**b**): *1*—grease container; *2*—roller («shaft»); *3*—«partial insert» sample; *4*—stationary disc; *5*—pins

Disks of D = 90 mm in diameter and h = 1.5…2 mm thick as well as cylindrical samples (“pins”) of d = 6 mm in diameter and 1.10… 12 mm long are used in tests on a pin-on-disc friction setup. Working area size of «partial insert» samples for the SMT-1 machine is 2 sm^2. The working surface total area of three samples is 1 sm^2.

All samples are processed pretest by emery paper and degreased with acetone and carbon tetrachloride. Then they are aged in silicone fluid PES-V-2. Wear-in quality is estimated visually; process is considered complete when the worn-in area take more than 90% of sample work surface. Wear-in modes are given in Table 3.1.

Experiments on research of adsorption of liquid crystal additive from solution on of dynamically contacting body surfaces are performed at the following modes. Tests are carried out on friction machine SMT-1 at the speed of 0.5 m/s and under load of 720 N (3.6 MPa), paraffin oil with addition of 1% LC is used as a lubricant. Lubrication occurs with roller dip. Lubrication volume during each tests is 15 ml.

Modes are changed taking into account the experience specific features in tests on pin-on-disc friction setup. Tested lubricant in amounts of 5% is smeared on a disk.

Besides, triboengineering test using «shaft–insert» scheme are carried out on a pendulum tribometer.

The original methods to increase an accuracy, resolving power and self-descriptiveness in determining tribophysical characteristics of dynamically contacting couples of friction on these devices are developed. They are considered in the following chapters.

Table 3.1 Wear-in modes of friction couples

Friction machine	Speed (m/s)	Load (MPa)	Materials of samples
SMT-1	0.5	0.8	Steel 45
Pin-on-disc setup	0.15	1.0	Steel 45, copper M1

3.1.2 Integral-Counting Method for Estimation of Small Variations of Oscillation Parameters for High-Precision Tribometry

It is presently beyond the question that precision tribotests could be realized by methods based on oscillation processes [1–4]. These processes are realized using physical pendulum (Fig. 3.2).

Pendulum oscillation amplitude is registered during tests as well as kinetic dependences describing character of frictional interaction are obtained.

Using this method some fundamental results in the friction of solids and lubricity of some matters have been obtained [1, 2]. It was shown that the inclined pendulum method is fairly sensitive when studying both dry and lubricated friction (Fig. 3.2c). In this case, the plane of pendulum oscillation makes an angle φ with vertical [1, 3]. Vertical deviation of oscillation plane is due to contact of pendulum with inclined surface. This surface could be without or with lubricants.

It is shown that decrement of inclined pendulum could be exponential or linear depending on thickness of lubricant films of polar molecules and roughness of rubbing surfaces. The linear dependence (shear resistance is independent on velocity) is taken to be characteristic of Coulomb friction. In contrast, the exponential decrement curve (shear resistance depends on velocity) is typical for viscous friction. In the latter case one should take into account the visco-plastic behavior of both the rubbing bodies and the lubricant since their contribution results in the deviation of the decrement curve of the pendulum oscillation amplitude from the linear one [1, 5].

At the same time, analysis shows that the view of the decrement curve of the oscillation amplitude is determined greatly by the correlation between the radius of the forming along which friction occurs and the radius from the point of suspension to the pendulum center of mass in addition to visco-plastic properties of materials

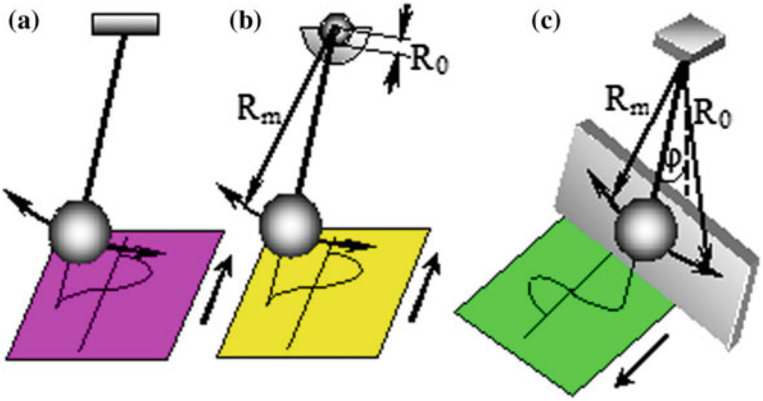

Fig. 3.2 Oscillation processes and options of pendulum tribometers

and media involved in friction. Really, according to [3, 4], their correlation governs the power of the exponential dependence. Hence, it is obvious that the resolution of the inclined pendulum is maximal compared to the similar methods for the evaluation of tribological characteristics using the decrement curve since under these conditions the radius of the friction generatrix coincides with the radius from the point of suspension to the pendulum center of mass. Consequently, the effect of these radii on the exponent is maximal. For the inclined pendulum method, more pronounced dependence of the decay law of the oscillation amplitude on viscous resistance in the friction zone is observed. As a result, a small change of the latter is arising, for example, when varying thickness of lubricating films formed by polar molecules. This change varies the decrement curve shape, that is, the curve transforms from linear into exponential one or vice versa. Therefore, the change in the viscous resistance is registered well by the inclined pendulum method.

Under conditions similar to the real operation of friction units (shafts of machines and mechanisms, human joints, etc.) friction is realized along the generatrix with the friction radius being much smaller than the radius from the point of suspension to the pendulum center of mass. The resolution of the pendulum method obviously decreases at least by an order of magnitude when using these supports since the radius of the friction generatrix (and consequently, the power of the exponential dependence) decreases by the same value [3]. As a result, the effect of viscous resistance caused by friction in the support under investigation becomes so weak that it cannot be determined by the common time dependence of oscillation amplitude decrement or, in other words, by common methods and means for the measurement of oscillation amplitudes.

Problem formulation. The consideration of the problem in more detail shows that oscillation amplitude and its attenuation are informative characteristics in tests with pendulum tribometer. First, the amplitude variation per period of pendulum oscillation is a measure of the friction force acting in the support during the same period [6]. Second, with consideration for the previous note, the dependence of oscillation amplitude variation on the number of cycles is the dependence of the friction force on the sliding velocity in the support [1, 7].

The latter fact is important because with this interpretation it becomes possible to determine the mode of friction in the support under study by the pattern of dependencies of oscillation amplitude variations on the number of cycles as well as by the pattern of velocity dependencies of the friction force (descending, ascending, or constant). Moreover, since the amplitude variations are considerably smaller than the amplitudes, they will be more sensitive to changes occurring in the support. With such approach, resolution is not smaller than in the inclined pendulum method. In addition, precision tribological measurements in real friction conditions become possible. Yet, the problem is how to determine reliably small variations of damping oscillations.

Analysis shows the development of the aforesaid method and its hardware implementation to be a rather complex problem. On the one hand, requirements to the measurement accuracy of the oscillation amplitude become stricter. On the other, because the amplitude variations registered during a cycle are small, more accurate consideration and estimation of interference and noise in a useful signal become necessary. In addition, it should be taken into account that interference and noise can be commensurable to or exceed the oscillation amplitude variations (Fig. 3.3).

In this case, it is obvious that known methods of measuring the maximal signals, e.g. devices for selection with storage or peak detector circuits [8, 9] are inapplicable here. This is caused by the fact that due to considerable scattering of data, we can lose the real pattern of amplitude dependence on the number of cycles (Fig. 3.4, curve *3*).

The proposed method and devices [10–12] allow eliminating the above disadvantages and to achieve a high measurement accuracy of the damping oscillation amplitude and its variations (Fig. 3.4, curves *2* and *4*). The method involves the ideal strobing integration of the input signal and determination of values proportional to the areas of odd or even oscillation half-waves and then, on the basis of the results, the estimation of the oscillation amplitude and its variations per period.

The method can be obviously implemented in both analog and digital variants. The digital variant is advantageous due to general merits of digital circuits compared to analog ones including the absence of intrinsic noise and drift, almost unlimited range of the test variable, etc. It is of particular importance that the digital results are not subjected to drift [13, 14].

In the general case, the digital variant of the suggested method for the estimation of small variations of the damping oscillation amplitude is implemented in accordance with the following algorithm.

The pendulum mechanical oscillations are transformed into the analog signal. Then during time intervals corresponding to the duration of the even oscillation half-waves, the signal under investigation is subjected to integrating analog–digital conversion. It consists in transforming voltage varying during the given time intervals into frequency and counting pulses followed by their transformation, as will be shown below, into the values of the damping oscillation amplitude and memorizing the obtained results.

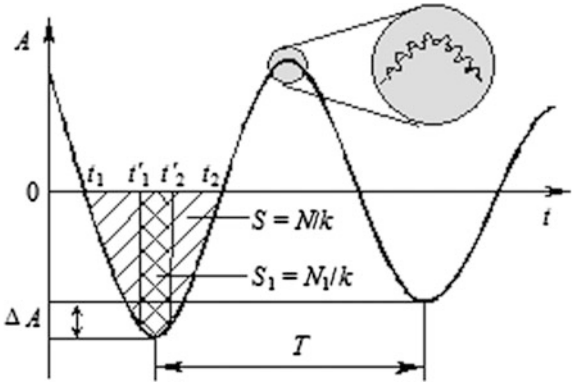

Fig. 3.3 The decrement curve of the pendulum oscillation and its segment given interferences and noises are present in a useful signal

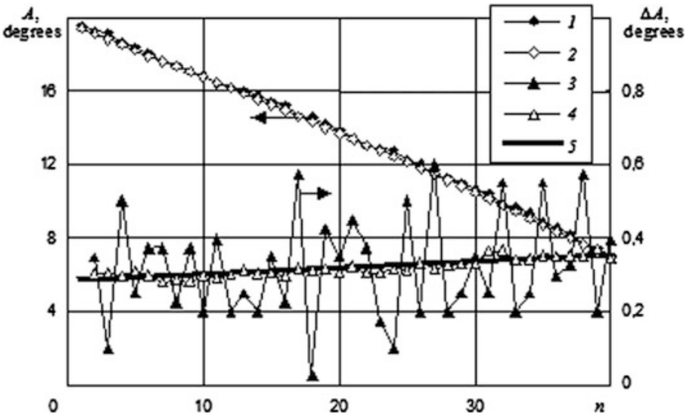

Fig. 3.4 Dependences of amplitude of pendulum oscillation angles (*1*, *2*) and its variations per period (*3*, *4*) for steel–steel pair ("shaft–insert" geometry) lubricated with mineral oil MC-20 under a load of 10 N obtained by different methods: *1*, *3*—known method of signal selection in the region of maximum value; *2*, *4*—proposed method; *5*—linear approximation of experimental data *3*

Further, the results following each other are compared to determine the difference equaling the variations of the amplitude of the oscillations per period. By these procedures, the digital averaging of the experimental data is performed and their high accuracy and reliability are provided (Fig. 3.4, curves *4* and *5*). In case of weak oscillations the algorithm can be changed by estimating, for example the half-waves of the oscillations not following each other, but following in some specified time intervals being multiples to the duration of the half-waves.

Mathematical Model and Errors of Method. For simplicity, let us consider pendulum oscillation damping by the arithmetical law (Fig. 3.3). Then the expression for analog signal describing the pendulum displacement at each moment of time will be written as

$$y = A\cos\omega t, \tag{3.1}$$

where $\omega = 2\pi/T$—is circular frequency.

Then, in line with the proposed investigation method we find the areas of even or odd oscillations half-waves by integrating function (3.1) over the time intervals between the moments when the pendulum passes its equilibrium point. Taking into account the designations introduced the areas can be presented after respective substitutions and transformations in the following way:

$$S = A(\sin\omega t_2 - \sin\omega t_1)/\omega. \tag{3.2}$$

Multiplying the left-hand and right-hand sides of relation (3.2) by transformation coefficient k or introducing the conditions required to implement the digital variant of the method we obtain the digital expression for the areas of oscillation half-waves:

$$N = Sk = Ak(\sin \omega t_2 - \sin \omega t_1)/\omega. \tag{3.3}$$

From relation (3.3) we obtain the general formula for the calculation of the oscillation amplitude in the digital form:

$$A = N\omega/k(\sin \omega t_2 - \sin \omega t_1). \tag{3.4}$$

Using symmetry property of trigonometric ratios:

$$\sin \omega t_1 = -\sin \omega t_2, \tag{3.5}$$

as well as the circumstance that the trigonometric functions have peak unit value when pendulum passes its equilibrium point, we obtain the resultant expression for oscillation amplitude value:

$$|A| = N\omega/2k. \tag{3.6}$$

Therefore, the formula (3.6) is a mathematical expression for determining amplitude values by the developed principles of the strobing integration of damping oscillations and the integral-counting method for their analysis. Let us evaluate the advantages of such a method for finding signal amplitude compare to the known methods and means.

For this purpose, we find the number of pulses N_1 that corresponds to a signal sampling in some region close to the region of the signal amplitude by formula (3.3) taking into account the developed integrating analog–digital transformation (Fig. 3.3):

$$N_1 = Ak\left(\sin \omega t'_2 - \sin \omega t'_1\right)/\omega. \tag{3.7}$$

The number of pulses that corresponds to the same signal sampling with consideration for the known methods for the analog–digital transformation also can be determined as:

$$N'_1 = Ak\left(t'_2 - t'_1\right). \tag{3.8}$$

Then using formulas (3.7) and (3.8), as well as the fact that in both cases the same elements of the analog–digital transformation are used (for example, the “voltage–frequency” transformation) and the condition $N_1 = N'_1$ is satisfied we obtain the expression for the amplitude in the region of the signal sampling:

$$A_1 = \frac{N_1'}{k(t_2' - t_1')} = \frac{A(\sin \omega t_2' - \sin \omega t_1')}{\omega(t_2' - t_1')}. \quad (3.9)$$

The analysis of this expression shows that the value of the signal amplitude A_1, i.e. the value obtained by the known analog–digital methods for its selection, is always less than its true value A being the value obtained by the developed integrating analog–digital method. In the limit at sufficiently narrow samplings expression (3.9) tends to A since in this case the condition: $\sin \omega t = \omega t$. Then, it follows from formula (3.9) that $A_1 = A$. In other words, with decreasing sampling time the error in determining the signal amplitude decreases. However, decrease in sampling time results in decreasing the number of counted pulses N_1 and, hence increasing the reduced counting error σ_{N1}. The latter is determined as a value, which is the inverse of the number of the pulses counted and expressed in percent. Consequently, $\sigma_{N1} > \sigma_N$. One can show that the reduced counting error σ_N of the proposed integral-counting method of determining the amplitude of oscillations is $1/\sin \omega t$ times less than the similar error σ_{N1} of the known analog–digital methods of determining the same characteristics of oscillations.

Moreover, analysis shows that, as samplings are made considerably shorter to obtain the closest coincidence between the signal amplitude being measured and its true value the function $\sin \omega t$ tends to zero. At the same time the value, which is the inverse of the function tends to infinity. The advantage of the proposed method for estimating the oscillation amplitude and its variations over the known methods is seen to be obvious.

Practical implementation. Figures 3.5 and 3.6 show the design and functional diagram of electronic pendulum tribometer with microprocessor data computing and storage as circuit realization of integral-counting method for estimation of small variations in oscillation amplitude. The schemes describing its operation are shown in Fig. 3.7.

The electronic pendulum tribometer includes: pendulum block 1, sensor 2, rectifier 3, voltage controlled oscillator 4, zero-level detector 5, pulse counter 6–8, commutators 9–10, counting pulse oscillator 11, decoder 12, invertor 13, interface block 14, computer 15.

Electronic pendulum tribometer operates in the following manner.

Through the mechanism of a platoon of the pendulum 1 is deflected from the equilibrium to some angle, and then pendulum is released and begins to oscillate. Sensor 2 transforms the mechanical oscillations of the block 1 into analog electric signal (Fig. 3.7a) synchronous with pendulum oscillations.

Analog electric signal delivers from sensor output 2 to rectifier input 3. Rectified signal sent out from output of rectifier 3 (Fig. 3.7b) is fed to inputs of voltage controlled oscillator 4 and zero-level detector 5. The latter forms square oscillations with unit amplitude (Fig. 3.7c) coincident with output signal (3.7b).

The signal is sent out from zero-level detector 5 output to the first data entries of the first 9 and second 10 commutators and counter input of the second pulse counter 6. Logical value 1 changed to 0, when the pendulum passes the equilibrium

Fig. 3.5 Design of electronic pendulum tribometer with microprocessor data computing and storage

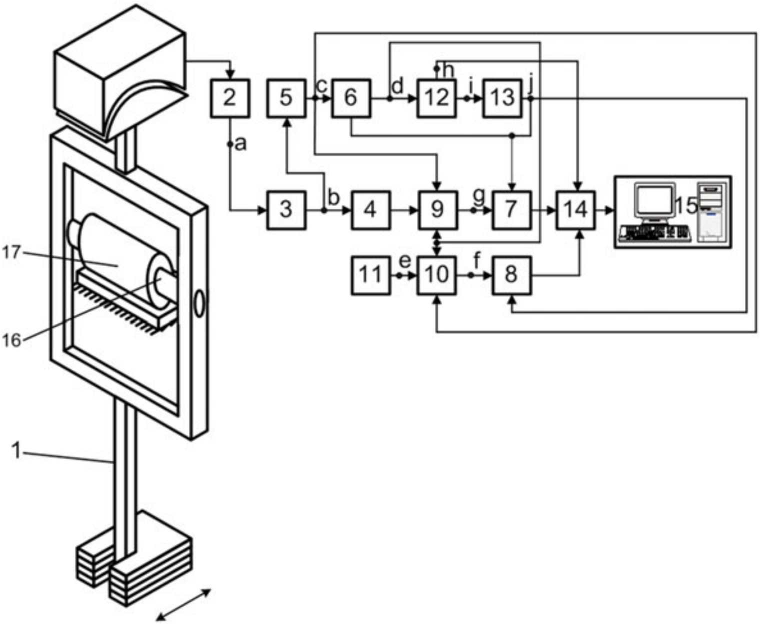

Fig. 3.6 Functional diagram of electronic pendulum tribometer with microprocessor data computing and storage

Fig. 3.7 Voltage diagrams in typical points of scheme shown in Fig. 3.6

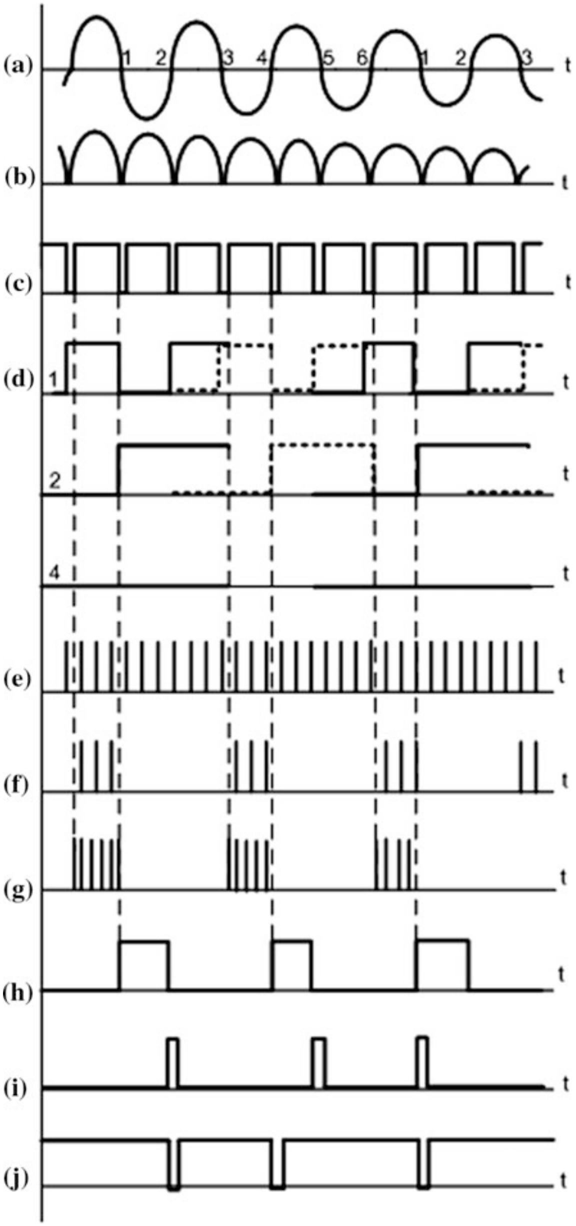

position, and the second pulse counter 6 (Fig. 3.7d) reading in oscillation half waves is activated. The binary-coded signal delivers from counter output to address input of the first 9, second 10 commutators and input decoder 12 converting binary code into decimal. As a result, the first conversion of square oscillation from 0 to 1

(Fig. 3.7c), corresponding to the start of oscillation half wave, connects voltage controlled oscillator 4 to counter input of the first pulse counter 7 through the first commutators as well as the counting pulse oscillator 11, generating constant-interval pulses (Fig. 3.7e), to counter input of the third pulse counter 8 through the second commutator 10.

The pulse counters 7 and 8 starts to read the pulses entering into counting inputs from output of counting pulse oscillator 11 (Fig. 3.7f) and voltage controlled oscillator 4 respectively (Fig. 3.7g).

The second conversion of square oscillation from 0 to 1 (Fig. 3.7c), corresponding to the end of oscillation half wave, disconnect the voltage controlled oscillator 4 to the first pulse counter 7 through the first commutators 9 (Fig. 3.7g) as well as the counting pulse oscillator 11 to the second pulse counter 8 through the second commutator 10 (Fig. 3.7g). Simultaneously, a recording pulse is formed on decoder output (Fig. 3.7h) and parallel loading of counter results occurs from outputs of the first 7 and third 8 pulse counter to interface block 14 for storage and further transfer to a computer 15. The number of pulses from the first counter 7 is in proportion to half-wave square (Fig. 3.7g), as well as from the third counter 8—to the half-wave length (Fig. 3.7f). Experimental data are saved on the hard disk in a text file for further analysis.

The 0/1 conversion appears (Fig. 3.7i), on relevant decoder output (here on the third one) in period multiple of a finite number of half-waves calculated by the second counter 6 (processes for a finite number equals to 3 are shown in Fig. 3.7) and resets the first 7, second 6 and third 8 pulse counters through the invertor 13 by means of 1/0 conversion (Fig. 3.7j). Since the reset pulse duration from the invertor 13 (Fig. 3.7j) of less pulse duration of square oscillations (Fig. 3.7c) is selected, the next 1/0 conversion on zero-level detector 5 output triggers the second counter 6 (Fig. 3.7d). Then the above process is repeated.

The microprocessor unit of the computer 15 accumulates the counter results, read by pulse counters 7 and 8, corresponding to squares and durations of oscillation half-waves. According to them, the amplitude of the oscillations and variations in the period are determined in terms of the above formula (3.6).

After that, computerized microprocessor circuit *15* processes the experimental data according to studies [10–12] and the features of the earlier described processes following the formula:

$$f_n = \frac{\Delta A}{4(n-1)r}, \tag{3.10}$$

where: f_n is the friction coefficient; ΔA is—the attenuation of the pendulum oscillation amplitude per period, *m*; *r* is the radius of major friction unit shaft, *m*.

As a result of mathematical operations performed on the computer 15, the values of the friction coefficients f_n when sliding shaft 16 in the tested friction unit 17 for various lubricating medium per period or cycle *n* of pendulum oscillations and their dependence on the number of oscillations are determined (Fig. 3.4).

Practical Application of Method and Discussion of Results. The method was performed on the pendulum tribometer with microprocessor data computing and storage (Fig. 3.5) when studying time dependencies of the friction coefficient in the support of "shaft–insert" type made of steel 45 and lubricated with a liquid-crystal (LC) lubricant at different temperatures. The shaft diameter was 0.012 m, the pendulum length was 0.51 m. Liquid-crystal compound of cholesterol with the mesophase at 20–35 °C was used as a lubricant. The temperature was kept constant by thermostatic control of the support.

Time dependencies of the oscillation amplitude and friction coefficient obtained by the developed method for the support under study lubricated with LC lubricant at different temperatures are presented in Fig. 3.8.

It is seen that despite a high accuracy of the measurement of the pendulum oscillation amplitude the time dependencies don't give information on the mode of friction occurring in the friction pair. This is because in all cases the shape of these curves is almost independent of the processes occurring in the given friction unit and therefore they are absolutely identical.

A different behavior is noticed for time dependencies of oscillation amplitude variations or, what is the same, of time dependencies of the friction coefficients under the same test conditions. Here it should be noted that the estimation results of friction with LC lubricant under consideration illustrate quite well the most efficient use of the method. In this case all three typical time dependencies of the friction coefficient are observed for the lubricant depending on temperature.

According to papers [1, 4, 7] the dependencies can be interpreted as follows.

At test temperatures that correspond to those of the lubricant mesophase (Fig. 3.8, curve *4*) viscous resistance to movement is proportional to the sliding

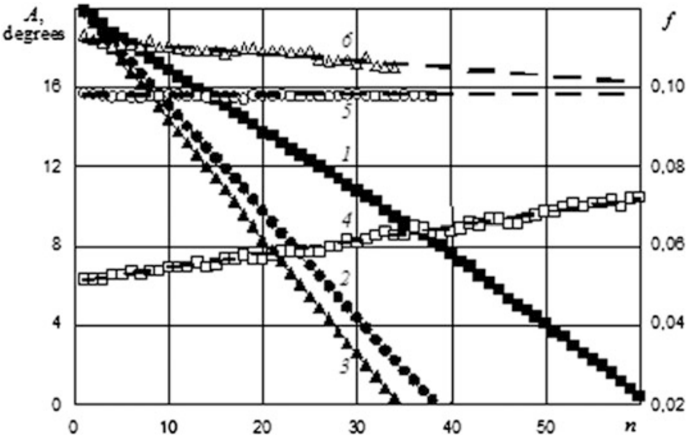

Fig. 3.8 Time dependencies of angle amplitude of pendulum oscillations (*1–3*) and friction coefficients (*4–b*), obtained by the developed method. Friction pair "steel–steel", scheme "shaft–insert", load—20 N, LM—LC-compound of cholesterol at various temperatures: *1*, *4*—22.5 °C; *2*, *5*—43; *3*, *6*—50 °C

velocity but inversely proportional to the thickness of the lubricating film. Therefore, when the shaft penetrates into the film friction increases thus yielding the effect observed in the experiment.

At higher temperatures that correspond to those of the transition from LC-phase to isotropic liquid (Fig. 3.8, curve *5*) when the strength of the lubricating film is still rather high then it evens the microrelief of the rubbing surfaces; as a result, the friction force remains constant being independent on velocity.

With further elevation of the temperature (Fig. 3.8, curve *6*) the lubricating film becomes weaker and fails thus leading to the direct contact of rubbing surface asperity summits. It is their visco-plastic contact that causes the proportionality of the friction force to the velocity and, consequently, decreasing friction force observed in these experiments. In other words, in the experiments with elevating temperature of LC lubricant a gradual transition of one mode of viscous resistance to another one occurs, namely the viscous resistance of the lubricant into the visco-plastic deformation of the material of the rubbing surface asperities. This is revealed in the aforesaid patterns of time dependencies of the friction coefficient. But this is not revealed when analyzing time dependencies of pendulum oscillation amplitude.

Therefore, the proposed integral-counting method for estimating small variations of oscillation parameters possesses adequate information on tribological characteristics and can be recommended for usage in high-precision pendulum tribotests.

3.1.3 Experimental Setup for the Simulation of Friction Processes in Natural Rubbing Organs–Joints

The processes of friction in joints of living organisms there are unique. This is due to discovering of peculiar and mechanism of abnormal low friction in natural rubbing organs–human and animal joints as well as search of more acceptable explanation of effect of these mechanisms on nature of recovery and friction interaction of joint cartilage. Analysis shows that experimental data in this area have been obtained on the reciprocating and rotatory friction machines as well as pendulum tribometers [3–6, 15].

It is obviously that the application pair of friction “cartilarge–cartilarge” in the pendulum is the best prerequisite for simulation and investigation of the mechanisms of friction of joints. In this case, friction is achieved when the articular cartilage rubs on the cartilage rather than on glass or other artificial material.

Investigating of nature of pendulum attenuation makes it possible to study the properties of joint and mechanisms of friction therein.

Nonetheless, a critical review of the published data reveals considerable differences both in assessments of the nature and mechanisms of friction and lubrication in natural joints and in measurements of their friction coefficients [3–5]. These discrepancies are due primarily to the poor sensitivity of the methods and equipment used to register the characteristics of the attenuating oscillation process and to methodological difficulties that introduce extra error into the measurement results. These difficulties include the pendulum working conditions and the accuracy of alignment of the planes of pendulum oscillations with the axes and planes of joint movement [6, 16].

Thus, to improve the methodology of use of the freely reciprocating pendulum for the study of natural joints and their lubricating fluids, the following problems should be solved: (1) accurate and sensitive methods and equipment for measurement of the characteristics of the oscillation process (amplitude, etc.) should be developed; (2) the optimal methods of transformation and digital processing of registered signals should be elaborated and applied; (3) instruments for investigation of articular friction equipped with devices permitting to adjust correctly the pendulum working conditions should be designed. They should ensure the right spatial orientation of the joint studied in relation to the frontal and sagittal planes and the congruence of the rubbing surfaces in the process of experimentation.

It is obviously that successful solution to these problems involves the creation of unified experimental complex ensuring high accuracy and validity of the results, which could be efficiently used in research of friction in joints of living organisms. The proposed method of investigation of the friction processes in natural joints is as follows. Natural synovial fluid is injected into an animal joint partitioned beforehand; the pendulum is set in motion and the area of deflection of the pendulum on each side of equilibrium is determined; and the two adjacent areas are compared and the difference between them is used to determine the friction coefficient in the joint. Then the synovial fluid is removed and replaced with the studied lubricant and the measurement procedure is repeated. The difference between the results allows comparison of the lubricity of each fluid [10]. The principle of working of the such electronic tribometer is based on the conversion of pendulum oscillations into analog electrical signals that are then transformed into a sequence of pulses. The pulses are counted per period of oscillations and the results are processed and recorded.

Figure 3.9 presents the functional circuit of the electronic pendulum tribometer with microprocessor data computing and storage for the simulation of friction processes in joints of living organisms. Figure 3.10 shows the diagrams of stresses in the typical circuit points, wherein the time *t* is counted along the X axis and the deflection of the pendulum from the equilibrium and the level of stresses are plotted along the Y axis as logical values 0 and 1.

The pendulum tribometer (Fig. 3.9) comprises the base 1 of the pendulum with fixing members 2 of the fixed part 3 (the joint socket) of the joint and pendulum 4 comprising fixing members 5 of the mobile part 6 (the ball) of the joint in contact with detector 7 and the mechanism of platoon of pendulum 8.

The pendulum tribometer operates in the following manner. The preselected joint is partitioned, then joint ball *6* is attached to pendulum *4* with fixing members *5* and placed into the joint socket *3*. The latter, with the introduced lubricating medium, is fixed on rigid base *1* of the pendulum mechanism. The mechanism of platoon *8* deflects the pendulum *4* from equilibrium to some angle. After that, the

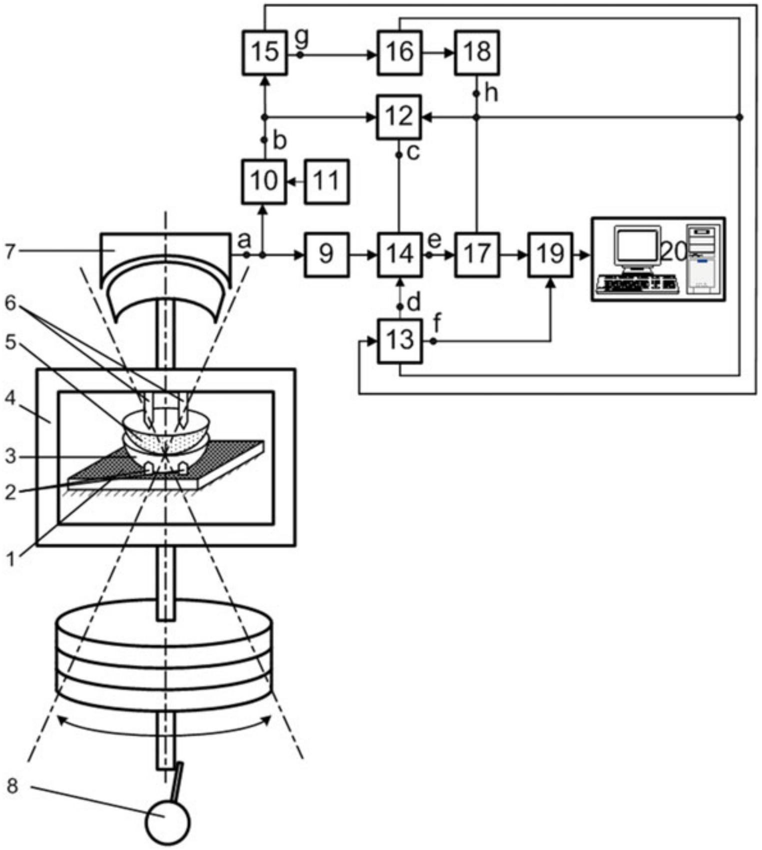

Fig. 3.9 The functional circuit of electronic pendulum tribometer with microprocessor data computing and storage for the simulation of friction processes in joints of living organisms

pendulum is released and begins to oscillate relative to the equilibrium position (Fig. 3.10a). Detector *7* transforms the mechanical oscillations into a sinusoidal signal delivered to the input of voltage–frequency transducer *9* (VFT) and to the first input of comparator *10.* In the second input of comparator *10* receives the reference voltage from source *11* and the comparator compares it with the original analog signals and shapes output pulses (Fig. 3.10b). Then, these pulses are fed to the S input of trigger *12* and through inverter *15* to the S input of trigger *13* and the counting input of pulse counter *16.* Once the pendulum passes through the equilibrium position, logical value 0 changes to 1 at the first output of trigger *12* (Fig. 3.10c) corresponding to the start of the first oscillation half wave (see Fig. 3.10a), and through element AND *14* voltage–frequency transducer *9* is connected to the counting input of pulse counter *17.*

The next passage of the pendulum through the equilibrium position corresponds to the end of the first oscillation half wave (see Fig. 3.10a) and switches over trigger

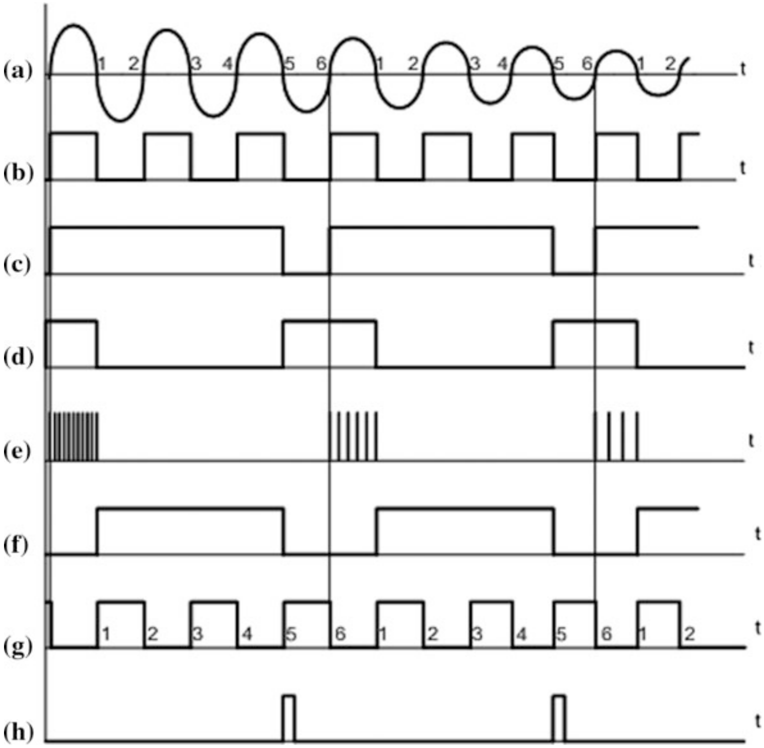

Fig. 3.10 The stresses in the typical circuit points presented in Fig. 3.9

13; its inverse output changes from logical 1 to 0 (Fig. 3.10d) and through element AND *14* disconnects VFT *9* from pulse counter *17.* Thus, the sinusoidal electric signal from the output of sensor *7* goes to the input of VFT *9* and the latter generates a burst of output pulses (Fig. 3.10e); their number is proportional to the area of the first half wave of oscillations. These pulses via member AND *14* proceed to the input of pulse counter *17* where they are summed up and transformed into parallel digital code also corresponding to the first oscillation half wave. The conversion from logical 0 to 1 at the direct output of trigger *13* (Fig. 3.10e) shapes a write pulse that commands parallel loading of the count result from the output of counter *17* into interface block *19* in order to save it and transfer to computer *20.* Simultaneously, the signal inversed by inverter *15* (Fig. 3.10g) by the conversion from logical 0 to 1 triggers pulse counter *16* with its output connected to the output of decoder *18.*

As a result, after the pendulum passes through the equilibrium position the number of times specified after the cycle of measurements (Fig. 3.10 shows five passages of the pendulum through the equilibrium position), conversion from logical 0 to 1 occurs at the corresponding output of decoder *18* (Fig. 3.10h), returning triggers *12*, *13* and pulse counters *16*, *17* to their initial zero state, ready for further measurements. The next passage of the pendulum through the equilibrium position corresponds to the even number after the cycle of measurements ends (Fig. 3.10a, g) and sets logic 1 in trigger *12* (Fig. 3.10c) so that the described processes repeat. Interface block *19* receives the counting results from pulse counter *17* corresponding to the areas of even and odd oscillation half waves. Then the data are transmitted to the computer, where the relevant formulas are used to determine the amplitude of oscillations and their deviations per period. The experimental data are saved to a hard disk in text file format for subsequent analysis.

Formulated differently, the proposed method of simulation of the friction processes in natural joints is embodied in the present pendulum tribometer according to the following algorithm.

The mechanical pendulum oscillations are transformed into analog signals. Then, after the intervals corresponding to the durations of, for instance, even oscillation half waves, they are integrally transformed from analog into digital signals. This means that the time-variable voltage is transformed into the frequency and the resulting pulses are counted. This is followed by their transformation with the relevant formulas into the amplitude of attenuating oscillations and saving of the results. Then the consecutive results are compared in order to determine the difference between them that is equal to the oscillation amplitude variations per period. After that, computerized microprocessor circuit *20* processes the experimental data using the results in [6] and the features of the earlier described processes following the formula:

$$f_n = \frac{\Delta A}{4r}, \tag{3.11}$$

where f_n is the friction coefficient; ΔA is the friction coefficient; and r is the radius of the convex part (the ball) of the joint, *m*.

As a result, the values of the friction coefficient f_n are determined for the cases when joints are lubricated with some lubricating medium per period or cycle n of oscillations, as well as the dependence of the f_n on the number of oscillations (Fig. 3.11).

It has been established that the available methods of measurement of maximum signals, such as sampling circuits with memorizing or peak detecting circuits [8], are not applicable in this case. Because of the substantial data scatter that these circuits produce, the proposed analysis of variations of oscillations can lose sense when the dependences on the number of cycles are used to derive information on the friction characteristics of joints (Fig. 3.11, curve *3*).

The proposed method [10] makes it possible to overcome the above disadvantages and reach highly accurate measurement of the amplitude of attenuating oscillations and the amplitude variations (Fig. 3.11, curves *2* and *4*). This instrument performs perfect strobe integration of the output sinusoidal signal and determines the values proportional to the areas of odd and even half waves of oscillations. The obtained results can be used to assess the amplitude of oscillations and its variation per period, thus determining the friction coefficient.

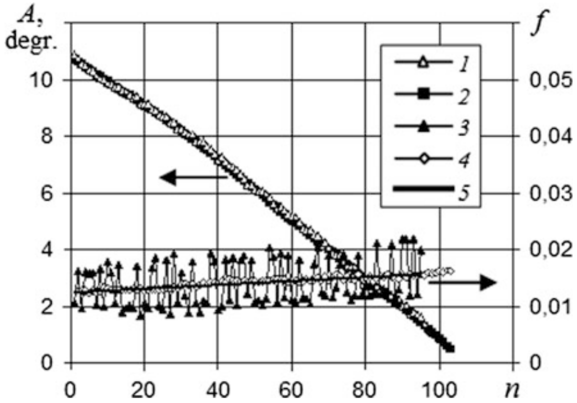

Fig. 3.11 Time dependences of angle amplitudes of pendulum oscillations (*1*, *2*) and friction coefficient (*3*–*5*) obtained with different methods during tests of joints lubricated with natural synovial fluid: *1*, *3*—with known method of signal sampling within maximum signal range; *2*, *4*—with developed method; *5*—linear approximation of experimental data *3*. Load—44.8 N

These operations can be used for digital averaging of the experimental data, ensuring their high accuracy and validity (Fig. 3.11, curves *4* and *5*).

If the oscillations vary only slightly, this algorithm can be modified to assess, for instance, half waves of oscillations that do not follow one after another but rather follow at preset intervals of some multiple of the half-wave duration.

Thus, the proposed method and the experimental computerized system ensure high accuracy and validity of the results and can be useful for study of the processes of friction in the joints, optimization of the lubricating compositions, and the development of new medicinal preparations for healing afflicted joints.

3.1.4 Tribometric Equipment for Precision Tests of Metal- and Biopolymer Coupling

A detailed study of the influence of lubricant media on tribotechnical characteristics of friction pairs from different materials contributes to improve the known and to develop new highly experimental methods and means. One of the effective solution approach is a combined use of present-day developments of precision measurement technique in triboengineering. The latter is defined by the fact that experimental research of various lubricants require high evaluation precision of tribotechnical characteristics over a wide range of measurements.

Analysis shows that research in this area is inseparably associated with study of friction mechanisms of joints in case when, for example, it is required to determine the coefficients of friction with sufficiently low value in the range of 0.005–0.02. A wide experience in application of foreign trigonometric devices implementing friction of cartilage against the glass is currently known [5, 17–19]. However, it should be noted that commercially available domestic friction machines are generally not suited for this purpose.

They have a low accuracy and resolution, especially in the case of measuring the tribological characteristics (friction coefficients etc.) at rather low loads and sliding speeds.

Therefore, the an original pin-on-disc friction setup, that allows us to accurately measure and automatically control during the tests the friction force, linear wear, deformation of dynamically contacting surfaces with varying within wide limits both rotation velocity and loading has been developed [3].

The design of this setup is presented in Fig. 3.12.

It consists of thyristor direct-current drive that gears the working shaft with counterbody placed in insulating plate using belt gearing. Fluted disk of nonimpact rotation speed measuring device is established at the bottom of the working shaft. Besides, the working shaft by means of coupling nipple is connected with mercury slip ring, which enables reliable electrical connection when related testing with metal counterbody. The metal counterbody could be replaced with a counterbody made of any other material.

Three pin samples by demountable collets are fixed to measuring plate, which by means of ball support and box-coupling connected with shaft of precision friction torque measuring instrument.

Ball support in measuring plate provides pin samples self-adjusting during tests. Friction torque measuring instrument can move vertically in sliding bearing of bronze. This provides centering of the instrument and tested samples relative to rotating counterbody.

Loading is carried out through the level-type loading mechanism. Interaction of individual electronic device is done through data control and logging unit.

The temperature in near-contact zone is measured using thermocouples and registered on multiple-point automatic potentiometer RSP-4. Friction force, rotation speed of counterbody and linear wear are registered at the same time and place.

A precision friction torque measuring instrument with adaptable datum is used in the developed pin-on-disc friction setup.

The principle of its operation is as follows: The base, where the torque of the torsion elements is measured, get an overtravel having the same direction and equal-in-magnitude to linear motion of dynamically contacting specimens caused by their wear and counterbody's bearing.

Give it in other words, the friction setup is modified with original torque test system fitted with three inductive sensors that exclude the effect of angular and vertical displacement of torsional elements on the accuracy of torque measurement (Fig. 3.13).

Moreover, one of the sensors is deployed while the other two are in standby during the experiments. This allows making transition from one measuring range to another directly during the test, i.e. without breaking the frictional contact of interfacing surface.

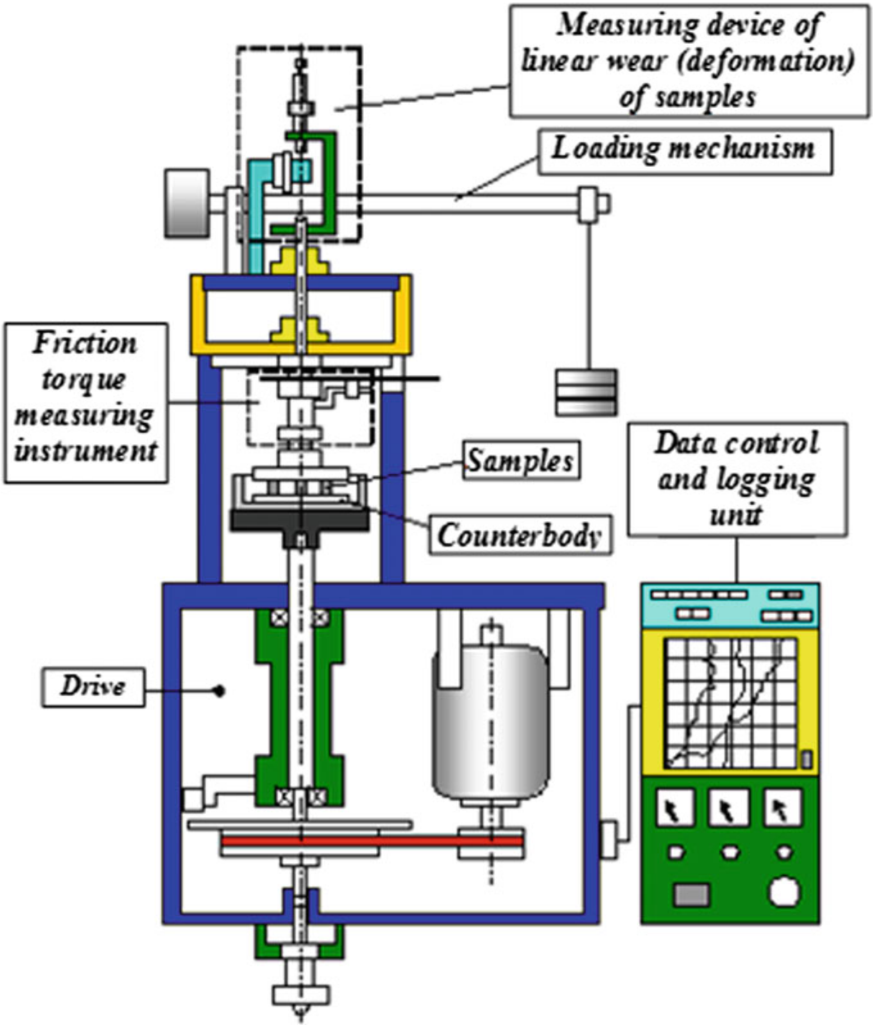

Fig. 3.12 The design of developed pin-on-disc friction setup

In addition, the used original friction calibration system makes it possible to control calibration directly during the test. Also, leverage at calibration and in experiments remains constant, which enables to register the friction force instantly.

An inductive sensor linear-displacement transducer 221 model connected with P 385 K digital measuring system with digital recording is used to measure linear wear. Digital form of displayed data allows us not only to improve accuracy of measurement of sample linear displacement but to get the same errors (about ±0.5 μm) over a rather wide range of sample size variation due to their wear and deformation during the tests.

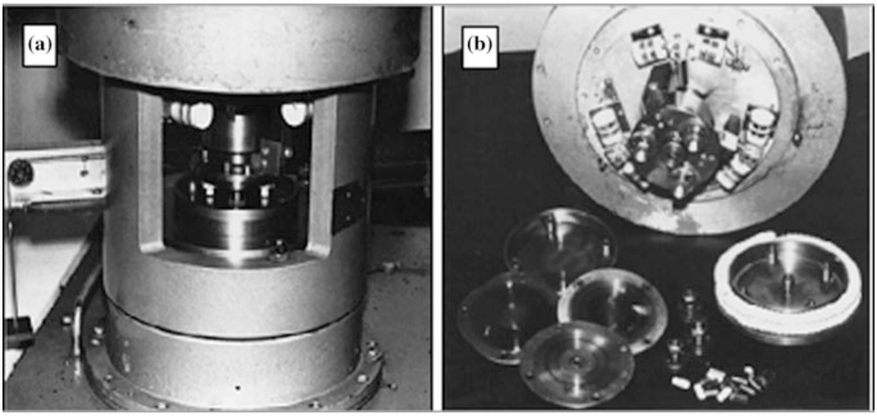

Fig. 3.13 Precision device to measure torque (**a**, **b**) and samples for test (**b**)

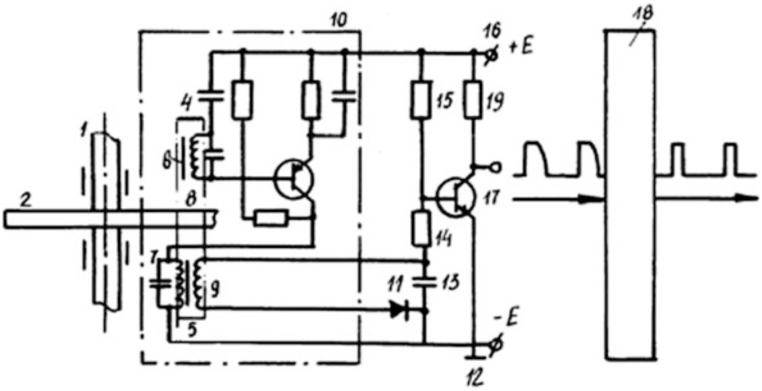

Fig. 3.14 Circuit schematic of rotation speed measuring device (copyright certificate USSR No. 1055247)

Thyristor DC-drive determining stepless speed regulation of counterbody within the speed range from 0.05 to 1.5 m/s is used in the setup. The nonimpact rotation speed measuring device that does not create a static torque on the shaft is used for measuring and automatic control of rotation speed [20]. Its circuit schematic is shown in Fig. 3.14.

The relevancy of this rotation speed measuring device is caused by high setup requirements.

Supplement of additional electronic elements and its structural connection allowing to get steep impulses independent on rotation speed is original in the rotation speed measuring device. This engineering solution promotes a high accuracy (measurement error is less than 1%) of rotation speed definition in a wide range from 0 to speeds limited by mechanical component strength.

The benefit of developed device is the absence of static moment on the shaft. Besides, line output providing easy of speed change registration is in possession of the device. That makes it possible to take into account and define the dependence of tested samples on rotation speed.

The use of offered device together with electronic computers with BCD notation output allow robotizing of research. One of the examples of automatic transition from one rotation speed to another in this device is shown in Fig. 3.15. What is more, automation with the developed rotation speed measuring device can be carried out by other parameters, by load etc.

Nonetheless, other modifications of friction devices are used for triboengineering tests by now. A known lubricant test friction machines e.g. consists a base, a fixed stand, two coaxial shafts meant for allocation of spherical samples on their end-faces, the ring wrapped around the shafts, meant for allocation of three key balls-countersamples inside, contacting with spherical samples, the cup, wrapped around the ring, in sectional electric heater, a roll drive, ball loading frictional moment recording units [21].

A four-ball friction machine for lubricant tests is widespread nowadays. Its top ball is fixed with peg in a holder rotating at a definite speed of a spindle [22]. Three bottom balls are attached fixedly in a cup using screw-nut and washer. The cup is filled with tested lubricant, and then three bottom balls are dipped into it. The bottom balls are pressed to the top by force transferred from removable masses to the cup through a disc, axial bearing, bronze and rubber spacers and a level fulcrum bearing. Consequently, rotation speed of a top ball is set.

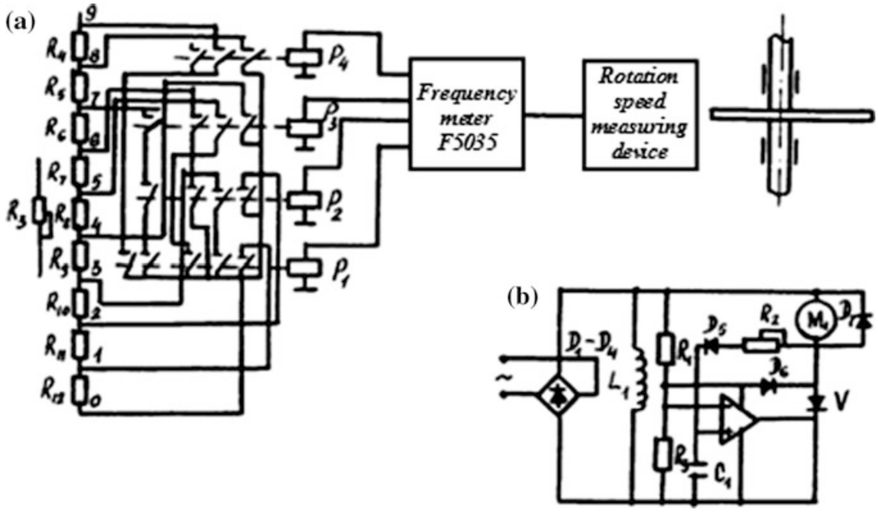

Fig. 3.15 Schemes: **a** automation of research on rotation speed; **b** drive, which speed is regulated by resistor R_3

Sometimes other forms of friction parts are used instead of balls. In particular, four-roll friction machine, serves to research the tribotechnical characteristics of lubricant materials at boundary friction, are not less common [23]. In this machine, a top tapered sample with taper angle 45° is set in a collet of removable spindle and comes in contact with three cylindrical counter-samples using rotatory drive. These roll-samples are centered about an rotation axis of spindle using separator and filler-fungiform and sandwiched between a fillet and a cover in arbor. All arbor with roller-counter-samples is established in oil cap of friction machine equipped with heater. Loading of friction unit is carried out through a jar and an axial bearing, that can move axially freely. Value of friction moment is determined from torque angle of torsion centered about a rotation axis inboard a jar.

However, low accuracy of friction force definition, especially during long-time tests, is a common disadvantage of known friction machines. It caused by zero-rate level, occurring under bending of elastic sensitive element, torsion e.g., and impossibility of measuring and correcting of friction zero-reading during the tests. Besides, limited range of measuring of friction force is another disadvantage of such friction machines. This is due to the fact that only one elastic element with a certain torsion limit could be used in the jar. It is hard to reach. That's why its replacement is allowable only if the friction machine is put out, that breaks friction contact and has a negative impact on processes and results of tests.

Analysis shows that development and application the devices based on precision measurement systems of friction with adaptable reporting base in tribometric equipment and enabling to use some element with different sensitive one-by-one and to control and account zero-rate level directly during the tests could successfully rectify the defects, i.e. increase accuracy and extend a range of friction measurements.

The developed friction machine is an example of solving the application tasks [24, 25].

A general view of the developed friction machine is presented in the Fig. 3.16.

It consists two platforms 4 and 5 fixed on the base 1 through the stands 2 and 3. The shafts 6 and 7 installed coaxially on the platforms 4 and 5 are designed to fix the arbor-adapters 8 and 9. The machine is also consists pin samples 10 and disc counter-samples 11, load center 12, friction measuring system 13, rotation speed measuring unit 14, rotary drive 15 and heating unit 16. The friction measurement system is designed as flat elastic element 17 located on horizontal plate 18 fixed on the shaft 6, that is able to move axially freely. A conical plate 20 centered about the rotation axis of countersample arbor-adapters 9 is located in the rolling bearing 19 on the shaft top. It is compatible with bottom of the countersample arbor-adapters 9 through the first spherical seating 21 and two vertical pin-supports 22 fixed in the top conical part; as well as with elastic element 17 through buckling 23, pivoted to bottom plate part of tapered plate 20. Tension members 26 and 27 with loads 28 and 29 embedded perpendicular to buckling 23 in the opposite directions through the blocks 24 and 25. To calibrate and compensate the friction force during tests, the shaft lower endface is connected with the level 31 pinned in support arm 32 fixed in the bottom of plate 4 serves to fix the loads of load center 12.

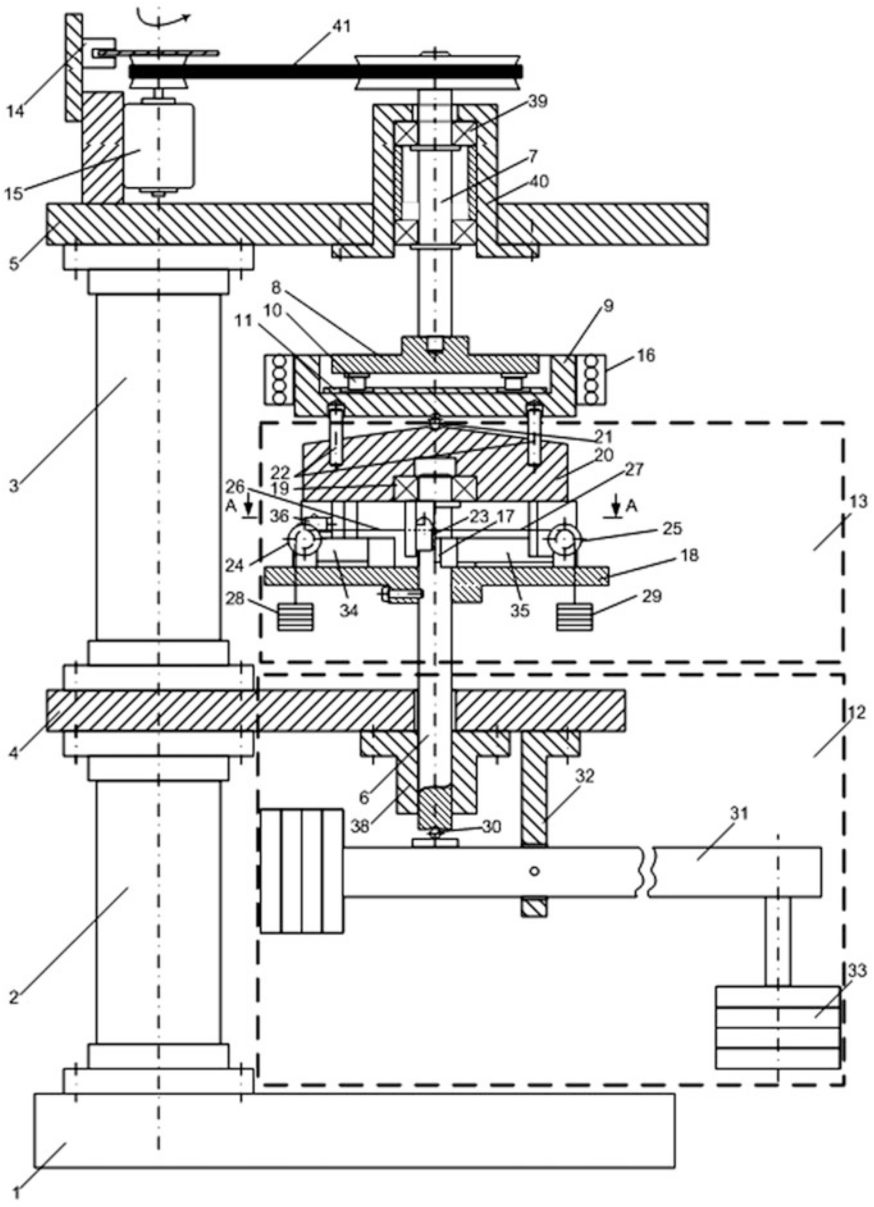

Fig. 3.16 A general view of the developed friction machine

To extend the measurement range of friction force, the friction measurement system 13 consists some flat elastic elements of different thickness (Fig. 3.17), e.g., 17, 34, 35 and the same number of bucklings 23, 36 and 37 pivoted to bottom plate

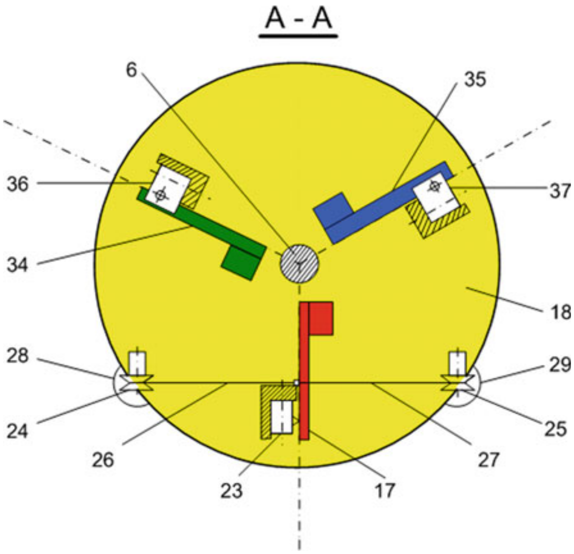

Fig. 3.17 Arrangement of the elastic elements of different thickness in the friction machine (Fig. 3.16—section A-A)

part of tapered plate 20 and circumferentially spaced at an angle 120°, e.g., to rotation axis. One buckling is operable during the tests, but the others are in stably and compatible only with own elastic elements.

Each elastic element should have tension-sensors or interact with linear motion inductive sensors. The latter is located on horizontal plate 18 fixed on the shaft 6. Torque moment occurring during tests at friction of pin samples 10 and disc-countersample 11 with or without lubricant is estimated by sensor signal. The shaft 6 is established in the plain bearing 38, fixed on the platform 4 moving axially. The shaft 7 in the plain bearings 39 located in cylinder guide 40 on the platform 5 does not move axially, vice versa. The drive 15 transmits rotation to shaft 7 through V-belt gear 41.

The friction machine operates as follows.

The pin samples 10 and disc-counter-sample 11 are fixed up in the arbor-adapters 8 and 9, and their friction with or without lubricant are studied, if necessary. Then rotating torques, occurring when applied load 29, are calibrated each after each using the load 29, the tension members 27 and the bucklings 23, 36 and 37 pivoted to bottom plate part of tapered plate 20. Then one buckling engaged with the thinnest elastic element of the friction measurement system is brought into position. For the buckling 23 and the elastic element 17 a zero reading of rotating torques (give it in other words, friction zero reading) is registered. The least load 33 is installed on the level 31 of load center 12; pin samples 10 contact with the disc-countersample 11 through spherical seating 30 and shaft 6 when the latter moves axially. A certain rotation speed of the shaft 7 and pin samples 10 fixed on it with the arbor-adapters 8 is set by means of rotary drive 15. Studies are carried out for a certain period of time, while rotating torque is registered, the friction force, occurring when friction interaction between pin samples 10 and disc-countersample

11, is estimated by use of calibration diagram. Then, elastic element 17 is unloaded, i.e. balanced out the friction force during the tests, with the loads 28 through the block 24 and tension member 26. The obtained data are checked with friction zero reading. The attained results are used as a basis if data do not change due to permanent strain of elastic element, i.e. zero drift does not happen. Otherwise, correction for error, appearing during the tests due to zero drift, is made using loads 28 and 29. Further, the experiments, measurements and control of friction force continue and repeat with a larger load 33 of load center 12. In a case of significant bend of elastic element 17, transfer to a thicker elastic element, here element 34, takes place by means of other buckling, e.g. buckling 36. What is more, that transfer from one elastic element to other could be made directly during the tests, i.e. without breaking the friction interaction between tested samples and counter-sample. Then in case of significant bend of elastic element 34, transfer to even thicker elastic element happens by means of the next buckling 37, and measurements of friction force and control its zero drift is repeated.

Since the elastic elements 17, 34 and 35 placed on a horizontal plate 18, fixed on the shaft 6 and, as a result, could move axially freely at wear of contacting samples, the offered friction measurement system is essentially a system with adaptable reporting base. Its operating principle is as follows: the base, relative to which the measurement of friction torque is made, gets overtravel coinciding in direction and equal in magnitude to linear displacement of dynamically contacting samples, that caused by their wear or beats of disc-counters-sample. Consequently, angular and vertical displacements of elastic elements during the tests do not have an effect on measurement accuracy of friction force.

In summary, the application of original mechanical features, allowing to get a precision friction measurement system with adaptable reporting base, and using the elastic elements of different thickness each after each in the friction machine, as well as control and report of zero drift directly during the tests increase accuracy and extend the measurement range of friction force.

Extensive experience in use of friction units shows that temperature caused by friction and heating the thin surface layers of coupled bodies and lubricant film is one of the most important factors having influence on all properties of rubbing materials determining their antifriction properties. This temperature could be generated in the lubricant layer or in the points of bodies contact. A variety of friction machines was created to simulate these processes in laboratory conditions. They allow performing the friction and wear tests of the lubricant materials and additives in dependence to contact temperature of solid bodies.

Let us consider some the most widely used of them nowadays. These friction machine for determining the temperature resistance of lubricant materials during friction, generally, provide trials of lubricants according to six schemes (Fig. 3.18): A—rotary ball—three stationary balls; B—rotary ball—spherical fillet on the ring endface; C—rotary ball—three stationary tabular samples; D—rotary ball—three cylindrical rollers; E—rotary taper sample—three cylindrical rollers; F—rotary taper sample—tapered fillet on the ring endface [26].

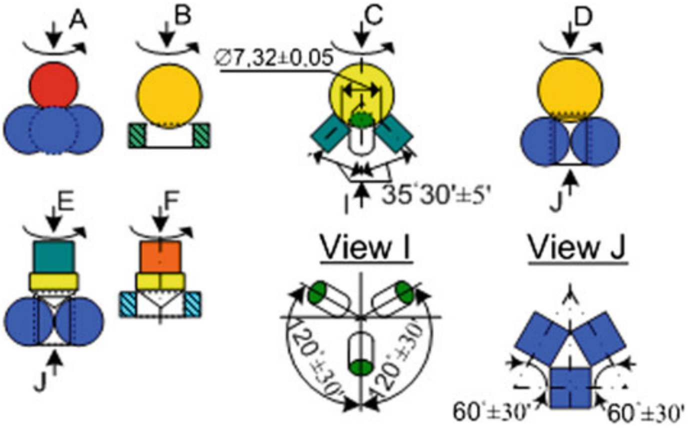

Fig. 3.18 Typical test circuits of lubricant materials

Operating principle of these machines is as follows. A vertical spindle has a chuck for upper rotary sample (ball or cylindrical sample with tapering working surface), that contacts with stationary counter-samples (according to one of described schemes), fixed in a cup with tested lubricant. By means of electric heater the temperature of friction unit and enveloping lubricant layer is changed within the range from 20 to 300 °C and maintained on a level with an accuracy ±3 °C.

A known lubricant test friction machines consists of a base, a fixed stand, two coaxial shafts meant for allocation of spherical samples on their endfaces, the ring wrapped around the shafts, meant for allocation of three key balls-countersamples inside, contacting with spherical samples, the cup, wrapped around the ring, inside the sectional electric heater, a roll drive, ball loading frictional moment recording units [21].

Nevertheless, the most widely used device for thermal-friction tests is a four-ball machine KT-2 designed to investigate the friction in boundary lubrication regime and estimate the critical temperature of lubricant boundary layer on the friction surfaces [27]. The device contains a housing with a stand, carrying a moveable bush with a support arm, where a live spindle with an upper ball-sample fixed on ball-bearings, a drive, including electric motor and V-belt drive, an oil cup with a cage for three bottom balls-countersamples, an electric heater, placed on a axial bearing in a movable barrel related to loading level, a loading level system and a friction measuring unit. The oil cup has a double bottom: the electric heater made of nichrome wire 0.5 mm in diameter (total resistance is about 50 Ω) at the voltage of 127 V or 0.3 mm in diameter (total resistance is about 90 Ω) at the voltage of 220 V is located between the bottoms. Tests of lubricant materials are carried out according to GOST 9490–75 [28]. The electric heater raises the bulk temperature of friction unit and ambient lubricant within the range from 293 to 573 K and maintains it on a level with an error no more than ±5 K. Test period with predetermined temperature is 60 s. The temperature in the bulk lubricant and the friction torque between the samples are registered during one minute.

The use of electric heaters as a heating system is a one of the most typical disadvantages of the known devices for thermal-friction tests. It brings about insufficiently high accuracy (±3–5 K) of the bulk temperature maintenance on a level for a relatively short time (60 s). The accuracy is getting worse during more durable tests, especially when it is necessary to create small heating temperatures of lubricant materials, i.e. electric heaters temperature changes depending on supply voltage time. The use of special control device, thyristor e.g., for temperature regulation of electric heaters requires significant complication of electric heating system and provides maintenance of predetermined temperature within certain limits. This leads to temperature variations in studied friction unit. It is specially undesirable when testing lubricant materials such as cholesteric LC-nanomaterials, which structure is rather temperature-sensitive. Consequently, if they are present in a dynamic contact area, even small temperature changes could cause sufficiently great changes of friction coefficient [29].

The temperature range of the used electric heaters is limited by room temperatures from below (≈20 °C). This is another disadvantage of such systems, because conducting experiments in a wider range, i.e. at lower, including subzero, temperatures becomes necessary when testing lubricant materials.

In addition, the common lack of such heating systems with electric heaters is necessity to supply them from a source at the voltage of 127–220 V, that requires to provide tightened security when testing on these friction devices.

It is obviously, that improving accuracy in maintenance of preset temperatures when it steps in the friction zone for extended periods and range extension of temperature regulation are important tasks to solve these problems when testing the heterogenous lubricants.

This is achieved by means of construction of the device for thermal-friction tests of lubricants. It consists the base, two platforms with coaxial shafts designed to fix the arbor-adapters of samples and counter-samples, a load center, the measuring systems of friction force and rotation speed, a rotary drive and the heating system using a Peltier module as a heating element. The module is attached to a bottom external surface of counter-samples arbor-adapters by one of working surfaces and supported in the packing of thermal insulating material by the other. The packing is connected through the curved plate spring with the bottom of empty cylindrical cup, which is connected coaxially by the endwall surface through a ring-type packing of thermal insulating material to a ring area of bottom external surface arbor-adapter of countersamples; as well as by a bottom through the spherical support and two vertical supports to the load center and through the buckling to the friction measuring system and regulated power supply of the Peltier module [30]. To extend the range of temperature regulation the heating system consists some Peltier modules, that is connected either parallel, or in tandem, and a programmable voltage supply used as regulated power supply of Peltier modules. What is more, the reverser, which reverses the voltage supply polarity of Peltier modules, is located between the Peltier modules and the power supply.

Then, not only heating but also cooling of studied lubricant could be carried out in the suggested friction device. These processes are based on Peltier effect. It involves that when passage of current through a Peltier module made-up of plenty of tailor-made semiconductor slices, some of them heat up, and others get cool at given current direction and vice versa at other current direction. Within this framework, one of the working surfaces of Peltier module, contacting with the surfaces of tailor-made semiconductor slices, heats up integrally, and another one, contacting with other surfaces cools integrally. That said, the temperature of working surfaces of Peltier modules is almost linearly-dependent on supply voltage of Peltier modules and determined by polarity of power supply connection. What is more, the differential temperature between the hot and cold working surfaces depends on a number of semiconductor slices and is always equal for a given supply voltage value. If the differential temperature is 40°, then at the temperature of hot surface equal to 50° the temperature of cold one is 10°. At the 20° on the hot surface—20° below zero on the other cold working surfaces. Peltier modules could be connected in parallel or by tandem—each hot pole of one module to a cold pole of other. Then a high differential temperature, approximately equal to sum of differential temperature of all modules (linear relation is valid for two–three modules) occurs between the hot and cold parts of outermost modules.

Therefore, using the Peltier modules in the offered friction device for thermal-friction tests the heating or cooling are carried out down to subzero temperatures of arbor-adapters of countersamples, and, consequently, of tested lubricant in the friction zone. Herewith the high accuracy of preset temperature maintenance for extended periods is achieved when it steps in the friction zone, i.e. Peltier modules are made on the semiconductor elements, which surface temperature linearly depends on the value of applied supply voltage and maintained to a high precision at a given voltage value. The temperature control over a wide range and the range extension to lower, including sub-zero temperatures are performed by means of the regulated programmable voltage supply and the pole reverser of its connection to Peltier modules. It should be noted that the Peltier modules do not require the high feed voltages (usually they do not exceed 12–15 V), that, in comparison with electric heater, confirms the safer use.

A general view of the developed device for thermal-friction tests of lubricants is shown in the Fig. 3.19. It consists the base 1, two platforms 4 and 5 fixed on it through the stands with coaxial shafts 6 and 7 designed to fix the arbor-adapters 8 and 9 of samples 10 (shown on the Fig. 3.19 is pin samples as samples, and on the Fig. 3.18 are rotary ball, rotary taper sample).

These samples are fixed in the arbor-adapters 8 when required and counter-samples 11 (the disc is shown in the Fig. 3.19 as counter-sample; shown on the Fig. 3.18 are three stationary balls, spherical fillet on the ring endface, three stationary sample with flat surfaces, three cylindrical rollers, tapered fillet on the ring and face). The mentioned counter-samples are fixed in the arbor-adapters 9 if necessary, a load center 12, the measuring systems of friction force 13 and rotation speed 14, a rotary drive 15 and the heating system 16 using a Peltier module 17 as a heating element. The module is attached to a bottom external surface of

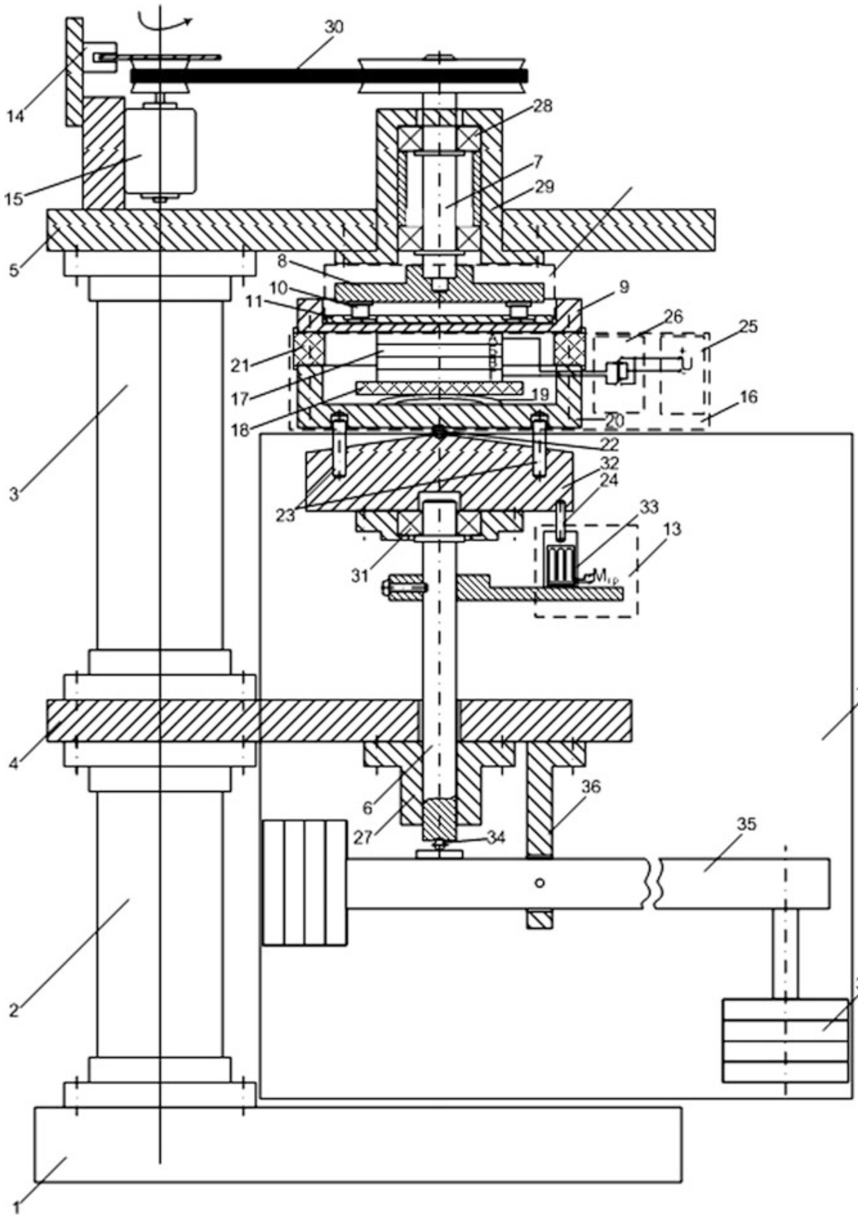

Fig. 3.19 The device for thermal-friction tests of lubricants

counter-samples arbor-adapters 9 by one of working surfaces and supported in the packing of thermal insulating material 18 by the other. The packing is connected through the curved plate spring 19 with the bottom of empty cylindrical cup 20, which is connected coaxially by the endwall surface through a ring-type packing of thermal insulating material 21 to a ring area of bottom external surface arbor-adapter 9 of countersamples; as well as by a bottom through the spherical support 22 and two vertical pin-supports 23 to the load center 12 and through the buckling 24 to the friction measuring system 13 and regulated power supply 25 of the Peltier module.

To extend the range of temperature regulation the heating system consists some Peltier modules 17 (A, B, C, D etc.) connected either in parallel or in tandem, and the programmable voltage supply is used as regulated power supply of Peltier modules. Besides, the reverser, which reverses the voltage supply polarity of Peltier modules, is located between the Peltier modules and the power supply. A shaft 6 is set up in the plain bearing 27 fixed on the platform 4 moving axially. The shaft 7 in the plain bearings 28 located in cylinder guide 29 on the platform 5 does not move axially, vice versa. The drive 15 transmits rotation to shaft 7 through V-belt gear 30. A load center 12 made as the shaft 6 is able to move axially freely. On its upper endface in the rolling bearing 31 the V-shaped plate 32 is located with ball bearing 22, two vertical pin-supports 23 fixed in its upper V-shaped part and buckling 24 in the bottom plate part. Angular rotation of the cup 20 through the ball bearing 22, vertical pin-supports 23 and buckling 24 of V-shaped plate 32 has an effect on the elastic element 33 of the friction measurement system 13. Bottom endface of the shaft 6 through ball bearing 34 in connected with the level 35, pinned in the support arm 36, set on the plate bottom 4 and meant for fixing the loads 37 of the load center 12.

The device operates as follows.

The samples 10 and counter-samples 11 are fixed in the arbor-adapters 8 and 9 according to lubricant test configuration, shown in the Figs. 3.18 and 3.19, and the tested lubricant is located between them. Then a contact between the samples 10 and counter-samples 11 is brought about using the load center 12 through the level 35 with the loads 37 and the shaft 6, when the latter is moved axially. The voltages with preset value and polarity are applied on the Peltier modules 17 by means of the regulated power supply 25 and reverser 26. Heating or cooling down to subzero temperature and the temperature maintenance at a pre-determined level for the required period of the studied lubricant material in the contact zone between samples 10 and counter-samples 11 are carried out in consequence of close contact of one of working surfaces of Peltier modules with a bottom external surface of arbor-adapters 9 of counter-samples 11 according to switch position 26 and supply voltage polarity. The shaft 7 with samples 10 is rotated by means of the drive 15 through the V-belt drive 30. The friction forces occurring in contact of sample 10 and counter-samples 11 turn about rotation axis the arbor-adapters 9 and connected to it the cylindrical cup 20, which affects the elastic element 33 of the friction torque measurement system 13 through the spherical seating 22, two vertical pin-support 23 and buckling 24, steady on the V-shape plate 32. The properties of tested lubricant material at certain temperature are estimated by the obtained friction torque. Then the samples 10 and counter-samples 11 are replaced with new samples, new batch of lubricants is introduced into their contact; then the next temperature level in the dynamic contact area is preset using the regulated power supply 25, and the trials are repeated at the other temperature of the friction unit.

The parameter definition of wear scars contacting dynamically during testing in the various lubricants of balls as accurate as possible isn't less important task when tribotests, especially on the four-ball friction machine.

The technique and device for estimating anti-wear and antiscoring properties of lubricants by virtue of evaluation of ball wear scar, obtained after friction using "rotary disk–stationary ball" scheme [31] is known.

The experimental device for trial of lubricant is known, including a four-ball friction machine, a sample stage (to fix the tested samples) and a toolmaker microscope for analysis of ball wear scars after testing on the four-ball friction machine [32]. The microscope contains a focusing system. A subject of research is located on the sample stage; the adjustment of object is fulfilled using, at least, two axes X and Y. On stage adjustment knobs the divisions are marked; reading is carried out at testing bigger wear scar diameter, along an X-axis e.g., and smaller diameter along an Y-axis, or vice versa. The properties of lubricants (abrasive wear index and critical load) on the four-ball machine are determined by GOST 9490-75 [33].

The most common today is the device for trial of lubricant under laboratory conditions, containing a four-ball friction device, a sample stage and a toolmaker microscope, allowing to determine the wear scars of balls fixed on the sample stage in the diametrically opposite direction by means of screw displacement of micrometer eyepiece [34].

Known devices for estimating wear scars when testing lubricant material has a significant disadvantage. The measurement process of wear scars diameters after testing on the four-ball friction machine requires realization of several stages (setting tested balls on a microscope sample stage such that the biggest wear scar diameter is measured along one of axes of movement of stage or screw micrometer eyepiece, and the smallest—along other axis; movement of the stage or the screw micrometer eyepiece to measure in orthogonally related directions, etc.). It takes a lot of time. At that, accuracy of measurement result is directly dependent on magnification power of the used microscope; and a full, rather than fractal, dimension of tested wear scar is should be definitely observed in its eyepiece field. It should be noted that eyepiece field has limited and rather small dimensions, generally. There are no recording of micro relief nature of studied wear scars and archiving their pictures and parameters in the known devices. They are necessary in the aggregate e.g. for the following more detailed comparative analysis of durability of various lubricants.

The analysis shows that one of the most effective ways to eliminate the noted disadvantages is creation of such devices, where improving accuracy of measurement and informativeness would be achieved by means of imaging wear scar, computer processing of its characteristics and archiving the obtained results.

The device for measurement of wear scars when testing lubricant materials is one of example of problem solving. It consists four-ball friction machine, a sample stage, a microscope with attached video camera and a data-processing unit. What is more, a digital video camera is fixed such that a CCD matrix would be in focus of the microscope [35, 36].

An image of the subject is transported from the digital camera to data-processing unit in real time, the ball with wear scar is positioned according to image on the monitor. As a result, accuracy of estimate of wear scar boundary line, and consequently an accuracy of estimating wear scar diameters increases by means of additional (if other conditions, e.g. microscope magnification, remain constant) increase in wear scar when image is displayed and much the largest size of vision area of the display compared with microscope eyepiece field e.g.

For imaging of tested surface of wear scar, the following stages are fulfilled. The plane defined by ellipse of wear scar border is located perpendicular to a lens. Image sharpness is set up by focus change to increase in brightness levels, from which the scars and back-ground will be determined later. A software package is started to record and save the images. With help of test objects for all used lens types, scale coefficients, allowing to calculate an actual increase in observed image, are set up. In other words, measuring system of actual sizes on monitor is calibrated with chosen magnification.

The biggest D_1 and smallest D_2 wear scar diameters (Fig. 3.20), is defined in orthogonally related directions, the scar parameters are estimate by obtained data during tests using software automatically or interactively, whatever position of subject (a ball) on the sample stage. A scar profile is studied according to certain section or developed 3D model. It should be noted, that the software, used in the proposed device, makes it possible to study of surfaces of not only oval-shaped, but free-form object. Obtained testing data are archived for further more detailed analysis.

Shown on Fig. 3.20 is a flowchart of the device, and on Fig. 3.21—one of examples of its realization in real form with the use of up-to-date computer technology.

The device for measurement of wear scars (Fig. 3.20) consists of a four-ball friction machine 1, a microscope 2; a sample stage 3 with adjustment knobs for position control of studied object in horizontal 4 and in vertical directions 5.

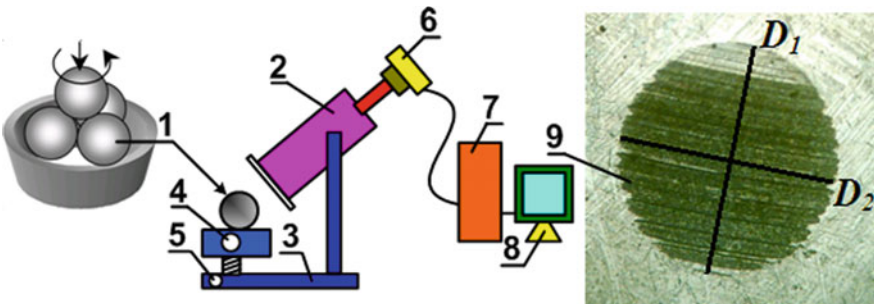

Fig. 3.20 Flowchart of device for measurement of wear scars when testing lubricant materials

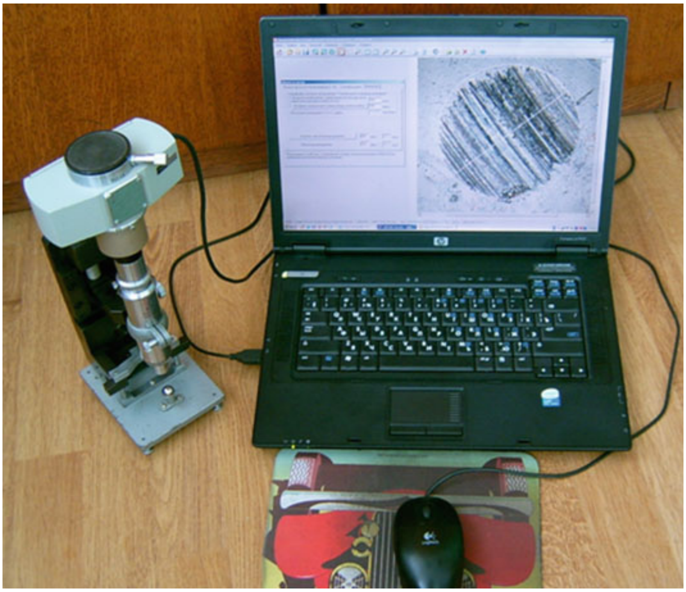

Fig. 3.21 PC-based device for measurement of wear scar when testing lubricant materials

The ball under test with wear scar is established on the microscope sample stage. A digital video camera 6 is fixed on the microscope such that a CCD matrix would be in focus of the microscope. Data-processing unit 4 equipped with monitor 8. Software package is a component of device performance and allows visual inspection of tested surface as bitmap image 9 suitable for interactive indication of the research area and a section selection.

The device operates as follows. The bottom ball is set on the sample stage 3 after testing by a four-ball friction machine 1 so as to a plane defined by ellipse of wear scar border is located perpendicular to a lens. Then the software package of the data-processing unit 7 is started. A camera 6 is adjusted to obtain a clear picture of wear scar on the monitor 8. The required measurements of 9 wear scar image are made by a program complex automatically or interactively. Then they are saved (archived) for further processing.

It should be noted that such comprehensive implementation of these devices and intended use of the described precision devices and systems has significantly improved precision and accuracy at determining tribotechnical characteristics of metal- and biopolymer friction pairs. Eventually, it has made possible to receive a high reproducibility of experimental data when studying friction of not only artificial, but natural rubbing elements, as well as research of lubricating ability of used lubricants and medical preparations.

3.2 Methods to Determine the Structuring Additives and Their Content in the Basic Compositions

3.2.1 *Infrared Spectroscopy*

The additive concentration in the base compositions was evaluated by Fourier transform infrared spectroscopy (FTIR) on a spectrometer Nicolet 5700. Oleic acid cholesteryl esters and oleic acid were used as the additives. Liquid paraffin and polyethylsiloxane PES-V-2 are used as base oils.

The concentration of oleic acid cholesteryl esters and oleic acid in lubricant were estimated by absorption band intensity, 1750 and 1720 cm^{-1} respectively. These bands correspond to oscillations in C=O bond in acids and esters.

The 2% solution of both liquid-crystal nanomaterials and oleic acid were selected as the subject of research on determining the adsorption onto copper, iron and glass powders. Friction surface adsorption upon dynamically contact of steel 45–steel 45 pair is estimated by changes in concentration of 1% LC solution in liquid paraffin. These experiments are based on the technique described in the paper [37].

Its solutions with known concentration were previously investigated for construction of the calibration graphs of dependencies of absorption strength of the spectral line on additive content in the base oil. The graphs constructed using the obtained data are shown in Fig. 3.22.

Experiments to detect adsorption in static contact of the oil solutions with copper, iron, and glass powders were carried out as follows. The pre-rinsed in acetone and air-dried powders of tested materials (6 g) were added to 2% initial lubricant solution (10 ml). The samples were selected immediately after the mixing of these powders with the 2% solution of the oils as well as one day after mixing.

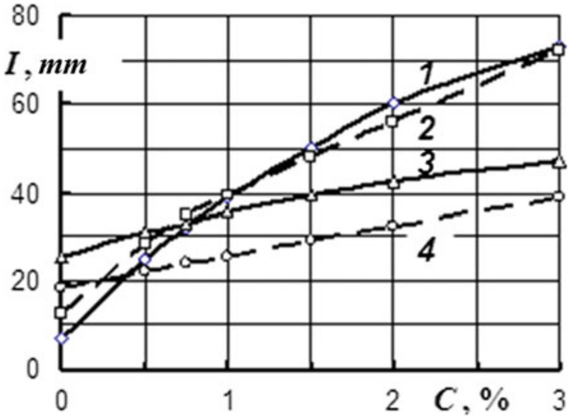

Fig. 3.22 The calibration graphs of dependencies of absorption strength of the typical IR-lines on content of follows additive in the liquid paraffin (*1*, *2*) and organosilicon fluids (*3*, *4*): *3*—oleic acid cholesteryl esters; *2*, *4*—oleic acid

The collected samples were filtered to remove the powder residues. As the filtering takes a certain time, the solutions selected immediately after adding powders still were in contact with the latter about an hour.

3.2.2 *Determination of the Concentration of the Liquid Crystal Additive in the Base Compositions by Measuring a Rotation Angle of Polarization Plane*

Infrared spectroscopy is one of the traditional methods of estimating the concentration of additives in the lubricant. Absorption strength of a certain wavelength intrinsic to the additive is measured through a layer of matter with the additive; content of the additive in the base oil is determined by intensity variation of the absorption band. This method is quite accurate and universal. Nevertheless, another possibility of control of content of cholesteric liquid-crystal nanomaterials in oil solutions based on their optical activity exists.

The cholesteric structure is known to be distinguished from the others by ability to rotate the light polarization plane. It is due to both its organization and molecule structures possessed a chirality [38–41]. This fact was the basis for the study of potential for use of this property of cholesterics to determine their content in the solution (base oil).

The studies of dependencies of optical rotation on LC nanomaterials concentration in the test solution were carried out by means of saccharimeter SU-4.

The operation principle is based on comparison of the brightness polarized light beam, crossed over through the basin with studied solution and then through an analyser, with a brightness of the same beam (control) crossed over only through an analyser.

Torsion angle of the polarization plane is determined based on the rotation angle of a compensated polarizer included in control beam path. Measurements were made in saccharous degrees (°S, $1° = 2.8885°S$) according to technique presented in [42] using the basin $L = 200$ mm in length.

To take off the temperature dependence of the rotation angle of the light polarization plane, the temperature condition is maintained by a thermostat.

The 1, 5 and 10 wt% solutions of cholesteryloleate and cholesterylacetate in Vaseline oil as well as custom medical liquid paraffin are experimentally studied. The results are shown in Fig. 3.23. As seen, injection of LC-nanomaterials in liquid paraffin leads to a change in the optical properties of the base oil, which is expressed in left-hand optical rotation.

Dependence of the angle of rotation of light polarization plane on LC-nanomaterials concentration in liquid paraffin is linear. The angle y is also dependent on type of used additive. So, specific value of polarization plane rotation (CH-16) for cholesteryloleate is $y = 1.35°S$ per 1% of the additive; and for cholesterylacetate (CH-3) that $y = 2.2°S$ (with polirimetric basin length

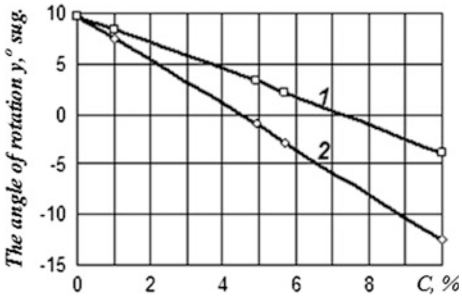

Fig. 3.23 Dependence of the angle of optical rotation of linearly polarized light on cholesteryloleate (*1*) and cholesterylacetate (*2*) concentration in liquid paraffin

L = 200 mm). The dependence of the intensity of the optical rotation on the certain composition of cholesterol ester is explained by both differences in the molecules structure (in particular, a radical of acetic acid is significantly shorter than oleic acid radical) and different molar weight of tested cholesterol compounds, that is 428.7 and 651.1 g for cholesteryloleate and cholesterylacetate, respectively.

The latter circumstance leads to different numbers of molecules per solution volume unit at equal weight concentrations of additives in the basic composition. In this case, the number of cholesterylacetate molecules is approximately by 1.52 times greater than cholesteryloleate.

Given the fact that the molar mass of cholesterylacetate is by 1.52 times more than cholesteryloleate, it can be said that the molecules of cholesteryl esters of acetic acid more optically-active than cholesteryloleate molecules.

Such measurements are possible due to the statistically homogeneous distribution of the liquid crystal molecules in the solution volume, as well as due to their chiral properties [3, 38, 41], when left and left and right directions become different, that causes dependence of optical activity on molecular spatial orientation. The light polarization plane rotates by each molecules through an angle φ, then total angle y is represented the sum of such unit rotations: $y = \sum \varphi_i$.

3.2.3 Development of Methods and Equipment to Control the Mesophase of Cholesteric Liquid-Crystal Nanomaterials and Their Compounds

As is known, control methods of temperature range of LC mesophase is based on physical peculiarities of liquid-crystal state of substance. The analysis shows that mesophase building-up process in smelting of CLC is defined by considerable latent heat and doesn't cause difficulties during tests i.e. it could be well-determined by thermography. This fact is in use in a differential thermal analysis (DTA) and a differential scanning calorimetry (DSC). At the same time, the latent heat of the mesophase–isotropic fluid transition is less by a huge ratio that makes it difficult to measure this transition by means of usual thermographic techniques. A more sensitive research method is needed for that purpose.

In our opinion, a optical rotatory power of CLC in a mesophase could be a base of this method; whereas in contrast an isotropic phase does not possess such a property [3, 41]. As a consequence, while heating of CLC, located between microscope crossed polaroids, light flux decreases almost in discrete steps when mesophase–isotropic fluid transition. It could be registered by means of a light cell embedded into the optical system. If we send a signal is from a light cell output to one of X-Y recorder input and from a warm stage thermal couple to another input, then the dependence of the signal from the light cell which is proportional to light flux passing through the studied sample, on the heating temperature of CLC (Fig. 3.24).

In consequence of step change of light flux when mesophase–isotropic fluid transition, such dependence for CLC has a pronounced kink corresponding to temperature of above transition (Fig. 3.25).

In addition, more detailed experiments have shown that the near-linear dependence of transition temperature of compositions to LC and isotopic liquid phases is present for two-component mixtures of LC-compounds of cholesterol, as against for multicomponent, in a wide range of concentrations.

It is noted that such pattern is most typical for mixtures of enantiotropic n-alkanoats of cholesterol, for which the linear dependence of phase transition

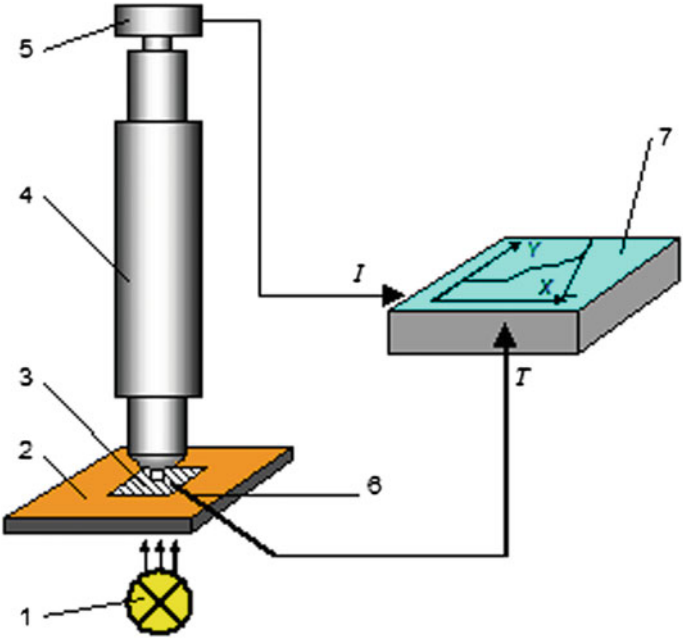

Fig. 3.24 Scheme of a laboratory setup to determine a mesophase temperature range from the light transmission intensity by liquid crystal layer: *1*—light source; *2*—warm stage; *3*—sample; *4*—microscope; *5*—light sensor (light cell); *6*—thermal couple; *7*—X-Y recorder

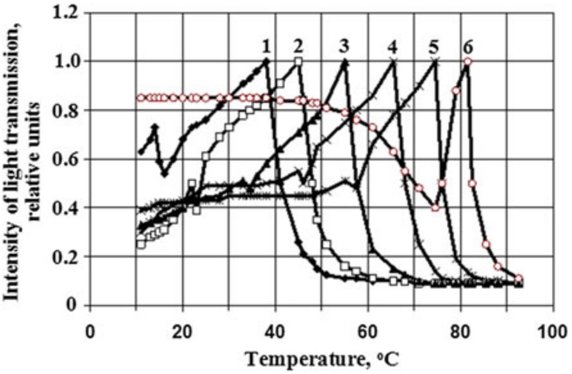

Fig. 3.25 Dependence of light transmission intensity of cholesteric LC-samples of compounds on basis of Tekon-20 and cholesteryl esters of pelargonic acid on the temperature with concentration of cholesteryl esters of pelargonic acid in Tekon-20: 1–0; 2–20; 3–40; 4–60; 5–80; 6–100 wt%

temperature on the composition is observed almost over a range of concentrations from 0 to 100%, and thus includes the transition temperature of primary components.

The scientifically-based control strategy of temperature characteristics of LC-compounds by means of simplification of multicomponent mixtures to two-component with certain temperature parameters and application for them of foregoing patterns typical for two-component mixtures is developed using the obtained results.

The enantiotropic LC-mixtures of cholesterol n-alkanes, effectively correcting the phase transition temperature of LC-compounds in the intended direction of temperatures, and the recommendations for use of such LC-compounds in medicated products and lubricants with the required temperature limit are produced [42, 43].

This method is tested on a polarizing microscope NU-2 equipped with a warm stage made for described purpose. A non-contact precision thermostat BTP-1-type, allowing to vary the heating rate within 0.5–10 °C/min, is used to provide a given heating rate. A PDA-1 type recording gage is applied as X-Y recorder.

The experiments showed that the method performed well in the study of liquid-crystal cholesteric compounds. Furthermore, it distinguish itself by informativity and easy servicing among known thermographic research methods and could be suggested to control the mesomorphic properties of LC-compounds.

As can be seen from the above, the method and the hardware support allowing to view and control without interruption the changes of phase state of LC-preparation depending on the temperature are developed.

References

1. A.S. Akhmatov, *Molecular Physics of Boundary Frictio*n (Fizmatgiz, Moscow, 1963), p. 472 (in Russian)
2. P.A. Rebinder, *Physico-Chemical Mecanics: Selected Papers* (Nauka, Moscow, 1979), p. 381

3. S.F. Ermakov, V.G. Rodnenkov, E.D. Beloenko, B.I. Kupchinov, *Liquid Crystals in Engineering and Medicine* (Asar, Minsk, 2002), p. 412
4. A. Unsworth, D. Dowson, V. Wright, The frictional behavior of human synovial joints. Part 1. Natural joints. Trans. ASME. **F97**(3), 369–376 (1975)
5. R.A. Brand, in *Joint lubrication*. Ch. 13. The Scientific Basis of Orthopaedics, 2nd edn. (1987), pp. 373–386
6. I.C. Clarke, R. Contini, R.V. Kenedi, Friction and wear studies of articular cartilage: A scanning electron microscope study. Trans. ASME. **F97**(3), 358–368 (1975)
7. V.I. Savenko, V.P. Izmailov, O.V. Karagioz, The Application of the pendulum method for the analysis of mechanisms of energy absorption during rolling. Sov. J. Friction Wear **9**(2), 14–22 (1988)
8. A.G. Milekhin, *Radio Circuits on the Basis of Field-Effect Transistors* (Energy, Moscow, 1976), p. 208 (in Russian)
9. V.I. Nefedov, *Metrology and Electric Radio Measurements in Telecommunication Systems* (Vysheishaya Shkola, Moscow, 2001), p. 383
10. S.F. Ermakov, B.I. Kupchinov, E.D. Beloenko, USSR Invention Certificate 1630033, Int. Cl.^{5} A 61 F 2/76, no 4455100/14; Application 05. 07. 88; Published 22. 10. 90
11. S.F. Ermakov, B.I. Kupchinov, USSR Invention Certificate 1420480, Int. Cl.^{4}, G 01 N 19/02, no 4195328/25-28; Application 16. 02. 87; Published 30. 08. 88. Bull. Invention Discoveries. 32, 202 (1988)
12. B.I. Kupchinov, S.F. Ermakov, V.P. Parkalov, V.G. Rodnenkov, USSR Invention Certificate 1326903, Int. Cl.^{4} G 01 H 11/06, no 4012129/24-28; Application 09. 12. 85; Published 30. 07. 87. Bull. Invention Discoveries. 28, 143 (1987)
13. V.I. Vasiliev, Yu.M. Gusev, V.N. Mironov (ed.), *Electronic Industrial Devices* (Vysheishaya Shkola, Moscow, 1988), p. 380 (in Russian)
14. Y.L. Khotumtsev, A.S. Lobarev, *Foundations of Radioelectronics* (Agar, Moscow, 2000), p. 288 (in Russian)
15. Y.M. Chernyakova, Zh.V. Kadolich, L.S. Pinchuk, Electromagnetic field effect on tribological characteristics of synovial fluid. J. Friction Wear **24**(6), 636–641 (2003)
16. O.V. Oganesyan, S.E. Sosin, T.A. Maslikova, A.I. El'kin, The method of studying the frictional properties of joints of living. Orthoped. Traumatol. (1), 59–63 (1985) (in Russian)
17. S.F. Ermakov, Biomechanics of synovia in living joints. 1. Modern concepts of living joints friction, wear and lubrication. J. Friction Wear **14**(6), 97–109 (1993)
18. J.M. Mansour, V.C. Mow, On the natural lubrication of synovial joints: Normal and degenerate. Trans. ASME **F99**(2), 163–173 (1977)
19. P.S. Walker, D. Dowson, M.D. Longfield, Boosted lubrication in synovial joint by fluid entrapment and enrichment. Ann. Rheum. Dis. **27**, 512–520 (1968)
20. S.F. Ermakov, B.I. Kupchinov, USSR Invention Certificate 1055247, Int. Cl.^{4} G 01 P 3/48, no 3384094/18-10; Application 11. 01. 82; Published 15. 07. 83
21. V.I. Trofimov, E.S. Mikhailov, N.A. Grybnikov, USSR Invention Certificate 1250920, Int. Cl.^{4} G 01 N 19/02. Bull. Invention Discoveries. 30, 212 (1986)
22. V.V. Sinitsyn (ed.), *The Grease and the Assessment of Their Quality (Foreign Standards and Specifications* (Publishing standards, Moscow, 1975), p. 192 (in Russian)
23. R.M. Matveevskii, I.A. Buyanovskii, O.V. Lazovskaya, *Extreme Pressure Resistance of Lubricating Media at Friction in Conditions of Boundary Lubrication* (Nauka, Moscow, 1978), p. 192 (in Russian)
24. Patent No. 5125 U BY, Int. Cl. G 01 N 3/56. Friction Machine / S.F. Ermakov, no u20080218. Filed 27. 08. 2008. Published. 28. 02. 2009
25. Patent No. 94343 RU, Int. Cl. G 01 N 3/56. Friction Machine / S.F. Ermakov, A.P. Svirskiy, A.L. Bogdanov, V.I. Kolesnikov, A.P. Sychev, no 2009135517/22. Filed 23. 09. 2009. Published 27. 01. 2010
26. R.M. Matveevskii, V.L. Laxshi, I.A. Buyanovskii (ed.), *Lubricants: Anti-Friction and Anti-Wear Properties. Test Methods: Guide* (Mashinostroenie, Moscow, 1989), p. 224 (in Russian)

27. R.M. Matveevskii, *Temperature Resistance of Lubricant Layers and Solid Lubricant Coatings During Friction of Metals and Alloys* (Nauka, Moscow, 1971), p. 228 (in Russian)
28. GOST 23.221–84, *Method of Experimental Evaluation of Thermal Resistance of Lubricants in Friction*, p. 16
29. S.F. Ermakov, B.I. Kupchinov, Yu.M. Pleskachevskii, V.A. Shardin, Effect of temperature of mesomorphous state on lubricity of liquid crystals and their compositions. J. Friction Wear **24** (5), 60–65 (2003)
30. Patent No. 5317 U BY, G 01 N 3/56. Device for Thermal-Friction Tests of Lubricants / S.F. Ermakov, A.V. Mikelionis, no u20080670. Filed 25. 08. 2008. Published 30. 06. 2009
31. A.A. Kalinin, N.I. Zamyatina, V.G. Melnikov, S.V. Tonkushina, G.G. Gorboletova, Use of glass microspheres as grease fillers. Sov. J. Friction Wear **12**(3), 148–151 (1991)
32. V.A. Voitov, A.V. Levchenko, Integral criterion for assessment of tribological characteristics of lubricants using a four-ball machine. J. Friction Wear **22**(4), 71–76 (2001)
33. GOST 9490-75, *The Materials of Liquid and Plastic Lubricants. A Method of Determining the Lubricating Properties of Four-Ball Machine,* pp. 211–220
34. S. Ermakov, A. Bogdanov, A. Rybakou, V. Konstantinov, V. Danishevskii, in *Measuring the Wear Scar During Testing the Lubricant*. Scientific Proceedings «NDT days 2015», Sozopol', Bulgaria, vol. **2**, no. 165, pp. 353–355 (2015)
35. Patent No. 5241 U BY, Int. Cl. G 01 N 3/56. Device for Measurement of Wear Scars When Testing Lubricant Materials / S.F. Ermakov, A.P. Svirskiy, no u20080563. Filed 15. 07. 2008. Published 30. 04. 2009
36. Patent RU 91171, Int. Cl. G 01 N 3/56. Device for Measurement of Wear Scars When Testing Lubricant Materials / S.F. Ermakov, A.P. Svirskiy, V.V. Mulyarchik, no 2009126467/22. Filed 13. 07. 2009. Published 27. 01. 2010
37. A.A. Kut'kov, About the mechanism of a friction of the polymers greased with surface-active greasings. Mech. Polym. (1), 128−135 (1965) (in Russian)
38. A.S. Sonin, *Introduction to Physics of Liquid Crystals* (Nauka, Moscow, 1983), p. 320 (in Russian)
39. S.A. Pikin, L.M. Blinov, *Liquid Crystals* (Nauka, Moscow, 1982), p. 208 (in Russian)
40. V. de Gennes, *Physical Properties of Liquid Crystalline Substances* (Mir, Moscow, 1982), p. 160 (in Russian)
41. S. Morishita, K. Nakano, Y. Kimura, Electroviscous effect of nematic liquid crystals. Tribol. Int. **26**(6), 399–403 (1993)
42. S.F. Ermakov, *Tribology of Liquid-Crystalline Nanomaterials and systems* (Belarusian Nauka, Minsk, 2012), p. 380 (in Russian)
43. S. Ermakov, A. Beletskii, O. Eismont, V. Nikolaev, *Liquid Crystals in Biotribology. Synovial Joint Treatment* (Springer Cham, Heidelberg–New York–Dordrecht–London, 2016), p. 211

Chapter 4
Tribological Properties of Liquid-Crystal Nanomaterials

Development of the efficient lubricants can improve durability of tribosystems and save energy in machinery [1]. An optimum and cost-efficient trend is to improve tribological performance of the available lubricants by introduction of suitable additives [2]. The experience shows that liquid-crystal cholesterol compounds (LCCC) can acquire planar orientation on the bearing surfaces and thus reduce friction of lubricated surfaces and increase their load-bearing capacity [3–5]. It can be assumed that lubricant turns into a mesomorphous state where the molecules of the additive and lubricant acquire the ordered position.

4.1 Influence of Liquid-Crystal Nanomaterials on Friction of Chemically-Inactive Materials

There is a large class of LC-compounds which under certain thermodynamic conditions are structured not only near supporting surface, but also at some distance from it, even possessing flow properties [3, 6]. Besides, the different molecular orientations relative to the supporting surfaces can be present depending on nature of LC-compounds [7–9]. As previously noted (Chap. 1) they can form three structural models: smectic, nematic and cholesteric. Analysis of the studies on lubricity shows that the smectic lubricating layers were studied most often [10–12]. However with pressure increase their polymolecular layers change to monomolecular, that leads to step-like increase in shear resistance, and it was reported that they can realize the effect of absorption strength loss of solids [11, 12].

The cholesteric structures should not have these disadvantages, because they consist of twisted nematic layers, [6, 13]. If the thickness of the smectic boundary phase is equal to the molecule length (2–4 nm) [10] in the cholesteric phase it equals to single-crystal film height which is over the molecule length being in order of 200–550 nm depending on LCCC specifics [3, 7]. Due to the above-mentioned

S. F. Ermakov and N. K. Myshkin, *Liquid-Crystal Nanomaterials*, Springer Series in Materials Science 267, https://doi.org/10.1007/978-3-319-74769-9_4

properties the interfacial layers of cholesterics have a higher shielding effect than the interfacial layers of smectics.

Analysis of studies on boundary friction of metals with SAA shows that their molecules reduce friction more effectively [10, 11]. At friction of inactive solids, these surfactants are ineffective [10, 14].

Glass surface, as well as the surfaces of gold, platinum, nickel and chromium, are qualified as inactive surfaces. This fact has been used in our experiments. Moreover, the studies have been carried out using the homogeneous friction pair.

Vaseline oil is non-active to the test materials and its compounds with oleic acid and its cholesterol ethers are chosen as lubricants. For regular distribution of the additives, the mixtures are homogenized with a sonicator before testing.

Friction was investigated with the tribometer implementing the end faces of three pins against a disk. Glass pins were placed into contact with bottom surface of Petri dishes 100 mm in diameter rotating at speed of 0.1 m/s. A stable value of friction force was defined when pressure was applied. Then, the pressure was increased and the stable value of friction is defined again. The limiting value of pressure on the sample is determined by the significant increase in friction force and at exceeding the limit tribometer was automatically turns off.

Figure 4.1 shows the test data for the friction pair glass–glass at application of different types of lubrications [15].

Analysis of obtained dependences shows that adhesion of glass samples occurs in non-active Vaseline oil and with oleic acid almost under the same pressure 0.9–1.2 MPa.

The process of friction in Vaseline oil with addition of oleic acid is followed by visually observable filming of oleic acid on the friction track despite the fact that the lubricant has been homogenized before the experiment. Accordingly, the decrease of friction force in lubricant with oleic acid is caused by separation of surfaces by multimolecular layers of oleic acid. Low load capacity of such lubricant results from the low energy of interaction between oleic acid and glass surface [10] that is

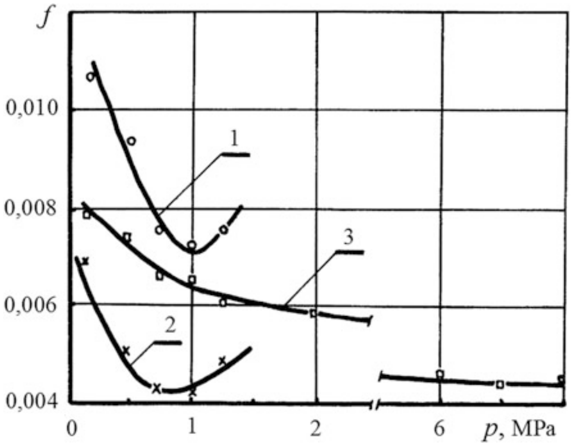

Fig. 4.1 Dependence of friction coefficient on pressure for glass–glass pair in case of lubrication by Vaseline oil (*1*), 3 wt% of oleic acid (*2*) and 3 wt% of cholesteryl oleate (*3*)

similar to the energy of interaction of Vaseline oil molecules with the same surface. According to [10], the glass is not apt to chemisorption of oleic acid molecules. So, interacting with each other by carboxyl groups the oleic acid molecules form dimers. Dimerized oleic acid molecules to some extent are similar to Vaseline oil molecules by their hydrocarbon radicals. It appears that this similarity determines the similarity of their lubricating properties in relation to the glass surface.

The research of friction surface obtained by SEM and profilometry testify in favor of the above mentioned supposition. The fracture pattern of rubbing surfaces in these cases is the same as at dry friction, i.e. associated with deep glass chipping (Figs. 4.2a–c and 4.3a–c).

The additive of LCCC into the inactive lubricant during friction of neutral surfaces leads not only to decrease in friction coefficient, but also to increase in load capacity.

For example, at friction of glass along glass the addition of 3.0 wt% of cholesteryl oleate in Vaseline oil produces the increase in load-carrying by a factor of 6–7 in comparison with medium containing oleic acid. At the same time, the formation of microgrooves on the rubbing surfaces (Fig. 4.4) is established by SEM and profilometry at pressure over 4 MPa.

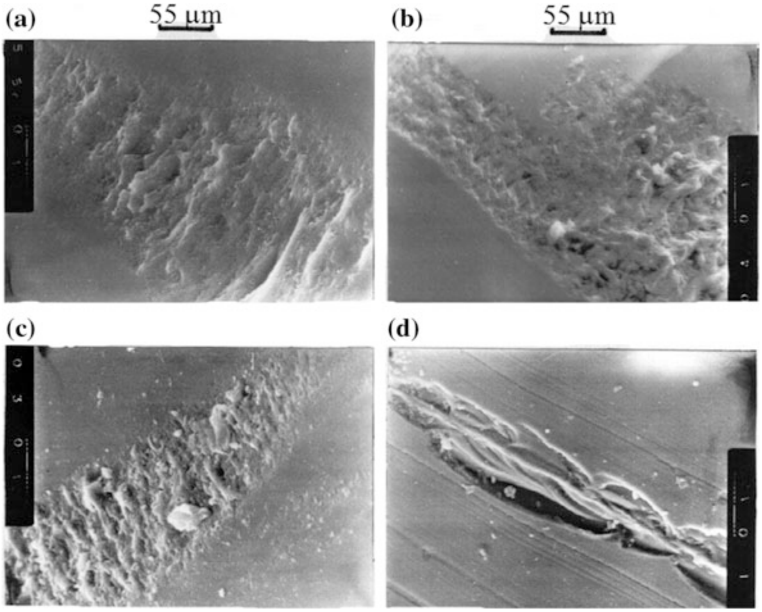

Fig. 4.2 Friction surfaces of glass samples: **a** without lubricants; **b** with Vaseline oil lubrication; **c** with addition of 3 wt% of oleic acid; **d** with addition of 3 wt% of cholesteryl oleate; (**a**–**c**) p = 1.2 MPa; **d** p = 7.0 MPa; V = 0.1 m/s

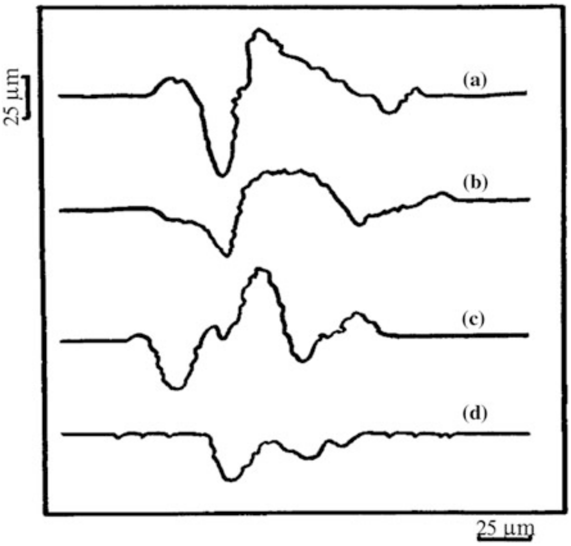

Fig. 4.3 Profiles of surfaces of glass samples after friction: **a** without lubricants; **b** with Vaseline oil; **c** with addition of 3 wt% of oleic acid; **d** with addition of 3 wt% of cholesteryl oleate; (**a**, **b**, **c**) $p = 1.2$ MPa; **d** $p = 7.0$ MPa; $V = 0.1$ m/s

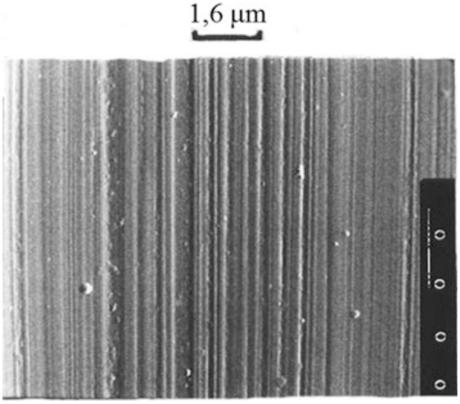

Fig. 4.4 Glass sample surface after friction with $p = 6.0$ MPa and $V = 0.1$ m/s in Vaseline oil with addition of 3 wt% of cholesteryl oleate

Optically active substances are found in the microgrooves by method of polarization microscopy (Fig. 4.5). According to [7, 8, 15] such surface texture determines the molecular arrangement of liquid-crystal nanomaterials oriented parallel to grooves and the cholesteric and nematic liquid crystals form a planar texture.

Cohesive energy of the LC molecules in this case can be significant. Electric field intensity more than 1×10^6 V/cm is necessary for changing the orientation of the LC molecule across a microrelief groove [3, 7]. This property can cause high load capacity of boundary lubricating layers formed by molecules of LCCC. It is proved by both increasing the load capacity and fracture pattern of rubbing surfaces. For example, in lubricant with addition of LCCC, failure occurs only in some parts

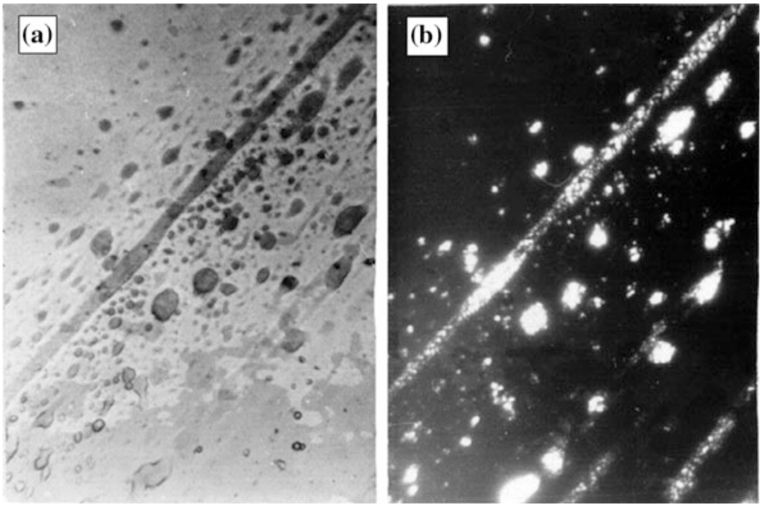

Fig. 4.5 Friction area on the surface of glass samples: **a** under unpolarized light; **b** under polarized light; (**a**, **b**) 435×

of rubbing glasses with pressure over 7 MPa (Fig. 4.2d). At the same time in media free from LCCC surface failure is present under pressure 6–7 times lower (Fig. 4.2a–c).

Therefore, results of the studies show that addition of LC-compounds into lubricant for neutral surfaces is highly effective as allows increasing by several times the load capacity of friction pair.

4.2 Influence of Liquid-Crystal Nanomaterials on Friction of Metal Tribosystems

According to the current knowledge, lubricity at boundary lubrication is not connected with either its viscosity or chemical transformations, but depends on the structure of the boundary layer at the solid–lubricant interface [10, 11]. It is evident that the role of lubricant is not only to reduce the shear resistance by localizing it in the lubricant film, but also depends greatly on volume of solid surface that undergoes deformation and damage at friction. The thickness of the monocrystalline film of oriented planar molecules of the cholesteric liquid crystals (CLC) surpasses that of the monolayers of LC molecules of the smectic type oriented in homeotropic manner by several orders of magnitude. So, it will be natural to admit that CLC will display more stable antifriction properties in contrast to fatty acids (e.g. oleic acid). The latter are known to ensure rather low coefficient of friction [12, 16].

The tribotests were conducted with the friction setup SMT-1 with the block-on-ring scheme. The medium-carbon steel 45 parts with the surface polished till R_a = 0.64–0.35 μm (ring) and 4–5 μm (block) were tested. The lubricant was in the form of specific LC-compounds of smectic type, e.g., cholesteryl oleate. These compounds are known to form [7, 8, 17] boundary layers on the contact surfaces with homeotropic and planar structural orientations. Vaseline oil (VO) was doped with cholesteryl oleate having the LC phase at room temperature which is preserved up to 345–359 K. Blend compositions were prepared by heating components until their complete dissolution was evident via mechanical agitation and endurance at the transition point temperatures of the CLC in the isotropic liquid followed by cooling. The concentration of CLC in the VO was varied in the range of 0.5–100 wt %. Investigations of the lubricant with the test machine SMT-1 were performed at sliding velocity v = 0.5 m/s and pressure p = 3.5 MPa.

Figure 4.6 illustrates the kinetics of the variations in the coefficient of friction for rubbing components made of steel 45 lubricated with LC compounds of the smectic and cholesteric types.

The results have shown that oleic acid that forms smectic-like lubricating layers on friction surfaces is sometimes able to promote lower values of the coefficient of friction than its derivative of the cholesteric type can under the same conditions. However, with lubrication by oleic acid, the dependence of f (Fig. 4.6, curve *1*) is cyclic with leaps in the coefficient of friction over the periods of 18–20 ks. The processes in the dynamic contact at a planar CLC structure in the lubricating layers are characterized exclusively by more stable behavior (Fig. 4.6, curve *2*).

The periodic character of friction in the pair lubricated by the oleic acid is apparently connected with the specific physicochemical processes that occur in the dynamic contact area. This supposition is supported, first, by the results of studying wear of the friction surface and, secondly, by IR spectroscopy of the lubricant before and after rubbing.

The investigations have shown that, despite the rather low coefficient of friction provided under friction in oleic acid, the wear rate (2.2 × 10^{-10}) of steel surfaces

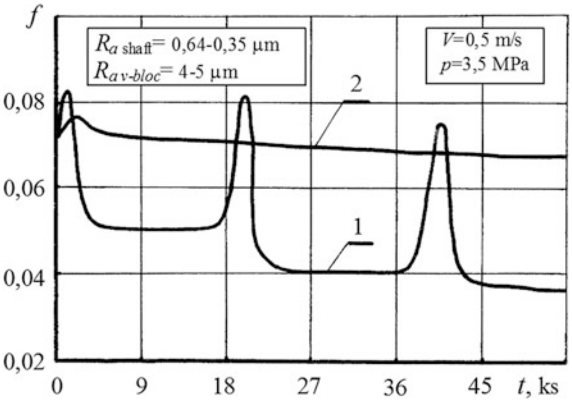

Fig. 4.6 Time dependence of the coefficient of friction for steel 45–steel 45 tribosystem at lubrication by CLC compounds: (*1*) oleic acid; (*2*) cholesteryl oleate

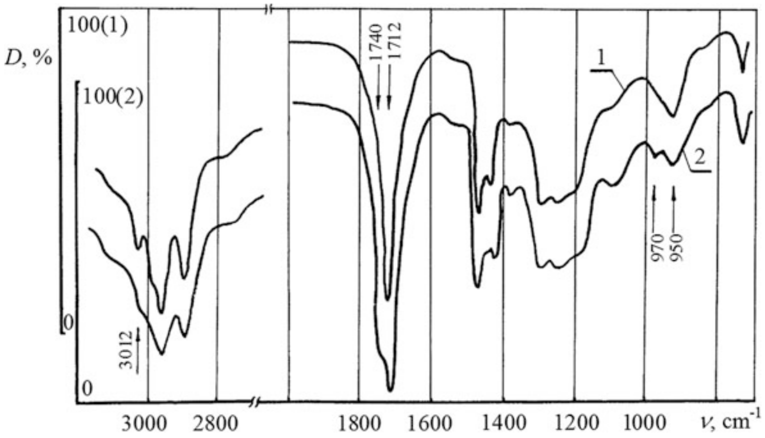

Fig. 4.7 IR spectra of oleic acid (*1*) before and (*2*) after operation in the friction zone

during fairly long periods turned to be an order of magnitude higher than at lubrication by its LC derivative of the cholesteric type (1.35×10^{-11}). However, it should be noted that, after rubbing, the IR spectrum of the oleic acid reflects an abrupt reduction in the intensity of the absorption band in the region of 3012 cm^{-1} that corresponds to valence oscillations of the CH group near the double bonds and the appearance of absorption bands in the regions of 970 and 1740 cm^{-1} that present the HF shoulder to the absorption bands in the regions of 950–1712 cm^{-1}, correspondingly (Fig. 4.7).

The appearance of a duplet 950 and 970 cm^{-1} in the oleic acid spectrum after rubbing is related to variations in the energy of hydrogen bonds of the dimerized molecules of the higher fatty acid. This behavior of the oleic acid spectrum after rubbing gives grounds to assume that the opening of double bonds takes place in the hydrocarbon radical of the oleic acid, along with the formation of high-molecular compounds.

Similar phenomena were observed elsewhere [18] in studies of steel surfaces at the presence of oleic acid with abrasives. According to these results, oleic acid polymerizes on the metal surface under certain conditions induced by mechanochemical transformations. In our case, these conditions probably occur due to high contact stresses because of the substantial roughness of the rubbing surfaces. As a result, such polymers cover the contacting surfaces with thick films, and the dissipative losses can be attributed to overcoming shear resistance between these films. This leads to abrupt growth in the coefficient of friction and, consequently, in the mechanical energy adsorbed by the polymer. The aforementioned phenomenon promotes the destruction of the polymer with formation of the active products that intensify the wear process of the metal body. The wear of the surfaces found in the dynamic contact and destruction of the polymer create conditions for the appearance of adsorption layers from oleic acid molecules on freshly formed metal surfaces that lead to decrease in the coefficient of friction. The aforementioned processes are recurrent and are accompanied by periodic growth in the coefficient of friction of the mating friction surfaces and their wear.

It should be noted that above-described mechanochemical processes are not observed on the metallic surfaces of similar roughness lubricated by CLC. This is supported by the absence of any changes in the IR spectra (Fig. 4.8) before and after frictional interactions with the LC medium, as well as by the stability of the friction mode during the whole test cycle (Fig. 4.6, curve *2*).

It is established the roughness of mating surfaces at friction in LC-compounds has a great impact on quantitative characteristics of frictional interaction. So, decreasing R_a parameter of partial insert from 4–5 μm (Fig. 4.6) to 0.85 μm (Fig. 4.9) leads to significant reduction of friction coefficient and temperature in the friction area.

Further decrease in roughness (Fig. 4.10a) of dynamically contacting surfaces to $R_a = 0.06$ μm causes an increase in given parameters of friction, especially at the beginning of the experiment (Fig. 4.9, curve *2*, *2′*).

However, as it appears from the results presented in Fig. 4.9, these diversities disappear as time goes on (over 40–45 ks).

In such a case, changing roughness parameters of the insert after such a period of time shows their increasing, in particular, parameter R_a varies from 0.06 μm at the beginning of friction process to 0.108 μm.

Besides, microrelief of rubbing surfaces becomes regular (Fig. 4.10b), which is optimal for low-dissipative friction process of cholesteric LC-compounds, as it follows from the obtained experimental data and studies of anisotropic surfaces of biopolymer [3, 5].

Consequently, obtained results confirm that there is the optimal *regular* roughness of mating surfaces for LCCC wherein the best performance of tribosystem are observed.

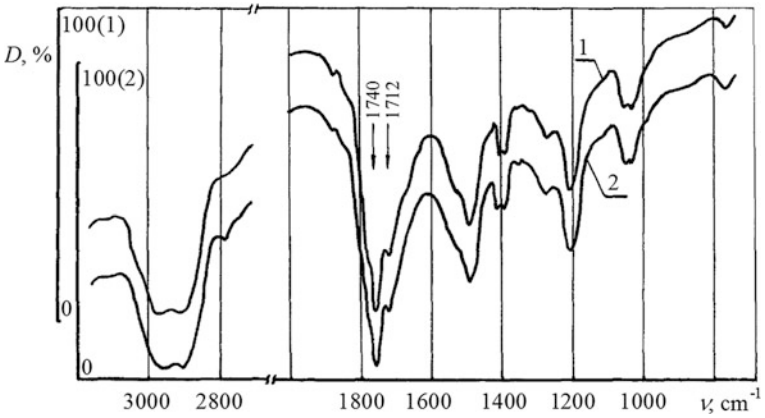

Fig. 4.8 IR spectra of cholesteryl oleate (*1*) before and (*2*) after operation in the friction zone

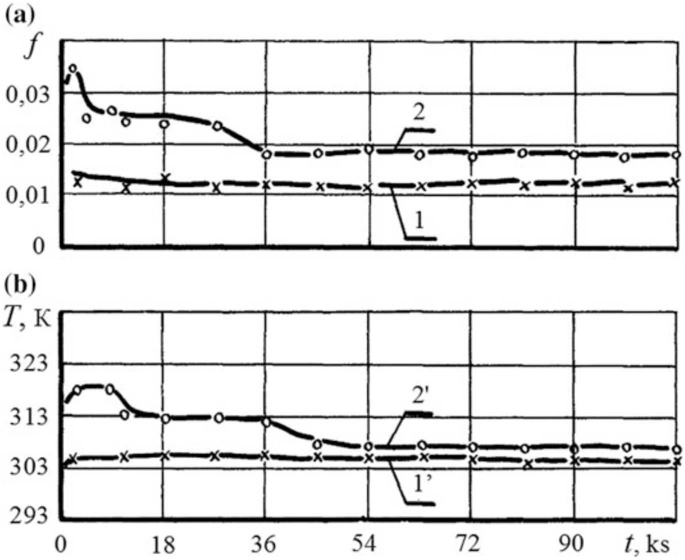

Fig. 4.9 Kinetics of friction coefficient (**a**) and temperature in the friction area (**b**) for pair steel 45–steel 45 when lubrication with cholesteryl oleate and different roughness of rubbing surfaces: *1*, *1′*—$R_{a\ v\text{-}bloc}$ = 0.85 µm, $R_{a\ \mathrm{shaft}}$ = 0.229 µm; *2*, *2′*—$R_{a\ v\text{-}bloc}$ = 0.06 µm, $R_{a\ \mathrm{shaft}}$ = 0.06 µm; V = 0.5 m/s; p = 3.5 MPa

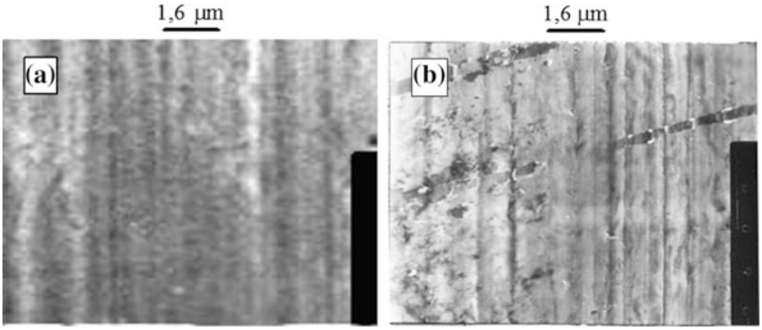

Fig. 4.10 Surfaces of the insert of steel 45 before (**a**) and after friction (**b**) within 45 ks at lubrication with cholesteryl oleate; V = 0.5 m/s; p = 3.5 MPa

As far as is known [3, 7, 13], two phase transitions are typical for thermotropic LC-substances: the first is the transition from solid phase to liquid-crystal, the second is from liquid-crystal phase to isotropic liquid. Phase state of LCCC in friction area seems to have impact on friction interaction of solids. This suggestion is verified experimentally.

Mixture of LCCC with mesophase has been chosen as samples for tests in the temperature range from 304 to 358 K (Fig. 4.11a).

Fig. 4.11 DTA data of the mixture of LCCC with mesophase in the temperature range of 304–358 K (**a**) and their relation to results of tribotests of pair steel 45–steel 45 ($V = 0.15$ m/s; $p = 1$ MPa) at lubrication with: **b** above-mentioned LCCC-mixture; **c**, *1*—Vaseline oil; **c**, *2*—Vaseline oil +1 wt% of LCCC; **c**, *3*—Vaseline oil +3 wt% of LCCC

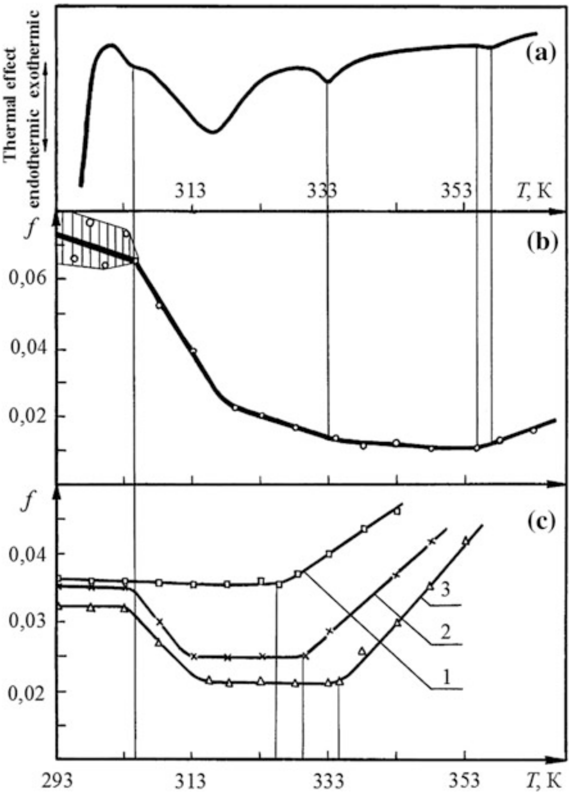

Temperature dependences of friction coefficient of pair steel 45–steel 45 at friction in the presence of these LC-compounds are shown in Fig. 4.11b.

The obtained results show that stick slip and step change of friction coefficient in the range of 0.06–0.10 occur at temperatures below 304 K (solid state). The LC-mixture under test is solid at given temperatures while discontinuous behavior of friction coefficient is rather similar in character and value to the results obtained at dry friction. So, these results testify to the fact that individual LC in solid state slightly possesses lubricity and the immediate contact between rubbing surfaces is present.

The friction process is stabilized as the transition temperature (304 K) of the LC-mixture from solid to liquid-crystal state is approached (Fig. 4.11b). When heated above this temperature a stick-slip stops and friction coefficient declines sharply down to 0.01 in the temperature range 333–354 K. In such a case fractures occur on the curve of dependence of friction coefficient on temperature that can be related to structural adjustment of LC-lubricant layers with temperature changes in friction area.

Indeed, according to [19] LCCC can form smectic phases in addition to cholesteric ones under certain thermodynamic conditions in statics. It appears that the same processes occur with temperature changes in friction area. The correlation between fracture temperatures found on curve of dependence of friction coefficient on temperature (Fig. 4.11b) and temperatures on endothermic peaks on DTA curve (Fig. 4.11a) for tested LCCC-mixture confirms this assumption. This is also illustrated by the fact that friction coefficient increases when temperature in friction area exceeds 354 K. This fact seems to be linked to another phase transition of LC-mixture under test: its transition from liquid-crystal state to isotropic liquid.

To check this suggestion the dependence of friction coefficient and temperature in friction area on pressure is investigated for steel-steel pair where LC-compounds with the second phase transition temperature 349 K are used as lubricant (Fig. 4.12, curves *1*, *1′*) [20, 21].

Analysis of results (Fig. 4.12) shows that a large increase in friction coefficient at lubrication with given LCCC occurs in the temperature range above the transition temperature of its liquid crystal phase to isotropic liquid. Consequently, friction coefficient for the test pair in LC-phase in a friction zone is lower than at lubrication with LC in isotropic liquid phase. This regularity is valid not only for cholesteric, but for nematic LC [15, 22, 23].

Hence, it can be concluded that minimal values of friction coefficient for individual LCCC and the mixtures are observed in the temperature range typical for their mesomorphous state. Therefore, if this conclusion holds for individual LCCC, then it is also true for their mixtures with mineral oils.

To prove this assumption the temperature dependences of friction coefficient of pair steel 45–steel 45 are tested at friction in the presence of Vaseline oil both without and with LCCC-additives having mesophase in the temperature range of 304–358 K (Fig. 4.11c). It is shown that lower and more stable values of friction coefficient (0.03–0.04) can be present at friction of this pair at temperatures below 304 K in contrast to individual LC (Fig. 4.11b). This effect seems to be linked to good lubricating properties of base oil in this temperature range.

Indeed, rather similar friction coefficient values of Vaseline oil without (curve *1*, Fig. 4.11c) and with LC additives (curves *2* and *3*, Fig. 4.11c) in this temperature range confirm this conclusion.

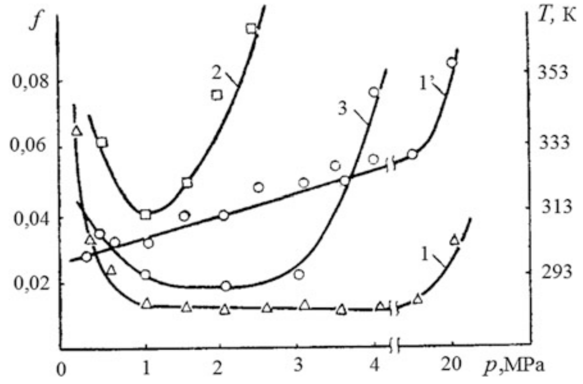

Fig. 4.12 Dependence of friction coefficient (*1*–*3*) and temperature in friction zone (*1′*) on pressure for steel 45–steel 45 pair at lubrication of LCCC at the temperature of the second phase transition 349 K (*1*, *1′*), Vaseline oil (*2*), Vaseline oil with LCCC additive at the temperature of the second phase transition 349 K (*3*)

Increase in temperature of the pair being under investigation above 304 K at lubrication by Vaseline oil with LCCC additives leads to decreasing friction coefficient, like in the case of lubrication by individual LCCC. This behavior pattern of friction coefficient when the pair is lubricated by individual LCCC and the oil solutions at the same temperature indicates the adequate mechanism of transition into the mesomorphous state.

It is established that as compared to lubrication by individual LC the start point of increasing friction coefficient on the curve of its temperature dependence shifts toward a range of lower temperatures and depends on LC-additive concentration (curves *2* and *3*, Fig. 4.11c). As their concentration in lubricant increases, the start point of rising friction coefficient shifts to higher temperatures. Therefore, it can be argued that the above conclusion on the minimum value of friction coefficient observed in the temperature range of lubricant mesomorphous state is valid not only for individual LCCC but for their mixtures with mineral oils.

LCCC possesses in LC-phase higher lubricity than in the other phase states both in homogeneous and heterogeneous friction pairs for metals, polymers, biopolymers and glasses [24–26]. High efficiency of lubricating layers planar-oriented on bearing LC-surfaces is confirmed by results of research on wear intensity of metal surfaces. So, the wear intensity at lubrication by LCCC in mesomorphous phase is much lower than when lubrication by oleic acid forming smectic liquid crystal structure [20, 21].

Figure 4.12 shows that introduction of LCCC into the Vaseline oil leads to decreasing friction coefficient in a steel pair. Similar influence of LCCC additives is observed also for mineral oils at friction of heterogeneous metal pairs (Table 4.1).

Table 4.1 Results of frictional interaction of metal friction pair at lubrication with LC-containing mineral oils

Friction pair	Base of lubricant	Temperature of the 2nd phase transition of LC-additive, K	Concentration of LC-additive, wt%	Friction coefficient/temperature, K under a pressure, MPa				
				1.0	3.0	5.0	10.0	12.0
Steel 45–steel 45	Vaseline oil	–	–	$\frac{0.04}{303}$	$\frac{0.11}{358}$	–	–	–
		349	5.0	$\frac{0.02}{303}$	$\frac{0.02}{303}$	$\frac{0.08}{380}$	–	–
		349	7.5	$\frac{0.02}{303}$	$\frac{0.02}{303}$	$\frac{0.08}{355}$	–	–
Brass L-63–steel 45	Spindle oil	–	–	0.11	0.06	0.09	–	–
		349	2.0	0.08	0.03	0.03	0.10	–
		361	2.0	0.07	0.02	0.02	0.03	0.06
		387	2.0	0.06	0.015	0.015	0.02	0.04
Brass L-63–steel 45[a]	Spindle oil	–	2.0	0.05	0.015	0.04	–	–

[a] Oleic oil is used as additive

Compared to lubricant containing oleic acid, LCCC-additives lead not only to decreasing wear intensity of the pair brass L-63–steel 45 (6.52×10^{-9} and 1.01×10^{-9} respectively), but to increasing load capacity of lubricating layers (Table 4.1).

The tests show that addition of LCCC to synthetic (polysiloxane) lubricants is the most effective (Fig. 4.13). For instance, addition of LCCC leads to decreasing friction coefficient by a factor of 4–10 times and the temperature by 30–50 K.

According to the investigations, introduction of LCCC to lubricant of different nature in friction pairs formed by different materials brings about pressure range extension of operational use of these lubricants.

So, for instance, if deep tearing at friction of glass surfaces lubricated by Vaseline oil with addition of oleic acid is observed under pressure of 0.9–1.2 MPa, then only weak adhesion of glass surfaces takes place under pressure higher than 7 MPa at the presence of LCCC-additive in Vaseline oil (Figs. 4.1 and 4.2). Addition of LCCC to synthetic lubricants causes decreasing friction coefficient in the pair brass L-63–steel 45 from 0.06 to 0.015–0.005 and increasing the load capacity of lubricant from 3 to 10–12 MPa (Fig. 4.13).

Analysis of the test results presented in Fig. 4.13 shows that load capacity of lubricant increases in a greater degree if LCCC with higher temperature of the second transition are used. It is indicative of influence of molecular structure of LCCC at tribotests.

The reasons for these differences in the properties of lubricants with LCCC are not understood because the LCCC generally dissolve in lubricants. It leads to decomposition of their structure and formation of the system of lubricant molecules and LCCC-molecules. However, it is assumed that in the contact of such system with a solid the molecules of both lubricant and LCCC would be observed on its surface. LCCC molecules can align the molecules of lubricant parallel to the direct axes owing to «guest-host» effect [7, 13]. Then realization of liquid crystal state of lubricating interlayer at friction surface seems to be possible.

As has been seen, the reduction of friction is achieved thanks to it. It is confirmed by the results of research on friction of brass–steel pair.

Fig. 4.13 Dependence of friction coefficient (*1–4*) and temperature (*1′–4′*) on pressure for brass L-63–steel 45 friction pair at lubrication with synthetic lubricants without (*1*, *1′*) and with LCCC-additives at the temperature of the second phase transition 349 K (*2*, *2′*), 361 K (*3*, *3′*) and 387 K (*4*, *4′*)

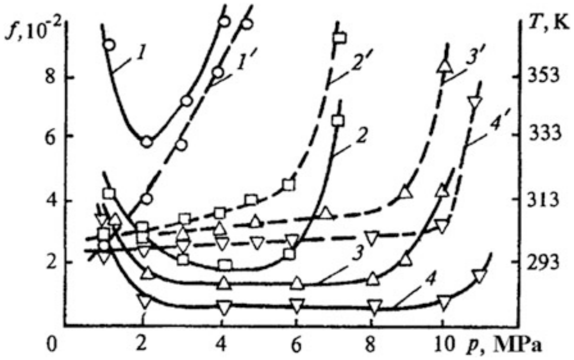

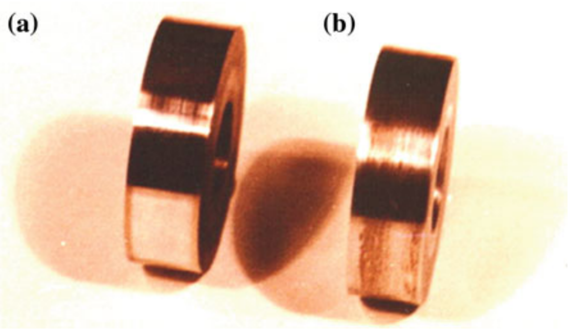

Fig. 4.14 Surfaces of steel rollers rubbed with brass L-63 in the presence of synthetic lubricant with (**a**) and without LCCC-additive (**b**)

It is established that smearing of copper on the steel surface takes place at friction in synthetic lubricant materials (Figs. 4.14 and 4.15) [27].

These processes do not lead to decrease of friction coefficient similar to the data given elsewhere [28] and confirm the high surface activity of lubricant to brass.

Introduction of LCCC to such lubricant makes building-up process of transition films impossible at friction of brass against steel. It seems to be linked with appearance of LCCC-films preventing appearance of transition films and serving as a particular screen on the friction surface.

Screening effect of LCCC during friction process is confirmed by the results of copper powders dispersion in lubricant materials with and without LCCC [21, 29].

Copper powders were milled for 60 min with steel balls in a steel container set on vibrator generating oscillations of $v = 26$ Hz and of amplitude 8 mm. The powders after milling were washed by distilled water and toluene. The particle size was determined using the photos of the powders. The differential curves of particle

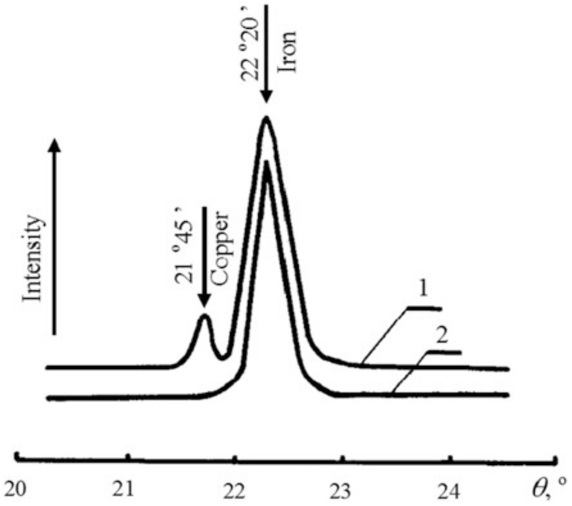

Fig. 4.15 X-ray graphs of surface layers of steel rollers at friction with brass L-63 in the presence of synthetic lubricant without (*1*) and with LCCC-additive (*2*)

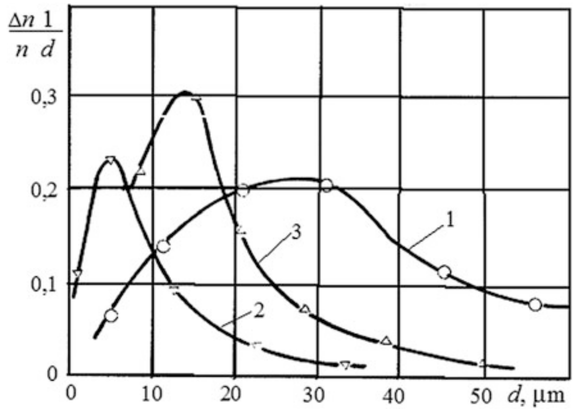

Fig. 4.16 Differential copper particle size distributions: *1*—initial powder; *2*—after dispersion in synthetic lubricant; *3*—after dispersion in synthetic lubricant with LCCC-additive at the temperature of the second phase transition 349 K

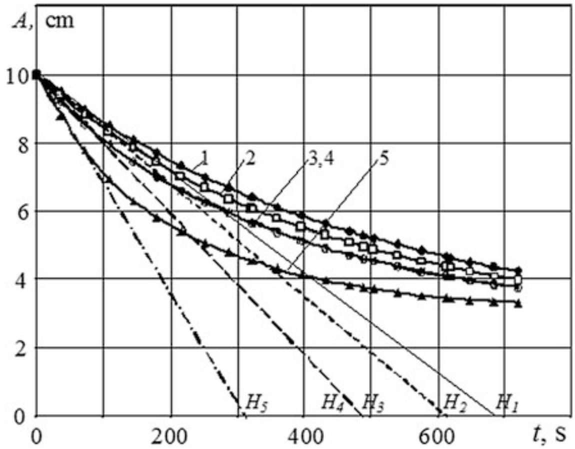

Fig. 4.17 Decrement of pendulum oscillation amplitude (*A*) based on copper surface and its hardness (*H*) by two steel indenters (r = 0.5 mm): *1*—in air (H_1 = 685 s); *2*—in Vaseline oil (H_2 = 620 s); *3*—in Vaseline oil with additive of nematic LC (H_3 = 489 s); *4*—in Vaseline oil with LCCC-additive (H_4 = 490 s); *5*—in Vaseline oil with additive of oleic acid (H_5 = 322 s)

distribution by size were plotted on the basis of the integral results of three independent measurements.

The data are shown in Fig. 4.16. It is seen that pure synthetic lubricant acts as a surfactant for copper and helps its particles break in dispersion. This is proved by the shift of maximum of the differential curve of particle size distribution to the region of finer sizes.

The maximum of the similar distribution after dispersion in the presence of LCCC is located to the right within the region of large particle size. In our opinion, it is related to the protective screening effect of LCCC in metal dispersion [21, 29].

Research results of influence of oleic acid solutions in Vaseline oil and its cholesteric derivative on decreasing surface hardness of copper obtained by means of pendulum sclerometry (presented in Fig. 4.17) are further prove of screening effect of cholesteric-nematic LC-layers on metal surface.

As follows from Fig. 4.17 the effect of traditional surfactants and cholesteric LCs is different. In contrast to oleic acid the hardness of copper decreases less in cholesteryl oleate. In other words, LC-layers of anisometric LCCC molecules inhibit stronger the penetration of indenters into the material under investigation and hence provide a higher screening effect than the layers of oleic acid polar molecules. Moreover, analysis of the experimental data shows the behavior to be characteristic for nematic LCs as well (Fig. 4.17, *3*, *4*).

A different nature of concentration dependencies for decreasing surface hardness (Δ*H*) of copper in the presence of these media also indicates to considerable difference in the interaction mechanisms of fatty acids and cholesteric LCs with the solid surface (Fig. 4.18).

If in the first case concentration dependence is extreme by nature then in the second case it is monotonous.

Actually, according to the data of [30, 31] extreme curves are typical of SA solutions in oils. Since extreme points are close to the critical concentration of micelle formation [11] then at higher concentrations the number of micelles in solution increases. Micelles have a softening effect on metals significantly lower than that of the OA molecules. This results in the extreme character of the test dependence (Fig. 4.18, *1*).

At the same time in case of monotonous dependencies the concentration curves Δ*H* can be considered as one of adsorption isotherms or, in other words, they are symbate to the respective adsorption isotherms [11, 32]. Moreover, since according to the data of [32, 33] hardness *H* reaches its minimum as the adsorption layer is saturated with oriented molecules then in our case (Fig. 4.18, *2*) we may assume that LCCC molecules are subjected to adsorption ordering on the copper surface.

Actually, according to the data of [30, 31] extreme curves are typical of SA solutions in oils. Since extreme points are close to the critical concentration of micelle formation [11] then at higher concentrations the number of micelles in solution increases. Micelles have a softening effect on metals significantly lower

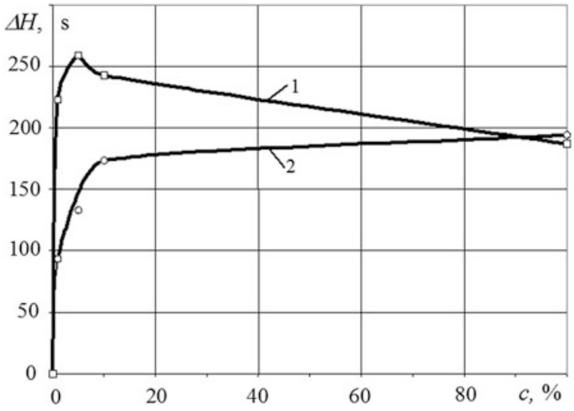

Fig. 4.18 Concentration dependencies of copper hardness decrease Δ*H* in the presence of VO with added OA (*1*), cholesteryl oleate (*2*)

than that of the OA molecules. This results in the extreme character of the test dependence (Fig. 4.18, *1*).

At the same time in case of monotonous dependencies the concentration curves ΔH can be considered as one of adsorption isotherms or, in other words, they are symbate to the respective adsorption isotherms [11, 32]. Moreover, since according to the data of [32, 33] hardness H reaches its minimum as the adsorption layer is saturated with oriented molecules then in our case (Fig. 4.18, *2*) we may assume that LCCC molecules are subjected to adsorption ordering on the copper surface.

Therefore, the investigation carried out indicates that mesogeneous cholesterol compounds on the metal surfaces form LC-layers that prevent the dynamic contact of the surfaces.

The established correlation of the second phase transition temperatures of LCCC with temperatures of significant increasing the friction coefficient (Fig. 4.13) demonstrates formation of LC state of lubricant in the friction zone. This correlation suggests that increase in friction coefficient is caused by destruction of liquid-crystal structure and formation of isotropic liquid that is characterized by great energy dissipations in contact area. This fast transition is similar to disorientation process of boundary lubricating layers observed during tests of the temperature resistance.

In summary, LCCC prone to planar orientation on surface in mesophase provide larger decrease of friction between different solids than in isotropic liquid phase and improve service performance (decrease of friction coefficient and increase of load capacity) of lubricants. Correlation between the second phase transition temperature of LCCC and temperature resistant of boundary lubricating layers formed by them is observed.

4.3 Adsorptive Properties of Liquid-Crystal Compounds

Theoretical and experimental data on the interaction of LC compositions with solid surfaces, particularly on their adsorption, describe the behavior of individual mesogenous substances and relate primary to the optical applications of LC compounds [7, 8, 15]. Meanwhile, information on the interaction between solutions of LC nanocompositions and dynamically contacting surfaces is of interest to tribologists.

Although there is a large amount of experimental data that describe the lubricity mechanism of LC-additives, the adsorption patterns of molecules of liquid-crystal nanomaterials from the solutions on the friction surfaces of solids and the influence of static and dynamic contact conditions on them are not clear enough [15]. On the one hand, taking into consideration the relative chemical non-activity of cholesterol ethers, we can assume that they are not adsorbed on the surfaces of metals and other materials. On the other hand, the experimental results presented elsewhere [15, 20] can be explained only by behavior of adsorption. The following are the experiments for answering the questions and sorting out the differences.

4.3.1 Interaction of Liquid-Crystal Nanomaterials with Hard Surface in Static Contact

Behavior of liquids of different nature at solid surfaces is of a great interest for many fields of science and technology [10, 11, 34]. Friction at the presence of LC-nanomaterials in the contact is no exception.

As known, thin polymolecular boundary lubricating layers are formed on the rubbing surfaces during a dynamic contact of metals, for examples, with SAA-containing lubricant [10, 11, 35]. A number of researchers have found that these layers have specific physical and mechanical properties, in particular they can resist very large normal pressures, but they are deformed in shear like elastic bodies [10, 36]. Indeed, building-up processes of such layers are competitive and associated with adsorption of components of lubricant. A number of original methods and techniques are developed to explain these features [10, 36, 37]. In our opinion, the method described in [36] is the most interesting. It takes into account the spectral characteristics of the solutions before and after contacting with powders of various materials.

Vaseline oil and organosilicone fluid PES-V-2 are used as base compositions for solutions in these experiments.

Mixture of cholesterol ethers with mesophase from 16 to 42 °C is used as LC-additive. Therefore, the noted additive is in liquid-crystal state in the temperature range used when the experiments are carried out. Additive of surface-active agent—oleic acid is used as control solutions.

A Nicolet 5700 spectrometer was used to assess variations of additive concentration with IR Fourier spectroscopy.

The concentration of the LC additives was determined by the intensity of the band 1740 cm^{-1} and that of the oleic acid by the intensity of the band 1712 cm^{-1}. Before the compositions with various concentrations of the additives were prepared, calibration graphs were plotted of the response of the intensities of the above absorption bands to the concentration of the additives in the oil. Then powdered copper, steel, and glass were added to the oil samples (10 ml) with 2% of the additives by mass.

It is suggested that change in concentration of tested solutions is indicative of adsorption of medium components on friction surfaces as well as a constant concentration gives evidence of similar activity of solution components relative to the materials being under test.

Directly after addition of powders into solutions, the filtered out specimens were selected, the concentration of additive was determined in the test composition. Since the filtering process takes some time, the solutions of oleic acid and liquid-crystal nanomaterials in Vaseline oil were in contact with given powders within an hour. Repeated samples for definition of the additive concentration in Vaseline oil were selected in a day after mixing (Table 4.2).

The described procedures were carried out also with the other base composition—organosilicone fluid PES-V-2.

Table 4.2 Change in concentration of oleic acid solutions and liquid-crystal nanomaterials after contacting with copper, iron and glass powders

Base composition	Contact conditions		Concentration of additive, wt%	
	Material of powder	Interaction time (h)	Oleic acid	Liquid crystals
Vaseline oil	Initial solution after filtration	–	1.8 ± 0.02	1.8 ± 0.02
	Copper	1	1.4 ± 0.06	2.0 ± 0.02
		24	1.3 ± 0.04	2.0 ± 0.05
	Iron	1	1.8 ± 0.03	1.9 ± 0.05
		24	1.7 ± 0.03	1.9 ± 0.05
	Glass	1	1.8 ± 0.04	2.0 ± 0.05
		24	1.7 ± 0.03	2.0 ± 0.05
Organosilicone fluid	Initial solution after filtration	–	2.1 ± 0.04	1.8 ± 0.03
	Copper	1	1.6 ± 0.04	2.0 ± 0.05
		24	1.0 ± 0.05	2.1 ± 0.06
	Iron	1	2.1 ± 0.04	2.0 ± 0.05
		24	2.0 ± 0.07	2.0 ± 0.05
	Glass	1	2.1 ± 0.04	1.8 ± 0.03
		24	2.0 ± 0.04	1.9 ± 0.03

Besides, concentration of additive in base oils was estimated for comparison after filtering the base 2% solutions. As studies have shown, the latter was of great importance, since a pronounced tendency for change in the concentration of the initial solutions after filtration has been present in all cases.

Figure 4.19 shows that a general nature of the interaction of oleic acid solutions in Vaseline oil with powders of the materials does not differ from the one described, for example, in the papers [10, 36]. Analysis of experimental data indicates that solutions of given SAA interact actively with copper (Fig. 4.19a) and slightly with iron and glass (Fig. 4.19b, c). It may be noted that changes in concentrations in the latter case are comparable with a measurement error. Nevertheless, a tendency to reduce the content of oleic acid in the solution when contacting these materials for a longer period of time is clearly visible (Table 4.2). This indicates that molecules of oleic acid possess higher adsorptive capacity with the surfaces of copper, iron and glass than molecules of base Vaseline oil do.

During experiments it has been found that the same pattern is typical for solutions of oleic acid and other base compositions, such as organosilicone fluid (Table 4.2).

However, as the results show, it is less pronounced for these compositions. So, if significant reduction of oleic acid content in the studied compositions is present when contacting the copper powders, then the noted tendency for decreasing

Fig. 4.19 Assimilation rate of IR-spectrum typical lines and concentration of 2% solution of oleic acid in Vaseline oil: *A*—initial solution after filtering; *B*—within an hour of presence of copper (**a**), iron (**b**) and glass (**c**) powders

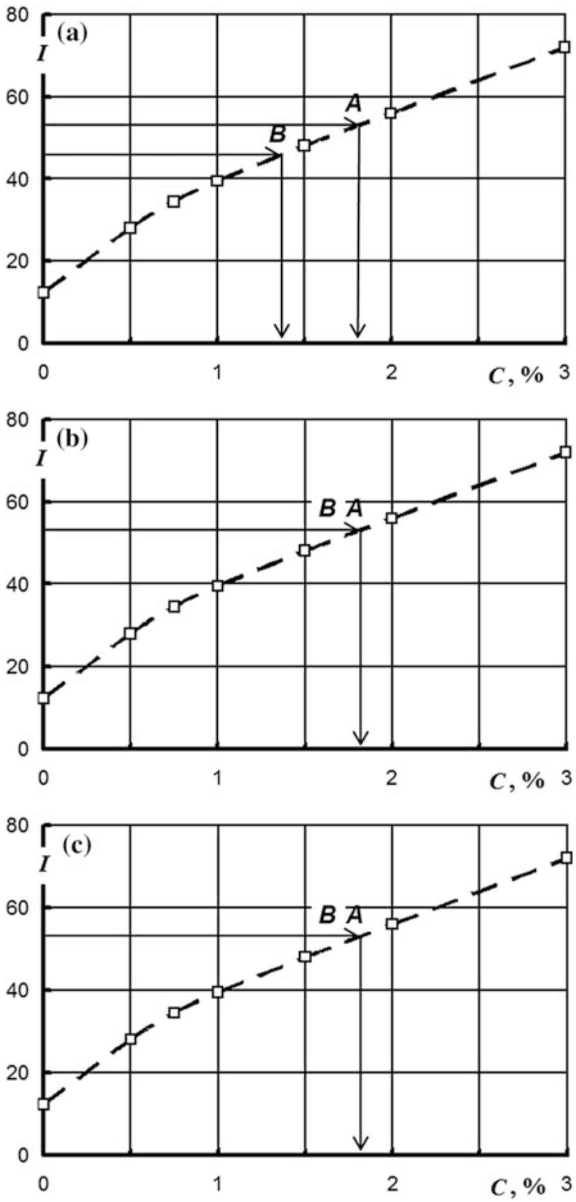

concentration of initial solutions is becoming less visible when these solutions contact with iron and glass powders.

The latter seems to be explained by a similar competitive capacity of the base oil molecules taking part in these processes and additive molecules. In other words, it is possible to conclude that constant concentrations of initial solutions observed in their contact with iron and glass powders imply a similar adsorptive capacity of oleic acid molecules and organosilicone liquid molecules on the surfaces of these materials.

The experiments with solutions of liquid-crystal nanomaterials have shown even more unexpected result (Fig. 4.20).

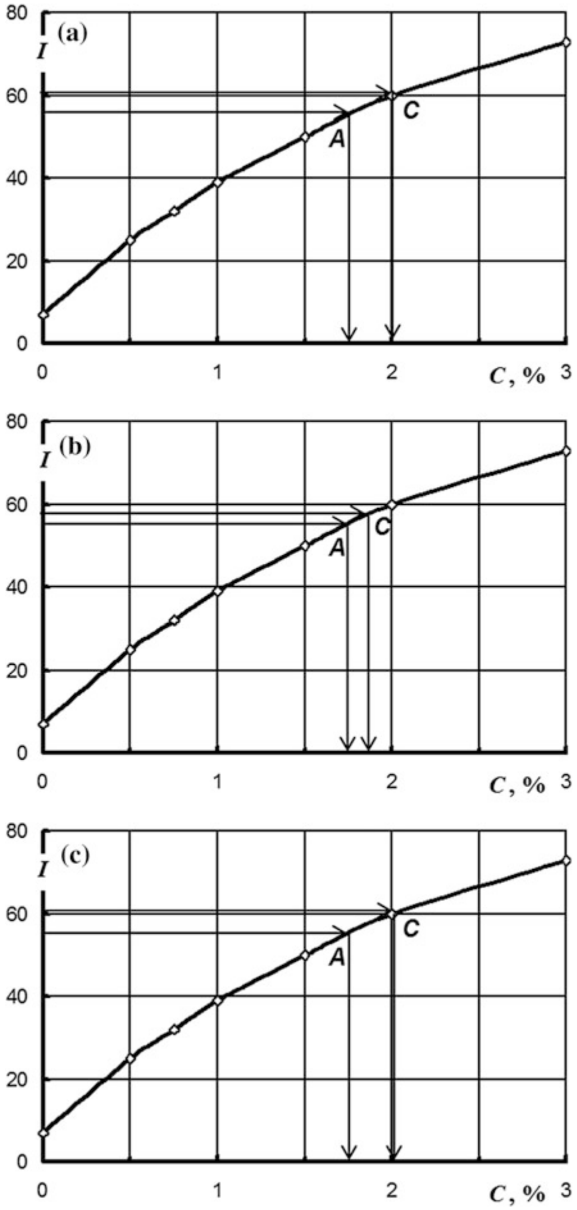

Fig. 4.20 Assimilation rate of IR-spectrum typical lines and concentration of 2% solution of LC-nanocompounds of oleic acid derivative in Vaseline oil: *A*—initial solution after filtering; *C*—within an hour of presence of copper (**a**), iron (**b**) and glass (**c**) powders

It is established the concentration of LC-additive in Vaseline oil after contacting with the powders of test materials have increased in each case (Fig. 4.20a–c). Although this change in some experiments is comparative with an error, it can be argued that adsorption of the cholesterics used in this experiment was not under way on the powder surfaces of copper, iron and glass, or at the least was much less than adsorption of base oil molecules, such as Vaseline oil.

The same situation existed for solutions of liquid-crystal nanomaterials in organosilicone liquid (Table 4.2) is also evidence in favor of this conclusion. In other words, we can assert that when contacting of LC-nanomaterials solutions with copper, iron and glass powders, i.e. in static conditions of experiment, adsorption capacity of LC-nanomaterial molecules is much less than such capacity of base oil molecules. As a result, the latest ones being adsorbed on fine powder surfaces of tested materials cause irreversible changes of a percentage ratio of solution components. Finally, it leads to concentration increase of liquid crystal nanomaterials in the initial solutions.

Oleic acid has not been observed in solutions interacting with copper powder in the test a year after the start of the experiment. In all other cases, the concentration of additives under investigation in base composition has remained at relatively the same level as a day after the start of experiment.

Therefore, the performed experiments have not supported a suggestion concerning adsorption of liquid-crystal cholesterol ethers from the solutions on the fine powder surfaces of copper, iron and glass. However, as it has been noted in the papers [36, 37], the results of such experiments in “statics” may differ significantly from the results expected in the conditions of dynamic (frictional) contact. That is why the additional studies have been carried out which tried to estimate the changes in concentration of LC-additive in Vaseline oil under conditions of friction, in particular when lubrication of homogeneous friction pair steel 45–steel 45 below other results of these studies.

4.3.2 Triboinduced Adsorption of Liquid-Crystal Nanomaterials Under Frictional Interaction of Solids

It is well known that various lubricants can reduce significantly the friction force and, as a result, wear, reducing stresses in surface layers of rubbing solids [37]. It is proved that the steady decrease of the friction coefficient under the influence of lubricant is generally determined by adsorption and chemical interaction of lubricating interlayer with friction surfaces [10, 12]. However, the issue is which components of lubricant play more active role in adsorption processes. It can be both liquid crystals and molecules of base oil. The adsorption process can be of additive nature and the prevailing effect of certain components of lubricant in competing processes during friction can also be observed.

Accordingly, the experiment with sampling and measurement of LC-additive concentration in lubricant has been carried out after work of tribosystem within 20 min, 1, 2, 3, 10 and 50 h. The obtained experimental data are presented in Fig. 4.21.

It is established that in dynamic contact the adsorption processes for LC-solutions differ fundamentally from the processes in static contact. Particularly, the reducing LC-additive content in used lubricant at friction of steel pair is observed (Fig. 4.21), rather than its increasing in static contact (Fig. 4.20). In other words, it can clearly be argued that adsorption of LC-molecules from lubricant is especially evident in dynamic contact in contrast to static one.

However, according to Fig. 4.21, this phenomenon becomes more complex as time goes by. At the least, three typical areas can be identified on the basis of the obtained dependence.

Reducing concentration of liquid-crystal nanomaterials in the samples of lubricant liquid is observed at the beginning of dynamic contact that is an evidence of domination of their adsorption over the adsorption of Vaseline oil molecules.

With increasing the time of friction, this process becomes balanced and dynamically-stable, that achieves the greatest effect at contact of the metal pairs within an hour. Probably, molecules of solvent, i.e. Vaseline oil, as well as molecules of added liquid-crystal nanomaterials are involved in the adsorption processes, for instance because of the same “guest–host” effect [7]. Accordingly, LC concentration in lubricant specimens is stabilized, while the process itself becomes additive.

Then, increase in the LC concentration is again indicated in the samples selected for analysis of the lubricant with time. In our opinion, the latest can be caused by the carboxylated compounds being a part of Vaseline oil [10] that possess higher adsorption capacity, extract the LC-nanomaterials molecules from rubbing surfaces, and adsorb on them and on wear debris in a competitive sorption. The experimental results obtained in statics with metal powders (Fig. 4.20) suggest this assumption.

Nevertheless, it is obvious that described phenomena can be realized only if the LC-molecules are physically adsorbed on metals without reaction with the friction

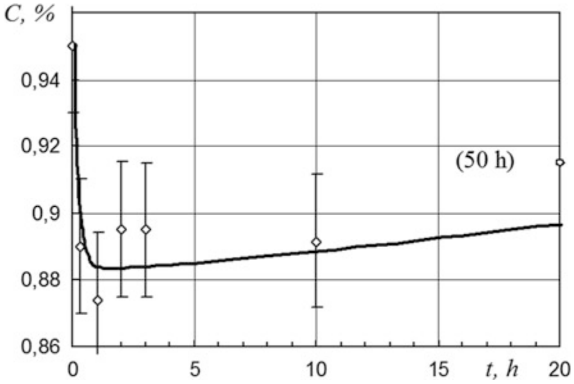

Fig. 4.21 Change in concentration of liquid-crystal additive in Vaseline oil at lubrication of friction pair steel 45–steel 45

surfaces and forming no new compounds such as soaps on them, as it has been observed for fatty acids [16, 17]. Infra-red spectra of LC obtained before and after friction and presented in Fig. 4.8 confirm this conclusion.

If we assume that all changes of mesogenous components concentration are caused by their adsorption on the solid surfaces, according to [7] for the mesogenous cholesterol ether molecules with length 1.5 nm and diameter 0.5 nm we can try to determine the surface area which they cover at close molecular arrangement.

The results of this estimation show that that operating friction pair within an hour the area, where a monomolecular layer of LC is adsorbed, must be equal $S_{\mathrm{LC}}^{\mathrm{pl}} \approx 0.07244\ \mathrm{m}^2$ when their planar arrangement and $S_{\mathrm{LC}}^{\mathrm{h}} \approx 0.01896\ \mathrm{m}^2$ when homeotropic. These values are several times greater than the total area of the dynamically contacting surfaces equal to $S_{\mathrm{fc}} = 0.0014566\ \mathrm{m}^2$. Undoubtedly, the latest is the evidence of polymolecular arrangement of adsorbed layers of LC-nanomaterials on the rubbing surfaces.

Furthermore, we can evaluate a thickness of polymolecular layer, providing that liquid crystals are adsorbed regularly on each surface changed during friction. According to paper [38], given a weighted average size of wear particle $d_{\mathrm{wp}} = 0.7\ \mu\mathrm{m}$ with the condition of their spherical shape and mean mass wear of friction pair about $D_{\mathrm{m}} = 0.58$ mg, the area capable to adsorption in the given system would be about $S_{\mathrm{ca}} = 0.0062\ \mathrm{m}^2$.

A simple calculation shows that with smectic-like molecular arrangement of mesogens they form a triple layer and more than ten layers at planar arrangement. In this case a total thickness of polymolecular layer is about 4–5 nm.

At the same time, if all liquid crystals are adsorbed only in the friction zone, then the thickness of liquid-crystal polymolecular layer is about 18–21 nm when testing the tribosystem within an hour [39]. It is not difficult to determine that at more long-time tests, when the concentration of LC-nanomaterials in used lubricant starts to increase, the thickness of estimated polymolecular layer decreases twofold.

However, more detailed analysis shows that this behavior of lubricant in this conditions can be apparent, as in this case a strong orientation effect (because of "guest-host" effect [7, 39]) of LC-molecules on base oil molecules is ignored. That can result in direct participation of base oil molecules in formation of the polymolecular layers described above. The results of paper [36] confirm that. According to them, under certain conditions the adsorption layers of not only polar molecules, but molecules of electrically neutral (non-active) substances can be formed on friction surfaces. It is seen that the thickness of lubricating layers in a friction zone under given conditions can be much higher, than we have obtained by the calculations, that don't take into account the influence of base oil molecules on the formation of polymolecular layers [23, 39].

From there it is clear that activation of adsorption capacity of liquid-crystal cholesterol ethers occurs at friction. It allows them adsorbing on friction surfaces. Considering possible causes of increasing adsorption activity of LC-additive we can note that it seems to be caused by "renewal" of friction surfaces in operation of pair, especially at the beginning of friction. Removal of the oxide layer and direct contact of lubricant with newly-formed metal areas allow the molecules of LC-component to interact with the areas of renewed surface and be finally adsorbed on them.

Obviously, increasing free surface energy of juvenile surface of dynamically contacting metals can give rise to additive increase of interaction between molecules of lubricant and friction surfaces [10, 40], including interaction of cholesterol ethers and solid body [7]. Occurrence of double electric layer at friction in lubricating interlayer can be also important [41]. Taking polarizing and orientation effect on liquid crystals, this layer can influence significantly the adsorption capacity at friction [22, 42]. For this reason, increase in adsorption capacity of LC-nanomaterials observed under these friction conditions can be explained by superposition of all this factors.

Because, according to obtained results (Fig. 4.21), the most intensive changes of LC-nanomaterials content in Vaseline oil happen during the first hours of tribosystem operation, the test has been significantly modified. During three hours of operation of steel 45–steel 45 couple the lubricants have been totally replaced with brand new ones at specific time intervals. Shown in Fig. 4.22 are the absolute changes in LC-additive concentration in each of the selected portions of lubricant under the given test conditions.

The combined graph of gradual accumulation of changes in LC concentration in oil and the curves of corresponding friction coefficient changes of tribosystem is presented in Fig. 4.23.

Analyzing the experimental data (Figs. 4.22 and 4.23), we can conclude that LC-additive concentration in Vaseline oil decreases the most significantly in lubricant portions worked-out in the initial period of time, i.e. about an hour of the test, remaining in other periods of time on almost baseline level. This behavior of LC content in lubricant is indicative of stabilization of adsorption in this tribosystem and occurrence of dynamic equilibrium.

It is noted that due to the chosen test procedure with complete replacement of lubricant in the friction zone the wear debris are removed regularly. They are formed the most intensively in the first intervals of operation, and then this intensity is decreasing. The fact that the initial concentration of liquid-crystal nanomaterials

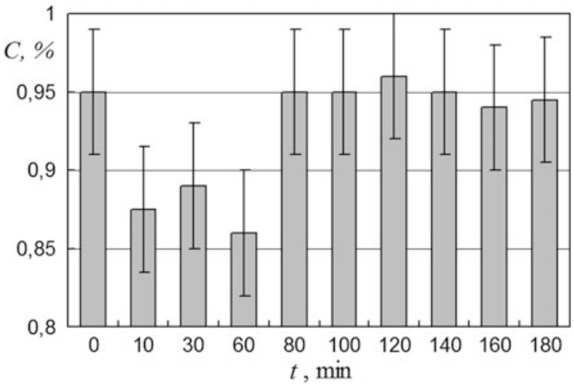

Fig. 4.22 Absolute changes in concentration of liquid-crystal additive in Vaseline oil when operating of friction pair

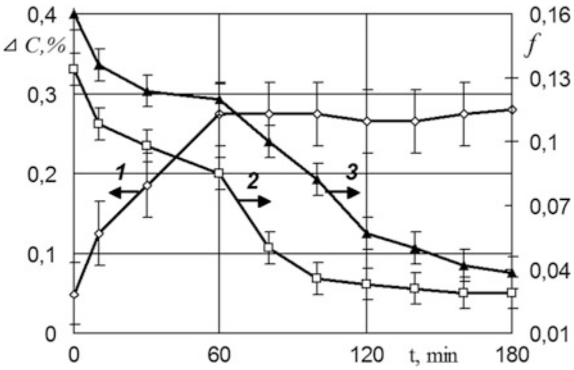

Fig. 4.23 Change in concentration of liquid-crystal additive (*1*) in Vaseline oil and coefficient of friction at 20 °C (*2*) and 40 °C (*3*) of a steel 45–steel 45 pair over the time period

in oil does not increase after a certain point of friction suggests the regular distribution of LC on all surfaces capable to adsorption, including the wear debris.

Indeed, if an assumption of LC adsorption from solution is correct only on surfaces in a friction zone, then, as it is observed during previous experiment, gradual increase in LC concentration in base composition would be expected, but however, it does not happen. It is evident that wear debris in friction play an important role in adsorption processes. Besides, stability of LC concentration over time in base oil indicates not only to stabilization of adsorption processes in the friction area, but absence of destruction of LC-component in lubricant. Otherwise, content of liquid crystals in it would decrease when using each new portion.

Moreover, analysis shows that correlation of LC content stabilization and descent of friction coefficient is no less important comparing the curves of friction coefficient and LC-additive concentration in lubricant (Fig. 4.23). Simultaneous occurring of knees of experimental curves confirms that. Practically, the dependence established in these experiments shows clearly at the fact that the adsorbed LC-layer starts to “work” at this moment [23, 39]. LC content in lubricant liquid and its adsorption together with structural and mechanical properties of lubricating layers, determines steady-state thickness of polymolecular layers, and consequently, a great drop in friction coefficient observed in the experiment [10, 37]. Estimations show, that the thickness of adsorbed layer formed only by molecules of LC-nanomaterials is around 10–12 nm during stable period of operation in this friction conditions.

However, as follows from the experimental data shown in Fig. 4.23, the adsorbed layers of LC do not start working effectively immediately; like SAA, they have some latency period [10]. It can be argued that the greatest decrease in the friction coefficient corresponds to the saturation of polymolecular layer by oriented LC molecules on the rubbing surfaces, and so to stabilization of their friction.

The difference of friction coefficient values at room temperature (curve *2*, Fig. 4.23) and at the temperature above 40 °C (curve *3*, Fig. 4.23) is caused by reducing the lubricant viscosity. Consequently, it means realization of more reduced lubricating film in the latter case. Less significant break on the curve *3* (Fig. 4.23) at the stabilization of LC-additive content in lubricant is also indicative of that. It also give evidence of reducing lubricant efficiency of LC when transition to isotropic liquid state.

Therefore, a previously unknown effect of significant increase in adsorption capacity of liquid-crystal nanomaterial molecules from solutions under the influence of dynamic contact of mating solids has been found during the studies. It is established that adsorption of LC-molecules at friction is clearly agreed with increasing and stabilizing their tribological characteristics.

It is obvious that the roughness parameters of friction surfaces at different LC concentrations in the lubricant would influence the speed with which adsorbed LC-film can cover a microrelief and shield the surfaces, redistributing the pressure more regularly [39, 43]. Here we can assume that the probability of more rapid formation of polymolecular boundary film of a sufficient thickness increases at higher concentration of the LC-additives in lubricant.

4.4 The Role of Liquid-Crystal Additives in Mechanism of Friction, Wear, and Lubrication of Tribosystems

According to [15, 39], the addition of LC-substances with planar orientation on the bearing surfaces reduces friction of lubricated solids and increases load capacity of tribosystem. It is likely to be achieved due to mesomorphous state of lubricant characterized by ordered oriented molecular arrangement.

Considering the structure of the lubricating layers formed by LCCC molecules and topography of surfaces, it can be assumed that the efficiency of such additives depends on their concentration in lubricant.

Block-on-ring couples were tested with friction machine SMT-1 [15, 20, 39]. The bodies of the friction pair were made from steel 45: surface roughness R_a = 0.64–0.35 μm (ring) and 1.40–1.50 μm (block). Vaseline oil (VO, USSR Standard GOST 3164-72) served as a lubricant with addition of LCCC. It has a liquid-crystalline phase at the room temperature and maintains it up to 345–359 K. The mixed compositions were prepared by heating the components of the test lubricant until full mutual dissolution and by thorough mechanical agitation followed by aging at a temperature about the point of transition of the LCCC into an isotropic fluid, then followed by cooling. The LCCC concentration in the VO was varied from 0.5 to 100% by mass. The lubricants were tested at sliding velocity v = 0.5 m/s and pressure p = 3.5 MPa.

Figure 4.24 presents the kinetic dependences of friction coefficient and temperature of the test pair for lubricants with different content of LCCC. Their analysis shows that decrease of friction coefficient and temperature in the friction zone are observed with addition of LCCC in Vaseline oil, but depending on LCCC content this occurs at various time intervals from the beginning of friction.

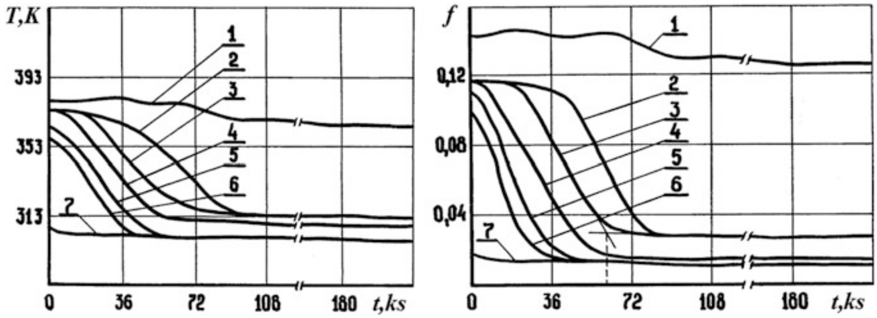

Fig. 4.24 Kinetics of temperature change in friction area (left) and friction coefficient (right) for pair steel 45–steel 45 at lubrication with Vaseline oil without (*1*) and with additive of LCCC: 0.5 wt% (*2*); 1.0 (*3*); 5.0 (*4*); 7.5 (*5*); 9.0 (*6*); 100 wt% (*7*). $V = 0.5$ m/s; $p = 3.5$ MPa

As it follows from Fig. 4.24 (curves *2–7*), increasing LCCC concentration in lubricant leads to shorter time before the beginning of decrease in friction coefficient and temperature in the contact area.

If the change of friction coefficient and temperature is not observed for Vaseline oil without LCCC-additive (curve *1*), then the length of time period after which the reduction of coefficient occurs is almost zero at lubrication with pure LCCC (curve *7*).

Shown in Table 4.3 are the time periods, after those a steady friction mode is established in the pair, obtained by comparing the tangents of slopes of experimental curves at the moments of reduction and stabilization of investigated characteristics (see Fig. 4.24, curve *3*), as well as the values of friction coefficients and temperatures under steady conditions.

Comparison of intervals before the beginning of steady friction mode *t* in the tribosystem and LCCC concentration in lubricant *C* shows a close correlation relationship between them ($r = 0.97$) described by the equation:

$$t = 75.1 - 5.5 \times C\,(\text{ks}) \tag{4.1}$$

Table 4.3 Relation between the test characteristics and content of LCCC in lubricant for friction pair steel 45–steel 45

Time before the steady friction mode start *t*, ks	Concentration of LCCC in lubricant *C*, wt%	Friction coefficient, F	Temperature at the friction contact *T*, K
73.3	0.5	0.03	316
62.1	1.0	0.03	316
50.4	5.0	0.025	313
33.3	7.5	0.02	308
25.2	9.0	0.02	308

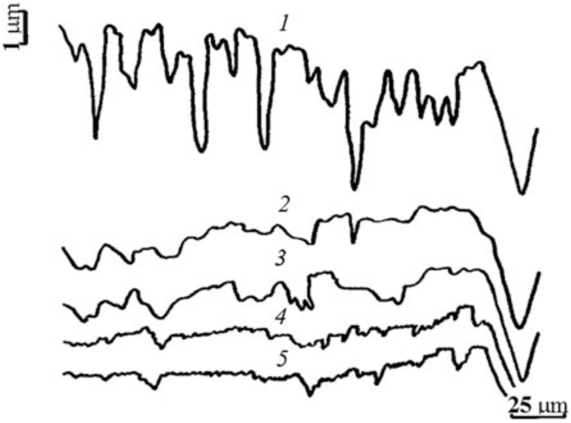

Fig. 4.25 Kinetics of change of surface roughness of an insert of steel 45 when friction in Vaseline oil with additive of 7.5 wt% LCCC in: *1*—0 ks; *2*—7.2 ks; *3*—28.8 ks; *4*—101.6 ks; *5*—216 ks

The kinetics of changes of the microgeometry of contact surfaces was studied during friction in VO with LCCC additives (Fig. 4.25).

It is established that the topography of steel surfaces in the initial period of friction undergoes noticeable changes and stabilizes in the steady regime. The investigation of roughness of contact surfaces reveals that the mean height of asperities before and after friction depends on the duration of friction contact and the LCCC concentration in lubricant (Fig. 4.26). It is established that the height of asperities does not practically change when the LCCC content is high. The maximum changes occur at low LCCC concentrations. According to our experimental data the roughness of the rubbing surfaces at a given LCCC concentration diminish from 1.40 to 0.28 µm, accompanied by simultaneous reduction of the friction coefficient and temperature in the friction zone. It follows that under definite friction conditions LCCC reveals a powerful polishing effect; hence the LCCC can be effectively used for surface finish [39, 44, 45].

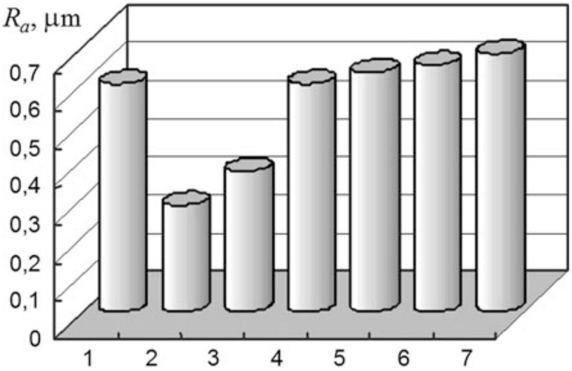

Fig. 4.26 Influence of lubrication composition on roughness mean values (R_a) of the insert: *1*—Vaseline oil; *2*—0.5 wt% of LCCC in Vaseline oil; *3*—1.0; *4*—5.0; *5*—7.5; *6*—9.0; *7*—100 wt% of LCCC

Within the time interval corresponding to unsteady friction, the parameters of the surface microrelief are intermediate between the initial ones and those corresponding to the period when friction coefficients are low.

The test results prove that low friction in the test pair is achieved only when we reach definite roughness parameters typical for each composition with LCCC additive. It was observed that the topography of the specimens is characterized by appearance of a flattop microrelief, with numerous fine depressions on the friction surface. Such surface texture provides apparently low contact stresses in the friction zone (real contact area expands), as a result heat generation and deformation losses reduce, as it has been observed in the test.

If low friction is provided by lubricating film that appears on friction surfaces and has a liquid crystalline structure, then at low LC concentrations the probability of the film formation which would prevent interaction between asperities is small. The cause can be (a) low LC concentration in the lubricant; (b) limited adsorption of LC molecules on friction surfaces or (c) relatively high asperities on friction surfaces.

Under such conditions during the initial stage of friction, the surface microrelief changes due to interaction between asperities resulting in deformation or wear [44, 45]. Metals do not come into contact when asperities are re-deformed, because they are apparently separated by oil and LC molecules located in microdepressions over the slopes of asperities on the friction surfaces. This assumption is based on the fact that friction pairs never seized under the above test conditions, nor catastrophic wear ever occurred. The friction coefficient was relatively high when the surface topography was changing. It diminishes until the friction surface microrelief permits LCCC molecules to form a continuous lubricating film at a given LC concentration that would prevent direct contact between asperities on friction surfaces. Then sliding proceeds in the LC layer. Profilometry of friction surfaces after their dynamic contact in lubricant with LC additive proves that a smoothed microrelief appears with asperities of a smaller order of magnitude than those that appear when lubricant without LC is used [15, 44, 45]. More detailed examination with the STM has revealed that introduction of LC additive into VO leads to the appearance of smaller asperities (Fig. 4.27) [44, 45].

It is obvious (Fig. 4.27) that the STM-profile of the specimen after running in pure VO (Fig. 4.27a) has typically a single-level microrelief with a period ≈0.3–1.0 μm and the asperities height ≈5–10 nm. At the same time the profile of the surfaces that were run in VO with LC additive (Fig. 4.27b) shows a distinctly two-level organization in which the microrelief with ≈8 μm spacing and ≈15 nm height is covered by submicrorelief with the parameters ≈0.3–0.5 μm and ≈1–3 nm, respectively. Comparison of the results of the STM examination with the experimental profilometer data shows that there is a submicrorelief with individual projections on the flattop microrelief in Fig. 4.27b.

The studies allow one to assume the following mechanism of processes that evolve in the friction zone at the presence of LCCC.

When the concentration of LCCC in the lubricant is low its molecules are adsorbed on the friction surfaces and orient its long axes along the hollows of the

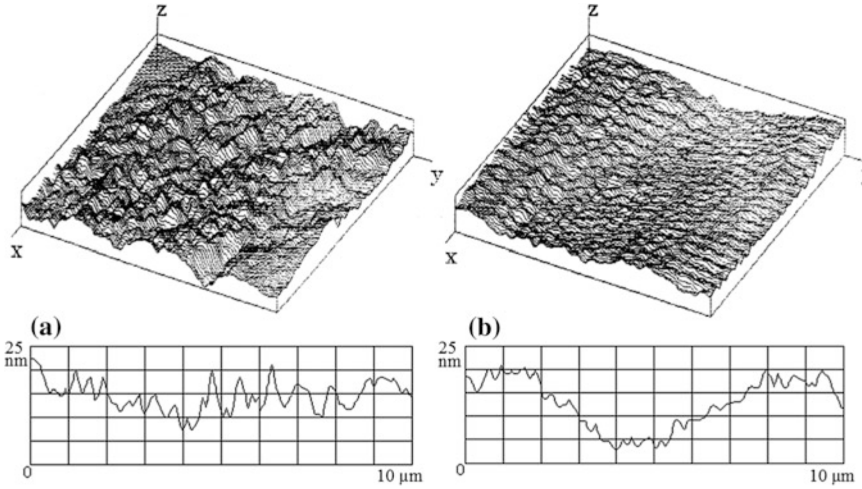

Fig. 4.27 STM pictures (10 × 10 μm) (top) and STM profile (bottom) of friction surfaces of steel samples after operation in Vaseline oil without (**a**) and with LCCC (**b**)

microrelief. Due to a scanty quantity of the LCCC and limited adsorption the appearing film is not continuous. In our view, the microrelief of friction surfaces at the initial stage of friction contact changes mostly due to re-deformation of asperities that are kept apart by LC molecules located in the submicrorelief hollows. Gradual, dosed and controllable action of LCCC molecules produces flattop microrelief of friction surfaces. After that LCCC molecules at a given concentration can produce a continuous lubricating film that reduces the friction coefficient due to localization of shear in the film.

A higher concentration of LCCC leads to more complete occupation of the hollows in the microrelief. When the LCCC concentration in lubricant is high enough, its molecules are in sufficient number to form a layer that can cover the asperities on the friction surface. As a result the friction surface microrelief does not practically change and low friction coefficients are achieved shortly.

Such behavior of the LCCC-modified oil is confirmed by the results of wear test for the mated steel surfaces in relation to LC concentration in VO (Fig. 4.28). It proves that the wear rate lowers proportionally to growth of LCCC concentration and stabilizes at a concentration >5% by mass ($\approx 10^{-11}$).

This mechanism of gradual wear or changes in the topography of the friction surfaces shows that it is possible to develop the efficient processing fluids containing LC for machining both metals and superhard materials.

Our study has shown that growth of LCCC concentration in lubricant shortens the time needed to achieve optimal tribological characteristics. It has been also observed that small LCCC concentrations in friction transform the initial microrelief into a flattop one.

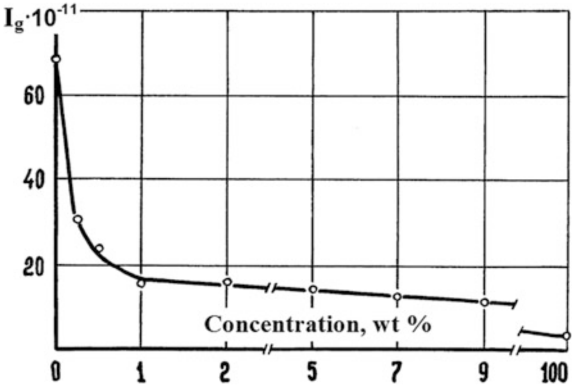

Fig. 4.28 Relation between wear rate *I* of steel 45–steel 45 pair and LCCC concentration in VO ($v = 0.5$ m/s; $p = 3.5$ MPa)

Scanning tunnel microscope has revealed that LC additives produce double-level topography of contacting surfaces when individual asperities on the flattop microrelief acquire a specific submicrorelief with the asperities of one order of magnitude smaller than those that can be obtained with lubricants without LCCC. It has also been observed that this topography of contact surfaces together with the adsorbed LCCC film is favorable for relieving local stresses in the contact zone and therefore reduces heat generation and deformation.

A mechanism of the lubricating action of LCCC is proposed according to which the gradual wear under the effect of LCCC changes the topography of contact surfaces. After that, molecules of LCCC are able to produce a continuous lubricating film that protects the contact surfaces.

4.5 Diagnostics of Liquid-Crystal Cholesterol Compounds in Lubricants by Optical Methods

The experiments indicate that concentration of LC-compounds has significant influence on tribotechnical characteristics of lubricant materials (LM). Accordingly, development of efficient methods and tools for defining their content in LM is of considerable importance from the tribological standpoint. Analysis shows that capacity of LCCC to change optical activity of their solutions in the range of visible frequency spectrum may be the basis of such works and these assumptions have been tested [46].

The experiments proved that petroleum oils and intermediate petrochemical products (hydrotreated vacuum gas oil, vacuum oil distillates etc.) are the appropriate test media and the torsion angle of their polarization plane is +9.5 to +9.75°S (saccharous degrees) (Fig. 4.29).

It is shown that addition of different LC-compounds of cholesterol into petroleum and synthetic oils, and intermediate petrochemical products leads to change in

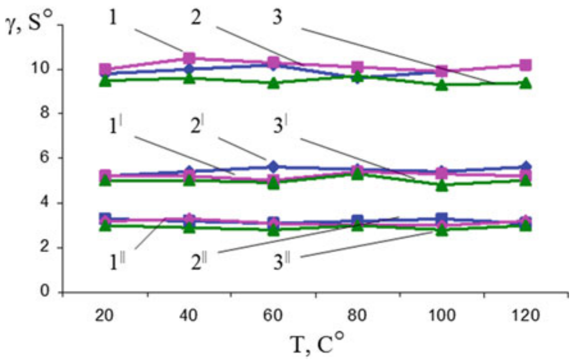

Fig. 4.29 Dependence of polarization plane rotation angle γ on temperature: 1—I-40A; 2—vacuum oil distillates (VOD); 3—Vaseline oil; 1^{I}—I-40A +3% of LCCC; 2^{I}—VOD +3% of LCCC; 3^{I}—Vaseline oil +3% of LCCC; 1^{II}—I-40A +5% of LCCC; 2^{II}—VOD +5% of LCCC; 3^{II}—Vaseline oil +5% of LCCC

their optical properties. It is marked by left rotation of light polarization plane of the investigated LM compositions.

It is noted that the value of rotational angle of light polarization plane of these mediums in a wide temperature range (to 110–120 °C) depends on LCCC concentration and does not depend on temperature.

Reduction of optical activity of the studied compositions of Vaseline oil with increasing length of alkyls used as additive of LCCC homologs is established for series of cholesteryl ethers of monocarboxylic aliphatic acids according to [47, 48] (Fig. 4.30).

It is shown that the dependence of the angle of light polarization plane rotation γ on the LC concentration in the Vaseline oil have is linear for all the studied cholesterics but the angle γ depends on what compound is used as the additive. For example, the specific polarization plane rotation for the cholesteryl stearate (X-7) was α = 0.33°S per percent of the LC-additives. Meanwhile for the cholesteryl acetate (X-3) it was α = 1.1°S (when the polarimetric cuvette length (*L*) is 200 mm). Dependence of the intensity of the light polarization plane rotation on the composition of the cholesterol ether is explained by the different structure of molecules (the acetic acid radical is significantly shorter than the stearic acid

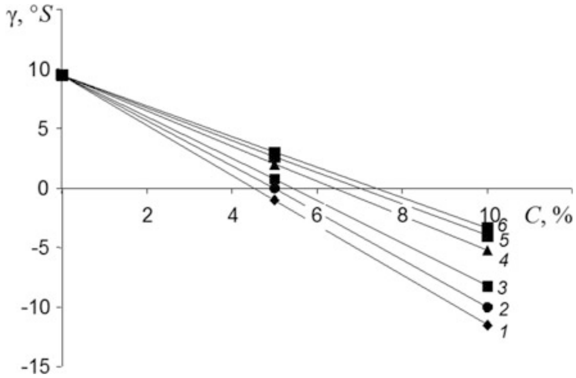

Fig. 4.30 Dependence of angle polarization plane rotation γ on concentration of CLC-components in VO: *1*—X-3; *2*—X-9; *3*—X-11; *4*—X-5; *5*—X-15; *6*—X-7. *Note* Results of tests of cholesterol coincide with line 1

radical) and the different molar mass of the tested compounds, 428.7 and 653.4 g, respectively, for the cholesteryl acetate and the cholesteryl stearate.

The latter circumstance leads to the similar mass concentration of the additives in the base composition, yet to different concentrations of LC molecules in the solution (the number of molecules for the cholesteryl acetate is approximately 1.52 times larger than that of the cholesteryl stearate). Taken into account that the molar mass of the cholesteryl acetate is 1.52 times less than that for the cholesteryl stearate, it can be asserted that the molecules of the cholesteryl acetate are optically more active.

These measurements become possible due to the statistically homogenous distribution of molecules of the cholesterics in the oil volumes and to their chiralic properties [7, 49] when the left and right directions become different so much that the optical activities depend on the directions of orientation of the molecules in space. The light polarization plane of each molecule rotates through the angle φ and the resulting angle γ is the sum of these single rotations: $\gamma = \sum \varphi_i$. It is observed when there are no chemical interactions between the oil and cholesteric molecules, and in the multi-component mixtures there are no interactions between the individual components. In other words, if chemical interaction or any noticeable effect of one component on the other take place, then the sum of contributions of each mixture component separately and together would be unequal.

The graph in Fig. 4.31 shows the dependencies of the angle of polarization plane rotation on the concentrations of cholesterol and cholesteryl ethers of the stearic acid (X-7) and their mixtures in the polyethylsiloxane fluid PES-5. It should be noted that the pure polyethylsiloxane fluid PES-5 does not show any optical activity and its angle of polarization plane rotation is 0°S.

Figure 4.31 shows that when 2.5% of the cholesteryl stearate by mass is introduced into the PES-5, the angle of its polarization plane rotation is $\gamma = -3.1°S$, while at 2.5% by mass of cholesterol it is $\gamma = -5.2°S$. The mixture of the cholesteryl stearate and cholesterol, with 2.5% by mass for each component, should rotate the polarization plane at the angle $\gamma' = -3.1 + (-5.2) = -8.3°S$. Straight line 3 in Fig. 4.31 demonstrates it vividly. For such mixtures $\gamma = -8.5°S$.

It is apparent that γ and γ' are practically similar. It is noteworthy that publications [50] indicate too that in the first approximation it can be assumed for binary

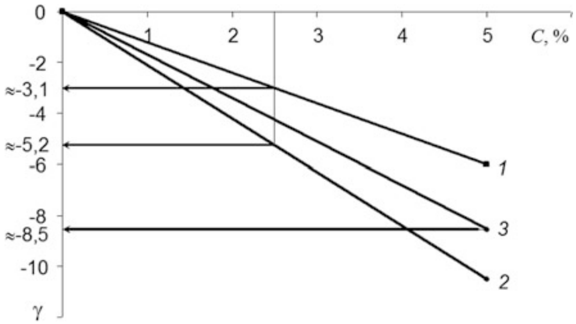

Fig. 4.31 Dependence of angle of polarization plane rotation γ on concentration of C LC-components in PES-5: 1—X-7; 2—cholesterol; 3—mixture of 2.5% by mass of X-7 +2.5% by mass of cholesterol

mixtures of cholesterols that the inverse length of the wave of selective reflection is the additive sum of concentration-weighed inverse lengths of waves of selective reflections from individual components.

The first approximation here implies that the mutual effect of the components (without introducing any special correction factors, such as, κ(A, B) Adams and Haas or β_{AB} Back and Labis ones).

The effective wavelength of selective reflection should be considered as some values (which relate to the effective steps of the spiral, hence, to the effective force of twisting). They show the relative contribution of the cholesteric into the resulting spiral structure of the mixtures: the larger the effective cholesteric wavelength is, the smaller its effective force of twisting and the larger the spiral pitch of the mixtures on its base are.

If the angles of twisting are compared with the parameters characterizing the structure of the cholesterics, the following experimental results can be obtained.

The data in Fig. 4.32 show the effect of the alkyl radical length on the optical activity of CLC solutions in the Vaseline oil. All the CLC in question contain the alkyl chain of the series $CH_3(CH_2)_n$ i.e. only the saturated cholesterol ethers.

Figure 4.32 shows that the concentrations 5 and 10% by mass manifest similar dependencies different just by the intensity of the light polarization plane rotation. If the point of cholesterol, which misses the alkyl chain, is ignored (i.e. $n = 0$), the analysis of the obtained curves shows a logarithmic dependence. For example, the following equation is obtained for the concentration 5% by mass:

$$\gamma = 1.8944\ \ln(n) - 2.4701 \tag{4.2}$$

The validity of approximation is 0.992; while for the 10% by mass concentration the equation is the following:

$$\gamma = 3.9995\ \ln(n) - 14.818 \tag{4.3}$$

and the validity of approximation is 0.9793.

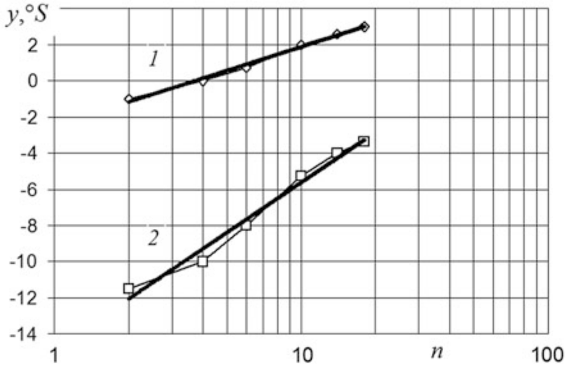

Fig. 4.32 Dependence of the angle of polarization plane rotation γ on number of carbon atoms n in alkyl chain of cholesterol ethers: 1—5%-concentration of cholesterol ethers in VO; 2—10%-concentration of cholesterol ethers in VO

Thus, with account of approximation, the test data are well described by the obtained equations. When cholesterol ethers are introduced into mineral and synthetic oils, the dependencies of the angle of light polarization plane rotation on the number of carbon atoms in the alkyl radical of cholesterol ethers for all the media have practically linear pattern in semi-logarithmic coordinates. It has been determined that with addition of LC-compounds of cholesterol in petroleum and synthetic oils the dependence of rotation angle of light polarization plane on a number of carbon atoms in alkyl of LC and their concentration in the base compositions is linear for all tested LC-compounds. The rotation angle of polarization plane of the also depends on the type of LCCC used as an additive. Such dependence is explained by both the differences in molecular structure and various molar mass of used LCCC.

We can draw a conclusion that the difference in molecular structure of LCCC leads to different amount of the molecules per unit volume of the solution at the same mass concentration in the base composition, and consequently to different optical activity of the test lubricants. Therefore, the obtained data is a real basis for quality evaluation of such lubricants.

4.6 Lubricity of Cholesteric Liquid-Crystal Nanomaterials and Their Mixtures Depending on Temperature

Extending the service life of equipment, reducing its energy consumption and intensification of technological processes in machine building are closely linked to development of efficient lubricants.

Variation of tribological behavior of lubricant materials and systems by varying their composition is known as a “passive control” of the friction coefficient [9]. In this context the liquid crystals (LC) are particularly promising due to their structural features [3, 5, 23, 51]. The experience shows that realization of LC mesomorphous state ensures their efficient application since they significantly affect the lubricity even in small quantities [23, 51].

In up-to-date practice also the systems of “active control” of the friction coefficient are known where friction is controlled not only by the contact pressure but friction force when varying the lubricant shear resistance [9, 16]. Moreover, the nature and structural properties of lubricant are of great concern in this case. Thus, in work [9] it has been stated that if some LC of nematic type are placed in the zone of dynamic contact then the friction force of the tribosystem can be varied by 20–25% by application of electric fields. On the other hand, if paraffin or alcohol is present in the zone of dynamic contact then the friction force can be varied by changing the tribosystem temperature [16]. However, even the process is reversible for paraffins and alcohols the sliding friction coefficient varies in a discontinuous manner. Taking account of the properties and chemical structure of cholesterol LC one should expect that “active control” of their lubricity by varying the friction force via heating would be smooth rather than discontinuous. Moreover, it will happen within rather wide limits of reversible variations of the friction coefficient.

Synthetic commercial enantiotropic cholesterol LC [52] was used in our investigation. To produce LC having a required range of mesophase an individual cholesterol thermotropic LC composite with mesophase within 74.5–81.5 °C (LC_3) temperature range was chosen. It was modified with industrial blends of liquid crystals LC_1 and LC_2 having much lower mesophase temperature ranges and known in practice as low-temperature LC sets for thermal indicators (Technical Specifications 6-09-06-1065-82). The temperatures of phase transitions of these LC-compositions of cholesterol are given in Table 4.4.

Medical VO was used as an inactive lubricant. Steel 45–steel 45 couple (42–46 HRC) was used as a tribosystem.

Blended compositions were formed by heating the components up to their full visible mutual dissolution accompanied by thorough mechanical mixing and holding at a temperature above the point of transition into isotropic liquid of the most refractory component followed by cooling.

To monitor the phase state of LC-preparations in response to temperature we used a polarization microscope NU-2 (Germany) equipped with a heating table and two-axis recorder (Chap. 3, Fig. 3.24).

Tribotests were carried out with the original pin-on-disc friction setup comprising digital circuit engineering, providing the reproducibility of the test data [53]. The setup allows us to measure and automatically control friction force, sliding velocity, linear wear, and deformation of surfaces within wide limits of rotation velocity and load. The discs 90 mm in diameter and 1.5–2 mm thick were used as well as pins 6 mm in diameter and 10–12 mm long. The total area of the working surfaces of the three specimens was 1 cm^2. Prior to the tests the specimens were polished with emery paper and degreased with acetone and carbon tetrachloride. The quality of the run-in was estimated visually and considered complete when the area of the friction contact was $\geq 90\%$ of the working surface of the specimen(-s). The run-in conditions were as follows: sliding velocity 0.15 m/s and contact pressure 1 MPa.

The friction experiments were carried out at environment temperature 8–10 °C. The required test temperature was measured by the thermocouple on the disc surface located 2 mm from the friction zone. It was specified and kept constant by controlling thermostatically the friction unit using a thermostatic switch. Before testing 10–12 drops of the test lubricant were applied to the disc surface in such a way, that in spreading it covered the whole contact surface. The experiments were carried out at sliding velocity 0.1–0.5 m/s and pressure 0.1–3.0 MPa.

Table 4.4 Temperatures of solid–liquid crystal T_{ph1} and liquid crystal–isotropic liquid T_{ph2} phase transitions

Component	T_{ph1} (°C)	T_{ph2} (°C)
LC_1	14	39
LC_2	–8	19
LC_3	74.5	81.5

It is a well-known that the cholesterol LC can rotate the polarization plane whereas the isotropic phase can not [49, 54]. As a result, with heating up LC compositions, placed between the crossed polaroids of the microscope, the light flow decreases practically stepwise at transition from mesophase to isotropic liquid. The latter was registered with the photocell mounted into the microscope optical system. In this case the signal was fed from the photocell output to one of the inputs of the two-axis recorder. The signal from the thermocouple of the heating table was fed to another input. The dependencies of the signal from the photocell being proportional to the light flow passing through the LC compositions were plotted versus the heating time (Fig. 4.33). It was found that these dependencies have well pronounced peaks that correspond precisely to the temperatures of the respective phase transition. In our opinion, this results from the stepwise variation of the light flow during transition from mesophase to isotropic liquid.

The solid-LC state phase transition for each LC specimen evidently lies in the region to the left from the mentioned peaks of intensity of light transmittance. In this case the character of the curves within this temperature range (Fig. 4.33) apparently results from the processes occurring in the structure and composition of the test LC. Nevertheless, a rather significant hidden heat characterizes the formation of mesophase at LCCC melting and it is easily monitored by thermograph.

Therefore, based on the test data we can clearly see that it is possible to control the temperature characteristics of enantiotropic LC blends and, hence, obtain LCCC with given temperatures of phase transition (Fig. 4.34).

The latter as it was shown earlier [3, 53] is important in terms of optimal application of LC compounds as antifriction additives to LM with required operation temperature range. At the same time it was suggested that the LC compositions could be efficiently applied as lubricants with tribological characteristics varying considerably within their mesomorphous state, i.e. in response to temperature effects.

The assumption has been verified experimentally.

A set of the temperature dependencies for shear resistance or friction coefficient for LCCC specimens (Fig. 4.35) was obtained as a result of tribotests. Moreover, it should be noted that the repeatability of the presented experimental data was

Fig. 4.33 Intensity of light transmission *I* versus temperature *T* of LC blends: 1—100% of LC_1; 2—80% of LC_1; 3—60% of LC_1; 4—40% of LC_1; 5—20% of LC_1; and 6—100% of LC_3

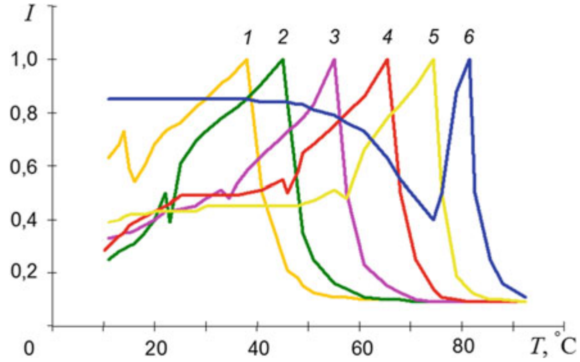

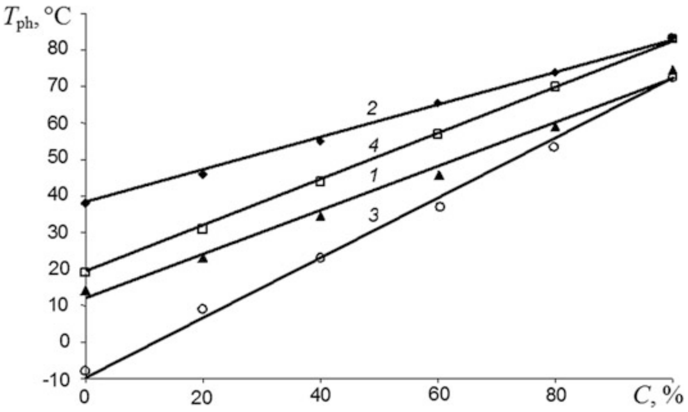

Fig. 4.34 Temperatures T_{ph} of solid-liquid crystal (1, 3) and liquid crystal-isotropic liquid (2, 4) phase transitions versus concentration C of LC_3 in LC_1 and LC_2: 1, 2—LC_3 + LC_1; 3, 4—LC_3 + LC_2 (LC_1 and LC_2 are multi-component composites of LCCC, LC_3—individual LCCC)

Fig. 4.35 Friction coefficient f versus temperature T: 1—LC_1; 2—LC_1 +40% of LC_3 by mass; 3—LC_1 +1% of LC_3 by mass; 4—BM; 5—BM +1% of LC_1 by mass; v = 0.3 m/s; p = 1 MPa

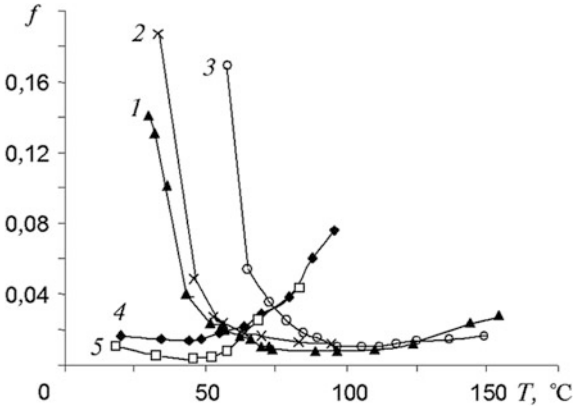

extremely high. In this connection the diagrams obtained for efficiency of the LC compositions can be considered as regular.

Actually, thermotropic cholesterol LC substances are characterized by two-phase transitions [7, 49]: the first one is transition from the solid state to the liquid-crystalline one (LC melting region) and the second one is from the liquid-crystalline phase to isotropic state (LC clarification region). At the temperatures lower than the transition temperatures of the aforementioned LC compositions from their solid state to the liquid-crystalline one the discontinuous sliding and stepwise variation in the friction coefficient within wide limits (0.06–0.20) was revealed (not shown in Fig. 4.35). At the given temperatures the test LC compositions are in solid state and discontinuous behavior of the friction coefficient is very much similar in pattern and value to the results obtained for dry friction. Therefore, the experiments indicate that cholesterol LC compositions in solid state don't have any lubricity and the rubbing surfaces contact directly.

As the temperature approaches the temperature of transition of LC compositions from the solid state to liquid-crystalline one the friction stabilizes. At further heating above these temperatures the discontinuous sliding is not observed for all the test LCCCs and the friction coefficient decreases monotonously achieving minimum within the temperature range including the temperature of mesophase existence (Fig. 4.35). In this case one can see a number of bends on the temperature dependencies of the friction coefficient. It can be due to the structural reorganization of LC lubricating layers with varying temperature in the friction zone. Actually, according to [7, 19] under certain thermodynamic conditions LCCC can form a smectic mesophase as well as the cholesterol one.

We have found that when the friction couple is lubricated with the LCCC-modified mineral oil the region of increasing friction coefficient on the curve of its temperature dependence is shifted to lower temperatures compared to lubrication with individual LCs and depends on the concentration of LC additives (Fig. 4.35, *5*). However, it was observed that with increasing additive concentration in the lubricant the region of increasing friction coefficient is shifted to higher temperatures. Therefore, one can state that low friction coefficients are observed at the temperatures corresponding to the mesomorphous state of the lubricant components not only for individual LCCC but their blends with mineral oils as well. It is clear from Fig. 4.35 that by adding 1% by mass of cholesterol LC into lubricant we can decrease the friction coefficient. Hence, the results are supported by the fact that even at this concentration the LC molecules can be adsorbed on the friction surface and reveal their lubricity [55, 56].

A more detailed analysis of the experimental data shows that, on the one hand, in LC blends the mesophase range widens depending on their blend composition and, on the other hand, the temperature range widens at which minimal friction coefficients are observed (Fig. 4.35). Therefore, under given test conditions the temperature resistance of the boundary layers of enantiotropic cholesterol LC compositions exceeds that of lubricating layers of the mineral oils either containing or not the LC additives. We note the fact that for the LCCC under consideration minimal friction coefficients are observed within the temperature range including the mesophase and partly the isotropic liquid phase. In other words, when the tribosystem is heated the friction coefficient increases in the temperature range where the test LC blends have long been isotropic liquids. Such an ambiguous behavior of the given LC blends resulting in shift in the temperature stability of their boundary layer to the region of temperatures characteristic of the isotropic liquid phase apparently results from the influence of the friction surface on the LC compositions. Actually, in line with works [3, 7, 8] under the action of the bearing surfaces the physical-mechanical properties of thin boundary layers of LC molecules can vary and differ significantly from their bulk properties. In other words, a decrease in the friction coefficient observed for test LCCC above their clarification points is not unexpected. Moreover, it is of some interest since in this case boundary lubrication is governed by lubricity of polymolecular lubricant films adjoining directly the solid surfaces. The results of work [9] also support this conclusion. In line with them an opportunity exists for LC-composites that the transition of the LC films from the ordered state to the disordered one occurs on the friction surfaces at temperatures significantly higher than the temperatures at which their bulk becomes clarified. Up to these temperatures LC molecules are capable of maintaining order (smectic, cholesteric, etc.).

So, it is shown experimentally that the friction coefficient varies for all test LCCC when they are in their LC state and, hence, can experience some structural transformations. The variations in the friction coefficient under the steady-state dynamic contact were proved to be reversible and highly reproducible.

The similar results are observed not only in case of continuous but also discrete or stepwise temperature variations, viz. during much longer testing of LC compositions. The testing time was 32–36 h reaching up to 8 h for each specific temperature. In this case the friction coefficient is also reversible for all test LCCCs, viz. the same friction coefficient corresponds to each temperature under the steady-state conditions irrespective of whether the characteristic is registered during heating or cooling of the LC blend. It should be noted that the given effect is observed not only within the LCCC mesomorphous state but also within a wider temperature range. The time of LCCC operation does not affect the friction coefficient. It remains constant and corresponds to a certain temperature both during heating and cooling of the LC tribosystem.

Based on the aforesaid one can draw the following conclusions.

1. Considerable variation and reversible lubricity of thermotropic cholesterol LC with temperature are revealed experimentally.
2. For the individual LC blends with low-temperature LC sets for thermal indicators a close to linear dependence is observed for the transition temperatures from liquid-crystalline phase to that of isotropic liquid state within a wide concentration range.
3. Thermotropic LC compositions of cholesterol compounds can be used efficiently not only as additives with required temperature range of operation but also directly as lubricants having a considerably higher thermal resistance of the boundary layers than that of mineral oils, and temperature-controlled tribological performance.

References

1. B.N.J. Persson, in *Sliding Friction. Physical Principles and Applications* (Springer, Berlin, Heidelberg, New York, 2000), p. 515
2. *A Handbook for Triboengineering: Volume 2. Lubricants, Machinery Lubricants, Bearings of Sliding and Rolling*, ed. by M. Khebdy, A.V. Chichinadze (Mashinostroenie, Moscow, 1990), p. 400 (in Russian)
3. S.F. Ermakov, V.G. Rodnenkov, E.D. Beloenko, B.I. Kupchinov, in *Liquid Crystals in Engineering and Medicine* (Asar, Minsk, 2002), p. 412 (in Russian)

4. B.I. Kupchinov, S.F. Ermakov, V.P. Parkalov, Study of influence of liquid crystals on the friction of solid. J. Friction Wear. **8**(4), 29–32 (1987)
5. S. Ermakov, A. Beletskii, O. Eismont, V. Nikolaev, in *Liquid Crystals in Biotribology. Synovial Joint Treatment* (Springer, Heidelberg, New York, Dordrecht, London, 2016), p. 211
6. B.V. Deryagin, Y. Popovski, B.A. Altoiz, Study the liquid-crystalline state occurring under the action of surface forces. Doklady USSR. **262**(4), 853–855 (1982)
7. A.S. Sonin, in *Introduction to Physics of Liquid Crystals* (Nauka, Moscow, 1983), p. 320 (in Russian)
8. J. Congrad, *Alignment of nematic liquid crystals and their mixtures* (Gordon and Breach, London, 1982), p. 104
9. Y. Kimura, K. Nakano, T. Kato, S. Morishita, Control of friction coefficient by applying electric fields across liquid crystal boundary films. Wear. **175**, 143–149 (1994)
10. A.S. Akhmatov, in *Molecular Physics of Boundary Friction* (Fizmatgiz, Moscow, 1963), p. 472 (in Russian)
11. G.I. Fuks, Adsorption and lubricating ability of oils. Sov. J. Friction Wear. **4**(3), 398–414 (1983)
12. *Fundamentals of Tribology (Friction, Wear, Lubrication)*, ed. by A.V. Chichinadze (Mashinostroenie, Moscow, 1995), p. 779 (in Russian)
13. A.S. Sonin, *A Way Century Long. History of Discovery and Study of Liquid Crystals* (Nauka, Moscow, 1988), p. 224 (in Russian)
14. D.N. Garkunov, in *Triboengineering* (Mashinostroenie, Moscow, 1989), p. 328 (in Russian)
15. B.I. Kupchinov, S.F. Ermakov, V.G. Rodnenkov, in *Introduction to Tribology of Liquid Crystals* (Informtribo, Gomel, 1993), p. 156 (in Russian)
16. F.P. Bowden, D. Tabor, *Friction and Lubrication of Solids* (Pergamon Press, Oxford, 1986), p. 543
17. D.F. Moor, *Principles and Applications of Tribology* (Pergamon Press, Oxford, 1978), p. 487
18. N.D. Bryuzgina, G.A. Gorokhovskii, T.V. Dmitrieva, P.N. Logvinenko, On influence of products of oleic acid mechanical-chemical transformation of metal dispersion. Sov. J. Friction Wear. **4**(4), 621–625 (1983)
19. *Cholesteric Liquid Crystals* (Collection of Papers) (University, Novosibirsk, 1976), p. 100 (in Russian)
20. B.I. Kupchinov, V.G. Rodnenkov, S.F. Ermakov, V.P. Parkalov, A study of lubrication by liquid crystals. Tribol. Int. **24**(1), 25–28 (1991)
21. B. Kupchinov, V. Rodnenkov, S. Ermakov, V. Parkalov, A study on mesogen lubrication, proceedings 5th international congress on tribology: “Eurotrib-89”. Helsinki. **4**, 219–225 (1989)
22. J. Cognard. in *Lubrication with Liquid Crystals, In book: Tribology and the Liquid-Crystalline State*, ed. by G. Biresaw (American Chemical Society, 1990), pp. 1–47
23. A.S. Vasilevskaya, E.A. Dukhovskoi, A.A. Silin, Effect of nematic ordering on sliding friction. Lett. J. Tech. Phys. **12**(12), 750–752, (1986) (in Russian)
24. A.A. Syslov, S.F. Ermakov, V.M. Ovchinnikov, Liquid crystals—A revolution in the field of lubricants. Locomotive. **11**(479), 25–27 (1996) (in Russian)
25. S.F. Ermakov, E.D. Beloenko, O.L. Eismont, Role of liquid crystals in tribological behavior of joint cartilages. J. Friction Wear. **25**(5), 486–491 (2004)
26. S.F. Ermakov, V.P. Parkalov, V.A. Shardin, R.A. Shuldykov, Effect of liquid-crystal additives on tribological performance of dynamically contacting surfaces and mechanism of their friction. J. Friction Wear. **25**(2), 87–91 (2004)
27. B.I. Kupchinov, V.S. Xaritonov, V.G. Rodnenkov, S.F. Ermakov, B.P. Bataev, Inv. Cert. No 1094341 USSR, C 10 M 3/14, no 3537510/23-04; Application 15. 10. 82; Published 22. 01. 84
28. V.F. Pichugin, On the mechanism of selective transfer when you wear a pair of copper alloy steel. J. Friction Wear. **5**(2), 71–79 (1984)
29. S.F. Ermakov, V.P. Parkalov, V.A. Shardin, Study of screening effect of cholesterol liquid crystalline compounds by pendulum sclerometry. J. Friction Wear. **24**(6), 63–65 (2003)

30. I.B. Gantsevich, L.I. Mirnaya, G.I. Fuks, The influence of the composition of the solutions of surfactants in non-polar liquids, the magnitude of adsorption of lowering the hardness of the steel. Colloid J. **34**(5), 832–837 (1972) (in Russian)
31. G.I. Fuks, S.G. Uskova, I.B. Gantsevich, Z.A. Kuteinikova, On the influence of the composition of the low-polar medium and solutions of surfactants on the mechanical properties of the surface layer of solids. Colloid J. **35**(5), 854–859, (1973) (in Russian)
32. P.A. Rebinder, in *Surface Phenomena in Disperse Systems. Physico–Chemical Mechanics: Selected Papers* (Nauka, Moscow, 1979), pp. 143–154 (in Russian)
33. P.A. Rebinder, in *Physico–Chemical Mecanics: Selected Papers* (Nauka, Moscow, 1979), p. 381 (in Russian)
34. N.K. Myshkin, C.K. Kim, M.I. Petrokovets, *Introduction to Tribology* (CMG, Seoul, 1997), p. 292
35. E.L. Aero, N.M. Bessonov, in *Micromechanics of Structural Liquid Layers Between Solids in Contact*, ed. by I. Nauki, I. Tekhniki. Ser.: “Mechanics of Fluids and Gases”, vol. 23 (Moscow: VINITI, 1989), pp. 237–315 (in Russian)
36. A.A. Kut’kov, About the Mechanism of a Friction of the Polymers Greased with Surface-Active Greasings. Mech. Polym. **1**, 128−135 (1965) (in Russian)
37. S.F. Yermakov, V.I. Kolesnikov, A.P. Sychev, N.A. Myasnikova, A.P. Svirskii, Some regularities of adsorption of cholesteric liquid crystalline nanocompositions during the friction of solids. J. Friction Wear. **29**(4), 288–291 (2008)
38. V.E. Ivanov, A.B. Kupchinov, Investigation of tribotechnical characteristics of mineral oils with liquid-crystal additives. J. Friction Wear. **9**(2), 128–130 (1988)
39. A.A. Syslov, S.F. Ermakov, Liquid crystals in tribology. Mater. Technol. Tools. **1**, 5–11 (1997) (in Russian)
40. *A Handbook for Triboengineering: Volume 1. Theoretical Fundamentals*, ed. by M. Khebdy, A.V. Chichinadze (Mashinostroenie, Moscow, 1989), p. 374 (in Russian)
41. A.S. Volokitin, in *The Electric Double Layer. Physical Encyclopedia*, ed. by A.M. Proxorov, vol. 1 (Soviet Encyclopedia, Moscow, 1988), pp. 562–563 (in Russian)
42. S.F. Ermakov, in *Tribology of Liquid-Crystalline Nanomaterials and Systems* (Belarusian Nauka, Minsk, 2012), p. 380 (in Russian)
43. A.A. Syslov, S.A. Chizhik, S.F. Ermakov, O. Yi, Komkov, Simulation of contact interaction of solid surfaces in the presence of anisotropic lubricant layer. Mater. Technol. Tools. **4**, 9–14 (1998) (in Russian)
44. A.A. Syslov, S.F. Ermakov, S.A. Chizhik, B.I. Kupchinov, The effect of the liquid crystalline additive on microrelief of stell surface. J. Friction Wear. **17**(1), 60–66 (1996)
45. A.A. Syslov, S.F. Ermakov, Liquid crystal additives in finish materials. Mater. Technol. Tools. **2**, 87–88 (1998) (in Russian)
46. S.F. Ermakov, V.A. Shardin, R.A. Shyldikov, The effect of the alkyl radical length on the optical activity of solutions of cholesteric liquid crystals. Mater. Technol. Tools. **12**(2), 50–55 (2007) (in Russian)
47. *Chemical Reagents and High Purity Substances. Directory.* (Khimiya, Moscow, 1983), p. 342 (in Russian)
48. V.G. Tishchenko, R.M. Cherkashina, in *Molecular Structure and Mesomorphism of the Derivatives of Steroids* (Coll of Papers: Cholesteric Liquid Crystals, Novosibirsk, 1976), pp. 26–34 (in Russian)
49. V.A. Belyakov, in *Liquid Crystals* (Knowledge, Moscow, 1986), p. 160 (in Russian)
50. V.A. Belyakov, A.S. Sonin, in *Optics of Cholesteric Liquid Crystals* (Nauka, Moscow, 1982), p. 360 (in Russian)
51. S.F. Ermakov, V.I. Kolesnikov, A.P. Sychev, Lubricity of cholesteric liquid-crystal nanomaterials in friction of solids. J. Friction Wear. **37**(2), 136–140 (2016)
52. G.M. Zharkova, V.M. Khachatruryan, in *Cholesteric Liquid Crystals, in Coll. of Papers: Cholesteric Liquid Crystals* (Novosibirsk, 1976), pp. 4–13 (in Russian)
53. B.I. Kupchinov, S.F. Ermakov, E.D. Beloenko, in *Biotribology of Sinovial Joints* (Vedi, Minsk, 1997), p. 272 (in Russian)

54. V. de Gennes, in *Physical Properties of Liquid Crystalline Substances* (Mir, Moscow, 1982), p. 160 (in Russian)
55. B.I. Kupchinov, S.F. Ermakov, A.A. Suslov, V.N. Kestelman, in *The Effect of Friction on Adsorption of Liquid Crystal*, Proceedings of the 4th International Tribology Conference of AUSTRIB ‘94, Vol. II, pp. 67–69, 1994
56. V.I. Kolesnikov, S.F. Ermakov, A.P. Sychev, Triboinduced adsorption of liquid-crystal nanomaterials under friction interaction of solids. Dokl. Phys. **54**(6), 269–272 (2009)

Chapter 5
Practical Application of Liquid-Crystal Nanomaterial in Engineering and Medicine

Increasing operating life of current equipment, reducing its energy capacity, as well as the intensification of technological processes in mechanical engineering is closely related to the time-effective development of new lubricants. Analysis of domestic and foreign experience shows that improving lubricant materials by means of introduction of LC-additives providing the ordered state of the lubricant layers in a friction zone is a promising approach for a number of these tasks. The above-mentioned results of theoretical and experimental laboratory studies of tribophysical properties of liquid-crystal nanomaterials generally bring hope that their high lubricating properties will present also in friction units of real machines and mechanisms both in the direct applicability and as additives for traditional lubricating and self-lubricating materials. It is obvious that the issues of creating methods and techniques for correction of joints being unparalleled in terms of lubricity mechanism are no exception since convincing evidence of liquid-crystal state of synovia medium and its global impact on frictional interaction in the joints has been found. Consequently, following are the more detailed information about use of liquid-crystal nanomaterials in triboengineering and arthrology.

5.1 Application of Liquid-Crystal Nanomaterials When Running-In of Internal-Combustion Engines

The run-in process relates to modifications of the geometry of friction surfaces and physico-technological properties of surface layers in the friction period friction that is governing for reliable and durable performance of internal combustion engines (ICE). One of the main factors that determine service properties of rubbing surfaces of cylinder-piston groups is the original microgeometry of surface layers that should contribute to fast expansion of the actual contact area between the sleeve and the ring reducing correspondingly contact loads with the least run-in wear. The existing

S. F. Ermakov and N. K. Myshkin, *Liquid-Crystal Nanomaterials*, Springer Series in Materials Science 267, https://doi.org/10.1007/978-3-319-74769-9_5

process of machining of ICE cylinders including operations of turning, followed by honing, fails to produce an optimal combination of mechanical parameters of the working contact of cylinders. Therefore, the engines after assembly are run-in on workbenches to finish the rubbing surfaces. In this way, the original roughness is balanced, residual stresses redistribute and microhardness changes, among other parameters [1].

Usually, the run-in process is checked under constant external conditions by monitoring reduction of the work if friction, temperature and wear rate. The run-in processes are intensified by using run-in lubricating materials containing an additive acceleration appearance of balanced friction surfaces, protecting them against scratching, seizure that are possible under loads unless the surfaces are run-in. commonly the additives contain various surfactants with chlorine, phosphorus, sulfur, fatty acids. However, use of liquid crystal compounds as run-in additives has made just first steps. The ICE was selected because it is the most standard and essential machine building process that serves, as a rule, to test latest engineering achievements. Therefore, the problems relating to studies of run-in processes of ICE parts, the effect of factors of roughness, temperature, pressure, speed, on their reliability and durability, are studied by numerous teams of researchers both in the CIS and in elsewhere [2–9].

It should be noticed meanwhile that many ICE run-in problems remain so far unresolved and a variety of recommendations how to run-in the ICE are still controversial. Until now there is no consensus about the engine run-in duration and methods. According to [2], the ICE run-in by different manufacturers lasts from 1 to 34 h.

Engine builders in the CIS practice to run-in ICEs for a short (up to 3 h) at the factory and then to prolong it in operation for 40–100 h [3].

To reduce the ICE run-in and to maintain the set quality standard would means to promote efficiency, save fuel and energy.

One of the main properties of run-in oils and additives should be their ability to influence the condition of surface layers of parts during their run-in.

In order to save the run-in of engines it was proposed to use low viscosity oil or oil mixtures. However, low viscosity oils can destroy boundary-lubricating layers in the zone of contact between rubbing surfaces and cause scratching or intensified wear.

Efforts to prevent these shortcomings with run-in additives like graphite, powdered charcoal, talc, yellow blood salt, borax, common salt, sugar, sulfophresol, sulfur, molybdenum bisulfide, oleic acid, stearin, etc. [3], sometimes fail to yield positive results.

Their insufficient performance in run-in processes is due to corrosion of parts and soot formation reducing the service life of engines. The additives that prevent smoking, varnish and carbon black appearance in the zone of combustion include metal-organic compounds with heavy metals of variable valence (Cu, Fe, Cr, et al.); they boost the speed and depth of oxidation hydrocarbons during combustion. However, irrespective of the efforts underway, these additives have not found way yet to practical application.

At present self-lubricating additives ALP-2, ALP-3 and ALP-4 are broadly used for running-in ICE.

During a number of years self-lubricating additives were tested [10] on automobile, transport, and marine diesel engines. It has been established that these additives enable to reduce somewhat the period of initial (factory) run-in of vehicles.

Meanwhile, the paper [11] that self-lubricating additives in fuel run-in mixtures deposit in sprayers reducing the efficiency of nozzles, upset the combustion process and diminish the engine power. The main cause of the disadvantage of self-lubricating additives is their corrosive attack due to the sulfur mercaptane.

It should also be noted that elevated temperatures in the combustion chamber cause decomposition of the self-lubricating additives resulting in aluminium oxide. Due its abrasive effect the running-in of coupled parts gradually intensifies, but the abrasive effect persists later in the initial period of operation of the ICE.

The above problems of running-in ICE and the ability of liquid crystals to produce balanced microroughness of friction surfaces (see Chap. 4) put forward the problem of effectiveness of application of liquid crystals in the ICE run-in processes.

A possibility of using LC as additives to fuel mixtures in order to intensify the run-in process of parts was tested in running-in two-stroke starter engines makes P-350, P10-YD and PD-10Y [12]. These tests were performed at the Gomel Starter Engine Factory.

An LC additive was introduced into the fuel run-in additive (FRM) consisting of a solution of diesel oil ДС-11 in gasoline [in the ratio 1:(15…20)]. The effectiveness of the additives was rated by the mean microroughness R_a of rubbing surfaces of the cylinder face, piston pin, concentration-rod upper head sleeve, by changes in the mass of piston rings. Alongside with these parameters, the engine was checked and losses for friction were rated by the moment of resistance to cranking before and after run-in.

The fuel run-in additives containing the additive ALP-4 are traditionally used for the purpose.

The test method was the following. The starter engine with the preset ignition dwell angle was mounted on the run-in bench. The moment of resistance to cranking was measured. Then it was started and idle revolutions were adjusted. The run-in was carried out at 3500 r.p.m. the run-in time was changed from 15 min (the standard conditions for run-in using the additives ALP-4) and shorter with an interval 3 min.

The optimum concentration of the LC additives was determined experimentally and it corresponded to 0.1–0.2% by mass. Table 5.1 shows the changes (in % of the original) of the tested parameters of the engines run-in with the ALP-4 and LC additives.

The analysis of the obtained results shows that the LC additives used for FRM of the standardized parameters of roughness of parts of cylinder-piston groups (CPG) and the moment of resistance to cranking change to a larger degree and within a shorter time interval than the ALP-4 additives affords to achieve.

Table 5.1 Results of testing of different additives for running-in of engines (% of changes of the original value)

Parameters	Additives and run-in time (min)			
	ALP-4		LC additive	
	7	14	7	14
Roughness of working contact:				
Cylinder face	−25	−41	−40	−53
Piston ring	−5	−38	−34	−60
Con-rod upper head	−15	−45	−56	−64
Mass of upper piston ring	−0.31	−0.33	−0.23	−0.27
Mean engine power	+2	+3	+10	+21
The moment or resistance to cranking	−25	−25	−25	−21

The profilograms of the cylinder face in the engines run-in with the LC additive prove that it acquires a flat-top microrelief while the ALP-4 additive fails to produce it (Fig. 5.1). Moreover, after running-in of the engines with the fuel mixture containing the LC additive, the piston rings under nominal conditions and within the same operation time wear 20–25% less than when run-in with the ALP-4 additive. It is because of the fact the main mechanism of changes in the microrelief of surfaces run-in with the ALP-4 additives is abrasion with aluminium oxide particles producing during thermal decomposition of the additives. With the LC additives the surfaces are run-in primarily by plastic deformation of microprojections and insignificant attendant fatigue wear.

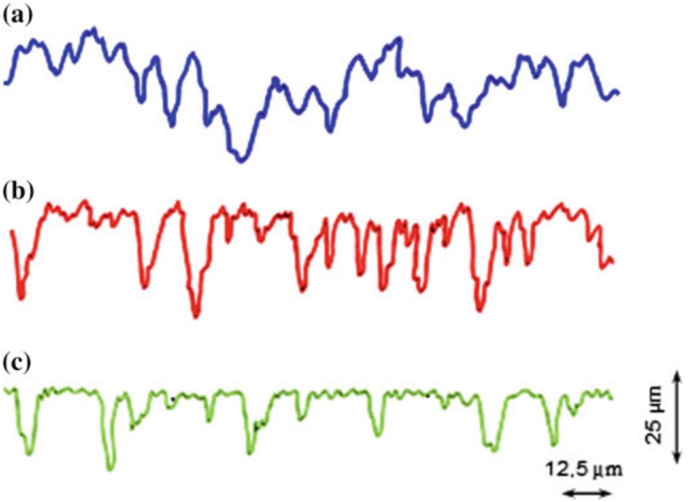

Fig. 5.1 Profilograms surfaces cylinder face starter engine before run-in (**a**), after run-in with additive ALP-4 (**b**) and with liquid crystal additive (**c**)

It has been established that slight additives (0.1%) of liquid crystals into the fuel mixture reduces the run-in of engines by 25%. The power of engines increases by 10% on the average, main fuel lines in the equipment are never blocked fuel and lubricating materials saved during the run-in process, labor consumption is reduced.

The flat-top relief resulting on contacting surfaces reduces wear of engines and energy losses for friction in operation.

The efficiency of liquid crystals as run-in additives was also studied with diesels D-240 on run-in braking workbenches KI-5542 GOSNIITI.

Figure 5.2 and Table 5.2 present the results. According to Fig. 5.2, introduction of LC nanomaterials into the motor oil leads to greater reduction of losses for the moment of resistance to cranking during cold run-in than when running-in with the pure motor oil. In the first case, losses for friction are 12% than in the second case. After 130 min of hot running in with the LC additives, they drop by the same value (Table 5.2).

Hot running in with the pure motor oil does not reduce losses for friction practically. It is observed after running-in of the engine with LC additives its power grows and specific fuel consumption reduces (Table 5.2) apparently due to lesser losses for friction.

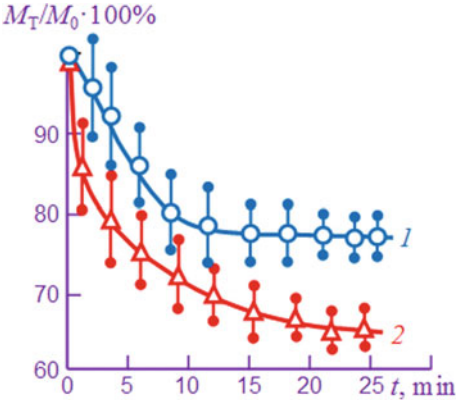

Fig. 5.2 Kinetics of relative moment or resistance to cranking diesel engine when running-in with pure motor oil (*1*) and motor oilwith liquid-crystalline nanomaterials (*2*)

Table 5.2 Parameters of diesels D-240 after run-in

Parameters	Run-in medium	
	Motor oil	Motor oil + LC additive
Power at nominal r.p.m., h.p.	73 ± 1	76 ± 1
Specific consumption fuel, g\l.s.h.	191 ± 4	181 ± 2
Relative moment of resistance to cranking ($M_T/M_0 \cdot 100\%$)[a]	77 ± 6	56 ± 1

[a] M_0, M_T—the moment of resistance to cranking before and after run-in, respectively

5.2 Liquid-Crystal Nanomaterials as Antiwear Engine Oil Additives

A number of commonly known causes necessitated search for substances capable to reduce losses for friction and wear, consumption of fuel by internal combustion engines. The result is a range of new antifriction additives to motor oils and friction modifiers. There are much fewer additives in the NIS; according to [13] they number ten. These additives were tested at the research center of the Volzhsky Automobile Works and yielded positive results permitting to recommend them as additives to motor oils.

They include Molycrystal, the liquid crystal additive developed at the Institute of Metal-Polymer Systems of the Byelorussian National Academy of Science. The additive was comprehensively tried during lab, Workbench and lab and operation tests.

A tentative test of the effect of Molycrystal showed that it improves the operation indices of a well run-in engine after 20–30 h run by 2–5%; hence, extra tests were performed. The lab tests were performed to assess the effect of Molycrystal on physico-chemical characteristics of the motor oil M-6_3/$12G_1$ (TS 38.101109987). In addition to the requirements set by the specification, the additives were checked for a tendency of the oil to foaming and compatibility with rubber.

Table 5.3 shows the results. Table 5.3 shows that Molycrystal in the oil M-6_3/$12G_1$ in a quantity 1.5% reduces the oil viscosity and the viscosity index at 160 °C. Absolute majority of the oil characteristics remain practically unchanged.

A four-ball friction machine served to test the effect of the additives on the oil lubricating properties; it revealed growth of the scratching index.

The workbench tests served to test a new VAZ engine to check the tendency of motor oils to produce low-temperature sediments and wear engine parts (Table 5.4).

The tests lasted 180 h. Before the tests and after every 60 h the engine and fuel consumption were checked. After the tests, the engine was disassembled to check the extent slam, scale on its parts, and wear by micrometering and weighing.

The accomplished studies revealed that Moly crystal in the oil M-6_3/$12G_1$ produces little slam on the engine parts. However, in general, the obtained results satisfied the provisional norms for the motor oils of the groups G_1. Nevertheless, it is noteworthy that papers [14, 15] report the mesomorphism of varnishes on engine parts. They analyze the conditions of appearance of the mesomorphous state and it is assumed that the liquid crystal phase is necessary on the surfaces of parts of cylinder-piston groups in order to prolong the service life by improving thermal stability.

Modifications of the engine characteristics in the process of workbench tests with the Moly crystal additive revealed that the mechanical losses rated by the moment or resistance to cranking have tendency of continuous reduction (Table 5.5); by the end of the tests they drop by 5.5% on the average. The largest reduction of the mechanical losses is observed after 60 h of operation of the engine.

Table 5.3 Results of tests specimens of pure M-6_3/12G_1 oil and with Molycrystal additive

Indicators	Oil specification norms	Oil	Oil + Molycrystal
Kinematic viscosity at 100 °C (cSt)	≥ 12	12.47	12.80
Dynamic viscosity at −15 °C (cPs)	<4500	3800	4100
Viscosity index	115	118	120
Stable viscosity	25	19.5	19.0
Sulfate ash content (%)	1.3	1.05	1.02
Alkaline number (mg of KOH/g)	7.5	7.97	8.00
Pour point (°C)	−30	−36	−36
Flash point (°C)	210	214	215
Corrosion on M-1copper	1a	1a	1a
Compatibility with rubber:			
Rubber 2801			
Change in volume (%)	±5	+2.64	3.11
Change in hardness, ISO units	±8	+3.0	+3.0
Rubber 5006			
Change in volume (%)	±8	+2.0	+2.61
Change in hardness, ISO units	±8	+4.0	+4.0
Concentration of mechanical impurities (%)	0.015	Rel.	Rel.
Lubricating properties in FBM			
Welding load (N)		2110	2000
Critical load (N)		800	1000
Scratching index		33	38
Wear spot diameter (mm)		0.43	0.40

Table 5.4 Results of wear of VAZ-2106 engine parts

Indicators	Measuring unit	M-6_3/ 12G1	M-6_3/ 12G1 + Molycrystal	% of changes
Camshaft mean wear	μm	12.2	4.7	−61
Mean wear of valve drive rods	mg	14.6	7.4	−49
Mean wear of piston rings	mg	32	29	−9.3
Mean change in piston ring joint gap	μm	73	69	−5.4

Reduction of mechanical losses by introduction of Moly crystal into motor oils boosts the engine power (Table 5.5) and reduces fuel consumption.

Lab and running tests with Moly crystal served to check fuel consumption by two VAZ-21083 vehicles. The scope of the tests was intended for 30 thousand run km of the vehicles and was counted after initial operation during 30 thousand run km. It means that the engines were well run-in and their and fuel consumption was

Table 5.5 Changes in characteristics of VAZ-2106 engine running with the Molycrystal additive

Characteristics of the engine	Test duration	Engine speed (min^{-1})		
		2283	3424	4566
The moment of resistance to cranking (Nm)	0	17.4	23.3	29.7
	60	15.8	21.6	27.7
	120	16.2	22.3	23.7
	180	15.4	21.4	23.4
Engine power (kW)	0	26.8	40.8	49.5
	180	27.4	41.4	50.4
% of power changes		+2.2	+1.4	+1.8

stabilized. Between 30 thousand run km and 45 thousand run km the vehicles operated with Moly crystal additive (1%), and between 45 and 60 thousand run km with the motor oil without any additives.

The fuel consumption in urban congestion was checked on run drums after 15 thousand run km. The fuel consumption by these vehicles was also checked with the Japanese 10-mode cycled used abroad to rate antifriction additives. Measurements were made every 5 thousand km staring with 35 thousand run km. It follows from из Table 5.6 that Moly crystal in the motor oil reduces fuel consumption by 4.5% on the average with both methods. It is noteworthy that the results with the first methods demonstrated that the effect of the additive persists after replacement of the oil too for 15 thousand run km at least.

Thus, the accomplished tests have shown that additive Molycrystal does not impair the physico-mechanical, detergent, or dispersant properties of the motor oil. It reduces wear of engine parts and mechanical losses for friction and fuel consumption by the vehicle by 4.45% in urban congestion.

It can be recommended for broad application as an additive to motor oils. Unlike the additives listed in [13] в отличие от перечисленных в работе [13] (Desta, Ecomin, Frictol, Resource, Remol, etc.), Molycrystal is ash-free without any environment armful substances, its tribological effectiveness is similar to the effect of friction modifiers.

Table 5.6 Results of the effect of the Molycrystal additives on VAZ-21083 fuel consumption

Vehicle	Fuel consumption (Q, l/100 km) based on coverage (thousand km)						
	30	35	40	45	50	60	Changes (%)
Urban cycle							
21083–95	9.22			8.9		9.1	−3.4
21083–37	8.67			8.19		8.08	−5.5
Mean (%)							−4.45
Japanese 10-mode cycle							
21083–95		9.22	9.10	8.90	8.90		−3.4
21083–37		8.70	8.60	8.22	8.20		−5.7
Average (%)							−4.45

5.3 Assessment of Liquid-Crystal Compositions' Efficiency When Polishing of Diamonds

Efficiency of introduction of liquid-crystal additives into the composition for polishishing of diamonds was verified when compositions was factory tested in Gomel MA "Kristall". The compositions made according to TS 25-1470.002-82 «Special salve-like diamond paste» [16] with addition of 3 wt% dispersed cholesteryl chloride into a salve base are used for experimental works at one of diamond production area.

During tests the diamond-cutters noted the following:

- polishing quality of work diamond surface improved;
- polishing zone on a diamond-cutting disc prepared in less time;
- discs cut softer that is leading to decrease in chipped teeth.

At the same time, resistance to drying of pastes has increased from 4–5 to 6–7 operating shifts.

To compare the efficiency of polishing of diamonds with base special salve-like diamond paste [16] and the same paste modified by 3 wt% of liquid crystals the laboratory studies of the artificial diamond («Almazot») surfaces treated with them are carried out. Pastes have been smeared on diamond-cutting discs in polishing zone.

Quality control of polished surfaces is carried out for six samples of artificial diamonds, three of which (for comparison) have been polished using base special salve-like diamond paste, and the rest have been polished with the application of the same paste with 3 wt% of liquid-crystal nanomaterials.

An atomic-force microscope (AFM) «Nanotop-202» and software package «Surface Soft» are used to evaluate the quality of surfaces.

A general nature of surfaces' microtopography (observed visually) and micro-geometrical parameters are analyzed, such as range of roughness height in the AFM picture A, arithmetic mean (AM) profile deviation Ra, root-mean-square (RMS) profile deviation σ (Table 5.7). The obtained data have been statistically processed.

It is noted that all samples being under test have high enough quality of processing, at that average altitude difference on the micro profiles equals $\sim$5–10 nm on the cut length of 5 μm [17, 18]. Nevertheless, full sized surface images of some samples haven't been archived because of non parallelism of two plate planes of the diamonds being under test.

Visual analysis of AFM images shows that the samples polished using pastes modified by liquid crystals, in comparison with results of application of base diamond pastes have smoother surface with less irregularities and much less pronounced marks of mechanical contact with a processing tool (Fig. 5.3).

Statistical analysis of microgeometric parameters of two groups of samples shows that more high surfacing quality by contrast to original composition is the

Table 5.7 Microgeometric parameters of surface area of the samples under investigation determining by an atomic-force microscope

AFM image (No sample-No area)	Scanning field size (μm × μm)	*A* (nm)	R_a (nm)	σ (nm)
Paste with LC				
1-1	13 × 13	128.3	32.9	3.7
1-2	13 × 13	37.1	9.7	2.7
1-3	13 × 13	65.1	19.5	3.7
1-3-1	5.6 × 5.6	66.5	21.3	9
3-1	5.6 × 5.6	9.5	3.6	1.2
3-2	5.6 × 5.8	14.6	6.2	1.4
5-1-	13 × 13	39	16	1.5
5-2-1	5 × 5	30	8.3	2.3
5-3	13 × 13	51.1	10.9	2.2
Base paste (without LC)				
2-1	13 × 13	200.5	49.3	10.8
2-2	13 × 13	196.3	46	11.2
4-1	7 × 8.5	13.5	4.1	1.1
4-2-1	1.6 × 1.6	2.8	1.1	0.2
4-2	6.4 × 6.4	12.1	2.8	1
6-1	5.2 × 5.2	139.5	91.4	14
6-1-	3.2 × 2.3	38.2	18.5	6.3
6-2	7.0 × 7.6	76.6	28.4	7

result of using the paste with edition of liquid-crystal nanomaterials when polishing of diamonds (Fig. 5.4).

In this case slightly less range of heights (Fig. 5.4a) on scanned fields, less arithmetic mean (Fig. 5.4b) and root-mean-square (Fig. 5.4c) profile deviations are achieved. This combination of values of given characteristics is indicative of increasing surface working quality of diamonds using modified paste with LC-compounds, i.e. shift of the process to formation of microroughnesses of lower order (submicroroughnesses) of the surface of the polished diamonds.

The compositions for surface working of solid and ultra-hard materials are proposed on the basis of the test results [18, 19]. Therefore, special salve-like paste modified by liquid crystals when using for polishing of diamonds allows to get the surfaces with higher quality of final polishing under otherwise equal conditions.

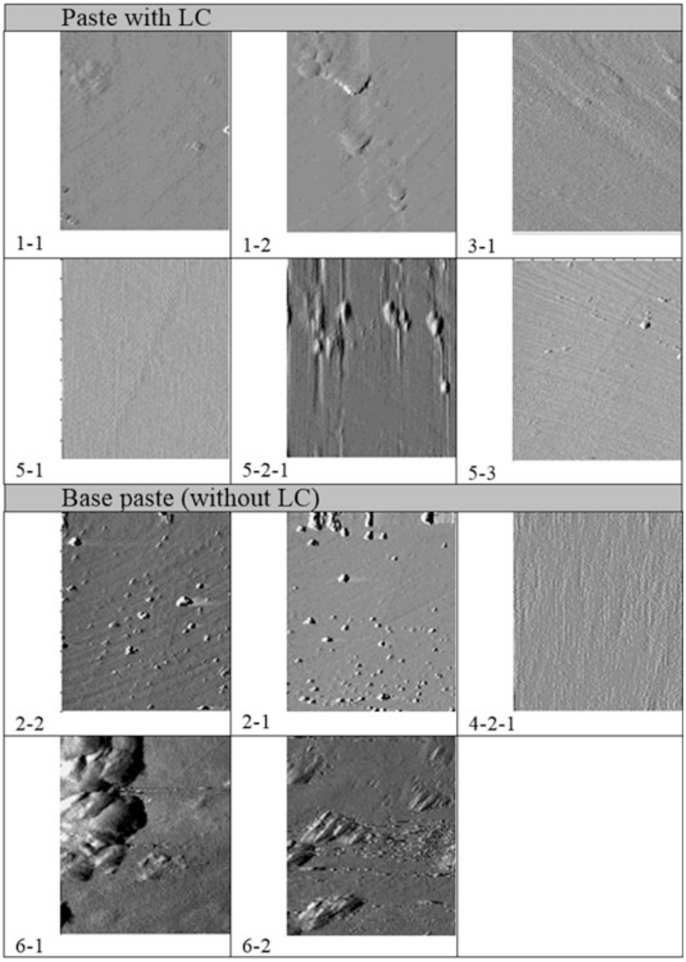

Fig. 5.3 Examples of characteristic AFM images of surface areas of artificial diamonds, polished with the use of base and modified pastes

5.4 Artificial Mediums Based on Liquid-Crystal Nanomaterials for Correction of Joint Tribology

The experiments revealed that synovia ensures the low friction of cartilages due to liquid-crystalline state of the lubricant in the friction zone. The obtained results were used to develop experimental samples of quasi synovial fluids and preparations intended to improve joint lubrication.

The effective protection of cartilage against destruction can be observed in articular tissue of histologic specimens after one- or three- fold introduction of

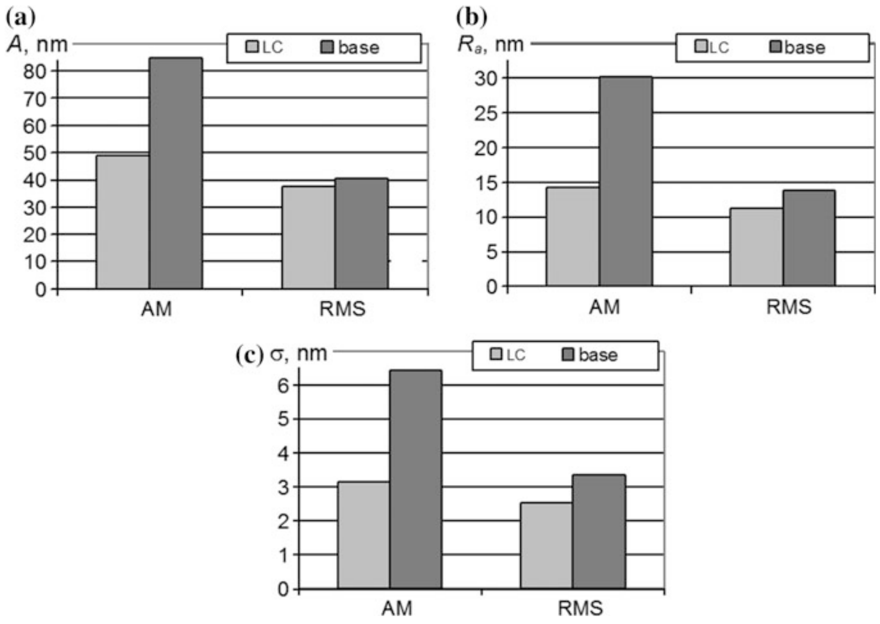

Fig. 5.4 Comparison of statistically average microgeometry parameters for two groups of samples of artificial diamond surfaces polished using base and modified pastes: **a** range of roughness height A; **b** arithmetic mean profile deviation R_a; **c** root-mean-square profile deviation σ

LCCC-containing quasisynovial liquid in a chronic phase of experimental osteoarthritis (Fig. 5.5a) [20, 21].

The surfaces have sharp contours and have been flat all along. LCCC-containing quasi synovial liquid has been more bio-effective when three-fold intra-articular introduction than one-fold.

Pronounced protective effect of LCCC-containing quasisynovial liquid has been found out also after intra-articular introduction of a specimen into knee joints of rats in an acute phase of osteoarthritis. A fairly wide surface area and uniform thickness with sharp contours keep in articular cartilage (Fig. 5.5b). Effective protection of collagenous articular structures without sacrificing their tangential area has been observed when van Gieson's stain.

In knee joints histologic specimens of the animals being under test both after intra-articular introduction of 0.2 ml LCCC-containing quasi synovial liquid in chronic phase of experimental osteoarthritis and on the 61st day after test work the articular cartilages have uniform sickness, sharp contours of a surface band (Fig. 5.5c). Structure of cartilage matrix has no any changes and been practically the same as under conditions of physiological standard. No dystrophic modifications of cartilage elements have been observed

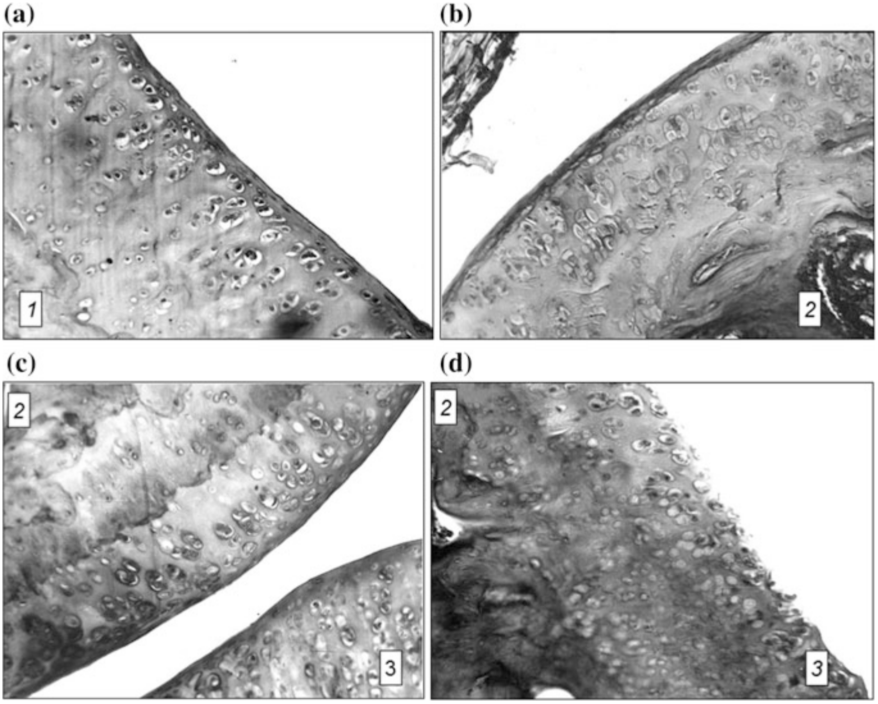

Fig. 5.5 Articular surfaces of knee cap (*1*), hip condyles (*2*) and shin bone (*3*) of knee joints of rats when experimental osteoartritis: **a**, **b** after three-fold intra-articular introduction of 0.1 ml LCCC-containing quasisynovial liquid in chronic and acute osteoarthritis phases, repetitively; **c** three-fold intra-articular introduction of 0.2 ml LCCC-containing quasisynovial liquid in chronic osteoarthritis phase; **d** experimental osteoarthritis; a stain by hematoxyline and eosine. ×140

Common symptoms of experimental osteoarthritis constituting erosions and full absence of cartilage surface layer in places and keeping only deep zones of cartilage matrix are present in control groups of animals after intra-articular introduction of physiological solution (Fig. 5.5d). Histology represents prominent chronic dystrophic processes, enzymatic and mechanical degradation of cartilage.

The finding suggests that the restoration character of structural and frictional functions of cartilage and synovial liquid under discontinuous load is similar to LCCC-containing quasi synovial liquid [21, 22]. Investigations on osteoarthritis models of animals' knee joints have demonstrated high chondroprotective efficiency of LCCC-containing quasi-synovial liquid, which involves protecting cellular and tissue structures affected by disease of articular cartilages against their biomechanical destruction.

The LCs can be introduced into the affected joint capsule not only by injection but by diffusion of cutaneously applied preparations trough the skin as well. The radioisotope technique established (Fig. 5.6) that the preparation accumulated on the femoral condyle surface.

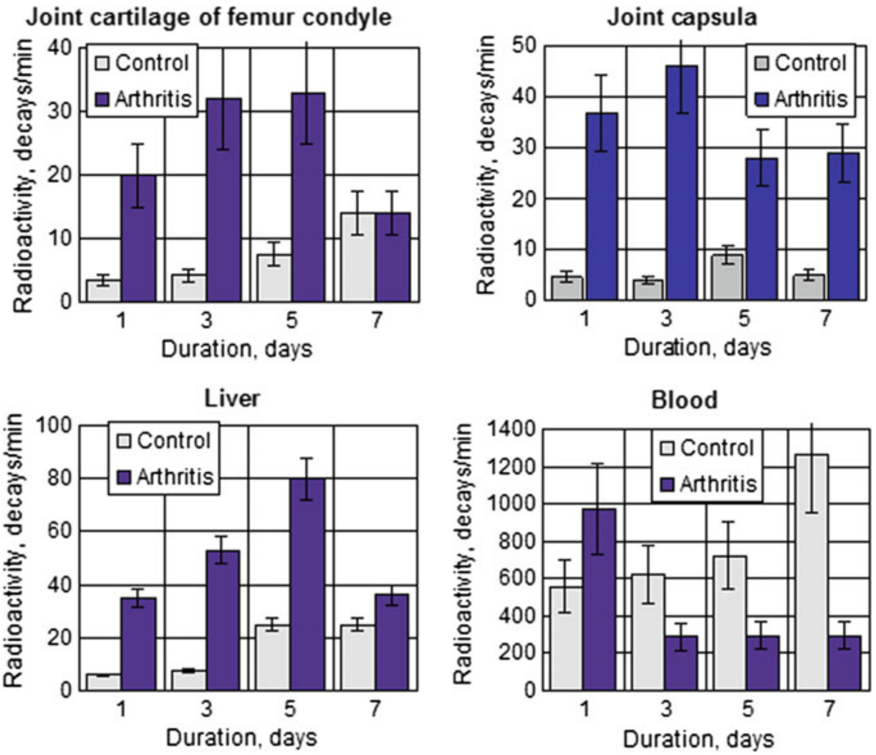

Fig. 5.6 Results of radioisotope investigation of cholesterol esters (labeled 1, 2 ^{3}H) diffusivity through rats' skin. Control—group under physiologically normal conditions, Arthritis—group under adjuvant arthritis

With normal joints, the amount depended directly on the duration of the experiments, and hence, on the number of applications that were made on the joint region. Simultaneously, the preparation was detected in the blood flow, liver, kidneys and joint capsula. In case of adjuvant arthritis, radioactivity appeared in the tissues sooner and in larger quantities than when the joints were normal. However, it stayed higher only in joint tissue. Probably, this is associated with a higher permeability of the vessel bed.

Preparations containing liquid crystals were tested clinically on a group of volunteers. The patients' condition improved after five to seven applications made with the test preparation onto osteoarthritic knee joints. The preparations were useful in reducing joint pain and in creasing the flexor angle. They were more effective than the most widely used therapeutic agents.

5.5 Lubricants Based on Vacuum Oil Distillates and Liquid-Crystal Nanomaterials

Lubricats play a significant role in the progress of modern engineering thanks to their ability to improve wear resistance of tribosystems, remove seizure, and corrosion effects [23, 24]. Plastic lubricants are known to perform these functions much better than liquid lubricating materials [25, 26]. So far, plastic lubricants occupy a special place among other lubricating materials with regard to production and assortment volumes. The plastic lubricants represent a dispersed phase-dispersion medium system, in which the dispersed phase (thickener) includes hydrated calcium soaps of the higher acids of either artificial or natural fats and the dispersion medium consists of either petroleum or synthetic oil [23–26].

As the analysis has shown, the new calcium lubricants can be efficiently developed by using cheap products for the dispersion medium, and byproducts like vacuum oil distillates and other useful substances available at the oil-refining enterprises. However, the research in this direction needs further elaboration.

Byproducts of oil refining were chosen for testing so that their rheological properties hardly differed from I-40A industrial oil often most used for manufacturing calcium lubricants. The modifiers for the lubricants were the liquid-crystal nanomaterials. To improve the triboengineering properties of the developed general-purpose calcium lubricants, they were added ethanolamines. It is common to differentiate between monoethanolamine, diethanolamine and triethanolamine, which are colorless, viscous, hygroscopic liquids with a specific amine smell that have an unlimited ability to mix with water and are easily soluble in ethanol, benzene, and chloroform; they display the properties of amines and acids. Ethanolamines represent a weak base and tend to form salts while interacting with the mineral and strong organic acids. They are used in industry as emulsifiers (ethanolamine soaps) and are simultaneously strong anticorrosion agents.

Lubricity of plastic lubricants has been studied on a four-ball friction machine (ChShM) following *GOST* (State Standard) 9490–75. The duration of each experiment was 10 s. The wear spot diameters d_w^m of the lower balls after testing served as the wear resistance estimates of the studied lubricating material samples. The load was raised in steps according to *GOST* (State Standard) 9490-75. The critical load P_{cr}, as well as the diameters of the wear spots were measured on the balls 1, 2, 4 and 8 h after the tests under the loads 196 and 392 N in various lubricating media.

It has been established for the first time [27] that ethanolamines (mono-, di- and triethanolamines) are able to improve wear resistance without deteriorating rheological properties of lubricants having vacuum oil distillates as a dispersion medium (base oil) when introduced in 0.5–1.5 wt% amounts (Fig. 5.7, curves *3*–*6*).

And, vice versa, the introduction of ethanolamines in the same concentration (0.5–1.5 wt%) into a lubricants containing traditional refined petroleum oils (industrial oils) as the dispersion medium does not affect the antiwear properties (Fig. 5.7, curves *1* and *2*; Fig. 5.8, curves *1* and *2*).

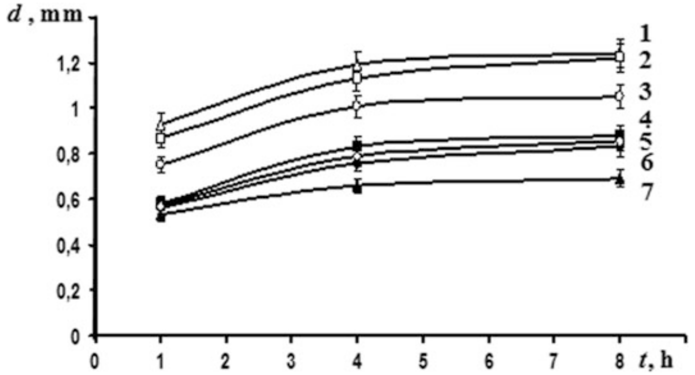

Fig. 5.7 Dependence of wear spot diameters *d* of steel balls versus time *t* at testing on ChShM machine under 392 N load in the presence of lubricants based on calcium soaps of the higher acids of natural fats containing industrial oil I-40A as a dispersion medium (*1*, *2*) and vacuum oil distillates (*3*–*7*): (*1*, *3*) without additives; (*2*, *4*) with addition of 0.5 wt% of triethanolamine; (*5*) 1.0 wt% of diethanolamine; (*6*) 1.5 wt% monoethanolamine; (*7*) with 0.5 wt% addition of triethanolamine and 3.0 wt% liquid-crystal nanomaterials

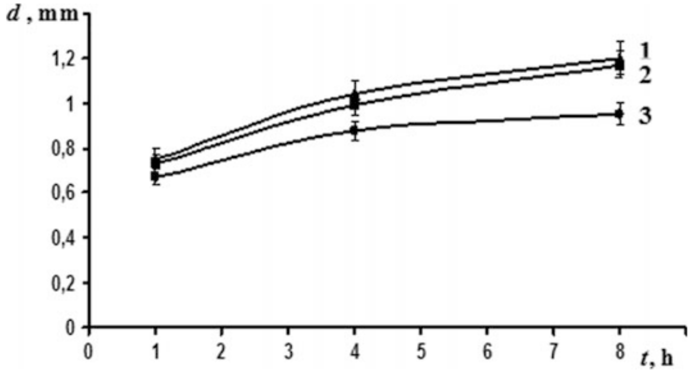

Fig. 5.8 Dependence of diameter *d* of wear spots of steel balls versus time *t* at testing on ChShM machine under 392 N load in the presence of lubricants based on calcium soaps of synthetic higher fatty acids containing oil I-40A as a dispersion medium (*1*, *2*) and vacuum oil distillates (*3*): (*1*, *3*) without additives; (*2*) with 0.5 wt% addition of triethanolamine

The aforementioned effect can be explained as follows. In contrast to the traditional highly refined industrial oils, the oil-refining byproducts (vacuum oil distillates in our case) contain petroleum oils (naphthenic, etc.) in small amounts, which are more chemically active than the fatty acids contained in general-purpose lubricants thickeners.

Therefore, they are able to form organic compounds while interacting with ethanolamines. These compounds display strong surface-active properties, where they form boundary lubricating layers with a strong screening effect that promotes the reduced wear of solids found in dynamic contact. This conclusion agrees with the experimental observations (Fig. 5.7, curves *3–6*).

Based on the aforementioned, the use of ethanolamines (mono-, di-, and tri-ethanolamines) in 0.5–1.5 wt% concentrations only makes it possible to enhance antiwear properties by as much as 1.2–1.4 times when plastic lubricants are added to the dispersion medium in the form of intermediate oil-refining products not subjected to special refining, e.g., vacuum oil distillates, with all other properties intact.

It should be noted that, in the case when the same ethanolamines are introduced into the plastic lubricants in amounts of 0.5–1.5 wt% with a dispersion medium in the form of the refined industrial oil and thickener based on both hydrated calcium soaps of higher acids of natural fats (Fig. 5.7, curves *1* and *2*) and hydrated calcium soaps of synthetic higher fatty acids (Fig. 5.8, curves *1* and *2*), then only a negligible effect of the wear spot diameter reduction is observed.

However, thorough microscopic and electron microscopic investigations of the wear spots on steel balls tested on the ChShM machine under severe conditions (392 N load during 8 h) show that, in both lubricantss containing refined industrial oils as the dispersion medium and thickeners based on hydrated calcium soaps of the higher acids of the natural fats (Fig. 5.9) and the hydrated calcium soaps of the synthetic higher fatty acids (Fig. 5.10) the introduction of ethanolamines in the lubricants promotes a significant reduction of the spots along with so–called cavitation wear, which appears on the edges of wear spots [27].

This type of wear is clearly seen as expressly defined, rather wide local damages (ultramicrocracks that result in the spalling of the material particles during propagation) near the contour of the wear spot in the direction in which the upper ball is brought into contact with the lower one (Figs. 5.9d, f and 5.10c, d). This fact also speaks in favor of the high efficiency of antiwear properties of ethanolamines used in the general-purpose calcium Lubricantss [27].

It has been found out that the introduction of 3 wt% liquid-crystal nanomaterials into the lubricants leads to an even stronger reduction of wear on the lower ball in the ChShM tests (Fig. 5.7, curve *7*). The presence of liquid-crystal nanomaterials in the lubricants provides for a softer frictional interaction mode between the solids. This is supported by the microrelief of the friction surface obtained by scanning electron microscopy after the ChShM sliding tests in the lubricants, just as without (Fig. 5.11a), so with the 3 wt% addition of liquid-crystal nanomaterials (Fig. 5.11b).

It follows from the results presented in this study that the microrelief of the friction surface shows principal differences between the two cases in question. For the case of lubricants studies without the liquid-crystal nanomaterials, we can observe furrows with multiple defects (Fig. 5.11a), the edges of which are blurred, while the friction surfaces are more damaged by long, deep pits. This is attributed to uneven and unstable friction process between the contacting bodies. It should be noted that the introduction of the liquid-crystal nanomaterials in the plastic lubricants imposes a noticeable reduction in the diameters of wear spots on the friction surfaces (Fig. 5.7, curve *7*) accompanied by the absolutely different morphological peculiarities of the anisotropic microrelief of the contacting surfaces.

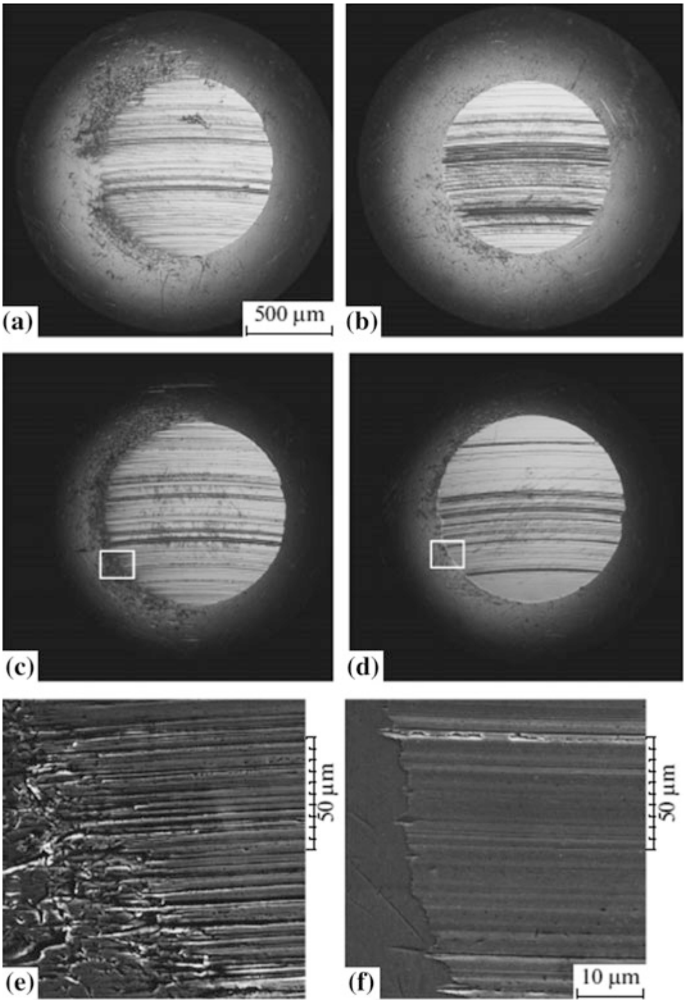

Fig. 5.9 Surface microrelief with different magnification of wear spots on steel balls after tests on ChShM machine under 392 N load for 8 h in the presence of lubricants based on calcium soaps of the higher acids of natural fats containing industrial oil I-40A as a dispersion medium: **a**–**c** without additives; **d**–**c** with 0.5 wt% triethanolamine

The microfurrows formed during sliding are characterized by higher regularities, while the tearing out is hardly observed and the microrelief is similar to the one observed in studies of liquid lubricating materials containing synthetic liquid-crystal nanomaterials. This means that it is characterized by more regular submicroroughness [23], which is known to be the most favorable for making strong cohesion with the liquid-crystal nanomaterials molecules. As a result, the above-described topography of surfaces found in dynamic contact with the

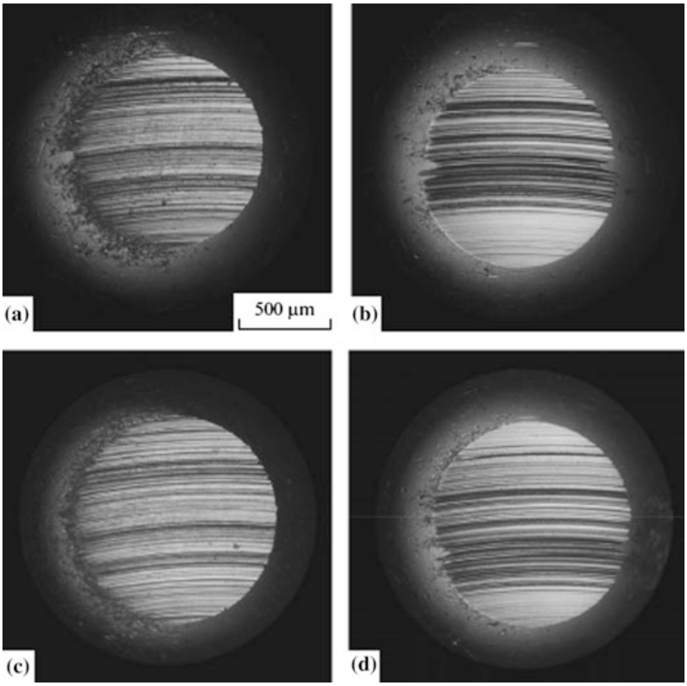

Fig. 5.10 Surface microrelief of wear spots on steel balls after tests on ChShM machine under 392 N load for 8 h in the presence of plastic lubricants based on calcium soaps of synthetic higher fatty acids containing industrial oil I-40A as a dispersion medium: **a**, **b** without addition of triethanolamine; **c**, **d** with 0.5 wt% addition of triethanolamine

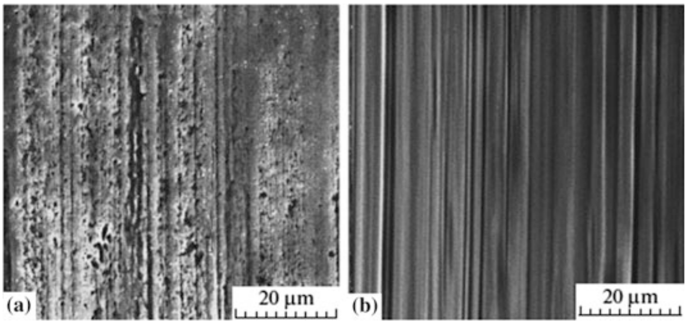

Fig. 5.11 Surface microrelief of wear spots on steel balls after tests on ChShM machine under 392 N load for 8 h in the presence of lubricants based on calcium soaps of higher acids of natural fats containing vacuum oil distillates as a dispersion medium: **a** without additives; **b** with addition of 3.0 wt% liquid-crystal nanomaterials

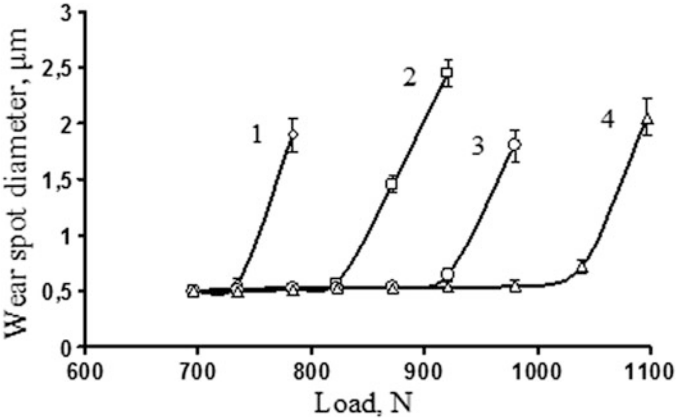

Fig. 5.12 Dependence of diameter of wear spot on axial load for calcium plastic lubricants: (*1*) general-purpose plastic lubricants GOST State Standard 1033–79; (*2*) plastic lubricants based vacuum oil distillates; (*3*) plastic lubricants based on vacuum oil distillates with addition of 0.5 wt % triethanolamine; (*4*) plastic lubricants based vacuum oil distillates with addition of 0.5 wt% triethanolamine and 3 wt% liquid-crystal nanomaterials

liquid-crystal nanomaterials film adsorbed on them is the most favorable for decreasing friction-induced losses and promotes the more stable operation of the metal tribopair, which has been confirmed experimentally.

ChShM tests of the developed lubricants under the critical loads have supported the above-mentioned conclusions (Fig. 5.12, curves *1* and *2*), as opposed to the traditional calcium plastic lubricants (Fig. 5.12). Compared to the known calcium plastic lubricants (Fig. 5.12, curves *1* and *2*), lubricants doped with liquid-crystal nanomaterials (Fig. 5.12, curve *4*) ensures a 1.25–1.4-fold increase in enduring critical load.

The results of present investigations have visualized that, in the creation of general-purpose calcium plastic lubricants based on vacuum oil distillates with improved antifriction properties for friction joints of machines and mechanisms, it is strongly advantageous to use ethanolamines, including those containing liquid-crystal nanomaterials.

References

1. E.V. Ryzhov, *Technological Methods of Improving Wear Resistance of Machine Parts* (Navukova Dumka, Kiev, 1984), p. 320 (in Russian)
2. V.A. Vladimirov, Trans. Res. Navy Inst. **227**, 34–44 (1977) (in Russian)
3. V.A. Vladimirov, L.M. Pekar, Calculation of duration and conditions of running-in of the marine diesel engine cylinder-piston group. Dvigatelestroenie **10**, 51–53 (1983) (in Russian)
4. L. Rodig, V. Bazika, Prisrevek k Probiematice Sledovani Zabehu Naftovych Motoru, Techniky Sbornik. VUCKD, Praga, **41**, 3–5 (1979)

5. V.N. Romanov, G.I. Romanova, Selection of the method of factory running-in of diesel engines. Dvigatelestroenie **10**, 53–55 (1984) (in Russian)
6. S.G. Arabjan, I.A. Kholomonov, Improvement of ICE running-in process. Dvigatelestroenie **8**, 43–45 (1981) (in Russian)
7. MKh Nigamatov, Accelerated running-in of engines. Tehnika v Selskom Hozjajstve **1**, 12–14 (1978) (in Russian)
8. G.J. Hillingman, S. Barrow, Shipboard in Vestigations with Selected Juels of Tomorrow, 14-th International Congress on Combustion Engines, Helsinki, D 63. (1981)
9. Running-in of Tractor Engines. Trans. Nat. Autotractor Inst. **216**, 54–56 (1972) (in Russian)
10. A.M. Kuliev, *Chemistry and Technology of* Additives *to Oils and Fuels*, 2nd edn. (Himija, Leningrad, 1985), p. 185 (in Russian)
11. M.Kh. Nigamatov, *Accelerated Running-in of Overhauled Engines*. (Kolos, Moscow, 1984), p. 178 (in Russian)
12. B.I. Kupchinov, S.A. Ermakov, V.P. Parkalov, V.G. Rodnenkov, Study of the effect of mesogenous additive to greases on the friction coefficient kinetics. Trans. Belarus. Acad. Sci. **33**(4), 340–343 (1989) (in Russian)
13. V.P. Dofman, Additive to motor oils. Za Rulem **3**, 20–21 (1991) (in Russian)
14. M.A. Gusev, Chem. Technol. Fuels Oils **5**, 30–32 (1985) (in Russian)
15. V.I. Bobrov, G.A. Tjuneva, Mesomorphism of peaches of distillate residues of diesel fuels and oils, in Structure and Properties of Liquid Crystals, Ivanovo (1989), pp. 84–91 (in Russian)
16. TS 25-1470.002-82, *Special Salve-Like Diamond Paste*. (1982), p. 6 (in Russian)
17. V.I. Kolesnikov, S.F. Ermakov, A.P. Sychev, Triboinduced adsorption of liquid-crystal nanomaterials under friction interaction of solids. Dokl Phys **54**(6), 269–272 (2009)
18. A.A. Syslov, S.F. Ermakov, Liquid Crystal Additives in Finish Materials. Mater. Technol. Tools. **2**, 87–88 (1998) (in Russian)
19. A.A. Syslov, B.I. Kupchinov, S.F. Ermakov, A.A. Baranovskii, A.T. Kozlovskii, Pat. 2210 C1 BY, C 09 G 1/02. The Composition for Polishing. No. 950789. Filed 21.07.95. Published 30.06.98
20. B.I. Kupchinov, S.F. Ermakov, E.D. Beloenko, *Biotribology of Synovial Joints* (Vedy, Minsk, 1997), p. 272 (in Russian)
21. B.I. Kupchinov, S.F. Ermakov, V.G. Rodnenkov, E.D. Beloenko, O.L. Eismont, Some results of studies in liquid-crystalline state of synovial lubricant in joints. J. Friction Wear **23**(3), 69–75 (2002)
22. S. Ermakov, A. Beletskii, O. Eismont, V. Nikolaev, *Liquid Crystals, Biotribology. Synovial Joint Treatment* (Springer Cham, Heidelberg, New York, Dordrecht, London, 2016), p. 211
23. A.S. Akhmatov, *Molecular Physics of Boundary Friction* (Fizmatgiz, Moscow, 1963), p. 472 (in Russian)
24. S.F. Ermakov, *Tribology of Liquid-Crystalline Nanomaterials and systems* (Belarusian Nauka, Minsk, 2012), p. 380 (in Russian)
25. V.V. Sinitsyn, *Selection and Application of Plastic Greases* (Khimiya, Moscow, 1974), p. 342 (in Russian)
26. V.V. Sinitsyn, *Plastic Greases in the USSR* (Khimiya, Moscow, 1984) p. 276 (in Russian)
27. V.V. Mulyarchik, V.G. Konstantinov, V.N. Danishevskii, S.F. Ermakov, R.A. Shuldykov, A. L. Bogdanov, A.P. Svirskii, Resp. Belarus' Patent 15897, MPK^8 S 10 M 101/02, Official Bull. (2012), no. 3, pp. 134–135 (in Russian)

Conclusions

The monograph covers results of investigation of triboengineering properties of LC-compounds and conceptual approach to explanation of their tribological efficiency at frictional interaction of different solids.

A wide range of information concerning the phenomena occurring between liquid crystals and other phases is presented. The lubricity of cholesteric-nematic LC-compounds is studied, their influence on tribophysical properties of natural of natural and artificial liquid mediums is determined; a link between parameters of LC-nanomaterials and technical features of metal- and biopolymer couples lubricated by them is established. A scientific concept of control of triboengineering parameters of natural and technical dissipative systems by means of implementing the ordered mesophase of boundary layers in dynamic contact area is proposed and discussed. Moreover, the medicines for the treatment of arthropathy, general in action mechanism and high-effective lubricants for machines and devices are created on the basis of the above concept.

New artificial lubricant mediums are developed on the bases of obtained experimental data. They contain cholesteric LC-nanomaterials inherent to natural synovia, possess its structural rheological and frictional characteristics and serve to both invasive and non-invasive application. The results of high chondroprotective efficiency of these preparations on osteoarthritis models and the benefits of clinical testing given in the book show that liquid crystals are of great importance for intra-articular friction reduction.

More detailed analysis of experimental data indicates that depending on their component structure, we can remark either mesophase range extension or temperature range increasing with minimal values of friction coefficient. Therefore, it is noted that in the circumstances the temperature resistance of boundary layers of cholesteric LC-mixtures exceeds the temperature resistance of lubricating layers with or without their mineral oils. Attention is drawn to the fact that the minimal values of friction coefficient for LC-compounds mixtures under consideration are observed in the temperature range including both mesophase area and a part of isotropic liquid. In other words, increasing friction coefficient in the process of tribosystem heating happens at temperatures when studied LC-nanomaterials have long been isotropic liquids. This ambiguous behavior of the LC-mixtures resulting

S. F. Ermakov and N. K. Myshkin, *Liquid-Crystal Nanomaterials*, Springer Series
in Materials Science 267, https://doi.org/10.1007/978-3-319-74769-9

in shift of temperature resistance of their boundary layers towards the temperature ranges relevant to the phase of isotropic liquid is caused by influence on LC-compounds of friction surfaces.

This is well evidenced by the fact that physical and mechanical properties of thin boundary layers of LC-compound molecules can change and differ from volumetric ones. In other words, decrease of friction coefficient observed for the cholesterol liquid-crystal nanomaterials above their elucidation points is of significant interest and not unexpected, as far as in this case boundary lubrication is defined by a mechanism where a lubricity efficiency is associated only with the properties of thin polymolecular films of LM which are border with solid surfaces.

The results presented in other works are also support this conclusion. According to them, there is a possibility that transition from ordered to disordered states of LC-films on the friction surfaces occurs at much higher temperatures then elucidation temperatures of their volume. As known, molecules of LC-nanomaterials can keep ordered (smectic, cholesteric etc.) structure until they reach this elucidations temperatures. It opens broad perspectives for using individual cholesterol liquid-crystal nanomaterials rather for their mixtures directly as lubricant materials with increased thermal resistance in relation to LM of different nature. As a result, a number of inventions related to new more effective liquid-crystal lubricant materials can be created on the basis of the finished research. Along with all these problems of tribology of liquid-crystal materials, there is a problem of their operational stability, what is meant both stability of the liquid crystals under conditions of the friction unit being in operating and stability over time of triboengineering parameters they provide. This problem solution is essential to the production on a large scale and application of tribotechnical liquid-crystal materials.

The studies in this area are currently under development and of great interest not only for professionals working in the field of liquid crystals but for tribologists and biophysicists. Such a situation in the lubricity research of cholesteric LC-nanomaterials makes the need for further in-depth works in this direction evident.

To sum up, it is hoped that the reported findings will attract the attention of tribology, arthrology and biophysics specialists and be used as background material to continue and intensify scientific work in research of unique triboengineering properties of liquid crystals, materials and preparations based on them.

Index

S. F. Ermakov and N. K. Myshkin, *Liquid-Crystal Nanomaterials*, Springer Series in Materials Science 267, https://doi.org/10.1007/978-3-319-74769-9